

**Thermodynamic, Morphological and Structural
Properties of Dissociated Fatty Acid Monolayers
at the Air-Water Interface**

Robert Johann

Potsdam 2001

Aus dem Max-Planck-Institut für Kolloid- und Grenzflächenforschung

**Thermodynamic, Morphological and Structural
Properties of Dissociated Fatty Acid Monolayers
at the Air-Water Interface**

Dissertation

zur Erlangung des akademischen Grades
Doktor der Naturwissenschaften (Dr. rer. nat.)
in der Wissenschaftsdisziplin Physikalische Chemie

eingereicht an der
Mathematisch-Naturwissenschaftlichen Fakultät
der Universität Potsdam

von
Robert Johann
geboren am 1.3.1970

Potsdam, im März 2001

abstract

Untersuchungen an Monoschichten amphiphiler Lipide auf wässriger Lösung sind in der Grenzflächenforschung von grundlegender Bedeutung. Aufgrund der Anwendbarkeit zahlreicher analytischer Methoden sind schwimmende unlösliche Monoschichten als Modellsysteme sehr geeignet, um Ordnung und Strukturbildung sowie den Transport von Materie in zwei Dimensionen oder die Wechselwirkung von Molekülen an der Grenzfläche mit Teilchen in Lösung (Stichwort "molekulare Erkennung") zu studieren. Aus dem Verhalten von Monoschichten lassen sich z. B. Rückschlüsse ziehen auf die Eigenschaften von Lipidschichten auf festen Substraten oder in biologischen Membranen.

Diese Arbeit befasst sich mit spezifischen und fundamentalen Wechselwirkungen in Monoschichten sowohl auf molekularer als auch auf mikroskopischer Ebene und deren Beziehung zu Gitterstruktur, Aussehen und thermodynamischem Verhalten von Monoschichten an der Wasser/Luft Grenzfläche. Als Modellsystem werden hauptsächlich Monoschichten langkettiger Fettsäuren verwendet, da in ihnen die molekularen Wechselwirkungen durch Änderung des Subphasen-pH-Werts über den Dissoziationsgrad gezielt und schrittweise verändert werden können. Ausser über die Subphasenzusammensetzung werden die molekularen Wechselwirkungen auch über die Temperatur und die Monoschichtzusammensetzung systematisch variiert. Mit Hilfe von Isothermen- und Oberflächenpotentialmessungen, Brewsterwinkel-Mikroskopie, Röntgenbeugung unter streifendem Einfall und polarisationsmodulierter Infrarot-Reflexions-Absorptions-Spektroskopie wird die Änderung der Monoschichteigenschaften als Funktion eines äusseren Parametern analysiert. Dabei werden aus den Röntgenbeugungsdaten quantitative Masse für die molekularen Wechselwirkungen und für die Kettenkonformationsordnung in Monoschichten abgeleitet.

Zu den interessantesten Ergebnissen dieser Arbeit zählen die Aufklärung des Ursprungs von regelmässigen polygonalen und dendritischen Domänenformen, die vielfältige Wirkung von Cholesterin auf die Molekülpackung und Gitterordnung langkettiger Amphiphile, sowie die Entdeckung einer abrupten Änderung in den Kopfgruppenbindungswechselwirkungen, der Kettenkonformationsordnung und des Phasenübergangsdrucks zwischen geneigten Monoschichtphasen in Fettsäuremonoschichten nahe pH 9. Zur Deutung des letzten Punkts wird ein Modell für die Kopfgruppenbindungsstruktur von Fettsäuremonoschichten als Funktion des pH-Werts entwickelt.

Research on monolayers of amphiphilic lipids on aqueous solution is of basic importance in surface science. Due to the applicability of a variety of surface sensitive techniques, floating insoluble monolayers are very suitable model systems for the study of order, structure formation and material transport in two dimensions or the interactions of molecules at the interface with ions or molecules in the bulk (keyword "molecular recognition"). From the behaviour of monolayers conclusions can be drawn on the properties of lipid layers on solid substrates or in biological membranes.

This work deals with specific and fundamental interactions in monolayers both on the molecular and on the microscopic scale and with their relation to the lattice structure, morphology and thermodynamic behaviour of monolayers at the air-water interface. As model system especially monolayers of long chain fatty acids are used, since there the molecular interactions can be gradually adjusted by varying the degree of dissociation by means of the subphase pH value. For manipulating the molecular interactions besides the subphase composition also temperature and monolayer composition are systematically varied. The change in the monolayer properties as a function of an external parameter is analysed by means of isotherm and surface potential measurements, Brewster-angle microscopy, X-ray diffraction at grazing incidence and polarisation modulated infrared reflection absorption spectroscopy. For this a quantitative measure for the molecular interactions and for the chain conformational order is derived from the X-ray data.

The most interesting results of this work are the elucidation of the origin of regular polygonal and dendritic domain shapes, the various effects of cholesterol on molecular packing and lattice order of long chain amphiphiles, as well as the detection of an abrupt change in the head group bonding interactions, the chain conformational order and the phase transition pressure between tilted phases in fatty acid monolayers near pH 9. For the interpretation of the latter point a model of the head group bonding structure in fatty acid monolayers as a function of the pH value is developed.

Contents

1. Introduction	1
2. Basic Features of a Monolayer	2
2.1 What is a Monolayer?	2
2.2 Monolayer Spreading	2
2.3 Monolayer Stability	4
2.3.1 Kinetic Stability	4
2.3.2 Thermodynamic Stability	5
2.3.2.1 Hydrophobic Effect	5
2.3.2.2 Effect of Other Solutes	6
2.3.3 Single Molecule Interactions	7
2.3.4 Chemical Bonding Interactions	8
3. Structural Order of Elongated Molecules in Two Dimensions	9
3.1 The State of Mesophases	9
3.2 Ordering in Smectic and Monolayer Phases	9
3.2.1 Classification of Smectic Phases	9
3.2.2 Order Parameters	10
3.2.2.1 Positional Order	10
3.2.2.2 Bond-Orientational Order	11
3.2.2.3 Herringbone Order	14
3.2.2.4 Tilt-Orientational Order and Tilt-Bond Coupling	15
1. Tilt-orientational order	15
2. Tilt-bond coupling	18
3.2.3 Classification of Monolayer Phases	23
4. Methods Used for the Investigation of Monolayer Systems	25
4.1 Filmbalance Technique	25
4.1.1 Instrument	25
4.1.2 Physical Fundamentals	26
4.1.3 Measurement and Interpretation	26
4.2 Surface Potential Measurement	28
4.2.1 Instrument	28
4.2.2 Physical Fundamentals	29

4.2.3 Measurement and Interpretation	30
4.3 Brewster-angle Microscopy	31
4.3.1 Instrument	31
4.3.2 Physical Fundamentals	32
1. Light reflection at an air-water interface	32
2. Light reflection at a film covered surface	34
4.3.3 Measurement and Interpretation	35
4.4 Infrared Reflection Absorption Spectroscopy	38
4.4.1 Instrument	38
4.4.1.1 Setup	38
4.4.1.2 Signal Processing	38
4.4.2 Physical Fundamentals	40
4.4.3 Measurement and Interpretation	41
4.5 X-ray Diffraction at Gracing Incidence (GID)	42
4.5.1 Instrument	42
4.5.2 Physical Fundamentals	43
4.5.3 Measurement and Interpretation	46
5. Phase Behaviour of Fatty Acid Monolayers	48
5.1 Neutral Fatty Acids	48
5.2 Dissociated Fatty Acids	49
5.2.1 Effect of pH	50
5.2.2 Electrostatics of the Interface	52
5.2.3 pH-Stability	58
6. Morphology of Dissociated Fatty Acid Monolayers	60
6.1 Observations	60
6.1.1 Effect of pH	60
6.1.2 Effect of Temperature	64
6.1.3 Influence of Cholesterol	65
6.1.4 Influence of Polyethyleneimine (PEI) in the Subphase	67
6.2 Forces Governing Domain Texture and Shape	70
6.2.1 Electrostatic Forces	70
6.2.2 Forces Determining Domain Texture	73
6.3 Explanation and Interpretation	77

6.3.1 On the Effect of pH	77
6.3.2 On the Effect of Temperature	78
6.3.3 On the Influence of PEI	80
6.3.4 Faceting of Monolayer Domains	84
6.3.4.1 Variation of an Arachidic Acid Monolayer with pH	84
6.3.4.2 Variation of a Monolayer of Heptadecanoic Acid Methyl Ester with Temperature	85
6.3.4.3 Variation of Composition in a Mixture of 1- <i>O</i> -hexadecyl- <i>rac</i> -glycerol (ETD) and 1-Palmitoyl- <i>rac</i> -glycerol (ESD)	87
6.3.4.4 Discussion	88
6.3.5 On the Influence of Cholesterol	90
6.3.6 Non-equilibrium Shapes	93
6.4 Quantification of the Line Tension	95
6.4.1 Theoretical Basis	96
6.4.2 Shape Analysis	97
6.4.3 Calculation	97
7. Structure of Dissociated Fatty Acid Monolayers	101
7.1 X-ray Analysis	101
7.1.1 Influence of pH on Chain Order	101
7.1.2 Influence of pH on Head Group Order	102
1. Steric interactions	103
2. Effect of solutes	105
3. Bonding interactions	105
7.1.3 Model of Fatty Acid Head Group Structure	107
7.1.4 Conclusion	109
7.2 Study of the Head Group Bonding by PM-IRRAS	109
7.2.1 Peak Analysis	109
1. Peak assignment	109
2. Peak fitting	111
7.2.2 Discussion	112
1. Variation of peak intensities with pH	112
2. Taking peak intensities for surface concentrations	113
3. Concluded variation of surface concentrations with pH	115
7.2.3 Conclusion	116

7.3 Effect of pH on the Stability of Monolayer Phases	117
7.3.1 Phase Shifting due to Head Group Ionisation	117
7.3.2 Optical Changes at the Phase Transitions	121
7.3.3 Indications of a Superior Division of the Phase Diagram	124
7.3.4 Possible Explanations of the Phase Shifting	125
7.3.5 An Alternative Mechanism for the NN/NNN Transition	128
7.4 Disclosure of Lipid-Solute Interactions by Simple Isotherm Measurement	128
1. Change of head group hydration	128
2. Indication of carboxylic acid dimer formation	130
3. Change of head group interactions	131
8. Summary and Outlook	133
9. References	138

Appendix

- I. Substances used
- II. Salt effects
- III. Dispersion energy of a tilted cylinder densely packed between six neighbours
- IV. Calculation of line energy (fig. 6.32)
- V. On monolayer-subphase interactions
- VI. X-ray diffraction data
- VII. List of symbols

Thesen

Lebenslauf

1. Introduction

Monolayers of organic molecules at the air/water interface have their permanent place in interface science from the beginning. Although this field has been subject to varying degree of interest in the lapse of time and other topics have been more in the focus of attention, monolayer science will certainly lose nothing of its importance also in the future.

The advantage of monolayers at the air/water interface is, that they are easy to handle, because of the peculiarity of the molecules to self-assemble at the interface and orient in a defined way and that their properties can be easily manipulated by relatively simple experimental means. The availability of a variety of newly developed surface sensitive techniques allows to study intermolecular interactions and molecular ordering, phase transitions, transport processes or the formation of condensed matter in two dimensions.

Such information is important under theoretical aspects, since in two dimensions systems are theoretically easier to treat and models easier to verify than in three dimensions. Of particular interest is the knowledge about the intermolecular interactions between monolayer lipids or between the monolayer and molecules in the aqueous subphase, such as proteins or polymers, for the understanding of processes and reactions in and at biological membranes. From the interactions between lipids revealed in a monolayer one can conclude on the properties of a membrane composed of these lipids, such as its stability, flexibility or permeability. Monolayers at the air/water interface also represent the basis for the formation of multilayers on solid substrates, which have potential application for electronic and optical devices.

Monolayers are not only of interest, because of their use as precursor or model systems. They still provide enough unresolved questions and hence need for investigation concerning their own nature. Important aspects are the specific and fundamental interactions between the amphiphiles of a monolayer and their influence on the properties and phase behaviour of the monolayer, the interactions between monolayer and solvent or solute molecules of the subphase, as well as the relation between the intermolecular interactions and the microscopic monolayer morphology.

In this work basic questions related to these aspects are accessed particularly by using monolayers of simple fatty acids. There the intermolecular interactions are varied gradually by changing the pH value of the aqueous subphase and the degree of dissociation in the monolayer. So far investigations on dissociated fatty acids are deficient and partially misleading. By means of a variety of surface sensitive techniques surprising and new results are obtained, which not only contribute to the understanding of monolayer features, but of the fundamental interactions between lipids and of processes at interfaces in general.

2. Basic Features of a Monolayer

2.1 What is a Monolayer?

A monolayer is an ultrathin film consisting of one layer of atoms or molecules, that is deposited on solid or liquid substrate at an interface between two different media. As the lateral dimension of a monolayer parallel to the interface exceeds its dimension perpendicular to the interface by far, a monolayer represents physically a two-dimensional system, which is described in terms of the occupied area. Monolayer investigation is advantageously performed on liquid, usually on aqueous subphase, where the monolayer can be easily manipulated by means of a film balance (see 4.1).

Molecules that are able to adsorb at an air/water or oil/water interface and to assemble to a monolayer must have a special chemical structure. Such molecules are called surface active agents, or briefly surfactants. A surfactant consists of a lyophobic (hydrophobic with water as solvent) part, which has little affinity to the solvent, and a lyophilic (hydrophilic for water) part with strong solvent affinity. Both parts are spatially clearly separated in the molecule. For surfactants assembling at an air(oil)/water interface the hydrophilic molecular section, referred to as head group, is highly polar or ionised, while the hydrophobic section, referred to as tail, is apolar and usually a hydrocarbon. Due to this dual nature the term amphiphile for surfactant is common. The balance between hydrophilic and hydrophobic character of the molecule determines, whether the substance prefers to remain in the 3D phase or spreads as a monolayer, whether it stays at the interface or dissolves into the subphase or evaporates. The simplest surfactants are fatty acids, alcohols, esters, amines, sulfates or sulfonates with a single unbranched saturated or unsaturated hydrocarbon chain. The chains are sometimes modified by replacing hydrogens by fluor atoms. The hydrophobicity is maintained but with increasing fluorine content the chains become less flexible and bigger in diameter. More complicated surfactants, that are found in biological systems are di- and triglycerides, phosphoglycerides, sterols or chlorophyll.

2.2 Monolayer Spreading

A monolayer is prepared most conveniently on a water surface by spreading some droplets of a dilute solution of the amphiphile in a water insoluble solvent onto the water surface by means of a microsyringe. The concentration of the amphiphile in the spreading solution is usually in the order of 10^{-3} M. Frequently used solvents are heptane or chloroform. In this

work the substances were dissolved in heptane to which sometimes 5 vol% of ethanol were added to enhance the solubility. As soon as a droplet of spreading solution touches the surface it spreads out over the entire accessible surface. The solvent evaporates and a monomolecular film of the amphiphile remains at the interface. It is recommended to let a short period of time elapse between spreading and commencement of monolayer investigation (for heptane several minutes) to allow the solvent to completely evaporate and the amphiphiles to adopt their equilibrium orientation. Slight effects of the type of spreading solvent on monolayer morphology and molecular order have been reported, which seem to originate mainly in different evaporation times of the solvent [Ger94, Hön92].

There are substances (e. g. alkanols) which spread in the pure state without solvent. If an excess amount of such a substance is placed on the surface as liquid droplet or solid crystal, molecules diffuse out of the bulk phase and distribute over the surface until a limiting pressure is reached, the so called equilibrium spreading pressure (Π_e).

The mechanism of the spreading process is not understood in detail yet and a matter of conjecture. It certainly depends on the solvent used and will be different with and without amphiphile. There are several possibilities known for the behaviour of a pure solvent droplet on a water surface:

- a) The droplet stays as it is and nothing happens
- b) The droplet spreads completely and covers the surface as a film
- c) The droplet partially spreads to a thin film or monolayer, which is in equilibrium with a droplet of excess solvent (at Π_e)
- d) The droplet first spreads completely, but immediately retracts to lenses that are in equilibrium with a thin film or monolayer (at Π_e). Famous example: benzene on water

The energetic situation, which governs a certain event, is described by the balance of the surface tensions τ at the three phase contact line fluid 1 (water), fluid 2 (spreading solvent), fluid 3 (air/vapour) (fig. 2.01). For the different cases it holds:

- a) balance of forces: $\tau_{13} = \tau_{12} \cos\theta_{12} + \tau_{23} \cos\theta_{23}$ (θ_{xy} : angle between \vec{t}_{xy} and $-\vec{t}_{13}$)
- b) spreading occurs spontaneously: $\tau_{13} > \tau_{12} + \tau_{23}$ corresponding to a positive spreading coefficient $S_\tau = \tau_{13} - \tau_{12} - \tau_{23} > 0$; for this case S_τ is usually large
- c) balance of forces: $\tau_{13} - \Pi_e = \tau_{12} \cos\theta_{12} + \tau_{23} \cos\theta_{23}$; if an amphiphile is dissolved and S_τ is positive, it is usually so small, that a monolayer forms more quickly by diffusion of the amphiphiles than by spreading of the solution
- d) at first case (b) holds and a film spreads, then a monolayer of solvent molecules adsorbs

onto the water surface and the film retracts, since $\tau_{13} - \Pi_e < \tau_{12} + \tau_{23}$;

finally state (c) is reached.

The spreading coefficient of heptane on water is only 2.6 mN/m (20°C) (compared to 8.8 mN/m for benzene on water [Mac90, Lid94]. Correspondingly it spreads only partially (case c). The situation drastically changes when a dilute amphiphile solution in heptane is used. Spreading is very quick and complete (case b), because τ_{12} is reduced by the amphiphile.

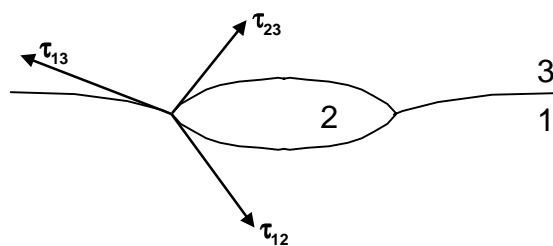


Fig.2.01: Solvent droplet (2) at the air(3)-water(1) interface in equilibrium

2.3 Monolayer Stability

2.3.1 Kinetic Stability

In many cases a monolayer does not represent a thermodynamically stable state and molecules escape from the interface in the course of time. The molecules can be solubilized by the subphase, evaporate or form 3 D crystals on the surface. The rate of substance loss depends on surface pressure, temperature and the ratio of hydrophilic to hydrophobic portion in the molecule. Below the equilibrium spreading pressure Π_e substance can only be lost via evaporation or solubilization, above this pressure the monolayer is metastable with respect to the transformation into 3 D matter. Π_e of stearic acid at 25°C is about 5 mN/m [Gai66]. The stearic acid monolayer can be compressed well above this pressure, however, film loss increases with pressure due to the formation and growth of 3 D nuclei within the monolayer. The so called collapse pressure represents the limiting pressure which cannot be exceeded as the crystal growth becomes very rapid or the film disrupts. For stearic acid on water at 25°C the collapse pressure is approximately 60 mN/m [McF93]. The solubility of stearic acid in water at 25°C is 3 mg/l [Gai66]. Hence, as an example, a monolayer of the acid at a molecular area of $0.2 \text{ nm}^2 \text{ mol}^{-1}$, that covers the water surface in a trough of 150 cm^2 area and 80 ml filling volume, should entirely dissolve in the subphase. The subphase could take 0.24 mg of the lipid, whereas the monolayer contains only 0,035 mg of it. However, the process of dissolution is so slow, that the monolayer appears stable within the time scale of monolayer investigation, which is usually in the order of hours. This implies that there is an energy barrier which prevents the monolayer molecules from submerging into the subphase. The fact

that the monolayer stability increases with increasing chain length of the amphiphile and that the solubility is higher in the expanded than in the condensed monolayer state indicates that the energy barrier results from the attractive chain interactions between the lipids. Monolayers of fatty acids and alcohols are fairly stable at room temperature for chain lengths ≥ 12 C-atoms ($\approx 0.1\%/min$ loss). With 18 and more carbon atoms film loss is negligible within the time scale of investigation [Gai66].

2.3.2 Thermodynamic Stability

2.3.2.1 Hydrophobic Effect

A monolayer is thermodynamically stable with respect to the formation of a bulk phase below Π_e . Its thermodynamic stability against dissolution is determined by the balance between hydrophilic and hydrophobic portion of the amphiphile. Assuming a low kinetic barrier to solution, an equilibrium between subphase and monolayer is established, and the monolayer is the more stable the larger the hydrophobic portion in the molecules. The origin of the hydrophobicity, i. e. of the fact that apolar molecular sections are expelled from the water phase, is the so called hydrophobic effect. This effect leads to the assembly of molecules on the water surface and to the formation of aggregates in water. Two aspects of the hydrophobic effect are distinguished: the "hydrophobic hydration" considers the interaction of a single non-polar solute (also gas) with the water solvent and accounts for the decrease in the solubility of the solute in water. The "hydrophobic interaction" refers to the apparent occurrence of attractive forces between apolar molecules in water leading to their association [Smi93]. Both aspects are based on the energetic changes connected with the distortion of the water structure in the immediate environment of the solute [Isr82].

A direct measure of the strength of the hydrophobic effect is the free energy necessary for transferring an apolar molecule from bulk phase into water. Considering a water phase in equilibrium with an apolar bulk phase, the free energy of the solute in the water phase (w), where its solubility is poor, is $\xi^w = \xi^0, w + RT \ln x$ and in the own bulk phase (b) $\xi^b = \xi^*, b$ (ξ : chemical potential). The free energy of transfer $\Delta\xi$ is $\Delta\xi = \xi^0, w - \xi^*, b = -RT \ln x_{eq}$ ($\Delta\xi > 0$ since $x < 1$). The enthalpy of transfer ΔH is obtained from the relation $\Delta H/T^2 = -d(\Delta\xi/T)/dT = -R d \ln x_{eq} / dT$. As for hydrocarbons the solubility in water decreases with increasing temperature ΔH is negative [Mac90]. This release of heat on solution of an apolar particle in water is ascribed to the strengthening of the hydrogen bonds between water molecules during the formation of a clathrate like cage around the solute [Cev87]. According to $\Delta\xi = \Delta H - T\Delta S$

the positive $\Delta\xi$ must arise from a negative entropy of transfer ΔS . The decrease in the entropy is caused by the loss in configurational freedom of the water molecules at the solute/water interface.

$\Delta\xi$ is proportional to the chain length of an alkane: $\Delta\xi/RT=3.55n(\text{CH}_3)+1.49n(\text{CH}_2)$ (in kJ/mole) [Cev87]. From the investigation of various hydrocarbons a proportionality between $\Delta\xi$ and the surface area of a hydrocarbon in contact with water has been revealed with a value for the "hydrophobic hydration" of approximately 10.5 kJ/mole per nm^2 [Cev87]. The dependence of the hydration energy on the shape of the solute leads to larger deviations from this value especially for very small solute volumes and large curvature of the solute surface [Wal95].

The dependence of the hydrophobic energy $\Delta\xi$ from the solute/water contact area allows the hydrophobic effect to be interpreted as the tendency of apolar groups to minimise their contact area with water, i. e. to dehydrate. It explains the reactions of apolar molecules in water, such as oil/water separation, protein folding and the formation of micelles, vesicles, membranes or of monolayers at the water surface.

When two apolar molecules in water approach, hydrophobic energy due to the breakdown of the solvent cages starts to be released already at some distance of the particles. It has been found to be more than two diameters of water molecules [Isr82]. The gain in molecular disorder gives rise to an attractive force between the particles, which is referred to as "hydrophobic interaction". The force decays exponentially over around 10 nm and may exceed the dispersion force by almost an order of magnitude [Isr82].

2.3.2.2 Effect of other solutes

The energy of the apolar solute in water is influenced by the presence of other kinds of solutes. A consequence can be the salting-in or -out of the apolar solute (see app. II).

2.3.3 Single Molecule Interactions

In this and the next section the fundamental interactions are presented, that molecules in monolayers are subject to. These interactions govern the stability of monolayers, their phase behaviour and morphology. They depend on the type of molecules and may be affected by the subphase composition.

1. Attractive London dispersion forces

By summing up r^{-6} dispersion potentials between the CH_2 -chain segments the attractive interaction between 2 parallel aliphatic chains of length L and distance D is [Sal62]:

$$F_L = \frac{\alpha}{4\gamma^2 D^4} \rho \left(3 \tan^{-1} \rho + \frac{\rho}{1 + \rho^2} \right), \quad \rho = \frac{L}{D} \quad (2.01)$$

Where α is a constant ($-1.34 \cdot 10^{-3} \text{ nm}^6 \text{ kcal/mole}$ [Sal62]) and $\gamma=L/N$ is the C-C distance of 1.27 \AA with N as the number of carbon atoms in a chain.

2. Repulsive dipole forces

Differences in electronegativity between different groups along the long axis of an amphiphile, especially between head group and tail, give rise to a dipole moment parallel to the axis. Permanent and induced dipoles of neighbouring molecules are uniformly aligned and hence repel each other. These dipole interactions strongly influence the shapes of condensed monolayer domains. The electrostatic energy of a two-dimensional array of parallel dipoles is:

$$F_p = \frac{1}{2} \frac{p_z^2}{4\pi\epsilon_0} \iint \frac{1}{|\mathbf{r} - \mathbf{r}'|^3} dN dN' \quad (2.02)$$

where p_z is the molecular dipole moment perpendicular to the plane, ϵ_0 the permittivity, N the number of molecules and $|\mathbf{r} - \mathbf{r}'|$ the distance between two increments dN and dN' of molecules. Replacing dN by ndA , where n is the molecular density dN/dA , and np_z by μ , one obtains [McC91]:

$$F_\mu = \frac{1}{2} \frac{\mu^2}{4\pi\epsilon_0} \iint \frac{1}{|\mathbf{r} - \mathbf{r}'|^3} dA dA' \quad (2.03)$$

where μ is the dipole density of the two-dimensional array. When the assembly of molecules is not surrounded by vacuum, but by a medium of different dipole density, for μ the difference of the dipole densities of both media has to be substituted.

Attractive interactions may arise from dipole contributions parallel to the monolayer plane.

With charged molecules additionally Coulomb interactions have to be taken into account.

2.3.4 Chemical Bonding Interactions

Much stronger than dipolar or dispersion forces are chemical bonding interactions. If they occur, they are usually dominating and determine the properties of condensed matter. Although these interactions are very short ranged being confined only to directly neighbouring molecules, they act on macroscopic scale by linking the molecules in a far ranging network. The formation of a network is based on the directionality of the atomic bonds, that is typical of these interactions.

The features of various monolayer systems are ascribed to the formation of hydrogen bonds between adjacent molecules (fig. 2.02). The strength of this bonding type can vary between that of relatively weak dipolar interactions and that of strong covalent bonds.

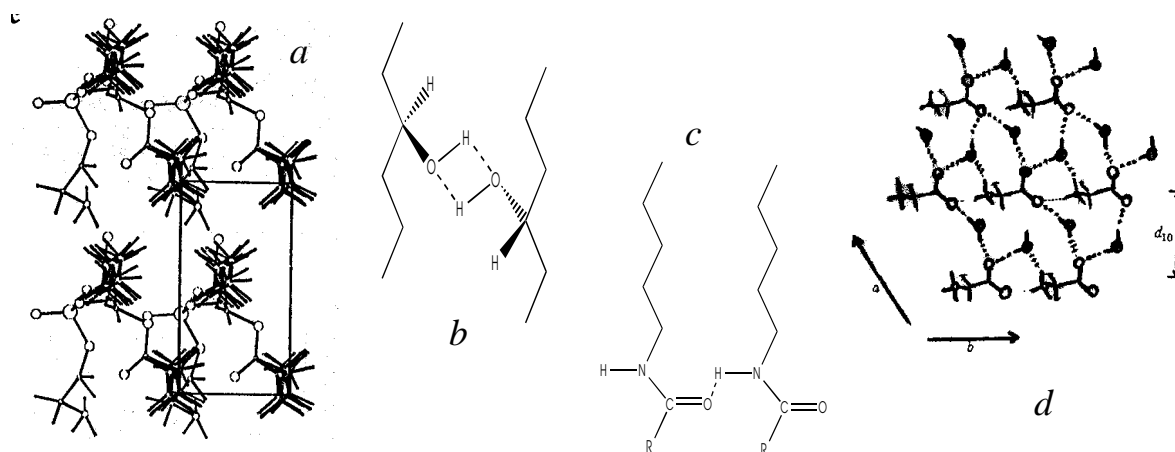


Fig. 2.02: Examples of hydrogen bonding in monolayers.

Assumed hydrogen bonding network in *L*-dipalmitoylphosphatidylethanolamine monolayers [Böh93] (a). Hydrogen bridging is indicated by low compressibility and relatively high crystallinity of a monolayer. High crystallinity is revealed by X-ray diffraction and usually manifests itself as rigid, needle-like and anisotropic growth forms of the condensed phase under the microscope [Mel97, Ase00, Wei96] (b, c). Modelled hydrogen bonding network between the amino acid head groups and water molecules in monolayers of $\text{CF}_3(\text{CF}_2)_9(\text{CH}_2)_2\text{OCOCH}_2\text{CH}(\text{NH}_3^+)\text{COO}^-$ [Jac90] (d)

3. Structural Order of Elongated Molecules in Two Dimensions

3.1 The State of Mesophases

The term mesophase or liquid crystal denotes a state of matter, that is between that of an isotropic liquid and of a crystalline condensed phase. Liquid crystals are fluid like liquids, but anisotropic like condensed phases. With certain substances one or more liquid crystalline phases are passed during melting before the liquid state is reached (thermotropic liquid crystals). Such phases can also appear when a substance is dissolved in a liquid (lyotropic mesophases). The persistence of the solid-like anisotropy in these phases is due to the particular geometry of the molecules, which are mostly long and straight or very flat.

The mesophase of lowest order is the nematic phase, in which rod like molecules align parallel with respect to their long axis (fig. 3.01a).

In the so called smectic phases the molecules are parallel and additionally arranged in layers (fig. 3.01b). There have been found many types of smectic phases, which can be classified with respect to the molecular order in two and three dimensions.

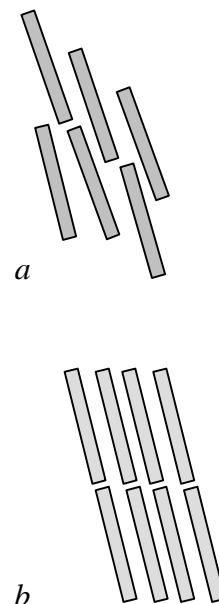


Fig.3.01: Nematic (a) and smectic ordering (b)

3.2 Ordering in Smectic and Monolayer Phases

3.2.1 Classification of Smectic Phases

Fig.3.02 [Hua92]: Most obvious is the distinction of the smectic phases between those, where the molecules are oriented with their long axes perpendicular to the layers, and those, where the molecular axes are inclined with respect to the layer normal. The tilted phases can again be subdivided by considering the orientation of the projection of the rod like molecule onto the layer plane with respect to different lattice directions (I vs. F vs. L, J vs. G vs. M, K vs. H vs. N; the tilt direction is indicated by arrows and arrow shaped triangles). The phases with upright molecules differ in the relative geometrical arrangement and position of the molecules with respect to each other. A source for a change of molecular packing can be a difference in the geometry of the molecular cross sections (elliptical: E, H, K, N vs. circular: all others). The different types of packing apply to the tilted as well as to the untilted phases. In the phases denoted as 'cry X' the positions of the molecules are correlated over different layers giving a three dimensional crystalline order, while in the other phases ('SmX' and 'HexX') the ordering is confined to the single layers.

NORMAL		TILTED			
Side View	TopView	Side View	TopView		
SmA		SmC			
HexB		SmI	SmF	SmL	
CryB		CryJ	CryG	CryM	
CryE		CryK	CryH	CryN	

3.2.2 Order Parameters

In this section the basic features, by which the types of smectic phases are distinguished and which were outlined in the previous section, are presented in more detail. It was found that there is strong resemblance between the structural features of single layers of smectic mesophases and those of monolayers of long chain amphiphiles on water. The same types of molecular order, i. e. the same order parameters, the variety of smectic phases are based on, can be applied to the description of the different phases of Langmuir monolayers.

3.2.2.1 Positional Order

Positional order means the coincidence of molecular positions with the point sites of an infinite crystallographic lattice. The degree of positional order is a measure for the spatial range, over which coincidence is fulfilled, i. e. a measure for the crystallinity. Quantitatively this is described by means of a density or position correlation function $G(r)$ [Sta71]:

$$G(\mathbf{r} - \mathbf{r}') = \langle n(\mathbf{r})n(\mathbf{r}') \rangle - n^2 \quad (3.01)$$

$n(\mathbf{r})$ and $n(\mathbf{r}')$ are molecular densities at positions \mathbf{r} and \mathbf{r}' , respectively, and n is the mean density of the sample. The brackets denote the statistical average. The product $n(\mathbf{r})n(\mathbf{r}')$ corresponds to the probability of meeting a certain density $n(\mathbf{r})$ at point \mathbf{r} and simultaneously a certain density $n(\mathbf{r}')$ at \mathbf{r}' . G expresses the correlation (degree of connection) of particle positions in dependence of distance and relative location. An example of a decaying correlation function is shown figure 3.03.

The position correlation or positional correlation is termed *long range*, when G is a constant different from zero for $r \rightarrow \infty$. For solids with infinite three dimensional translational order, this condition is fulfilled. In two-dimensional systems long-range periodicity of the lattice generally does not exist at temperatures above

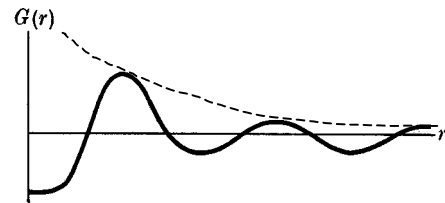


Fig. 3.03 [Sta71]:
Short range positional order

0°K. Thermal fluctuations destroy the correlation between movement and position of molecules over large distances, and G becomes zero for $r \rightarrow \infty$. The effect of temperature on positional order increases with decreasing spatial dimensionality of a system [Bro92]. However, true long range order in two dimensions seems not to be excluded by theory under certain conditions [Ove93a]. In two-and three-dimensional systems the decay of G with distance r is either found to follow a power law of the form $G \sim 1/r^{\eta(T)+d-2}$ (often referred to as algebraic decay, where d is the dimensionality of the system) or it is exponential according to $G \sim \exp(-r/\text{PCL}(T))$ [Hua92]. The critical exponent η and the position correlation length PCL are temperature dependent parameters. For the algebraic decay the corresponding position correlation is termed *quasi-long range*, as quasi-long range order and true long range order are hardly discriminated by means of X-ray diffraction methods. The position correlation of an exponential decay is called *short range*. Short range positional order is exhibited by disordered liquids and glasses.

3.2.2.2 Bond-Orientational Order

This order type concerns the relative geometrical arrangement of adjacent molecules. The preferred number of direct neighbours and the distances between them are compared. Long range bond-orientational order is given, when through the average directions of neighbours crystallographic axes can be laid, that reach to macroscopic dimensions (see fig. 3.06 b).

While the relative positions of molecules are disturbed by thermal fluctuations, the average direction of the vector connecting any two adjacent particles is not affected [Bro92].

The degree of order is described by a bond-orientational correlation function $G_n(r)$:

$$G_n(\mathbf{r}-\mathbf{r}') = \langle \Psi_n(\mathbf{r}) \Psi_n(\mathbf{r}') \rangle, \text{ where } \Psi_n(\mathbf{r}) = \frac{1}{N} \sum_{i=1}^N \exp(i\theta_i(\mathbf{r})) \quad (3.02)$$

is the bond-orientational order parameter for n -fold symmetry [Mur92]. $\theta_i(r)$ is the angle between a near neighbour bond at point \mathbf{r} and an external reference line (fig. 3.04). N is the number of direct neighbours. As the positional order, the bond orientational order can be long range, quasi- long range and short range. The corresponding functions for G_n are the same as described for the position correlation.

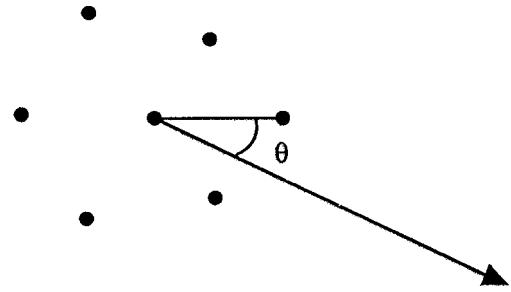


Fig.3.04: Definition of θ ; $N = 6$

Bond-orientationally ordered smectic or monolayer phases are usually of hexagonal or distorted hexagonal symmetry. Phases with short range positional order and long or quasi-long range sixfold bond-orientational order are termed *hexatic*. In known 2D systems, such as liquid crystals and assemblies of mutually repelling spherical particles of μm -size, prepared between parallel glass plates or as floating monolayers [Mur92], short range positional order is combined with quasi-long range bond-orientational order. The coupling of short range positional with long range bond-orientational order is only supposed for some systems [Kat92]. The hexagonal symmetry, which is observed for repelling as well as attracting particles, results from the lack of directionality of the bonding interactions between cylindrical chains, that closely pack, or from the isotropy of the electric and magnetic repulsion between spherical particles.

2D order-disorder transitions

	2D Solid		Hexatic		Liquid
Positional order	QLR	$\xrightarrow{T_m}$	SR	$\xrightarrow{T_i}$	SR
Bond-orientational order	LR		QLR		SR

Table 3.1 [Hua92] QLR: quasi-long range, LR: long range, SR: short range

This scheme illustrates the intermediate character of the hexatic mesophase, which has the positional order of a liquid and the anisotropy, due to bond-orientational order, of a solid.

The successive reduction in order during the transition from the solid to the liquid can be explained in a rather simple manner by the formation of two types of lattice defects, as is illustrated in figure 3.05.

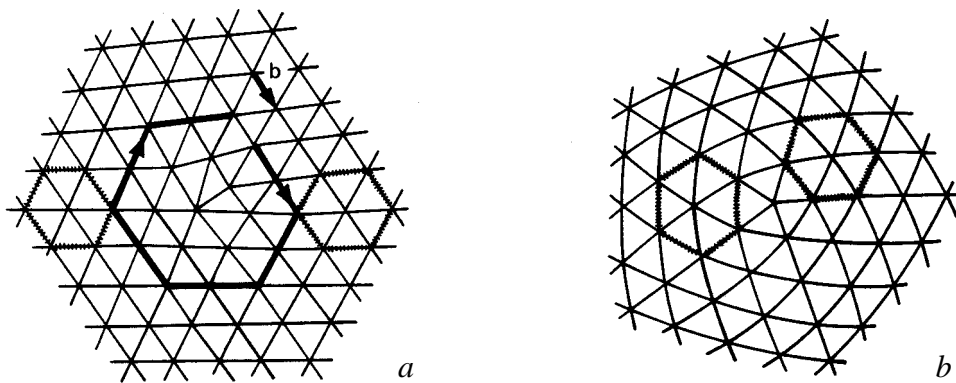


Fig.3.05 [Bro92]: Lattice defects in a two-dimensional triangular lattice. The insertion of an additional lattice line in the originally perfect lattice produces a dislocation, which is composed of a tightly bound pair of a seven- and a fivefold disclination, the midpoints of which are separated by one lattice spacing. This lattice defect destroys the long range positional order, but preserves the bond directions over long range (orientation of marked hexagons on opposite sides of the defect is the same)(a). The (quasi-) long range bond-orientational order is abolished together with the positional order, when the disclination pairs break up and separate. The two hexagons in (b) indicate the change of the bond orientations around a single fivefold disclination.

The position correlation length PCL is given as the mean separation of the dislocations and disclinations [Mur92] (fig. 3.05). In the regions between the defects the lattice is that of an ideal crystal.

The shape of X-ray diffraction peaks depends on the average extension of these crystalline regions. The peaks of monolayer phases are described quite well by Lorentz functions, which indicates short range positional order, i. e. exponential decay of G [Hel87]. The approximate value of the corresponding PCL is obtained from the peak width at half maximum, $fwhm$, of a peak resolved in the xy -plane (see 4.5):

$$PCL = \frac{2}{\sqrt{fwhm^2 - 0.89^2 nm^{-2}}} \quad (3.03)$$

The second term under the root takes into account the resolution of the detector, that may slightly vary; $0.82^2 nm^{-2}$ was used for it in chapter 6.3.5 and $0.89^2 nm^{-2}$ in chapter 7.1.

As already mentioned, the PCL is a measure of the crystallinity of the system. A large PCL corresponds to a low defect density and large crystalline regions. In this work the magnitude of PCL is put into direct relation to the interactions between the lipids in a monolayer. This seems reasonable, since the extent of crystallinity is governed by the interplay of inter-lipid bonding interactions, that force the molecules in definite lattice sites, and of thermal energy, by which the lattice order is disturbed. In chapter 6.3.5 and 7.1.2 it is demonstrated, how the

PCL can be used as a tool to reveal subtle variations in the inter-lipid interactions in monolayers. What is missing is a direct relation between the interaction energy and the value of the PCL.

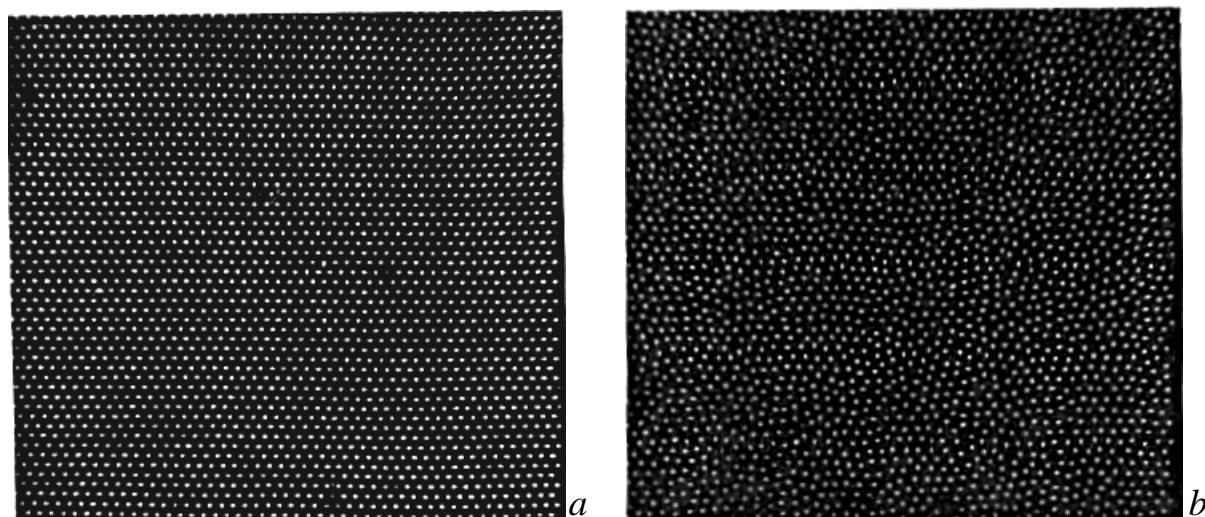


Fig.3.06 [Skj89]:

Monolayer of silica beads suspended in a ferrofluid between parallel glass plates and exposed to a magnetic field of varying strength. The degree of positional order (periodicity) within an array of particles is a function of the inter-particle interactions. A strong field produces hexagonal crystalline order (a); on reducing the field strength the extent of periodicity decreases to a few particle distances and a hexatic phase forms (b). The conservation of hexagonal symmetry one can proof by looking at a low angle on image b from different directions.

3.2.2.3 Herringbone Order

If the cross section is not circular but elliptical, the rod like molecules densely pack in the so called 'herringbone' pattern (fig. 3.02). An elliptical cross section is adopted by aliphatic chains in all trans conformation, as is illustrated in figure 3.07 (left) for long chain fatty acids. The packing symmetry in the plane perpendicular to the chain axes is then found orthogonal. When the number of gauche conformers in the chains increases, the cross sections become more circular and the packing symmetry approaches hexagonal (fig. 3.07, right). This is accompanied by an increase in the cross sectional area from about $0,18 \text{ nm}^2$ for herringbone packing to about 0.2 nm^2 for hexagonal packing. A free rotation of molecules in the hexagonal packing mode is unlikely, as for this an area of more than 0.25 nm^2 would be required [Sir97].

The conformational disorder of the chains of fatty acids is enhanced by increasing the temperature, reducing the chain length or by increasing the subphase pH (see 7.1.1). This can

be made plausible by assuming for the change from herringbone order (orthogonal) to disorder (hexagonal) the energetics of a discontinuous first order transition like for the LC-LE transition in a monolayer, which is also accompanied by a decrease in chain order from LC to LE (see 4.1.3). For the reaction to more disorder ($\Delta H, \Delta S > 0$) one may write: $\Delta G = \Delta H - T\Delta S$. Accordingly the equilibrium is left and more disorder produced ($\Delta G < 0$) by increasing the temperature or by reducing the attractive intermolecular interactions ΔH . ΔH diminishes with decreasing chain length or increasing electrostatic repulsion of the molecules. The latter is caused by increasing the subphase pH for dissociable amphiphiles.

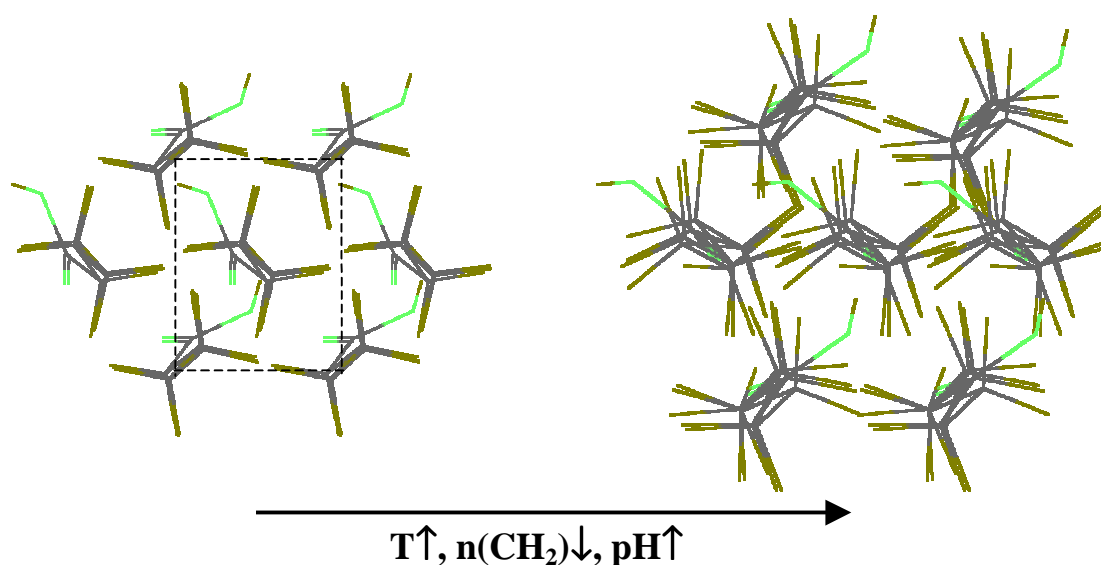


Fig.3.07: Fatty acid amphiphiles (viewed from chain end to head group) in all trans conformation (minimised with CS Chem3D Pro (3.5)) and herringbone packed (left). Approach of hexagonal packing mode by the increase of conformational disorder (right)

3.2.2.4 Tilt-Orientational Order and Tilt-Bond Coupling

1. Tilt-orientational order

The phenomenon that neighbouring rod-like molecules adopt the same tilt angle and align parallel to each other is denoted as tilt-orientational order.

Optical techniques, such as Brewster-angle microscopy (BAM) (see 4.3) and polarised fluores-

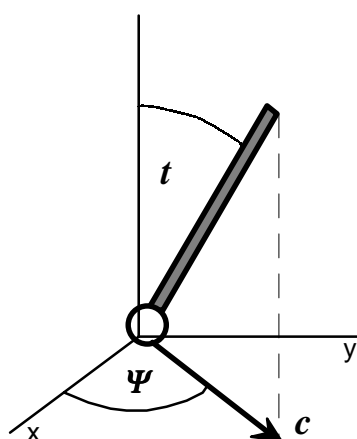


Fig.3.08: The orientation of a long chain amphiphile (head group depicted as sphere) is defined by the tilt angle t and azimuthal angle Ψ . The unit vector c indicates the orientation of the projection of the molecule in the monolayer plane x - y pointing towards the tail end;
 $c = x \cos \Psi + y \sin \Psi$

cence microscopy, reveal that in condensed monolayer phases the molecules can be ordered by this way over hundreds of microns.

In extended patches of condensed monolayers it is typically found that the uniform tilt order is interrupted by sharp boundaries subdividing the monolayer in a mosaic-like pattern (fig. 3.09). The formation of such boundaries requires energy and should therefore be unfavourable (the energy is proportional to the length of the boundary, see 6.2.2). Some observations suggest, that the pattern of a spread condensed monolayer (as in fig. 3.09) is kinetically stabilised. So it was observed, that a slowly evaporating spreading solvent favours the formation of larger domains in fatty acid monolayers [Hön92]. The domain size also increases by ageing [Hön92] and in a monomolecular film of fatty acid esters by exposing the film to higher temperatures [Gut95].

The pattern of LC domains in the LE-LC two phase region, the size of which is in the range of uniform tilt order (100 μm) (fig. 3.10), is determined by other factors. It largely depends on the line tension of the domain boundary to the expanded phase (see 6.2.2).

In monolayers the ordering strength of the three types of order appears to decrease in the sequence:

tilt-orientational \geq bond-orientational $>$ positional order

As a reason for the high stability of the orientations of tilted molecules one can imagine, that in tightly packed arrangements single molecules cannot move independently and are held in their orientations by neighbouring molecules. Another factor which influences the stability are the interactions between the molecules, that change with tilt angle and direction. In the following the latter aspect will be regarded more quantitatively with respect to the chain interactions.

Considering 2 straight aliphatic chains (fig. 3.11 a), their attractive energy F_L is given by eq. 2.01. For $L \gg D$, F_L can be approximated by [Sal62]:

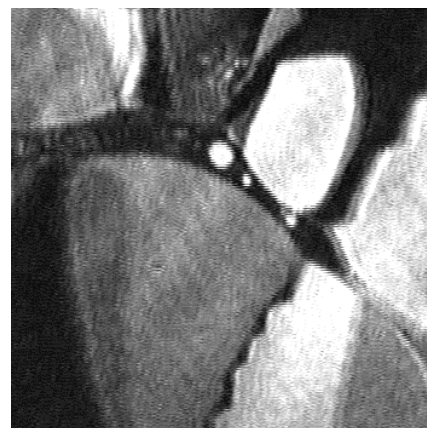


Fig.3.09:
Stearic acid, pH 3, 25°C. The shades of grey in the condensed phase observed with BAM correspond to regions of uniform tilt direction of the molecules. Size 287×287 μm^2

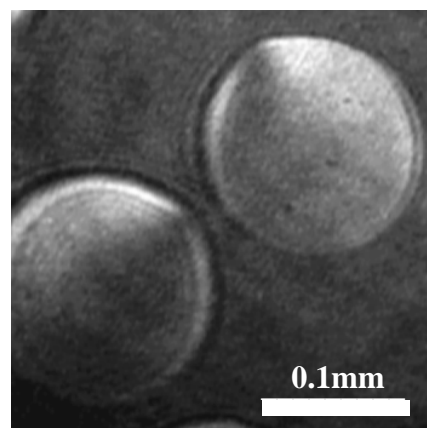


Fig.3.10:
BAM micrograph of two LC domains of pentadecanoic acid, pH 3, 25°C. The varying grey values indicate varying tilt direction within the domains

$$F_L = -g \frac{L}{D^5}, \quad \text{where } g \text{ is a constant} \quad (3.04)$$

D is d_{xy} in figure 3.11a,b. When the distance between the rods increases, also F_L increases (3.11 b). By tilting the molecules again approach and F_L decreases, but not all the energy is recovered (3.11 c). Neglecting the energy contribution of the chain ends without contact, F_l of two tilted chains is:

$$F_l = -g \frac{l}{D^5} = -g \frac{L - 2d_{xy} \sin t}{(d_{xy} \cos t)^5} \quad (3.05)$$

The notion, that tilted aliphatic chains in a monolayer are closely packed like straight cylindrical rods, where

$$d_0 = d_{xy} \cos t \quad \text{and} \quad A_0 = A_{xy} \cos t \quad (3.06)$$

(A_{xy} is the area per molecule in the monolayer plane, A_0 the cross sectional area of a chain) is in agreement with the results from X-ray diffraction experiments on monolayers [Kja89, Tip91].

There is a limiting distance $d_{xy}' > d_0$, below which the rods stay in the upright position. With known rod diameter d_0 this distance can be determined by using eqs. 3.04, 3.05, 3.06 and equalising:

$$\begin{aligned} F_L(D = d_0) - F_L(D = d_{xy}') = \\ F_l(d_{xy} = d_0) - F_l(d_{xy} = d_{xy}') \end{aligned} \quad (3.07)$$

The total energy of tightly packed chains is obtained by summing up the interactions with six neighbours regarding different lengths l and d_{xy} for different neighbours. Additionally at finite temperature the change in entropy has to be taken into account, since the thermal motion of the chains is restricted on going from state (b) to state (a) or (c) in figure 3.11 [Kag93a].

The dispersion forces between the chains are the larger the larger the contact lengths l between neighbouring chains. Therefore the arrangement of tilted chains according to figure 3.12a corresponds to the most stable one. The

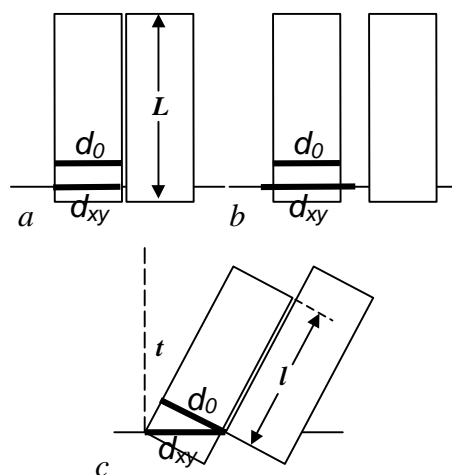


Fig.3.11: The dispersion interactions between a pair of aliphatic chains (modelled as cylindrical rods) decrease with increasing distance (a, b) or tilt angle (c)

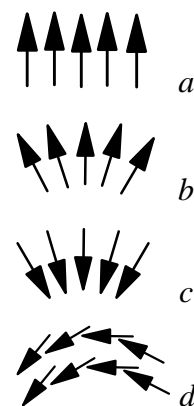


Fig.3.12: Different chain arrangements in monolayers (arrows are c -vectors, cf. fig. 3.08). Compared to case (a) the chain contact is reduced in splay (b, c) and bending patterns (d)

dispersion forces will be smaller in the cases (b-d). The energy differences give rise to different elasticities for bending the chains relative to each other. The patterns of figure 3.12 are found in the textures of LC monolayer domains. It seems reasonable to assume that the bending is the easier the shorter the chains, since the energy difference becomes smaller. Indeed the bending patterns 3.12c,d are observed in condensed monolayers of pentadecanoic acid (fig. 3.10), while for higher homologues pattern *a* is typical (see 6.2.2).

2. Tilt-bond coupling

a) Chain interactions

Three different tilt directions are distinguished with respect to the symmetry directions of a hexagonal lattice plane. It is the tilt in the (10)-direction towards the nearest neighbour (NN), in the (11)-direction towards the next nearest neighbour (NNN) and in an intermediate direction *I* between the NN and NNN direction (fig. 3.13). The dependence of the chain interactions on the tilt direction Ψ for a given tilt angle was calculated for hexagonally densely packed chains

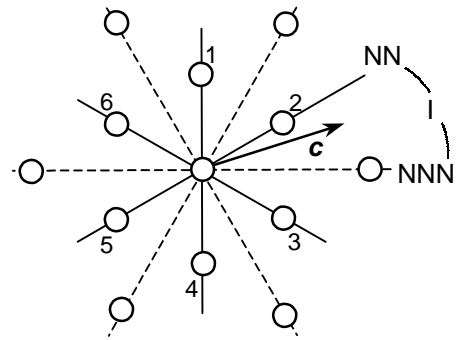


Fig.3.13: NN, *I* and NNN tilt directions in the hexagonal lattice

of cylindrical shape according to eq. 3.05 (appendix III). This dependence is shown in figure 3.14 for a rotation of a molecule within 60° for $t=20^\circ$, $L=25 \text{ \AA}$ and $d_0=5 \text{ \AA}$. It reveals that the tilt in NNN direction is energetically more favourable than in NN direction, in agreement with the considerations in [Kag93a, Sch97, Sch99]. This applies to any tilt angle, the energy difference increasing with the tilt angle for given L and d_0 (fig. 3.15). As the chain cross section can be considered as constant during the change in tilt angle [Kja89, Tip91], a contribution of conformational entropy to the interaction energy is negligible [Sir97, Kag99]. The lower energy of NNN compared with NN tilt becomes plausible from figure 3.13 by regarding the contact lengths l between each neighbour 1-6 and the central chain. For NN tilt along the 2-5 direction l is lowest and the interaction minimal with the neighbours 2 and 5 along the tilt direction, whereas it is larger with the neighbours 1, 3, 4 and 6. It would be maximal with chains perpendicular to the 2-5 direction, where $l=L$. For NNN tilt perpendicular to the 1-4 direction the neighbours 1 and 4 have the largest possible interaction with the central chain ($l=L$), whereas none of the other four neighbours lies along the tilt direction, where l is minimal.

b) Head group interactions

The separation of the molecules which finally leads to their tilting can be attributed to the repulsion between the head groups. At high pressure when the chains are upright and densely packed (fig. 3.11 a) the head groups are compressed to the size of the chain cross sections (fig. 3.16 a). As the pressure relaxes the heads can adopt their individual configurations and repulsive interactions between the head groups, because of thermal motion and the tendency for hydration, will result in an increase of d_{xy} . The chain interactions favour the separation in NNN direction. In the following it will be shown that separation in NN direction is favoured by the head group interactions. For this purpose the repulsive head group interactions are modelled as steric interactions between contacting elastic bodies. For simplicity the interactions are considered as isotropic and the bodies represented as spheres (fig 3.16). For NNN tilt the head group size cannot change perpendicular to the tilt direction in order to ensure tight chain contact (fig. 3.16 b). For NN tilt, however, the distance between the head groups enlarges in any direction with increasing tilt angle. Hence in contrast to NNN tilt the repulsive energy can decrease on isotropic head group expansion for NN tilt (fig. 3.16 c). The change in energy per head group may be described by:

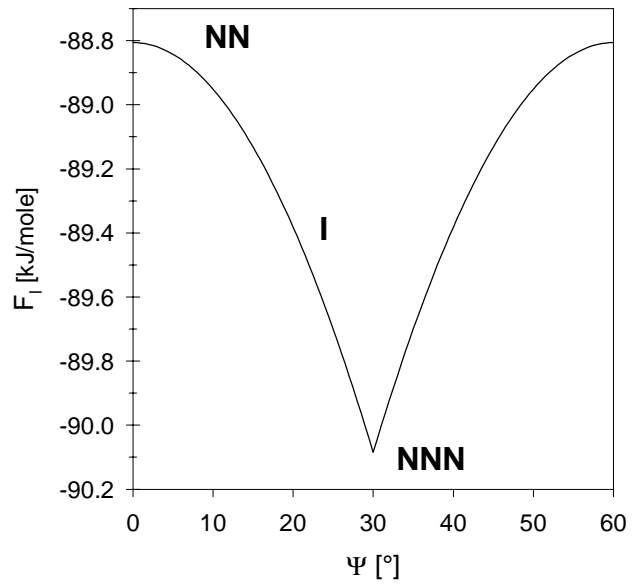


Fig.3.14: Calculated dependence of dispersion energy of a cylinder, that is surrounded by six other cylinders at close contact, on the azimuthal angle Ψ for constant tilt angle $t=20^\circ$ acc. to eq. 3.05 (see app. III). $L=25 \text{ \AA}$ and $d_0=5 \text{ \AA}$

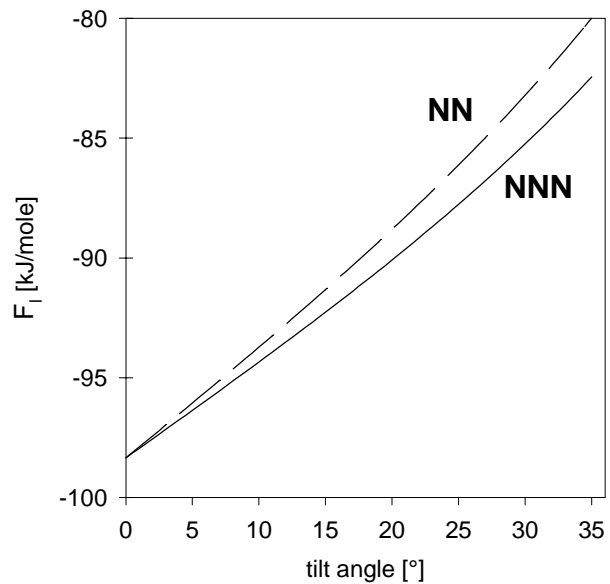


Fig.3.15: Same situation as in fig. 3.14, except that Ψ is fixed in NN or NNN direction and t is varying. The calculation shows firstly, that the chain interactions decrease with increasing tilt angle and secondly, that NNN tilt is more favourable than I or NN tilt at any tilt angle

$$dG = A d\pi \quad ; \quad K = -A \left(\frac{d\pi}{dA} \right) \quad \Rightarrow \quad dG = -K dA \quad (3.08)$$

where K is a measure of the elasticity of the head groups in the monolayer plane and A the cross sectional area of a head.

The change in A allowed with NN tilt is (see fig. 3.16 c):

$$\Delta A = \frac{\pi}{4} (d'^2 - d_0^2) = \frac{d_0^2 \pi}{16} \left(\frac{1}{\cos^2 t} - 1 \right) \quad (3.09)$$

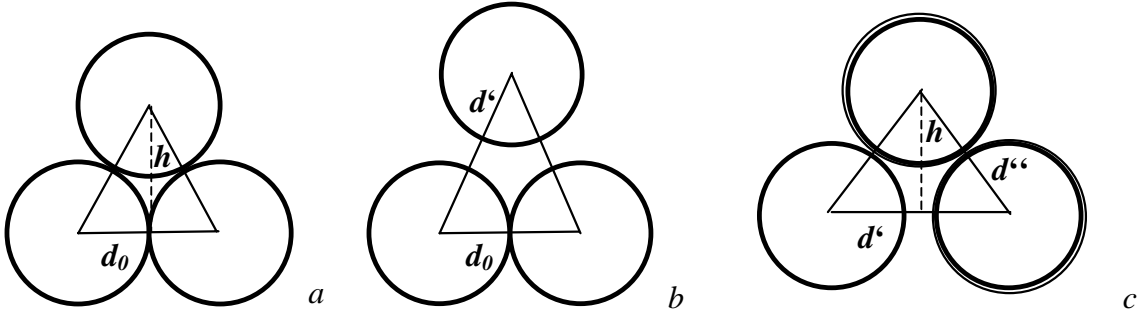


Fig.3.16: Illustration of the steric interactions between amphiphilic head groups (modelled as elastic spheres) in the upright (a), NNN (b) and NN state (c). With NN tilt the steric interactions between all neighbours decrease

In figure 3.17 $\Delta G \approx -K \Delta A N_L$ ($\Delta A/A$ is $< 10\%$ until $t=35^\circ$) is plotted versus the tilt angle t for an arbitrary $K = 0.33 \cdot 10^3$ mN/m. Below a certain tilt angle the energy for NN tilt due to NN chain and head interactions is lower than the energy of the NNN chain interactions. t at the phase transition point is the higher (and π the lower) the bigger K . A large value of K corresponds to a large size or a low compressibility of the head group. Interactions with subphase molecules may also contribute to the steric repulsion. According to this model changes in the head group interactions are reflected by a shift of the point of the NN-NNN phase transition with respect to that of the tilted-untitled transition (see fig. 3.17). In chapter 7.4 this is made use of in order to examine the effect of various solutes in the head group region of arachidic acid monolayers.

A similar concept was applied in [Sch99]. The repulsive head group interactions were described by a Lennard-Jones potential of the form

$$V(r) = \varepsilon_v \left[\left(\frac{\sigma_h}{r} \right)^{12} - 2 \left(\frac{\sigma_h}{r} \right)^6 + 1 \right] \quad (\text{for } r \leq \sigma_h, V(r) = 0 \text{ otherwise})$$

where σ_h corresponds to the head group radius and r is the head group distance. For $r < \sigma_h$ the head groups repel each other. The physical meaning of both approaches is the same. Not

regarded so far have been anisotropic head group interactions. The transition to the NN phase should be especially sensitive to the interactions along d'' (fig. 3.16 c), where the gap between the heads is smallest. Besides steric also bonding interactions may favour a certain head group arrangement and tilt direction.

Phases of intermediate tilt direction (I) often emerge between a NN and a NNN phase ([Kra00]; fig. 3.19). I phases are chiral because of the interactions between chiral molecules. The presence of an I phase with achiral fatty acids is therefore, at first glance, surprising. One may suggest that under certain conditions the chains distort to a chiral shape [Fis00]. Another possibility, however, which seems to me

more likely is, that chirality in fatty acid monolayers is caused by the restriction of the head group mobility. If the carboxyl head group is kept in a twisted position with respect to the chain backbone plane, the molecule becomes asymmetric (cf. fig. 3.07, left). This idea is supported by the fact that the I phase is only found at low temperature (fig. 3.19), where the mobility of molecular groups is expected to be reduced, and that the I region broadens toward lower temperatures.

Decreasing temperature may on the one hand increase the chirality of the molecules and on the other hand the chiral interactions between them.

The reason that the intermediate phase is frequently found between the NN and the NNN phase [Dur97, Kra00] may be as follows. At the NN/NNN transition the steric head group and the chain interactions compensate each other, so that neither the NN nor the NNN phase is preferred (fig. 3.14). Hence at this condition the chiral head interactions which are otherwise too weak can dominate and produce an I phase.

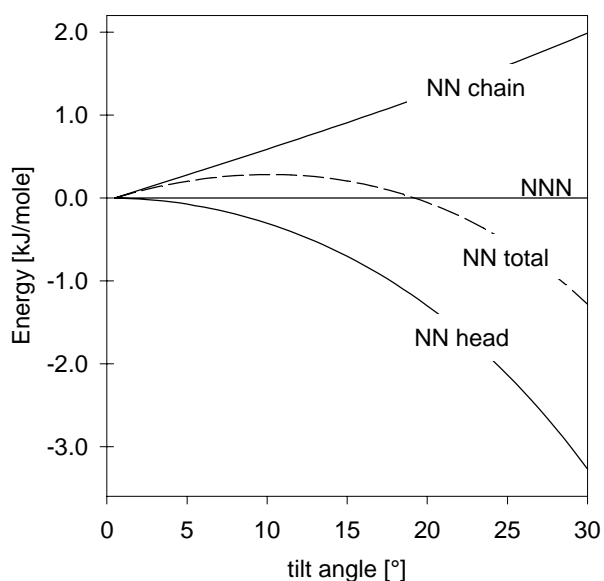


Fig.3.17: Calculated NN chain and head group interaction energy relative to that of NNN tilt (horizontal) as a function of the tilt angle (chain interaction calculated in fig. 3.15, steric energy of head groups calculated using eqs. 3.08, 3.09 and $K=0.33 \cdot 10^3$ mN/m). The interplay between chain and head group interactions leads to the transition between NN and NNN tilt at a certain tilt angle

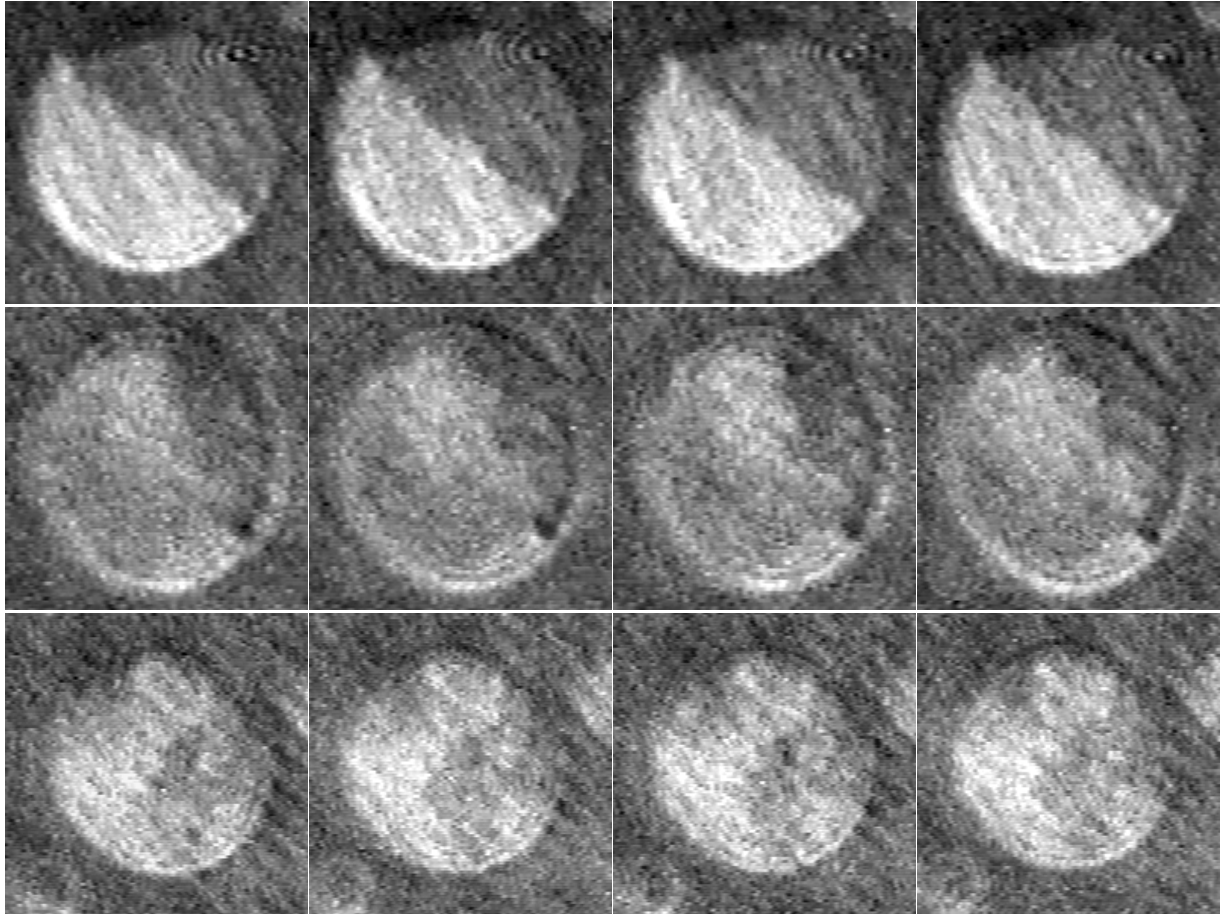


Fig.3.18: Illustration of tilt-bond decoupling and loss of long-range tilt orientational order at the NNN-U phase transition (U for untilted phase). Each BAM image shows an isolated circular LC domain of palmityl acetate embedded in a darker cholesterol matrix. Different shades of grey within a domain indicate different tilt directions. Flickering of the boundary between regions of different tilt direction with an amplitude of some tens of μm is observed between the NN-NNN and NNN-U phase transition (1st row; the 4 images of each row were taken within a quarter of a second). Near the NNN-U phase transition the boundary is destroyed and the range of uniform orientational order strongly reduced by a rapid change of tilt direction within patches of some tens of μm in size; the fluctuations are so quick that it looks as if it would 'boil' in the domain (unfortunately some images cannot convey the impression of a running video tape). However, a preferred distribution of the tilt directions is still displayed, which seems to be induced at the domain boundary (2nd row). At the phase transition vigorous rotation of the molecules and the absence of a preferred tilt direction is reflected by rapidly fluctuating patches all over the domain. The orientation of the molecules seems arbitrary and only subjected to thermal energy (3rd row). Beyond the transition, where the molecules are upright, the domain becomes uniformly bright. On leaving the transition region the original domain textures are recovered. This proves that the textures formed during domain growth correspond to equilibrium or lowest energy states. The tilt-bond decoupling, which may be expected for the NN-NNN transition from the foregoing discussion, is surprising for the NNN-U transition shown here. Perhaps the drastic increase in the mobility of the molecules is caused by cholesterol dissolved in the domains.

Size of an image: $150 \times 150 \mu\text{m}^2$ (The image contrast is poor because of the low tilt angle of the domain molecules and the low difference in reflectivity between domain and surrounding cholesterol film)

3.2.3 Classification of Monolayer Phases

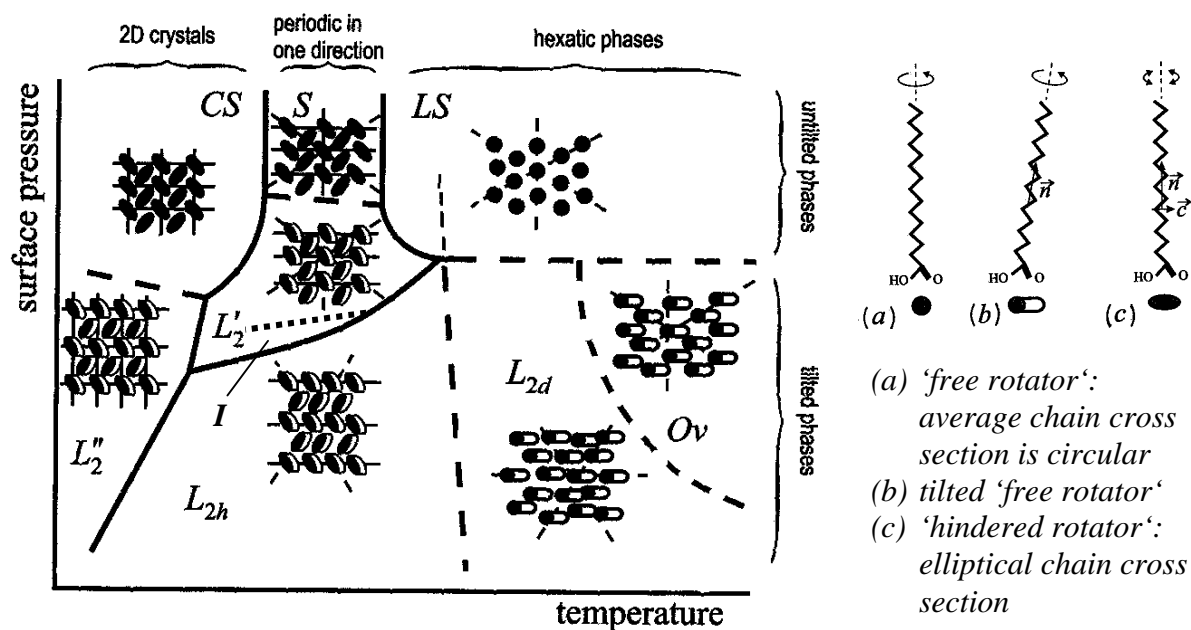


Fig.3.19: General phase diagram of long chain fatty acid monolayers. For different chain lengths the phases have to be shifted by 5-10°C to higher temperature per additional methylene group [Bib90, Kno90b, Kag99]. Solid phase boundaries correspond to discontinuous first order, hatched ones to continuous phase transitions. According to the own observations the L_{2d} - O_v transition is continuous (see 7.3), which deviates from the interpretations of other authors (cf. [Kag99]). The phases are designated according to the Harkins-Stenhagen notation. O_v denotes the phase discovered by Overbeck and Möbius [Ove93b]. The separation of the L_2 phase into herringbone ordered L_{2h} and disordered L_{2d} is proposed by Kaganer et al. [Kag99].

There is evidence that the dividing vertical hatched line marks a superordinate boundary between herringbone and hexagonally packed phases, at which the properties of fatty acids, such as their tendency of dissociation, change (see 7.3).

The different low order diffraction peaks in the S , L_2' and L_{2h} phases were found to have different peak widths indicating different PCLs for different lattice directions. This Kaganer et al. [Kag99] ascribed to the increase of the range of positional order in the herringbone ordered phases from short to quasi-long range in two steps. On entering the herringbone ordered smectic phases from the hexagonal phases first the lattice periodicity along one of the orthogonal (20) and (02) directions increases. For the S and L_2' phase it is the (20), for the L_{2h} phase the (02) direction, so that the positional order is increased perpendicular to the tilt direction. (fig. 3.20). In the second step the direction becomes ordered in both directions to give the CS and L_2'' phases. These phases are denoted as 2D crystals (although crystalline order does not exist in 2D as mentioned above), since the peak widths are below the resolution limit of the detector and therefore not distinguishable from those of true crystals. These widths correspond to PCLs of the order 1000 lattice spacings. In comparison the herringbone ordered smectic phases are all three dimensional crystals (fig. 3.02).

A thin region of a chiral phase with tilt direction between NN and NNN was found between the L_{2h} and L_2' phases in arachidic acid monolayers below 7°C [Dur97, Lau99].

The phases of fatty acid monolayers on pure water have been investigated most extensively. They can be classified with respect to the different order parameters like the smectic phases (table 3.2). The same types of ordering as in fatty acids have also been derived for other monolayer systems from isotherm and X-ray diffraction measurements [DeW98a, DeW98b, Dur95, Tee97, Bib91].

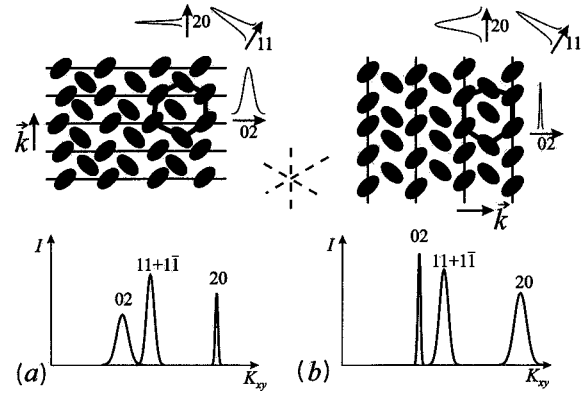


Fig.3.20: Experimental evidence for quasi-long range positional order in only one direction in Langmuir monolayers [Kag99]

Smectic	Monolayer	PO	BO	TO	T-B	HO
Sm A	LE	SR	SR	-	-	
Sm C		SR	SR	LR	-	
Hex B	LS	SR	QLR	-	-	SR
Sm I	L _{2d}	SR	QLR	LR	NN	SR
Sm F	O _v	SR	QLR	LR	NNN	SR
Sm L		SR	QLR	LR	I	SR
	S	SRQLR	(Q)LR	-	-	(Q)LR
	L ₂ '	SRQLR	(Q)LR	LR	NNN	(Q)LR
	L _{2h}	SRQLR	(Q)LR	LR	NN	(Q)LR
	I		(Q)LR	LR	I	(Q)LR
	CS	QLR	LR	-	-	(Q)LR
	L ₂ ''	QLR	LR	LR	NN	(Q)LR
Cry B		LR	LR	-	-	SR
Cry J		LR	LR	LR	NN	SR
Cry G		LR	LR	LR	NNN	SR
Cry M		LR	LR	LR	I	SR
Cry E		LR	LR	-	-	LR
Cry K		LR	LR	LR	NN	LR
Cry H		LR	LR	LR	NNN	LR
Cry N		LR	LR	LR	I	LR

Table 3.2: Classification of smectic and monolayer phases according to the order parameters PO: positional order, BO: bond orientational order, TO: tilt orientational order, T-B: tilt-bond coupling, HO: herringbone order. The range of order is abbreviated as in table 3.1, SRQLR means quasi-long range order in one lattice direction with short range order perpendicular to this direction. No value for TO means upright chains

4. Methods Used for the Investigation of Monolayer Systems

4.1 Filmbalance Technique

4.1.1 Instrument

To apply this technique the amphiphilic substance is spread (see 2.2) on the liquid surface of a filled trough. In most cases the liquid is water or an aqueous solution. But also other liquids are used, as for instance mercury. In order to manipulate the amphiphilic monolayer, it is placed between two barriers, at least one of which is movable. Leakage of substance out of the enclosed area through the barriers is prevented by keeping the liquid level above the bottom level of the barriers. Two types of film balances as viewed from above are shown in figure 4.01a,b. Figure 4.01a is a simple squared trough with two barriers, 4.01b is an example of a trough, the bottom of which is subdivided into two or more compartments. The compartments can be filled with different kinds of liquids and the monolayer be successively exposed to each of them by moving simultaneously both barriers with the same velocity around the surface. When a barrier moves over an edge that separates two compartments, a linkage between liquids of adjacent compartments is formed. To keep the time the linkage is maintained as short as possible and prevent the different liquids from mixing, edges with strongly dewetting surfaces are used, that cause the linkage to disrupt immediately, after the barrier has passed (for further details of this technique see [Sie97]).

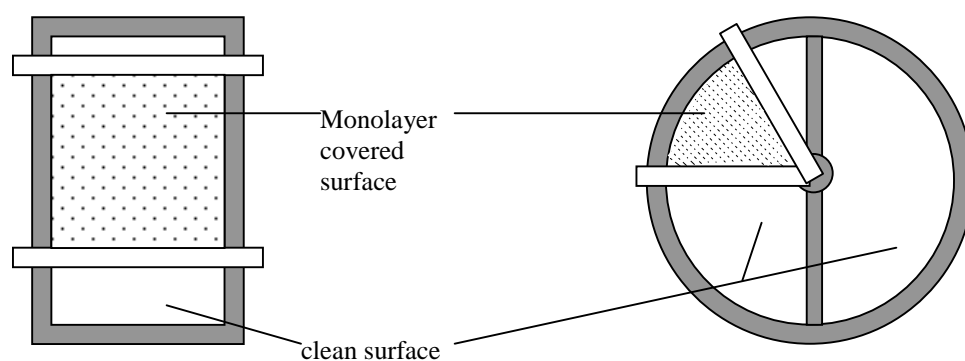


Fig.4.01: Simple trough (a), multicompartment trough with two compartments (b)

4.1.2 Physical Fundamentals

When amphiphiles adsorb at an initially clean air-water interface, either during spreading as an insoluble (Langmuir-) or from the subsolution as a soluble (Gibbs-) monolayer, the surface tension of the water surface τ_0 (72.75 mN/m, 20°C) reduces to a value τ (eq. II.1, app.). The change in surface tension $\tau_0 - \tau$ is commonly referred to as π and corresponds to a two dimensional surface pressure, that is exerted by the amphiphiles.

There are two methods in use in combination with a trough for recording continuous changes in π with time. They are based on the relation :

$$\tau = \left(\frac{\partial G}{\partial A} \right)_{\pi, T, n_i} = \left(\frac{dF}{dl} \right) \quad (4.01)$$

where F is the force exerted by the surface at an edge of length l

1. Langmuir float (fig. 4.02 a): Like a piston the floating barrier directly measures the lateral monolayer pressure π .
2. Wilhelmy plate (3.02 b): from the relation 3.1 the vertical force on a plate, that is wetted by the surface, due to the surface tension is the circumference of the wetted plate edge times $\cos\vartheta \tau$, where ϑ is the wetting angle. As this value is not known, plates are used that completely wet, i. e. where $\vartheta=0$, such as glass, filter paper or platinum. The buoyancy force and gravity of the plate are eliminated by measuring only the difference against the pure water surface.

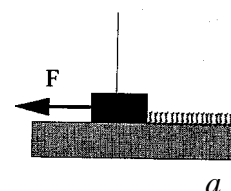
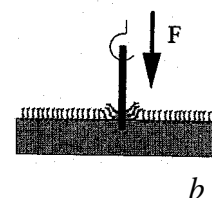


Fig. 4.02



The advantages of the floating barrier over the Wilhelmy system are, that one has not to take care of a wetting angle, the value of which can deviate from zero, if the plate is polluted and that a change of the water level due to evaporation during measurement does not play a role. Disadvantageous is the high delicateness of this method compared to the Wilhelmy method.

4.1.3 Measurement and Interpretation

By recording π against the monolayer area (usually expressed in terms of the mean area per spread molecule) information is obtained about thermodynamic properties and the characteristic phase behaviour of a substance. Monomolecular films were found to exhibit three states of different density that are comparable with the three dimensional gaseous, liquid and condensed state [Moo90, Mac90] (fig. 4.03).

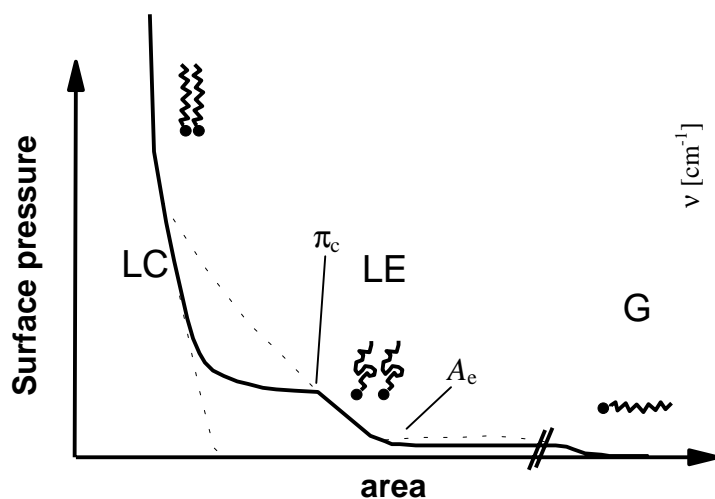


Fig.4.03: Sketch of a surface pressure-area isotherm with corresponding monolayer phases and molecular configurations

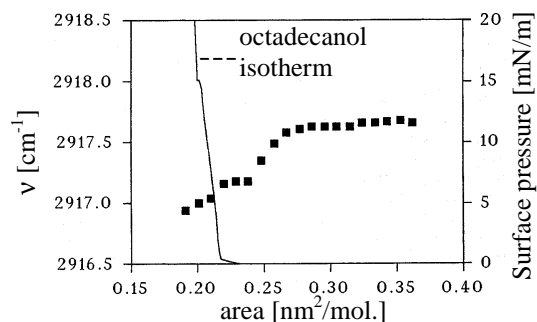


Fig.4.04: Illustration of sudden increase of the number of chain trans-conformations near the area where the isotherm pressure starts to rise. This is indicated by the decrease of the wave number of the asymmetric methylene stretching vibration [Ger94]

gaseous (G) phase: the equation of state: $\pi A = k T$, (4.02)

with A as area per molecule, is valid for very low density. π is on the order of a fraction of a mN/m. It may be considered as a 2D osmotic pressure and the barriers as semi-permeable membranes, that confine the molecules to a certain area but allow the solvent molecules to freely distribute. At very large A the hydrocarbon chains are assumed to lie flat on the surface (fig. 4.05 a) and to interact with the water surface due to a slightly positive spreading coefficient (cf. 2.2) of hydrocarbons on water. During the gas-expanded phase transition the hydrocarbon segments are ripped off the water surface [Kno90a] (fig. 4.05 b).

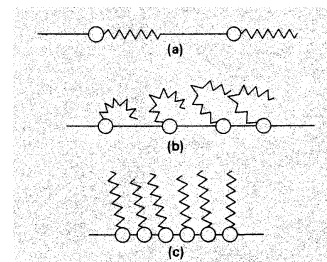


Fig.4.05 [Mac90]: Assumed configurations of long chain amphiphiles on a water surface in the gas (a), expanded (b) and condensed (c) monolayer state

expanded (LE) phase: the equation of state: $(\pi - \pi_0)(A - A_0) = k T$, (4.03)

corresponds to the 2D real gas van-der-Waals expression ($\pi_0 = f(A)$). The monolayer is in the pure LE state between the points A_e , which marks the end of the G-LE phase transition and the sharp inflection at π_c , where the transition from the expanded to a condensed phase occurs. The expanded state is characterised by a large conformational chain disorder (large number of gauche conformations) and high molecular mobility (fig. 4.05 b). As the chains try to minimise their surface energy and the contact area with air, the phase can be considered as

a thin hydrocarbon film. This is supported by the finding $\pi_0 \cong \tau_{w/a} - \tau_{w/hc} - \tau_{hc/a} =$ spreading coefficient (w: water, hc: hydrocarbon, a: air) [Mac90]. For an oil-water interface $\pi_0 \cong 0$.

condensed (LC) phase: the phase transition pressure π_c marks the onset of a flat plateau, which corresponds to the coexistence region of LC and LE phase. At the end of the plateau the pressure rises steeply. The relatively low compressibility of the condensed phase, defined as

$$C = -\frac{1}{A} \left(\frac{\partial A}{\partial \pi} \right)_T \quad (\text{order: } 10^{-3} \text{m/Nm}) \quad (4.04)$$

indicates straightened chains (fig. 4.05 c). Often the chains are tilted with respect to the surface normal and become upright at a certain pressure, that is indicated by a kink in the isotherm. Above this pressure the compressibility is much lower than in the tilted state. Head group and chain are compressed to the limiting area of 0.18-0.20 nm². The reduction in area in the tilted phase is essentially caused by a decrease in the tilt angle of the chains (eq. 3.06). The contribution of the increase in chain conformational order (cf. fig. 4.04) to the decrease in area is negligible [Sir97, Kag99]. This factor may determine the compressibility in the untilted state. The latent heat of the LE-LC transition may be determined by means of the Clausius-Clapeyron equation:

$$\frac{d\pi_c}{dT} = \frac{1}{T} \frac{H_{LE} - H_{LC}}{A_{LE} - A_{LC}} \quad (4.05)$$

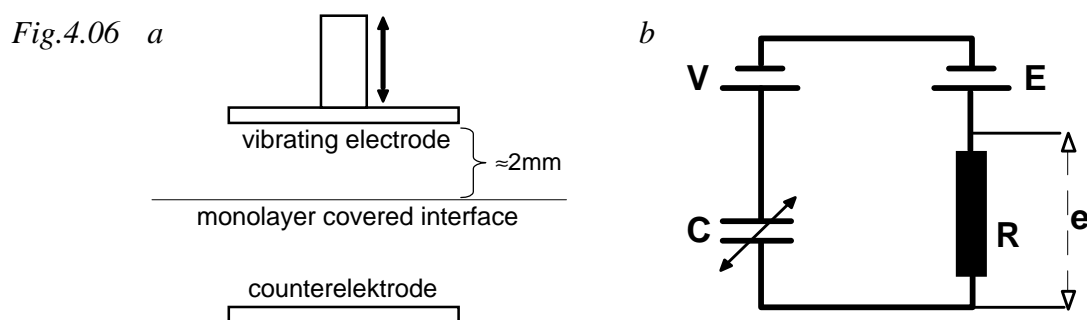
where H is the enthalpy, A_{LE} is the area of the expanded phase at π_c and A_{LC} is the area of the condensed phase at π_c , which is determined by extrapolating the isotherm section at lower pressures, i. e. if present of the tilted phase, to π_c . Far from the critical point, above which no condensed phase exists, π_c is usually found to vary linearly with temperature [Kel78]. In most cases π_c increases with increasing temperature.

4.2 Surface Potential Measurement

4.2.1 Instrument

For a long time isotherm and surface potential measurements were the most important methods for analysing monolayer systems. By both methods alterations in a monolayer are recorded as a function of the area, so that surface potential and pressure measurement may be combined in one experiment. There are two devices in use for measuring surface potentials: the ionising electrode and the vibrating plate method [Gai66]. The principle in each case is to detect the magnitude of the potential drop at the water interface to air or another medium, that

originates from the dipole moment contributions of the monolayer molecules normal to the interface. In this work the vibrating plate method was used. The schematic setup is shown in figure 4.06a. Figure 4.06b shows the simplified circuit by which the surface potential V is determined. A steady current is generated while the capacitor C is periodically vibrating at the interface. The current and the signal e become zero when the adjustable voltage E equals V [Gai66].



Schematic setup (a) and circuit (b) of the vibrating plate surface potential measuring device

4.2.2 Physical Fundamentals

A monolayer, in which the molecules have a dipole moment perpendicular to the interface, can be regarded as a charged capacitor. The potential V of the capacitor is

$$V = \frac{Q}{C} = \frac{\sigma l}{\epsilon \epsilon_0} = \frac{n p_z}{\epsilon \epsilon_0} = \frac{\mu}{\epsilon \epsilon_0} \quad (4.06)$$

where Q is the charge, C the capacity of the capacitor, l the distance of the charged planes, i. e. the length of the dipoles, σ the charge density of the planes

and ϵ the dielectric constant. For the meaning of the other symbols see under 2.3.3.

This V is measured as drop of the potential between vibrating and counterelectrode.

p_z of a molecule on water is only a fraction of the value of the isolated molecule [Gai66]. It is composed of the components of the molecule and a component ascribed to the reorientation of the subphase water molecules (see app. V) (fig. 4.07 a, the arrows point from negative to

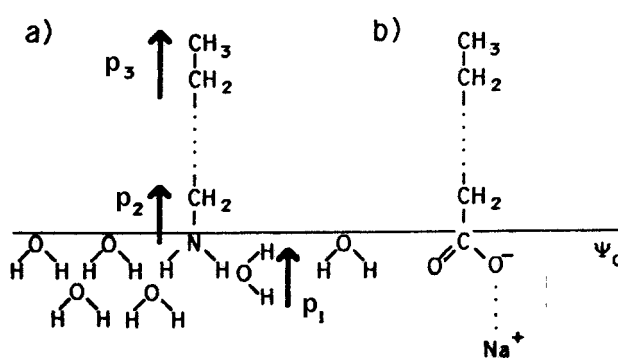


Fig.4.07: Molecular dipole moments and dipole moments perpendicular to the surface from interfacial water structuring (a) as well as a possible surface potential ψ_0 contribute to the surface potential ΔV

positive charge). A different structure of water at the interface compared with the bulk leads to the deviation of the value of ϵ from that of the bulk, which is near 80. It is much smaller, but the exact value is not known and it may be different for different monolayers. It is estimated to be 6-8 in the vicinity of monolayer head groups, 14-21 near zeolite surfaces and 36-46 near micelle interfaces [Vog88]. Hence the exact value of μ cannot be evaluated from equation 4.06. μ values in the literature are given for $\epsilon=1$ [Vog88, M6h89].

The potential is usually given as the difference ΔV between covered and uncovered water surface, as a definite value for the potential that is exhibited by a pure water surface has not been determined and it does not seem to be a constant neither for different measurements nor during one measurement [Gai66, Vog88] (obviously because there are several ways for water to structure at the interface). Positive ΔV , p_z and μ are defined by a dipole orientation with the positive charge pointing to the air.

If the *monolayer is charged*, ΔV includes the surface potential Ψ_0 (fig. 4.07 b):

$$\Delta V = \frac{\mu}{\epsilon \epsilon_0} + \Psi_0 \quad (4.07)$$

In the case of heterogeneous monolayers, μ and ΔV represent average values. Then ΔV is the sum of the potentials ΔV_i of the pure phases that are weighted by the relative areas x_i the phases occupy [Mil86a]:

$$\Delta V = \sum_i \Delta V_i x_i \quad \text{where} \quad x_i = \frac{A_i}{\sum_j A_j} \quad (4.08)$$

4.2.3 Measurement and Interpretation

Potential differences not only appear at the air-water interface, but also at the interfaces of the electrodes due to the adsorption of molecules from the environment. Water and possibly monolayer molecules adsorb onto the electrode in air, and in water solutes may adsorb. The potential only of the monolayer is obtained by keeping the potentials at the electro-de interfaces constant and measuring the difference against the pure water interface. In the own measurements it was waited a while before measurement was started, in order to allow the electrodes to get in equilibrium with the environment. Conditions were tried to keep constant by enclosing the trough and keeping the electrodes at a fixed position all the time. The accuracy of the measured surface potentials is 10 mV.

Figure 4.08 shows the π - A and π - ΔV isotherms of a monolayer of 1-palmitoyl-*rac*-glycerol at R.T.. It demonstrates the sensitivity of the surface potential to structural changes in the

monolayer, that are revealed in the π - A as well as in the π - ΔV curve by very similar features. In contrast to the π - A isotherm the heterogeneous gas-expanded coexistence region can clearly be recognised in the π - ΔV isotherm in the form of strong fluctuations. These are caused by patches of the different phases, that are floating in the monolayer. The patches are that large that they are resolved as different phases between the electrodes. At A_e the monolayer appears homogeneous due to a single expanded phase. On compression π and ΔV increase and also the density of the expanded phase. It is often found that μ of the expanded phase is independent of the molecular density. The onset of the condensed-expanded transition region is indicated by a break in the π - A curve. The change of μ in the condensed phase is little understood, since the contributions from water and head group are difficult to estimate and to separate.

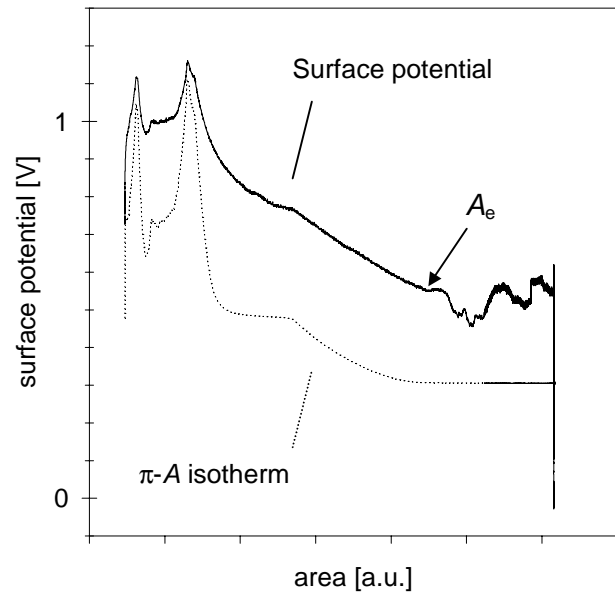


Fig.4.08: The features in the π - A isotherm and surface potential plot of 1-palmitoyl-rac-glycerol at R.T. are similar (meaning of A_e see p. 27)

4.3 Brewster-angle Microscopy

4.3.1 Instrument

The setup of a Brewster-angle microscope (BAM) is shown in figure 4.09. The measuring technique was developed separately by Hönig and Möbius [Hön91] and by Henon and Meunier [Hen91]. The BAM is usually designed for the investigation of thin films on surfaces of water or aqueous solutions at air. Instead of water also a transparent glass plate some millimetres thick may be used, the refractive index of which should not deviate too much from

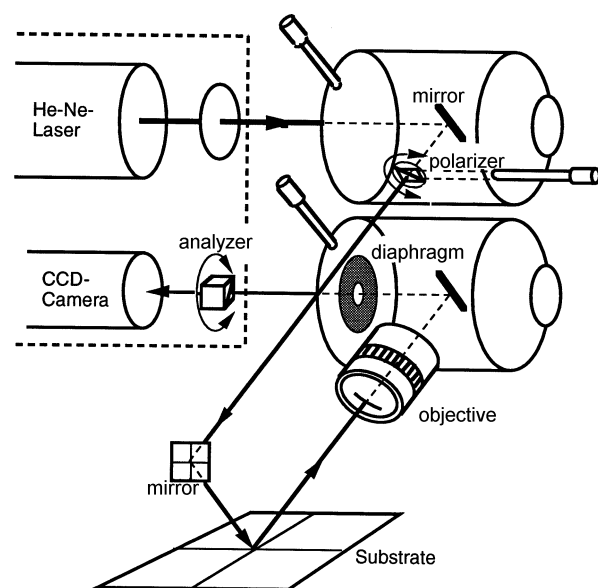


Fig.4.09: Setup of a Brewster-angle microscope

that of water, in order to work at convenient angles of incidence. The surface is imaged by detecting the laser light, which is polarised parallel to the plane of incidence and reflected at a certain angle from the surface, with a chip camera. An analyser may be switched into the beam path in order to reveal optical anisotropy of the film. If the trough is only a few millimetres deep, the rays reflected at the water surface and at the trough bottom have to be separated by placing an absorbing glass plate or a mirror at an angle on the bottom.

Since the surface is monitored at an angle, the original image is shortened in one direction, so that circular objects appear elliptic. The distortion is reversed either by means of an image processing software or by turning the camera chip by the same angle. As the laser beam, which has a diameter of nearly 1 mm, is reflected at an angle with respect to the surface, only a small stripe of the image in the direction perpendicular to the plane of incidence is focused by the lens and sharp. Usually BAM images are presented with the sharp stripe vertical. If a mirror is in the beam path of the reflected light (as in fig. 4.09) the recorded image is a mirror image of the object, which may have to be considered for the evaluation of chiral morphologies. As the objects on a liquid surface are usually in motion, local changes on the film like phase transitions can be followed by placing the substrate on an x-y table. With a separate electronic device it is possible to determine the reflectivity of the film as the summed intensity of the camera pixels.

Two BAMs were used in this work:

1. BAM 1 (He-Ne-laser, 10 mW, 633 nm (red), 4 μm resolution) with x-y table,
2. BAM 2 (frequency doubled 135 mW IR light, 532 nm (green), 2.5 μm resolution)

both from Nanofilm Technology GmbH, Göttingen.

The images were processed with the CompiC BIV software to select image size, improve contrast, change brightness and measure lengths, angles and areas.

4.3.2 Physical Fundamentals

1. Light reflection at an air-water interface

For visible light both air and water are isotropic and transparent (non-absorbing) media.

For infrared light of wavelengths above 1.85 μm [Ber89] air (free of carbon dioxide and water vapour) is transparent, but water is absorbing. The behaviour of a beam of light striking an interface between two media is shown in figure 4.10. The amplitudes of the electric fields of the reflected and refracted beams parallel and perpendicular to the plane of incidence are related to that of the incident beam by the Fresnel equations [Kle86]:

$$E_{r,p} = r_p E_{i,p} \quad ; \quad E_{r,s} = r_s E_{i,s} \quad \text{with} \quad r_p = \frac{\tan(\alpha - \beta)}{\tan(\alpha + \beta)} \quad ; \quad r_s = -\frac{\sin(\alpha - \beta)}{\sin(\alpha + \beta)} \quad (4.09)$$

$$E_{t,p} = t_p E_{i,p} \quad ; \quad E_{t,s} = t_s E_{i,s} \quad \text{with} \quad t_p = \frac{2 \sin \beta \cos \alpha}{\sin(\alpha + \beta) \cos(\alpha - \beta)} \quad ; \quad t_s = \frac{2 \sin \beta \cos \alpha}{\sin(\alpha + \beta)} \quad (4.10)$$

where r is the reflection coefficient and t the transmission coefficient; for the meaning of the other symbols and indices see figure 4.10.

The angles of reflection α and refraction β are related to the refractive indices n_1 and n_2 of the media by the Snellius law:

$$n_1 \sin \alpha = n_2 \sin \beta \quad (4.11)$$

The ratio of the refractive indices n_1/n_2 corresponds to the ratio of the velocities of light in the two media c_2/c_1 . For an absorbing medium n has to be replaced by the complex refractive index $n = n_{re} + ik$, where k is the absorption coefficient. On the way x through an absorbing medium the intensity I of light decays according to the Lambert-Beer law $I_t(x) = I_i \exp(-4\pi/\lambda kx)$ (λ : wavelength). The intensity is $I = |E|^2$. The reflectivity R for s or p polarisation is defined as $R_{s/p} = I_{r,s/p}/I_{i,s/p}$ or $R_{s/p} = |r_{s/p}|^2$.

According to a Maxwell equation for the components of E tangential to the interface it holds that $E_t = E_i + E_r$ for s and p polarisation (see fig. 4.10). This implies that the phase of the reflected wave can only be shifted by 0 or π with respect to the incident wave, otherwise the amplitude of the refracted wave would be modulated. An analysis of the Fresnel equations yields that the transmitted and incident beams are always in phase. With $n_2 > n_1$, there is a phase shift by π for both the s and p polarised reflected beam when $\alpha + \beta < 90^\circ$, and a phase shift by π only for the s polarised beam when $\alpha + \beta > 90^\circ$ [Hön94].

From equation 4.09 one obtains that r_p and hence the reflected intensity of p polarised light becomes zero for $\alpha + \beta = 90^\circ$, i. e. when the directions of reflected and refracted beam are

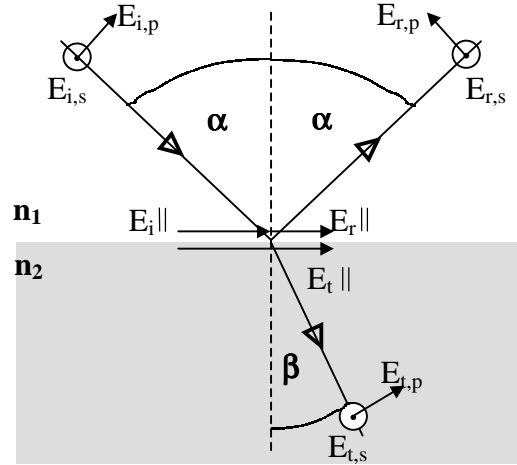


Fig.4.10: Reflection and refraction of light at a planar interface between two media of refractive indices n_1, n_2 .

α : angle of incidence and reflection;
 β : angle of refraction;

E : electric field, indices: i, r, t for incident, relected, transmitted, and s, p for perpendicular and parallel to the plane of incidence, resp.

The components of the electric field vectors parallel to the surface (\parallel) fulfil the condition: $E_i \parallel + E_r \parallel = E_t \parallel$ in the directions parallel and perpendicular to the plane of incidence.

perpendicular to each other. The corresponding angle of incidence is called Brewster-angle α_B . It can be determined from the relation $\tan\alpha_B=n_2/n_1$ using the Snellius law (eq. 4.11) and $\sin\beta=\cos(90^\circ-\beta)$. Taking $n_1=1$ for air and $n_2=1.33$ for water and visible light, α_B is 53.1° . In contrast to the p the s polarised component never vanishes.

2. Light reflection at a film covered interface

A surface illuminated with p polarised light under the Brewster angle appears dark. When now a film is placed at the interface, the Brewster-angles at both interfaces of the film will not coincide with that of the pure surface and reflection occurs (fig. 4.11). Hence the film covered surface appears bright. A method for determining the reflected intensity of a film of certain thickness is

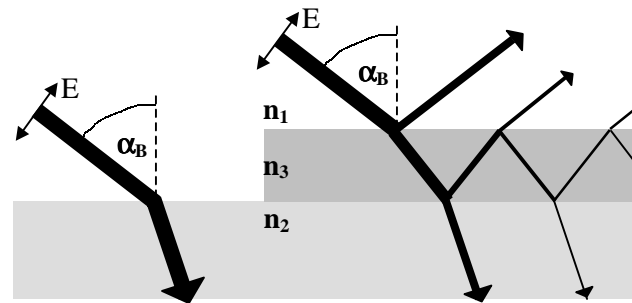


Fig.4.11: Principle of Brewster-angle microscopy. In contrast to the bare surface a film covered surface reflects light incident under the Brewster-angle

to assume repeated reflection within the film and to sum up the intensities of the single rays that are reflected or transmitted by the film regarding phase shifts. Convenient solutions are obtained by this way for optically isotropic films and for optically anisotropic films, where the refractive index in the film (x-y) plane is different from that perpendicular to the interface (z direction) [Hön94]. Such a case is represented by a monomolecular film with untilted elongated molecules.

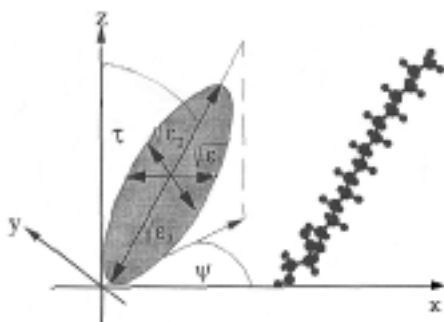


Fig.4.12: The figure illustrates the interpretation of macroscopic optical properties from the molecular level. The change of the refractive index with direction is ascribed to the anisotropy of the polarisability of a molecule (the polarisability is related to the permittivity ϵ , and $\sqrt{\epsilon}=n$).

For more complicated systems such as multilayers and anisotropic films with different refractive indices in x, y and z direction (including tilted molecules) the application of the Berremann formalism is more convenient [Hön94]. Important solutions for monolayers of molecules with long aliphatic chains are:

a) tilted, hexagonally packed ($\epsilon_1 \approx \epsilon_2 \neq \epsilon_3$) chains with average circular cross section

$$r_p = \frac{ih\pi}{\lambda\sqrt{1+n_2^2}} \left(\frac{n_2^2 / (\epsilon_3 - \epsilon_1) + \epsilon_1 \cos^2 \Psi \sin^2 t}{\epsilon_1 / (\epsilon_3 - \epsilon_1) + \cos^2 t} + \epsilon_1 - 1 - n_2^2 \right) \quad (4.12a)$$

$$r_s = \frac{ih\pi}{\lambda(1+n_2^2)} \left(\frac{\epsilon_1 \sin 2\Psi \sin^2 t - n_2 \sin \Psi \sin 2t}{\epsilon_1 / (\epsilon_3 - \epsilon_1) + \cos^2 t} \right) \quad (4.12b)$$

b) untilted chains with elliptic cross section ($\epsilon_1 \neq \epsilon_2 \neq \epsilon_3$)

$$r_p = \frac{ih\pi}{\lambda\sqrt{1+n_2^2}} (\epsilon_2 - 1 - n_2^2 + n_2^2 / \epsilon_3 + (\epsilon_1 - \epsilon_2) \cos^2 \Psi) \quad (4.13a)$$

$$r_s = \frac{ih\pi}{\lambda(1+n_2^2)} (\epsilon_1 - \epsilon_2) \sin 2\Psi \quad (4.13b)$$

The reflectivities apply for $n_1=1$ (air) and for a p polarised beam incident at the Brewster-angle; h : film thickness, λ : wavelength, n_2 : subphase refractive index, ϵ_i : film permittivities, for the definition of Ψ and t (or τ) see fig. 4.12, the x-z plane is the plane of incidence and the light is reflected into the positive x-z direction [Hön94].

One can see that s polarised light appears only, when the molecules are tilted and simultaneously rotated out of the plane of incidence in case (a) ($r_s=0$ for $t=0$ and $\Psi=0^\circ/180^\circ$) and when the molecules are oriented asymmetrically with respect to the plane of incidence in case (b) ($r_s=0$ for $\Psi=0^\circ, 90^\circ, 180^\circ, 270^\circ$). These conditions can be understood by imagining the molecules as vibrating dipoles that are excited by the incident p polarised light and emitting light polarised along the three polarisation directions (cf. fig. 4.12). Thus an s component can only be generated by a p component, if the molecule is oriented such that at least one polarisation direction is not parallel or perpendicular to the direction of p polarisation.

Variations of the molecular orientations Ψ and t within a monolayer are revealed by means of an analyser (A in fig. 4.13), the transmitted intensity depending on the relative portions of s and p polarised light:

$$I = |E_p \cos \varphi + E_s \sin \varphi|^2 \quad (4.14)$$

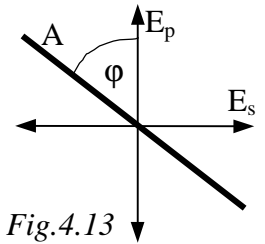


Fig.4.13

4.3.3 Measurement and Interpretation

Before film spreading, the Brewster angle, which particularly may vary with subphase composition, has to be adjusted by finding the minimum in reflectivity for p polarised light. At this angle the contrast of brightness between film and substrate is maximal, so that films even a molecular diameter thick are clearly recognised. Equations 4.12 and 4.13, valid for films of a thickness negligible compared to the wave length [Hön94], yield proportionality between reflectivity and the square of the film thickness for a certain wavelength. Besides variations in film height also variations in film density (as for G, LE, LC phase) lead to differences in reflectivity. Without analyser even variations in Ψ (and theoretically also in t) are revealed by a slight contrast. Anisotropy effects, however, can be distinguished from inhomogeneities in thickness or density by simply rotating the analyser. In the latter case the reflected intensity is varying uniformly over the whole image with changing analyser angle while in the first case the contrast between regions of different Ψ is varying.

The domains in figure 3.18 appear homogeneously bright, when no analyser is used, indicating uniform thickness. Therefore, as the height is related to the tilt angle by $h=L \cdot \cos t$ (L : length of a molecule, height at $t=0$), the fluctuations are caused by changes in Ψ rather than in t .

There have been attempts to use BAM as a quantitative tool for determining the parameters h , Ψ , t , ϵ_i on the basis of recorded intensities [Hos93, Tsa95, deM98]. The main problem arises from the noise in the images due to diffraction rings or poor focus, from the inhomogeneous intensity distribution of the laser beam and from the large number of unknown parameters. The accuracy of the results is therefore limited and the scatter usually quite large. Furthermore one has to take into account the response of the CCD camera, which is not a linear function of the reflected intensity [deM98]. The most reliable method for deriving molecular

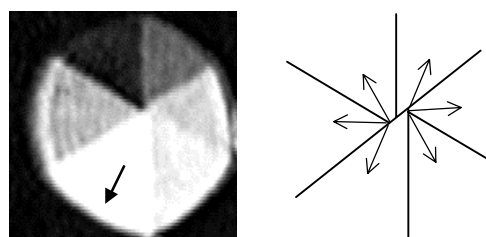


Fig.4.14: One of three different domain types occurring in the two phase coexistence region of arachidic acid monolayers on aqueous subphase of pH 11.7-12.0 at 25°C (size: $115 \times 115 \mu\text{m}^2$) (left).

A frequently observed feature of such domain types is that the wedges do not meet in a single point. In this case the arrangement of the wedge ends seems to correspond to that shown on the right.

This intersection region is also called defect core, because it is defined by the intersection of the, so called, defect lines, the boundary lines between regions of different tilt direction. The split of a defect point into two or more intersection points and the concomitant reduction of the number of different tilt directions starting from one point has probably energetic reasons (see 6.2.2) (right).

The arrows indicate the tilt direction (shown for 1 segment only on the left)

orientations Ψ within LC domains from the observed intensity pattern, appears to be to assume Ψ and to compare the calculated pattern with the imaged one [deM98, Ove94].

The kind of LC domain shown in figure 4.14 is common to many substances and is exhibited for instance by fatty acids and alkyl or glycerol esters.

The domain observed between crossed polarisers is subdivided into six wedge shaped segments of nearly equal size indicating six different tilt directions. The tilt direction is uniform within a segment and changes abruptly at the segment boundaries. One might expect that in domains of this type the tilt direction is the same in all segments. Furthermore the tilt direction should be symmetrical with respect to the segment and the domain boundaries, at least for achiral molecules. Put together, one of the patterns in figure 4.15 should be adopted.

Indeed, only the patterns *a-d* have been observed so far [Ove94, Fis96, Wei98a, b, 6.3.4].

a and *b* can be distinguished from *c* and *d* rather simply by inspecting the domains between parallel polarisers. For domains oriented as in figure 4.15 with the polarisation plane lying vertical, in case *a* and *b*, the two segments in the middle with tilt directions in the polarisation plane appear as the brightest among all six; in case *c* and *d* the two segments are the darkest of all (see also [Wei97a]).

a can be distinguished from *b*, or *c* from *d* by choosing a non-zero analyser angle. This is demonstrated by means of figure 4.16:

The reflectivity is plotted versus Ψ according to eqs. 4.12a,b for some analyser angles. The domain of figure 4.14 is shown below rotated

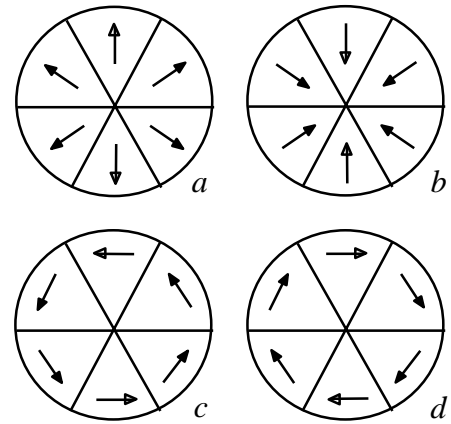


Fig.4.15: Expected tilt patterns (tilt along the arrows) in (achiral) domains with 6 wedge shaped segments and uniform tilt direction within the segments

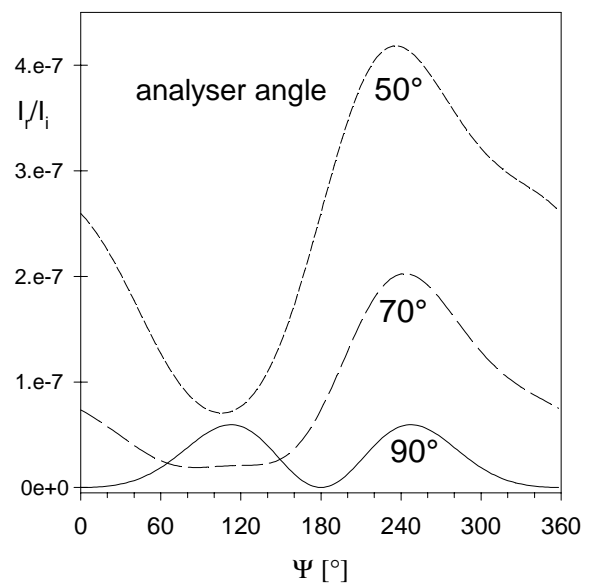
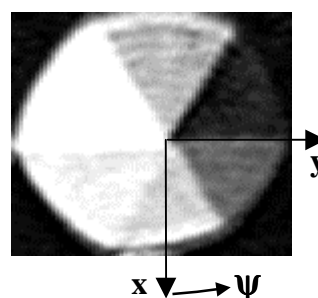


Fig.4.16:

curve parameters:

$h=2.5 \text{ nm}$
 $t=20^\circ$
 $n_2=1.33$
 $\lambda=532 \text{ nm}$
 $\epsilon_1=2.0$
 $\epsilon_3=2.1$



by 90° , which corresponds to the true reflected image. Figure 4.14 was recorded with BAM 2, where the reflected image is not mirrored but twisted by 90° . The position of ψ at the image is given for the case of figure 4.15a (ψ are multiples of 60°) and according to the definition in fig. 4.12 and the legend of eqs. 4.12 and 4.13. The reflectivity in the domain is minimal for $\psi=120^\circ$ and maximal for 240° which is in agreement with the calculations for the experimental analyser angle of $\phi=60^\circ$. Hence in the domain shown the molecules are tilted towards the domain boundary. However, because of the relatively broad minima or maxima, deviations from the symmetrical tilt directions in a segment by several degrees cannot be not resolved.

4.4 Infrared Reflection Absorption Spectroscopy

4.4.1 Instrument

4.4.1.1 Setup

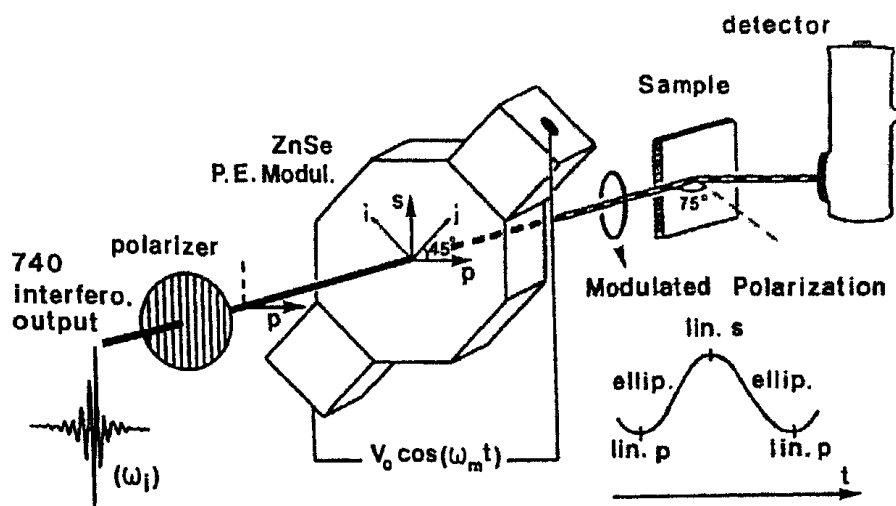


Fig.4.17: Optical setup of the FT infrared spectrometer working with polarisation modulation (PM) [Buf91, Dah98]. After leaving the source the polychromatic infrared light passes a Michelson interferometer. There the intensity of the light is modulated due to phase shifting and interference caused by the movement of the interferometer mirror. After the modulated beam has been p polarised it passes a photoelastic modulator (PEM). The PEM changes the polarisation of the light periodically with the frequency ω_m between linear p polarisation and an extreme elliptical or even s polarisation when the dephasing ϕ_0 is maximal, i.e. $(2n+1)\pi$, by applying a periodic voltage $V=V_0\cos\omega_m t$. The voltage V_0 at which maximum dephasing is achieved depends on the wavelength. Then the beam is focussed onto the water surface with an incident angle of 75° . A portion is reflected from the water surface and focused with a ZnSe lens onto a liquid-nitrogen-cooled MCT detector. The detected intensity is [Buf91]:

$$I = aI_0(\omega_i)\{R_p + R_s\} - 2aI_0(\omega_i)\{R_p - R_s\}J_2(\phi_0)\cos(2\omega_m t) \quad (4.15)$$

where a is a constant accounting for the transmittance of the optical setup, $I_0(\omega_i)$ the light intensity after the polariser, modulated with the frequency ω_i by the interferometer, R_s and R_p are the reflectivities of s and p polarised light and $J_2(\phi_0)$ the second-order Bessel function with ϕ_0 as the maximum dephasing introduced by the PEM.

4.4.1.2 Signal Processing

The R_p+R_s term of equation 4.15, which includes the intensity modulation, and the R_p-R_s term, which includes intensity as well as polarisation modulation, are separated by electronic filtering (using setup of ref. Dah98). At the output the two interferograms (R_p+R_s) and $J_2(\phi_0) \cdot (R_p-R_s)$ (fig. 4.18 a, b) are recorded simultaneously by multiplexing. After collection of 300 scans at 4 cm^{-1} resolution, the interferograms were Fourier transformed (fig. 4.18 c) and isotropic absorptions eliminated by setting the ratio

$$S = c J_2(\phi_0) \frac{R_p - R_s}{R_p + R_s} \quad (4.16)$$

(the constant c arises from the independent electronic processing of the two parts) (fig. 4.18

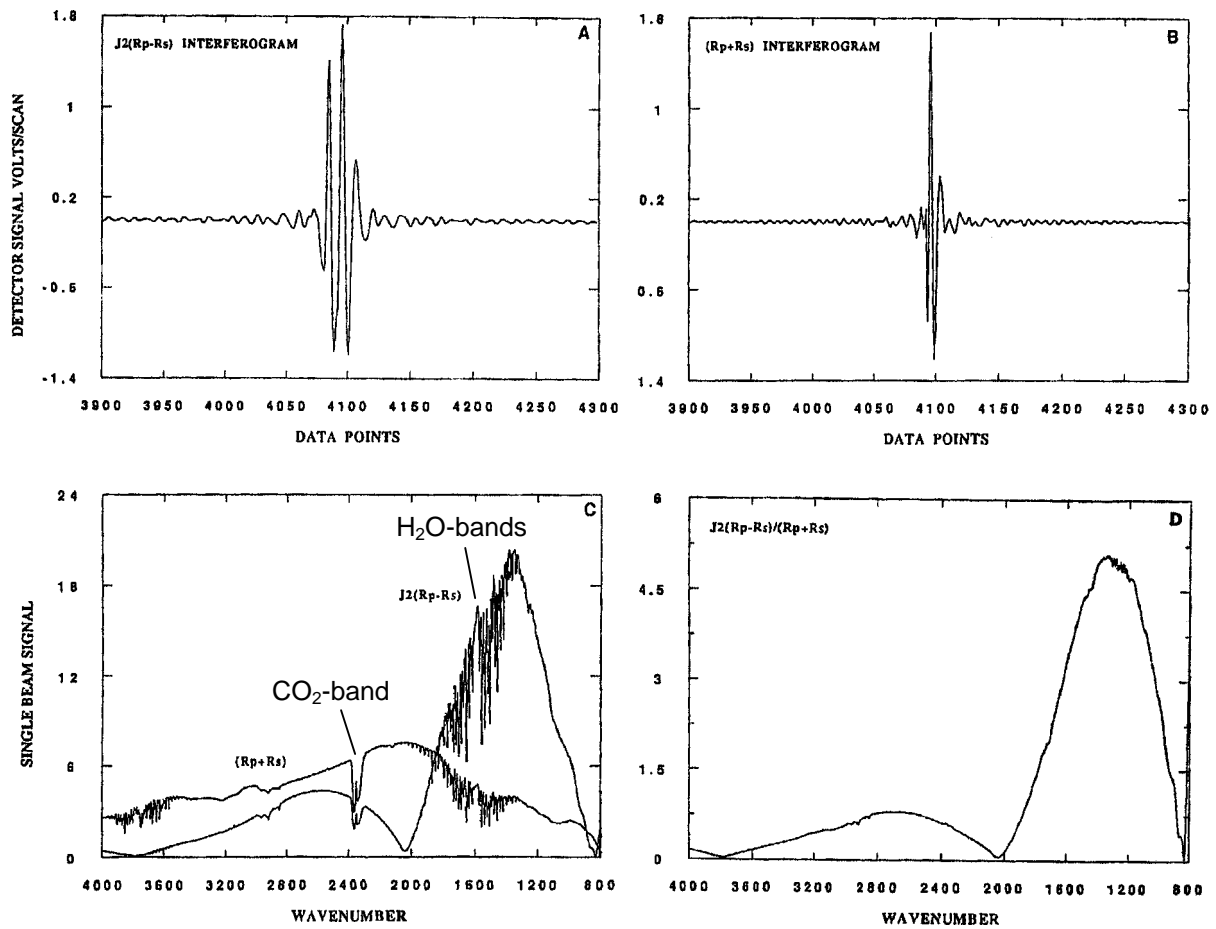


Fig.4.18: Interferograms $J_2(Rp-Rs)$ (a), $(Rp+Rs)$ (b); in the Fourier transforms of (a) and (b) one can see the CO_2 and H_2O absorptions (c). The shape of the ratio $J_2(Rp-Rs)/(Rp+Rs) \propto S$ is mainly determined by $J_2(\phi_0)$; CO_2 and H_2O bands are eliminated (d)

d). The signal S is optimal at maximum J_2 at maximum dephasing π . Maximum dephasing was set to 1650 cm^{-1} , i. e. a frequency within the region of interest. The intensity of the spectra is given as the normalised signal difference $\Delta S/S$ between covered (S_c) and bare water surface (S)

$$\frac{\Delta S}{S} = \frac{S_c - S}{S} \quad (4.17)$$

In the used setup the trough was movable perpendicular to the plane of incidence, so that film covered and bare water surface could be easily exchanged without the need to calibrate again because of different surface levels.

4.4.2 Physical Fundamentals

Infrared (IR) spectroscopy performed as transmission spectroscopy or as reflection-absorption spectroscopy (IRRAS or RAIRS [Hai87, Han91], ATR [Har67]) on various substrates is an analytical tool that provides information on the constitution and conformation of molecules and the type of substance. IR light interacts with a sample by exciting vibrational modes of the molecules, and absorption occurs at those frequencies in the IR spectrum, that correspond to the oscillating frequencies of the excited modes. The number of vibrational modes of a molecule is $3N-5$ for linear and $3N-6$ for non-linear molecules, where N is the number of atoms in the molecule (the relations are obtained by subtracting the 2 or 3 rotational plus the 3 translational degrees of freedom of the centre of gravity of the atom assembly from the $3N$ atomic degrees of freedom). There are two types of molecular vibrations: stretching (symbolised by ν) and bending (δ) vibrations. Stretching is involved with a change of bond distance and bending with a change of bond angles. Figure 4.19 shows the three most important vibrational modes at highest frequencies for non-linear triatomic groups or molecules, such as water, carboxylate or a methylene group. Modes are only excited by IR radiation, if a dipole moment is present and this dipole moment changes periodically during vibration. The intensity I_a absorbed by a mode is proportional to the intensity of the incident radiation, to the density of the excited groups and to the magnitude of the dipole moment change of the excited vibration. Furthermore it depends on the orientation of the transition dipole moment

$$I_a \propto \left(\frac{dp}{dR} \right)^2 \cos^2 \alpha \quad (4.18)$$

Where p is the dipole moment, R is the direction of dipole moment change and α is the angle between the dipole moment and the vector of the exciting electric field.

Equation 4.18 shows that for molecules oriented at an interface I_a depends on the state of polarisation of the light and the orientation of excited molecular groups with respect to the plane of incidence [Huo99].

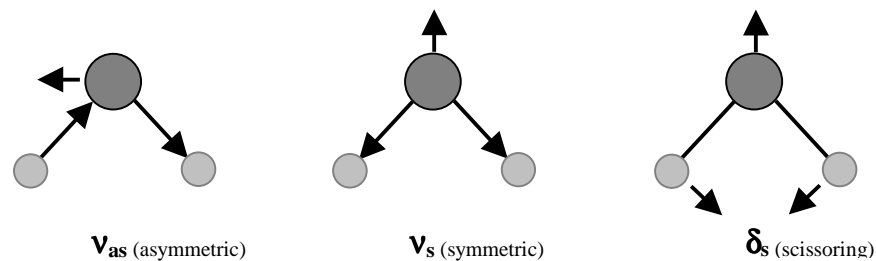


Fig.4.19: Basic vibrational modes of non-linear triatomic groups

4.4.3 Measurement and Interpretation

The main difficulties in the IR spectrometric investigation of monolayers on water are the low reflectivity of the water surface, which leads to a poor signal-to-noise ratio, and the superposition of the intense bands of water vapour and atmospheric carbon dioxide. The first problem is inherent to the system. The most elegant method to overcome the second problem is the use of PM-IRRAS. There the reflectivity is independent of isotropic absorption from gas or bulk water, which, however, is also the disadvantage of the method, since signals of isotropic structures at interfaces are compensated for and quantification becomes difficult.

A reflection-absorption spectrum can be interpreted similarly to a transmission spectrum, slight deviations in band frequencies can result from different dispersivities of bulk and film refractive indices [Ger94]. In the case of oriented molecules at the interface, with reflection-absorption spectroscopy the orientation of molecular groups can be derived from the reflected intensity [Sak98].

4.5 X-ray Diffraction at Grazing Incidence (GID)

4.5.1 Instrument

In order to detect reasonable intensities for the diffraction on monolayers, the energy of the incident X-ray beam has to be particularly large. This energy is provided by a synchrotron (the measurements were performed in HASY-LAB at DESY in Hamburg). A polychromatic X-ray beam, generated by the acceleration of electrons, is made monochromatic ($\lambda \approx 1.4 \text{ \AA}$) by a monochromator crystal and deflected onto the sample at an angle as low as 0.1° (fig. 4.20 a). The incident beam strikes the sample surface on an area of $50\text{mm} \times 5\text{mm}$ (footprint, fig. 4.20 b), which is determined by the input slit S_2 . The thermostated trough is enclosed in an air tight housing. Before starting measurement the housing is filled with helium gas. The time needed for complete gas exchange is about 30 min (which one has to take into account, when working with alkaline solutions without buffer, since the pH is reduced by atmospheric carbon dioxide). A glass block is immersed into the subphase below the footprint area and covered by only a few fractions of millimetres of solution in order to produce a smooth surface. Most of the intensity is reflected from the surface ($2\theta=0$, see 4.20 b), a part of it diffracted by the monolayer. The diffracted intensity is detected

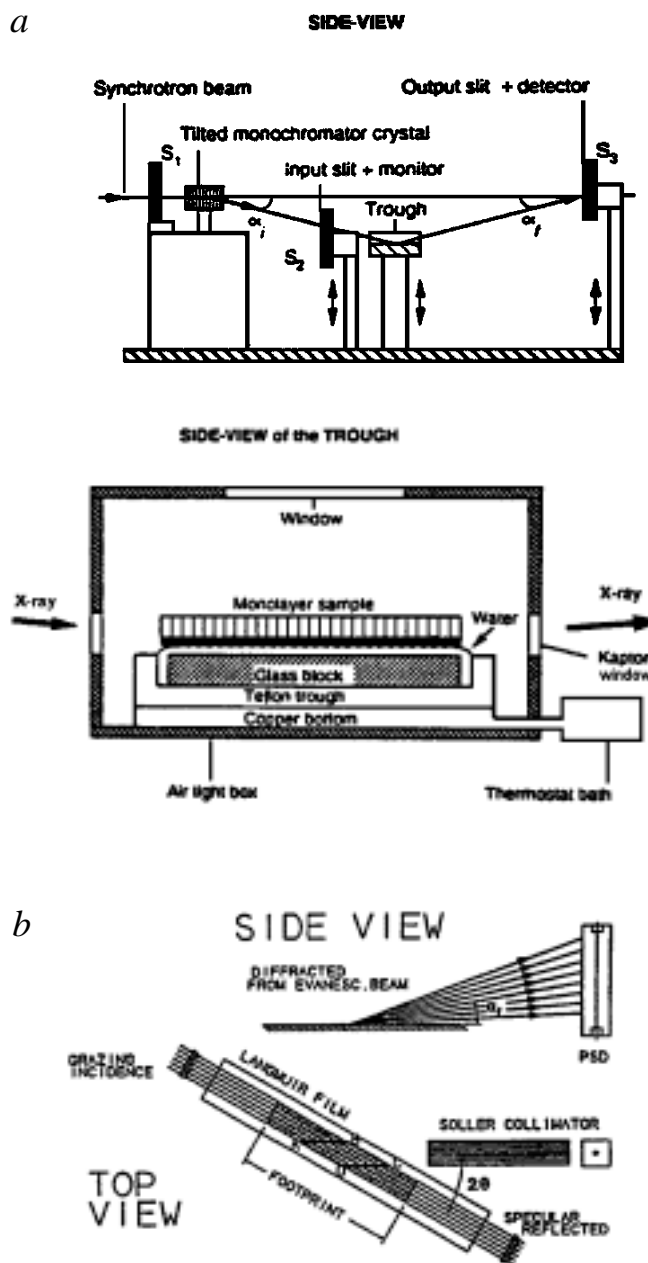


Fig.4.20: Sketch of apparatus setup with probe position and beam path for diffraction under grazing incidence (a). Geometric relation between incident and detected intensity in x-y-(top view) and z-direction (side view) (b)

by a position sensitive detector (PSD) simultaneously in x-y (monolayer plane) and z-direction. The z-direction is resolved by 220 channels within 13°. The resolution of 2θ in the x-y plane is limited to 0.9° and determined by a Soller collimator (S3 in *a*), which consists of 100 mm long parallel sheets of steel with a distance of 0.1 mm between two of such sheets (*b*).

4.5.2 Physical Fundamentals

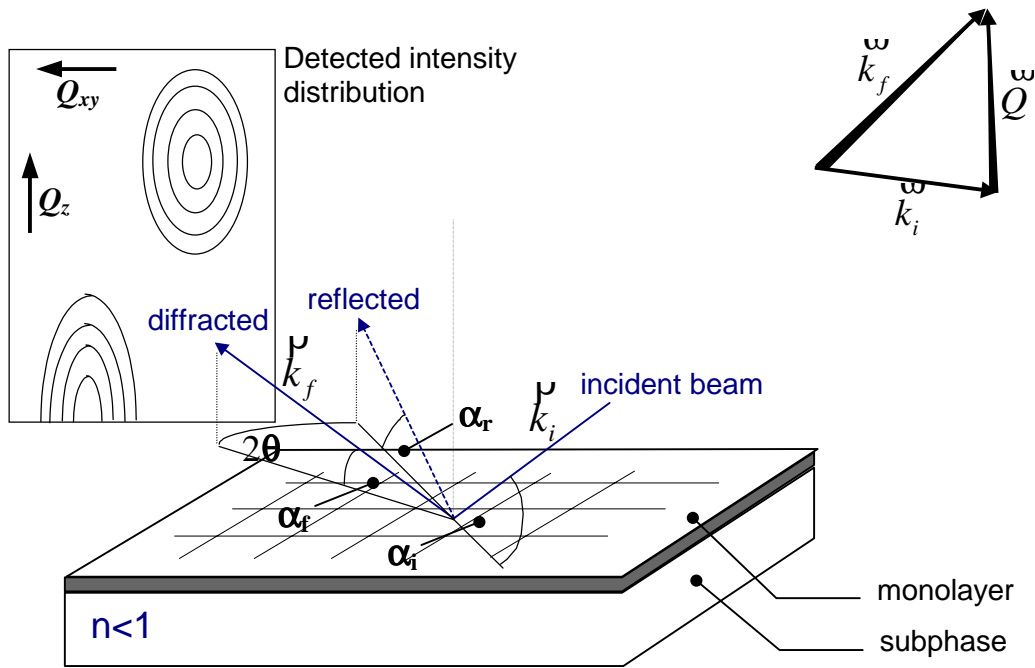


Fig.4.21: Diffraction geometry

For X-rays the refractive index n of a medium is given as:

$$n = 1 - \frac{e^2 \rho_{el}}{m_e c^2 k^2} = 1 - \delta \quad (4.19)$$

where $k=2\pi/\lambda$ is the wave vector and ρ_{el} the electron density of the medium; δ is in the order of 10^{-5} [Mel97a]. Hence for X-rays air is optically more dense than water and a beam incident from air can be totally reflected from a water surface. The critical angle of incidence for total reflection α_c is calculated from the Snellius law by setting the angle of the refracted beam zero (here the angles are measured with respect to surface, not the normal as in fig. 4.10):

$$\cos \alpha_c = n = 1 - \delta \quad (4.20)$$

For small α_c $\cos\alpha_c \approx 1-\alpha_c^2/2$ and therefore $\alpha_c=\sqrt{2\delta}$. For reflection on water with $\lambda=1.4\text{\AA}$, $\alpha_c=0.14^\circ$ [Böh93].

At the interface the electric fields of incident and reflected beam superimpose and cause the electrons of the molecules in this region to oscillate and to scatter X-rays in all directions. If the molecules are periodically arranged, the scattered X-rays interfere constructively only for definite directions, the directions of diffraction. The diffracted intensity, therefore, increases with increasing reflected intensity. For $\alpha_i \gg \alpha_c$ most of the intensity is transmitted through the subphase, and background noise due to the scattering of water molecules is large. The reflectivity increases with decreasing α_i and is maximal ($E_r=E_i$) for $\alpha_i = \alpha_c$. At this condition an evanescent field is generated at the reflection point, which decays exponentially into the water. The scattering and background noise caused by this field increases with increasing penetration depth. For $\alpha_i < \alpha_c$ phase shift occurs between incident and reflected wave and the reflected intensity decreases with decreasing α_i . The penetration of the electric field into the subphase, however, is strongly reduced.

Hence in practice α_i is chosen somewhat smaller than α_c ($\alpha_i = 0.85 \alpha_c$), in order to find the most favourable ratio between diffracted intensity and background noise [Als89].

By means of X-ray diffraction on monolayers one obtains the lattice parameters of the two-dimensional elementary cell a_1 , a_2 and γ (fig. 4.22 a), the molecular orientation by Ψ and t and the position correlation lengths in x-y (eq. 3.03) and z-direction (eq. 4.23).

From the scattering geometry (fig. 4.21) the lattice spacings d_{hk} (fig. 4.22 b) and thus the lattice parameters a_1 , a_2 and γ can be determined:

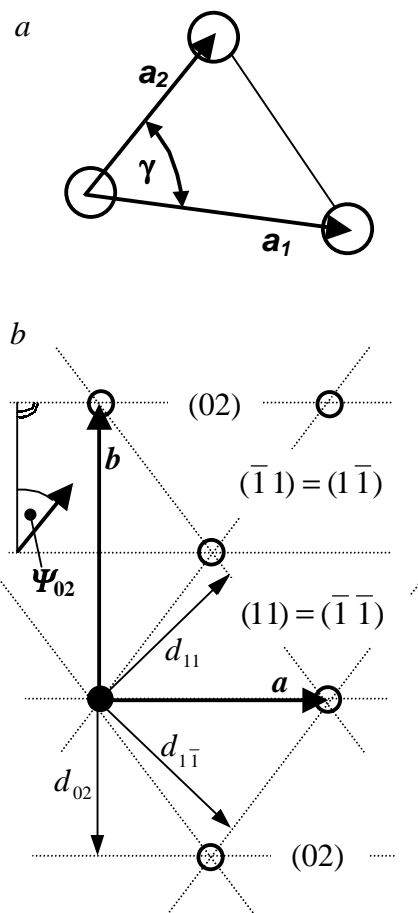


Fig.4.22: Smallest lattice unit of densely packed aliphatic chains (a). Description of the lattice by the orthogonal parameters a and b . The (02) , (11) and (-11) lattice lines and the corresponding lattice distances d_{hk} are indicated. Ψ_{hk} is measured with respect to the normal of the lattice line (hk) as shown for Ψ_{02} (the arrow indicates the tilt direction) (b)

$$\vec{Q} = \vec{k}_f - \vec{k}_i = \vec{Q}_{xy} + \vec{Q}_z \quad (4.21 \text{ a})$$

$$Q_{xy} = k \sqrt{\cos^2 \alpha_i + \cos^2 \alpha_f - 2 \cos \alpha_i \cos \alpha_f \cos 2\theta} \quad (b)$$

$$Q_{xy} \approx 2k \sin \theta \quad (\text{Bragg relation}) \quad (c)$$

$$Q_{xy}^{hk} = \frac{2\pi}{d_{hk}} \quad (d)$$

$$Q_z = k(\sin \alpha_i + \sin \alpha_f) \quad (e)$$

If the scattering centres would be confined to the lattice points of a two dimensional lattice, the diffracted intensity would appear as vertical stripes along Q_z (imaginable as a consequence of Bragg reflection at the $(hk0)$ planes). The finite electron density of the molecules, however, gives rise to an intensity within a defined range of Q_z . The peak position can be related to Ψ and t by modelling the aliphatic chain as a cylinder of homogeneous electron density [Böh93]:

$$Q_z^{hk} = Q_{xy}^{hk} \cos \Psi_{hk} \tan t \quad (4.22)$$

The peak width is dependent on the length L of the molecules:

$$L \approx \frac{0.9 \ 2\pi}{\sqrt{fwhm^2 - \Delta^2}} \quad (4.23)$$

where Δ is the detector resolution in z-direction (cf. eq. 3.03).

4.5.3 Measurement and Interpretation

Due to the low crystallinity, for monolayers in most cases only three peaks are observed that correspond to the densest lattice rows with the lowest Miller indices. Depending on the lattice symmetry a peak can be non-, two or three fold degenerate.

The number of peaks, however, is sufficient to solve for the unknowns Ψ (measured with respect to an arbitrary lattice direction) and t (there are as many eqs. 4.22 as number of peaks).

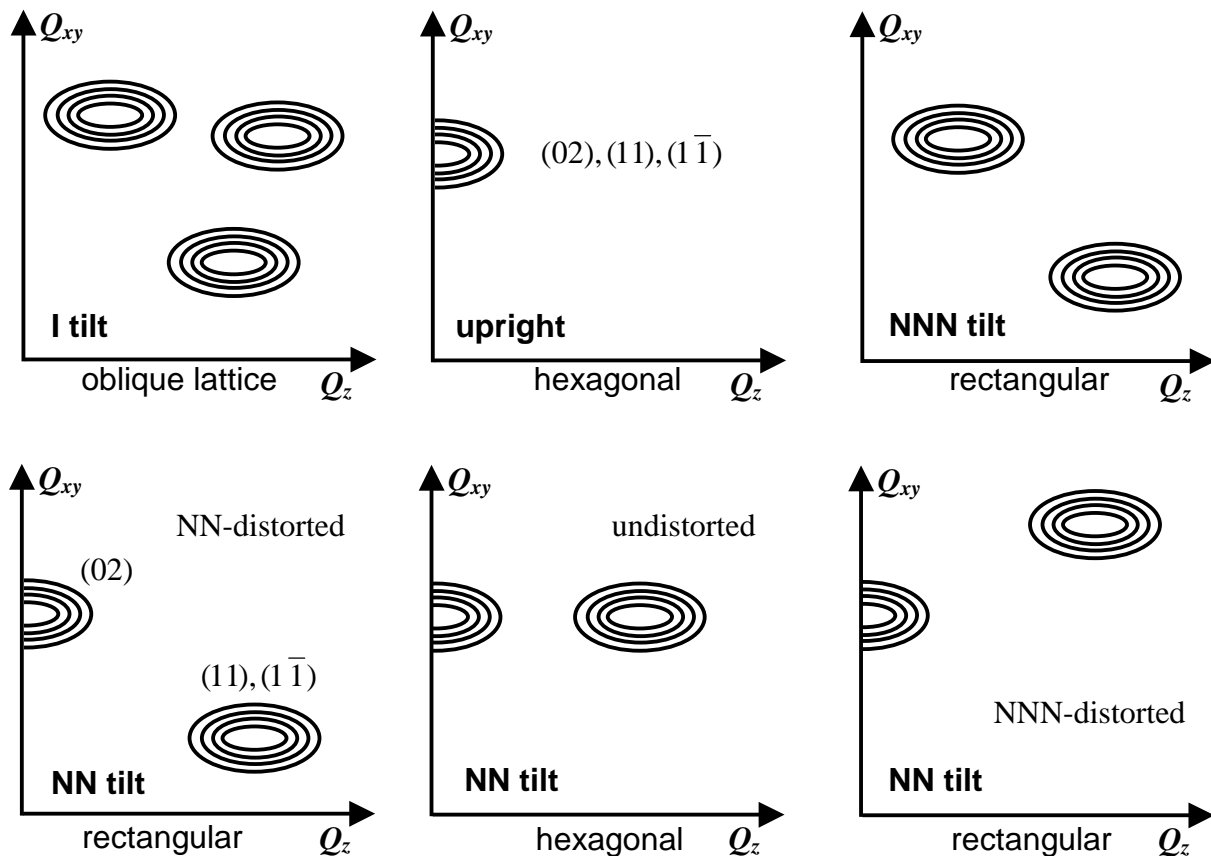


Fig.4.23: Typical contour plots of NN, I, NNN and upright phases in monolayers.

The presence of peaks with $Q_z > 0$ indicates chain tilt (eq. 4.22). In an oblique lattice all three sides of the smallest triangular lattice unit (fig. 4.22 a) are different. In a rectangular lattice two sides are equivalent and in a hexagonal one all three. The three peaks (degenerate and non-degenerate ones) are linked by the relationship $Q_{1z} + Q_{2z} = Q_{3z}$, where peak 3 is the one with the largest Q_z [Kag95a]. The different kinds of distortion, which are shown for NN tilt but also apply to NNN tilt, refer to the distortion of the lattice in the monolayer plane (alternatively one may regard the lattice perpendicular to the chain axes). The kinds of distortion are described in fig. 4.24.

A unit cell can be distorted to rectangular symmetry by chain tilt or by herringbone ordering of the chain backbone planes [Kuz98, Kag95a] (see 3.2.2.3). If both factors act in

perpendicular directions, a point exists at which they compensate each other and the cell is hexagonal even when the molecules are tilted (see fig. 4.23).

The distortion can be described by the ratio of the two axes of the ellipse through all six neighbours of a given molecule (fig. 4.24). The magnitude of the distortion ζ is expressed as $\zeta = (e^2 - f^2)/(e^2 + f^2)$ with e and f as the major and the minor axes of the ellipse, respectively.

One may regard the distortion of the lattice in the monolayer plane or perpendicular to the chain axes, which is identical for upright molecules. The distortion perpendicular to the chain axes is independent of tilt and due to herringbone ordering. If the degree of herringbone disto-

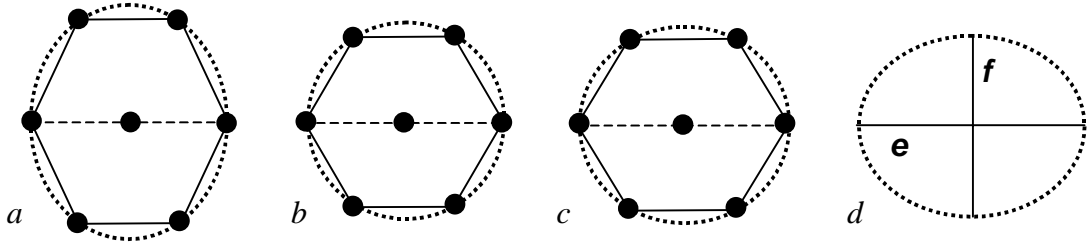


Fig.4.24: Lattice distortion in NNN (a) and NN (c) direction and an undistorted hexagonal unit cell (b). The distortion can be described by the ratio of the diameters of the ellipse that connects the 6 next neighbours of a molecule (d).

rtion is independent of the tilt angle, the distortion parameter d follows the linear relationship:

$$d = d_0 + m \sin^2 t \quad (m \text{ and } d_0 \text{ are constants}) \quad (4.24)$$

where d_0 (d at $t=0$) is a measure for the distortion due to herringbone ordering and the second term corresponds to the distortion in the x-y plane due to tilt. A negative value for d_0 implies that the distortion of the unit cell due to herringbone ordering is perpendicular to the tilt direction [Kag95a]. d is obtained from the experimental Q_{xy} values by means of the equations:

$$d = \frac{8}{3} (Q_{xy}(11) - Q_{xy}(02)) / (Q_{xy}(11) + Q_{xy}(02)) \quad (4.25)$$

for NNN tilted phases, and

$$d = \frac{8}{3} (Q_{xy}(02) - Q_{xy}(11)) / (Q_{xy}(11) + Q_{xy}(02)) \quad (4.26)$$

for NN tilted phases.

For rectangular distortion, with the tilt into NN or NNN direction, $|d|$ is ζ [Kag95a]. The degree of herringbone distortion is expressed in terms of e and f by equating $|d|$ to ζ .

5. Phase Behaviour of Fatty Acid Monolayers

5.1 Neutral Fatty Acids

Most studies on fatty acid monolayers are performed at pH 2 or 3, since ionisation is negligibly small and the system well defined.

Figure 5.01 shows the surface pressure-area isotherms of undissociated fatty acids at ambient temperature. Stearic acid and higher homologues are condensed (G-LC phase equilibrium) under these conditions. No plateau is also detected for palmitic acid. The relatively large compressibility of the condensed phase at low pressure, however, indicates that a LE-LC two phase region is present and that the temperature is near the critical point.

Figure 5.02 shows the schematic area-temperature phase diagram. From this one can see that the G-LE-LC triple point marks the temperature, at which a plateau (LE-LC coexistence region) in an isotherm starts to emerge. In the literature the triple point for pentadecanoic acid was found to be about 17°C [Moo90] and for stearic acid around 40°C [Kel78, Ove93b]. Taking into account the temperature shift for 1 methylene group of 5-10°C the triple point of palmitic acid is estimated to be near 25°C.

The acids of lower molecular weight exhibit a plateau region, the onset pressure π_c of which increases linearly with increasing temperature (cf. 4.1.3). Since an increase of 5-10°C corresponds to a decrease of chain length by 1 methylene group, π_c increases also linearly with decreasing chain length. For myristic acid the critical point is reached near 31°C [Sur88]. Therefore myristic and pentadecanoic acid are the only fatty acids which can be

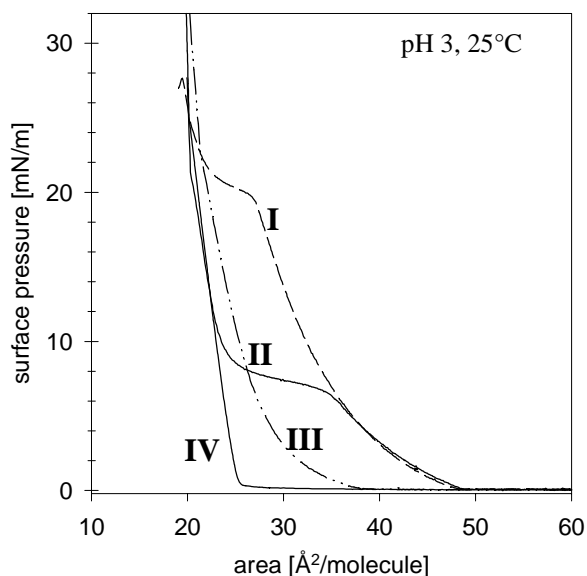


Fig.5.01: π -A isotherms of
I Myristic acid $C_{13}H_{27}COOH$
II Pentadecanoic acid $C_{14}H_{29}COOH$
III Palmitic acid $C_{15}H_{31}COOH$
IV Stearic acid $C_{17}H_{35}COOH$

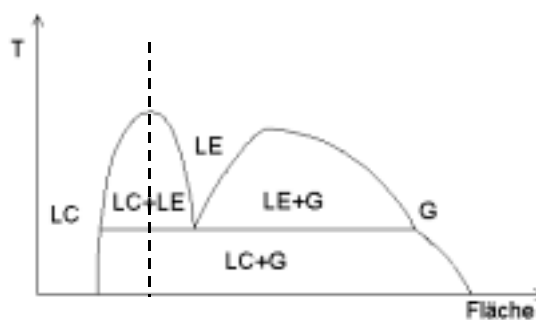


Fig.5.02: A-T monolayer phase diagram

conveniently studied in the two phase region at room temperature and in the neutral form.

One can clearly see that the plateaus in figure 5.01 are steep, i. e. that the pressure within the plateau region increases with decreasing area. If, however, the plateau marks the region of coexistence during the transition between two phases (see 4.1.3), according to the Gibbs' phase rule the phase transition has to occur at constant pressure, i. e. with horizontal plateau, for a given temperature. The unambiguous proof that the plateaus in the isotherms of neutral fatty acids on water represent first order transition regions with a two phase coexistence has been provided by optical microscopy [Moo90, Kno90a, Hön92] (cf. fig. 3.10). Consequently the origin of the slope in the plateaus is not clear. There are experimental and theoretical approaches for explanation [Mil86, Kno90b and ref. therein, Fai96]. However, the considerable influence of impurities on the slope is unquestionable [Mil86, Kno90b and ref. therein].

5.2 Dissociated Fatty Acids

5.2.1 Effect of pH

When the pH value of the subphase is increased, fatty acid molecules in the monolayer dissociate. The portion of charged carboxylate in the fatty acid monolayer varies as a function of pH (fig. 5.03). The substitution of carboxylates for neutral fatty acid molecules in the monolayer leads to a change in the intermolecular interactions. Most obvious is the appearance of ionic repulsive interactions. Hence the phase behaviour of fatty acid monolayers is expected to depend on the subphase pH. There is evidence that fatty acids start to dissociate and change their behaviour measurably at a pH value around 6 [Ave90]. Figure 5.05

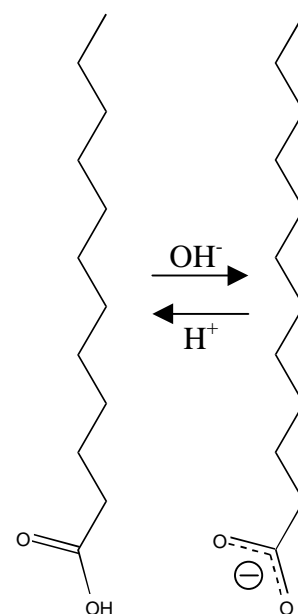
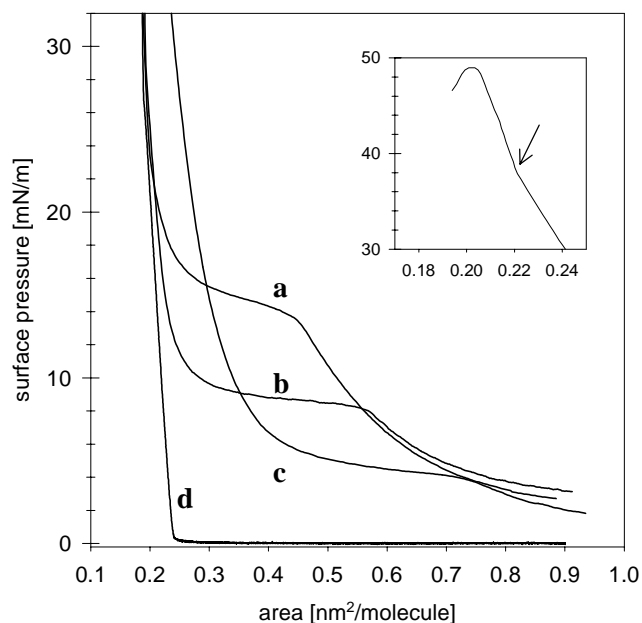


Fig.5.03

demonstrates, that monolayers of fatty acids, that are condensed on neutral subphase (fig. 5.04 d), become fluid at high pH. As the fluid phase is compressed a plateau emerges at the onset of which the formation of condensed phase is observed (fig. 5.05 a). The illustration of the two phase coexistence in figure 5.05 provides unambiguous evidence, that the plateau in the isotherms of fatty acid monolayers at high pH represents a fluid-condensed phase transition region analogous to the shorter chain homologues at low pH. However, there seems to be a difference in the character of the fluid phase at low and high pH. At low pH the pressure of the liquid expanded phase decreases steeply to zero indicating the transition to LE-G

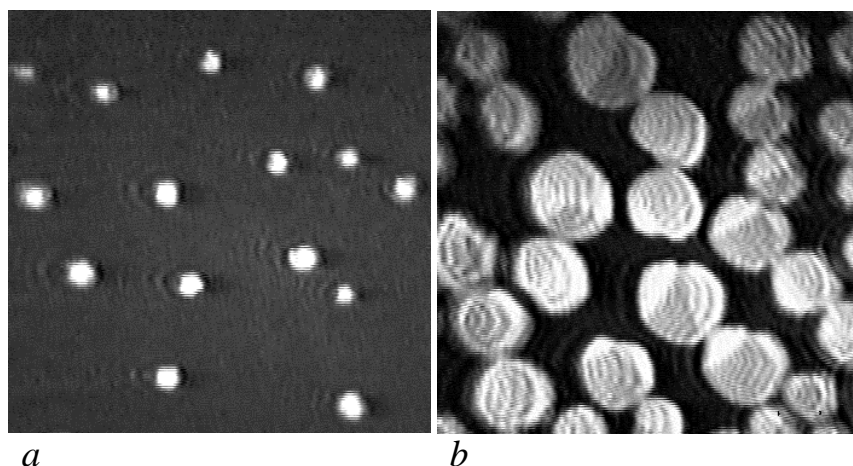
coexistence above $0.5 \text{ nm}^2/\text{mol}$. (fig. 5.01, cf. fig. 4.03). At high pH the zero pressure is approached asymptotically (fig. 5.04, 5.06).

Figure 5.06 shows that the plateau onset pressure π_c (see fig. 4.03) is, within a certain range of pH, a linear function of the subphase pH at constant temperature (inset). As π_c also increases linearly with the temperature (fig. 6.17), this implies, that the increase in pH is equivalent to an increase in temperature or a decrease in chain length. The increase of the plateau pressure with increasing pH can be understood as the result of the cost in energy for overcoming the electrostatic repulsion of the approaching charged molecules during their transition from the fluid phase into the condensed phase.



*Fig.5.04: π -A isotherms, $T=25^\circ\text{C}$
 (a) Stearic acid on subsolution of pH 11.0 containing 0.2 M NaCl , $1 \cdot 10^{-5} \text{ M EDTA}$,
 (b) Arachidic acid at pH 12.0, $1 \cdot 10^{-4} \text{ M EDTA}$,
 (c) Behenic acid at pH 13.0, $1 \cdot 10^{-3} \text{ M EDTA}$,
 (d) Arachidic acid at pH 3,*

The inset shows the kink in the high pressure part of the isotherm of behenic acid (curve c).



*Fig.5.05:
 (a) Nuclei of arachidic acid developing at the onset of the plateau; image: $230 \times 230 \mu\text{m}^2$;
 (b) domains of condensed phase growing in the plateau region; $580 \times 580 \mu\text{m}^2$
 (pH 11.7-12.0, $0.5 \cdot 10^{-4} \text{ M EDTA}$)*

The part of the isotherm referring to the fluid phase is unaffected by the pH. This and the fact that the pressure was found to vary inversely with ionic strength, suggests, that the fluid phase is completely dissociated [Pat72]. The condensed phase is probably only partially dissociated [Ois97]. The increase in the plateau pressure is then caused by the increase of the electrostatic

interactions due to continued dissociation of the condensed phase. To check the effect of the sodium ions, the pH was kept constant at 12.0 and only NaCl was added to adjust the sodium concentrations to the values present at the different pH values. There sodium was added with NaOH. Indeed the plateau pressure was found to increase also with increasing ion concentration, but only to a fraction of the value observed when NaOH was added instead of NaCl. This finding indicates that the fatty acid monolayer is not yet completely dissociated at pH 12 (for the action of ions see 5.2.2).

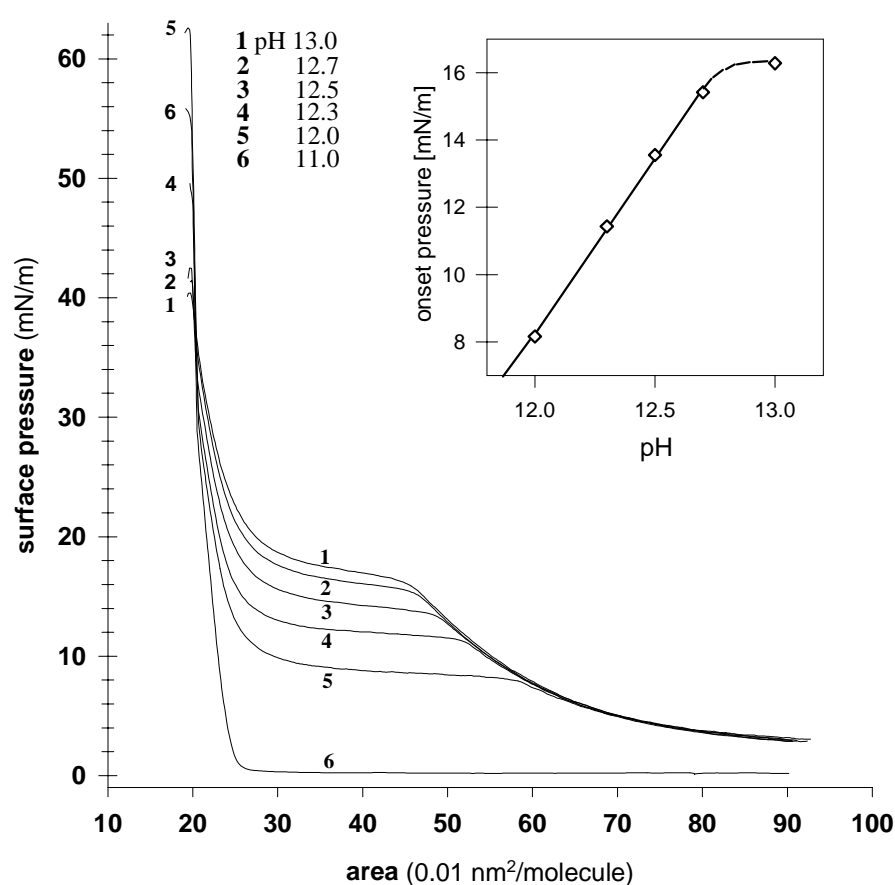


Fig.5.06: π -A isotherms of arachidic acid at 25°C for different pH values. The plateau onset pressure π_c (cf. fig. 4.03) is a linear function of the subphase pH at constant temperature (inset). From the insets in this and figure 6.17 one can derive that an increase in temperature by 10°C leads to the same pressure increase as an increase in pH by about 0.4 units. Hence the increase in the electrostatic energy of the phase transition on an increase of the pH by about 0.3 units corresponds to the energy for a decrease in chain length by one

CH₂ group. The increase in π_c is ascribed to increasing degree of deprotonation of the condensed phase. The pH value linearly extrapolated to zero plateau pressure is 11.5. The deviation from linearity above pH 12.7 indicates saturation and completeness of dissociation. The collapse pressure decreases quickly with increasing pH above pH 12.0. The coincidence of the isotherm parts at the limiting area for the different pH values up to highest pressures confirms the pH stability of arachidic acid monolayers.

5.2.2 Electrostatics of the Interface

When a fatty acid monolayer is spread on a basic subphase, it partially dissociates and becomes negatively charged. The hydrogens and positively charged metallic ions are attracted to the interface from the bulk solution and their concentration is enhanced in the immediate vicinity of the monolayer compared to the bulk. The balance between the attractive forces on the ions towards the interface and their diffusion back into the bulk creates a diffuse double layer. Introducing some approximations this system can be described by the Poisson-Boltzmann approach. It neglects the discreteness of charges on the surfactants and considers the charge as homogeneously distributed over the interface. Ions in the solution are regarded as point charges and the dielectric constant of the solvent is assumed to be constant going from the bulk to the interface. Image charge effects, that arise when the permittivities on both sides of the interface are different, are also neglected. In spite of many simplifications included, this model proved to correctly predict the correlation between the ion concentration of the bulk, the charge density and the electric potential at the interface in a number of systems investigated [McL77, Lak83]. Refinement and corrections concerning only a single aspect of the model resulted mostly in a larger disagreement with experimental findings than the application of the unmodified Poisson-Boltzmann relation [Blo90]. This is because the inadequacies of the assumptions compensate so excellently that the model provides a satisfactory description of experimental systems over rather wide ranges of surface charge density and bulk ion concentration [Dav63]. The error in taking smeared instead of discrete charges is insignificant, when the charge distance in the monolayer is smaller than the Debye screening length $1/\kappa$ and also ion size effects are negligible when the ions are smaller than $1/\kappa$ [Blo90]. The value of the electric potential Ψ in a space filled with electrical charges obeys the Poisson equation:

$$\text{div}(\epsilon\epsilon_0 E) = \rho \quad E = -\text{grad}\psi \quad (5.01)$$

where ϵ is the dielectric constant, ϵ_0 the permittivity of free space and ρ the electrical charge density. The ions of species i are Boltzmann distributed normal to the interface:

$$n_{i,s}(x) = n_{i,b} \exp\left(-\frac{z_i e \psi(x)}{kT}\right) \quad (5.02)$$

where n_i is the ion density, the indices s and b refer to surface and bulk resp. and z_i is the ion valence. With $\rho = \sum z_i e n_{i,s}$ and (5.01) and (5.02) the Poisson-Boltzmann equation is

$$\frac{d^2\psi}{dx^2} = -\frac{e}{\epsilon\epsilon_0} \sum_i z_i n_{i,b} \exp\left(-\frac{z_i e \psi(x)}{kT}\right) \quad (5.03)$$

First integration yields

$$-\frac{d\psi}{dx} = E(x) = \left[\frac{2kT}{\epsilon\epsilon_0} \sum_i n_{i,b} \left(\exp\left(-\frac{z_i e \psi(x)}{kT}\right) - 1 \right) \right]^{1/2} \quad (5.04)$$

The second integration gives the electric potential profile along x

$$x = - \int_{\psi=0}^{\psi=\psi(x)} \frac{d\psi}{\left[\frac{2kT}{\epsilon\epsilon_0} \sum_i n_{i,b} \left(\exp\left(-\frac{z_i e \psi(x)}{kT}\right) - 1 \right) \right]^{1/2}} + x_0 \quad (5.05)$$

x_0 is a constant from the integration from $\Psi=\Psi_0$ (at $x=0$) to $\Psi=0$. In the case of symmetric 1:1 electrolytes an analytical expression can be derived (Gouy-Chapman equation). The Potential Ψ_0 at the interface plane ($x=0$) is determined in dependence of the ion concentrations in the bulk and the surface charge density σ by means of eq. 5.04 and $(d\Psi/dx)_{x=0} = E(0) = \sigma/(\epsilon\epsilon_0)$

$$\sigma = \left[2kT\epsilon\epsilon_0 \sum_i n_{i,b} \left(\exp\left(-\frac{z_i e \Psi_0}{kT}\right) - 1 \right) \right]^{1/2} \quad (5.06a)$$

or

$$\sigma = (8kT\epsilon\epsilon_0 N_A c_b)^{1/2} \sinh\left(\frac{ze\Psi_0}{2kT}\right) \quad (5.06b)$$

for a 1:1 electrolyte with c_b as bulk salt concentration in mol/m³ and N_A the Avogadro constant. Eqs. 5.06a and 5.06b are known as the Grahame equation which was originally derived from the electroneutrality condition $\int \rho dx = \sigma$ [Gra47]. A second relation between Ψ_0 and σ that is needed for determining the unknowns, is provided by the conception of the Gouy-Chapman-Stern theory, that the ions are not only attracted to the interface forming a diffuse double layer but can also attach to lipid molecules in the monolayer by chemical and/or electrostatic forces. By this the charges of the lipid head groups are neutralised and the surface charge density is reduced. The specific ion binding to monolayer molecules is described by the mass action law:

$$K_M = \frac{\{RCOOM\}}{[M^+]_0 \{RCOO^-\}} \quad (5.07)$$

according to the equilibrium $RCOO^- + M^+ \rightarrow RCOOH$, where $[M^+]_0$ is the concentration of hydrogens or monovalent metallic ions next to the monolayer of a fatty acid, $\{\}$ denote surface concentrations. The surface charge density is

$$\sigma = \frac{e}{A} \frac{\{RCOO^-\}}{\{RCOO^-\} + \{RCOONa\} + \{RCOOH\}} \quad (5.08)$$

where A is the mean molecular area and H^+ and Na^+ are used as cations.

Using (5.07) and (5.02) with $\Psi(x)=\Psi_0$, (5.08) becomes

$$\sigma = \frac{e/A}{1 + \{K_H[H^+] + K_{Na}[Na^+]\} \exp(-e\psi_0/(kT))} \quad (5.09)$$

Combining eqs. 5.06 and 5.09 to the Poisson-Boltzmann-Stern equation and solving numerically yields Ψ_0 and σ . The effect of bulk salt concentration on Ψ_0 and σ is different for a monolayer with a fixed number of charges and a monolayer where σ is varied by the binding of ions. In the former case where σ is constant at constant monolayer area an increase in the salt concentration leads to a decrease of Ψ_0 and a faster decay of $\Psi(x)$ with x (screening effect). At constant ion concentration Ψ_0 varies like σ . In the latter case an acid monolayer with deprotonizable groups and non-binding cations in the bulk may be considered. At a certain pH an increase in the amount of salt will reduce Ψ_0 and thus $[H^+]_0$ (eq. 5.02). Due to the equilibrium (eq. 5.07) the fatty acid dissociates and σ increases, while Ψ_0 becomes smaller due to the screening. This shows that the degree of monolayer dissociation sensitively depends on the ion concentration in solution. The assumption that the concentration of the ions that are in equilibrium with the monolayer simply follows eq. 5.02 with $\Psi(x)=\Psi_0$ bears some uncertainty. At the interface the conditions are least defined and understood. The ion concentration there may deviate from the calculated value by image charge effects, that tend to repel the ions from the interface, by the volume of the ions limiting their density and the lessened electrical screening ability of the solvent in the interfacial region ($\epsilon \approx 20-30$ [Toc90]) compared with that in the bulk ($\epsilon \approx 78$). Performing corrections for the ion size and the permittivity a lower value for the number of ions at the interface is obtained but the coincidence with the Poisson-Boltzmann approximation is the better the smaller the bulk ion concentration and Ψ_0 [Fra79]. The pH value at the interface is different from that in the bulk solution and can be derived by applying eq. 5.02 to the hydrogens with $\Psi(x)=\Psi_0$

$$pH_0 = pH_b + \frac{e\psi_0}{2.3kT} \quad (5.10)$$

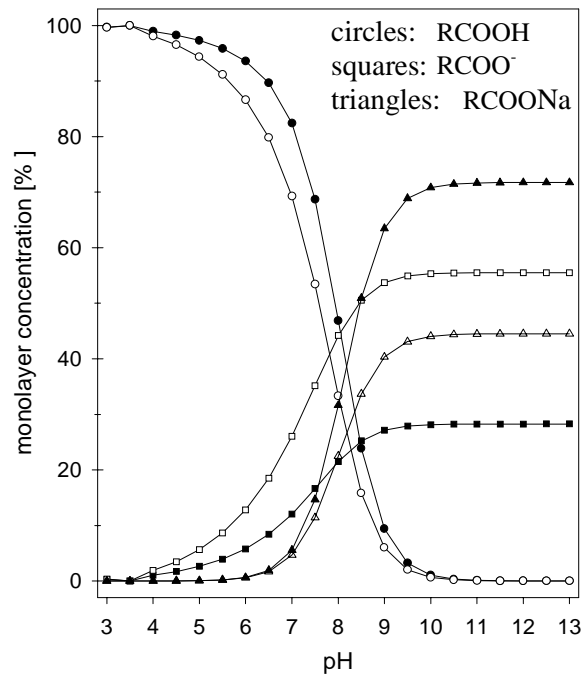
The acidity of a fatty acid molecule in a monolayer, expressed by the apparent pK_a value, and one in bulk solution ($pK=4.8$) is not the same. The reason for this are the peculiar conditions at the interface such as the existence of image charge effects that make monolayer dissociation more unfavourable, the changed dielectric properties due to orientation of water molecules at the polar or charged head groups, the possible formation of hydrogen bonding networks engaging head groups and water molecules which hinder the release of protons [Toc90, Bog87] or the strong binding of cations to the monolayer affecting the pK . The pK_a of the monolayer, which corresponds to that pH value of the bulk where the monolayer is half

dissociated, is not a constant but determined by the hydrogen concentration at the interface. It therefore strongly depends on Ψ_0 that is altered with the salt concentration and the packing density of the monolayer and may also depend on the concentration and sort of ions, that affect the water ordering and dielectric properties in the interfacial region. Table 7.3 contains data on the electrochemical conditions and the ion binding at the monolayer for the ion concentrations and pH values investigated as determined from the Poisson-Boltzmann-Stern equation. The degree of deprotonization D_H of the monolayer is

$$D_H = \frac{\{RCOO^-\} + \{RCOONa\}}{\{RCOO^-\} + \{RCOONa\} + \{RCOOH\}} = \frac{1 + K_{Na} [Na^+]_0}{1 + K_{Na} [Na^+]_0 + K_H [H^+]_0} \quad (5.11)$$

and the portion of sodium ions associated with lipid molecules is described by

$$A_{Na} = \frac{\{RCOONa\}}{\{RCOO^-\} + \{RCOONa\} + \{RCOOH\}} = \frac{K_{Na} [Na^+]_0}{1 + K_{Na} [Na^+]_0 + K_H [H^+]_0} \quad (5.12)$$



a

The values for the Debye length $1/\kappa$ are always much larger than the size of a hydrated ion (≤ 1 nm [Mit93]) and the distance between charged molecules in the monolayer, which is about 0.5 nm with 100% and on average around 1.6 nm with 10% free carboxylate.

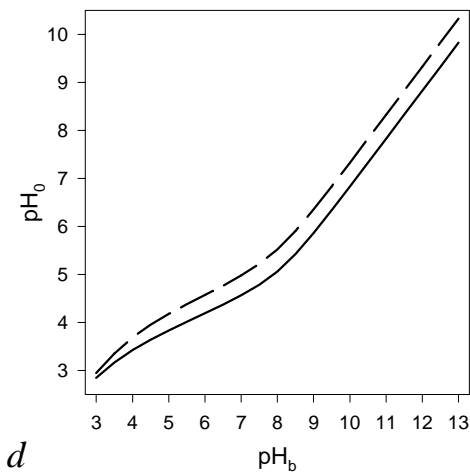
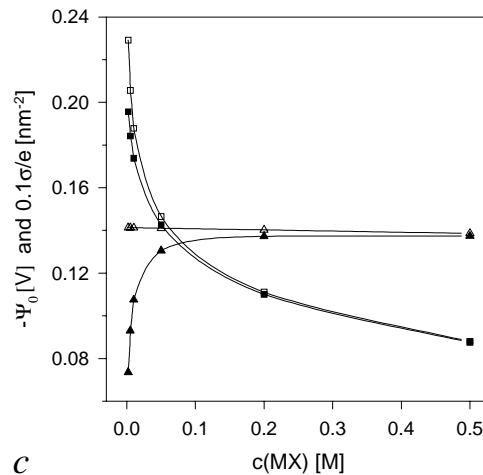
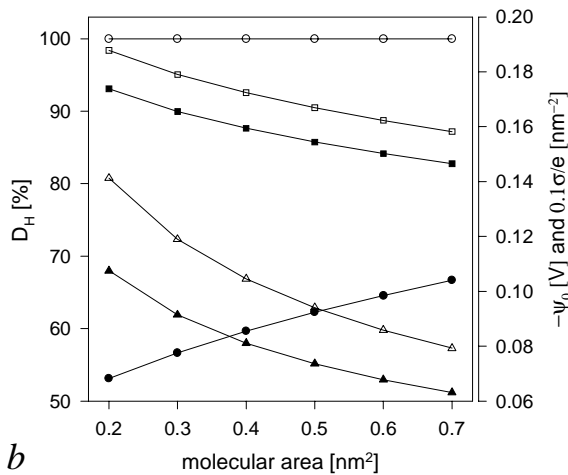
Fig.5.07:

(a) Calculated variation of the composition of a fatty acid monolayer with pH for 25°C, $0.20 \text{ nm}^2/\text{mol}$. (closed symbols), $0.70 \text{ nm}^2/\text{mol}$. (open symbols), with $\epsilon = 78$, 0.01 M 1:1 electrolyte, $K_H = 10^{5.4}$, $K_{Na} = 10^{-0.771}$ [Loc97].

The degree of dissociation increases with increasing molecular area

(b-d) closed symbols: pH 8.0 (partial dissociation), open symbols: pH 12.0 (complete dissociation), circles: D_H , squares: Ψ_0 , triangles: σ

In figure 5.06 the increase in plateau pressure of an arachidic acid monolayer of about 8 mN/m between pH 12 and 13 has been ascribed to the increase in dissociation of the condensed phase and the increase in the electrostatic energy of the phase transition. The fluid phase was assumed to be completely dissociated at these pH. The electrostatic energy of the phase transition arises from the difference in the charge densities $\Delta\sigma$ of fluid and condensed phase.



Regarding $\Delta\sigma$ as the difference in σ between 0.2 and 0.7 nm²/mol. $\Delta\sigma$ increases by 0.176 e/nm² from pH 8 to pH 12.0 for 0.01 M ionic strength (b) and by only 0.0025 e/nm² from pH 12.0 (0.01 M salt) to pH 13.0 (0.1 M salt). The increase in $\Delta\sigma$ from pH 12-13 is caused by the increase in ionic strength, the difference in dissociation between these two pH values is negligible and does not contribute to $\Delta\sigma$ ($D_H=0.9999$ (pH 12.0)/1.0000 (pH 13.0) for 0.2 to 0.7 nm²/molecule). However, it is obvious from experiment, that the change of the ionic concentration alone can not be the reason for the increase of the plateau pressure.

Apparently the Gouy-Chapman-Stern approach fails to correctly predict the conditions at the interface for this pH range and the degree of dissociation is overestimated (according to the calculations the monolayer is dissociated to 99% already at pH 10).

There are two explanations imaginable for this obvious disagreement: either the limits of the theory are exceeded at such high pH or, which idea I adhere more, the assumptions on the properties of the fatty acid monolayer included in the theory are insufficient. Experimental findings indicate, that the fatty acid head groups in the condensed phase are hydrogen bonded (chpt. 7), so that the ability of dissociation of the fatty acids is influenced by the pH value. Hence a better agreement between theory and experiment may be obtained by applying more than one or a pH dependent K_H value. The calculations, however, agree with the above assumption in that point, that the fluid phase is completely dissociated above pH 12.

(c) illustrates the effects of the ionic strength (MX: electrolyte) on a partially dissociated monolayer at pH 8 on the one hand and on a completely dissociated monolayer or a monolayer of constant charge density on the other hand. In both cases the surface potential Ψ_0 decreases with increasing ionic strength due to the screening of the surface charges by the counterions. This leads to the reduction of the proton concentration at the interface and to the increase of dissociation and surface charge density σ for a partially dissociated monolayer.

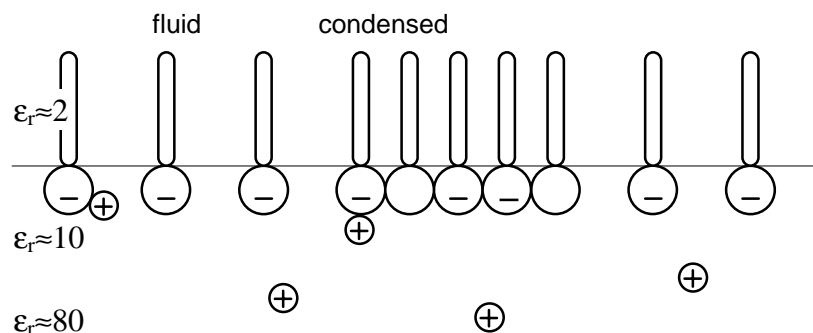
(d) comparison of pH_b of the subphase with the corresponding pH_0 at the monolayer of a fatty acid with $\text{p}K_a=5.4$ for 0.2 nm²/mol. (solid curve) and 0.7 nm²/mol. (hatched curve) at 0.01 M ionic strength. The monolayer is dissociated to 50% when $\text{pH}_0=\text{p}K_a$. For 0.2 nm²/mol. This

condition is fulfilled for a bulk pH of about 9. Above this point the surface pH varies linearly with the subphase pH_b, where the value at the surface is about 3 units lower than the bulk value.

Scheme of the state of a partially dissociated monolayer in the state of two phase coexistence:

Fig.5.08: The charge density in the condensed phase is higher than in the fluid phase, while the degree of dissociation is lower in the condensed phase (fig. 5.07 b).

The concentration of oppositely charged ions in solution is higher near the surface than in the bulk. One part of the sodium counter ions is bonded to charged head groups representing the Stern-layer, the other part is distributed at the interface constituting the diffuse Gouy-Chapman double layer.



Importance of EDTA

As noted in figure 5.04 some of the chelating agent EDTA was added to the alkaline subsolutions. Without the addition of EDTA the onset of the plateau was blurred and not pronounced. Also the morphology was affected. Without EDTA the size distribution of the condensed phase domains was very uneven with a large portion of very small domains, that did not grow. Furthermore the optical structure (texture) within the domains was irregular. These effects are probably caused by traces of polyvalent metal ions, such as calcium or magnesium, which bind to the dissociated fatty acids and change the properties of the monolayer. EDTA removes these impurities. The following example calculation demonstrates, that a tiny concentration of a binding metal in bulk solution suffices to considerably influence a highly charged monolayer at high pH:

The binding constant for the reaction $\text{Ca}^{2+} + \text{RCOO}^- \rightarrow \text{RCOOCa}^+$ is $K = \{\text{RCOOCa}^+\} / (\{\text{Ca}^{2+}\}_0 \cdot \{\text{RCOO}^-\}) = 10^{0.5}$ [Loc97]. $\{\}$ refers to monolayer concentration, $[\text{Ca}^{2+}]_0$ to the calcium concentration at the monolayer. The latter is related to the bulk ion concentration $[\text{Ca}^{2+}]_b$ by the Boltzmann equation $[\text{Ca}^{2+}]_0 = [\text{Ca}^{2+}]_b \cdot \exp(-2e\Psi_0/(kT))$. Assuming a surface potential Ψ_0 of -0.2 V, a $[\text{Ca}^{2+}]_b$ of the order of 10^{-8} mole/l suffices to obtain binding to up to 50% of the fully dissociated monolayer ($\{\text{RCOOCa}^+\} / \{\text{RCOO}^-\} \leq 1$).

The impurities could not be removed, despite taking care of cleanliness of the trough and substances. Possibly the polyvalent ions were etched out of the glass vessels containing the basic stock solutions. Although this source can be excluded by using quartz vessels, it seemed

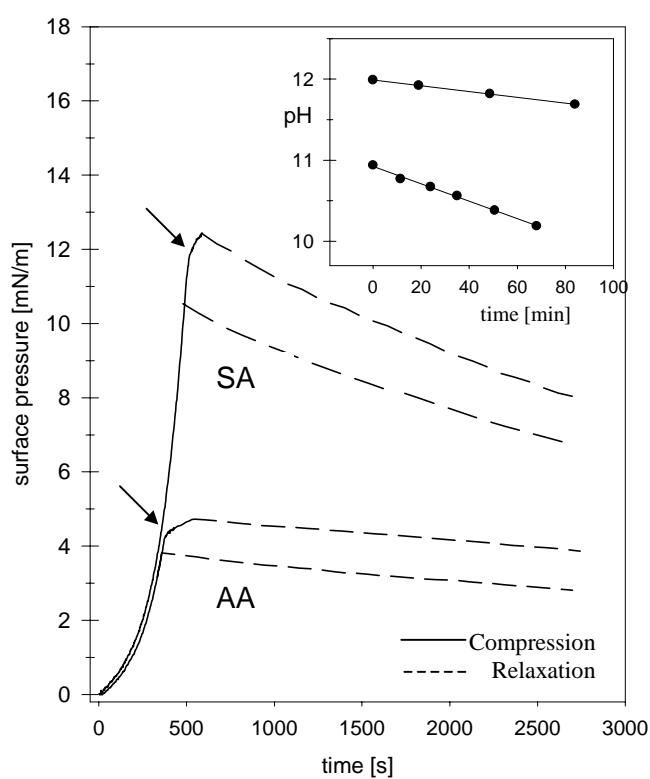
the safest to take EDTA, which has been a common ingredient in former investigations concerning monolayers at high pH [God67, Pat72, Lös88]. On adjusting the pH, the added amount of EDTA has to be taken into account, since EDTA is an acid (see app. I).

5.2.3 pH-stability

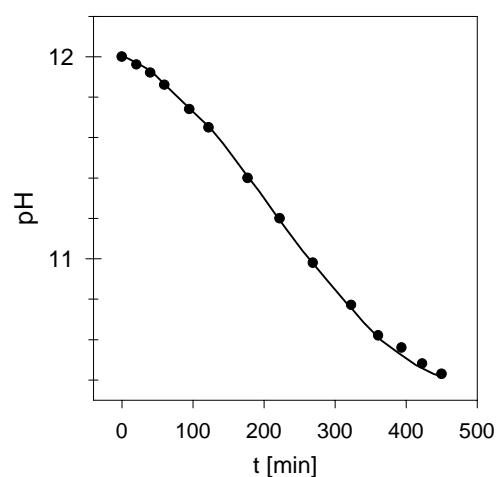
The stability of fatty acid monolayers is strongly influenced by the pH value and the ionic strength of the subphase. Because of the higher solubility of carboxylate compared to the neutral fatty acid and the repulsion of equal charges in the monolayer, fatty acid monolayers be-

Fig.5.09:

(a) Relaxation of the monolayers of stearic acid (SA) at pH 11.0 (0.2 M NaCl) and arachidic acid (AA) at pH 12.0, 25°C at constant area. The arrows mark the change in slope of the compression curves and the entering of the two phase region. Relaxation was performed for two different initial surface pressures for each acid. One pressure was chosen in the fluid region (lower curve for each acid), the other in the two phase region (upper curve for each acid). A very similar decrease in pressure with time is observed for both cases, although the origins of the pressure drop are different. The relaxation in the fluid region is due to desorption by solubilization. Desorption occurs also in the plateau region, but desorbed fluid phase is recovered at the expense of the coexisting condensed phase and as long as condensed phase is present, the pressure decreases only slightly within the plateau region. As the decrease in pressure is much larger and condensed phase domains were observed throughout the measuring period, the decrease in pressure, which corresponds to the plateau pressure, is not caused by desorption. The plateau pressure is probably reduced by the formation of carbonic acid in the subphase from atmospheric CO₂ and the concomitant decrease in the pH.



a



b

The carbon dioxide does not play a role for the fluid phase, since the pressure of the fluid phase is independent of the subphase pH above pH 11.5 (fig. 5.06). In the inset the decrease of the subphase pH with time due to CO₂ is shown for AA from pH 12.0 and for SA from pH 11.0 (the pressure was set to zero as it started to increase noticeably on compression, so the plateau onset pressures are lower than those in the isotherms in fig. 5.04)

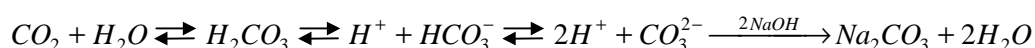
(b) Decrease in pH over more than 7 hours because of the penetration of atmospheric CO₂ into the subphase. The pH values were measured in a trough of 1200 cm² area containing 1600 cm³ solution.

come more and more unstable with increasing pH (2.3; eq. II.3, app.). The ionic strength has two effects: on the one hand the degree of dissociation increases with increasing ionic strength at constant pH due to increased electrostatic screening (see previous chapter). On the other hand the solubility of the molecules decreases with increasing ionic strength by unfavourable solute-solvent and solute-ion interactions. The latter effect is named salting-out (2.3.2.2).

With stearic acid on 0.005 M borate buffer solution film loss is substantial at pH 9.7 at room temperature. With 0.01 ionic strength of the subphase (adjusted with NaCl) the monolayer of stearic acid is found to be stable well above pH 10 [Spi63]. Figure 5.09a shows the stability for 0.2 M NaCl at pH 11.0 in a pressure range below the plateau onset pressure (cf. fig. 5.04 a). Without adding salt stearic acid desorbed quickly and the monolayer could not be compressed. The increase of dissociation with increasing ionic strength is indicated by the formation of a fluid phase of stearic acid at pH 9.2 after the addition of 0.2 M NaCl. On compression condensed domains of characteristic texture develop at nearly zero pressure (fig. 6.01 b). Still with 0.1 M NaCl the monolayer is already condensed after spreading.

The solubility decreases with increasing chain length. At room temperature arachidic acid and behenic acid prove to be relatively stable up to pH 13 (figs. 5.04, 5.06, 5.09 a, 6.17).

At the interface to air the gas exchange between subphase and atmosphere has to be taken into account. In water carbon dioxide forms carbonic acid, which lowers the pH of pure water from 7 to ≈5.6 and neutralises the base in alkaline solutions:



Between pH 12 and 13 the pH decreases only by about 0.1 unit within the measuring time of about 30 min for an isotherm (fig. 5.09). So no buffer was used at these pH. The same stability of pH was obtained for the pH range 8-10 by using 0.005 M borate buffer (H₃BO₃/NaBO₂+1·10⁻⁶-10⁻⁵ M EDTA, s. app. I). The efficiency of the borate buffer compared with other buffers, such as tris or carbonate buffer, which were found to interact with fatty acid monolayers [Pat75], was proven by Goddard et al. [God66].

6. Morphology of Dissociated Fatty Acid Monolayers

6.1 Observations

6.1.1 Effect of pH

Texture and shape of condensed phase domains in fatty acid monolayers are found to depend sensitively on the pH of the subphase and on the concentration and sort of counterions.

From the infinite number of possibilities to vary pH, amount and sort of ions, in this section selected examples are presented, from which clear interrelations can be deduced between the structure of the condensed phase and the subphase conditions.

The point of main effort of this work is the study of the effect of dissociation on the properties of fatty acid monolayers without the effects involved with the binding of ions. This ideal case is approached by using sodium counter ions, which interact with the carboxylate in the monolayer only weakly and essentially by electrostatic forces. Similar effects as with sodium are expected for larger monovalent ions, such as the heavier alkaline metal ions or ammonium or trialkylammonium ions (an exception in the behaviour of alkaline ions represent the small lithium ions, which have a rather high tendency for the formation of complexes with organic compounds [Sch91]).

At pH 8 and 25°C palmitic acid develops a variety of segmented domains with uniform tilt directions within the segments (fig. 6.01 a). The condensed phase spread at 25°C on pure water (cf. fig. 5.01) displays splay and bending, and domains grown on water at 32°C look like those of pentadecanoic acid at 25°C having the typical 'boojum' pattern (fig. 3.10).

Different domain types are also formed by stearic acid at different conditions of pH and ionic strength (fig. 6.01 b, c). Above 40°C and on pure water the domains of stearic acid are found to be circular with uniform tilt orientation over the whole domain area.

The fundamental effects of pH on the morphology of ionizable monolayers is illustrated by means of arachidic acid:

1. Domain 'superlattice'

The order in the spatial distribution of the domains, i. e. the correlation of the domain positions, decreases with increasing pH. The decrease in order is most pronounced between pH 12.3 and pH 12.5. The lower order in domain distribution at pH 12.5 and above is accompanied by a high tendency for the fusion of domains.

2. Domain shape and size

a) *Increasing ratio of domain perimeter to domain area*

Between pH 11.7 and 12.0 the domains are circular; on increasing the pH the distortion of the domain boundary to polygonal shape gradually increases and at pH 12.3 the domains have straight edges and sharp corners appearing like two dimensional faceted crystals. Between pH 12.5 and 13.0 the domain shapes become irregular and the ratio of domain boundary length to domain area is strongly increased. Within this pH range sometimes the formation of fine lamellae together with the compact domains is observed.

b) *Decreasing domain area*

With increasing pH the average size of the domains decreases. The difference in size is more obvious between pH 12.3 and 12.5 than between pH 12.0 and 12.3.

3. Tilt orientational order and domain texture

The degree of tilt orientational order and consequently of the order of the inner domain structure decreases with increasing pH. Up to pH 12.3 the range of uniform molecular orientation extends to several tens of microns. At pH 12.5 the range of uniform tilt has strongly reduced to about 5 μm . The conservation of structural and long range NNN tilt order in arachidic acid monolayers up to pH 12.5 is proved by the diffraction pattern in figure 6.04a. Beyond pH 13.0 no long range NNN tilt orientational order exists any more (fig. 6.04 b). The coupling of tilt and bond directions has weakened such, that simultaneously phases with NN and NNN tilt appear, in which the molecules are uniformly aligned at least over roughly 100 lattice spacings.

The morphology of behenic acid at pH 13.0 (fig. 6.03) is very similar to that of arachidic acid at this pH (not shown). Possibly the disorder in the tilt orientation is the same as with arachidic acid. That the molecules in the condensed phase are tilted below ≈ 39 mN/m is evident from the change in the slope of the corresponding isotherm at high pressure (fig. 5.04, inset).

In chapter 5.2.1 it has been evaluated, that with respect to the phase behaviour an increase of about 0.6 pH units at around pH 12 corresponds to a decrease in chain length by two CH_2 -units. Comparing the similar textures, ranges of tilt orientational order and domain shapes of stearic acid at pH 11, arachidic and behenic acid one may suggest that this relation holds also for the morphological features. However, the study of the temperature dependence of the morphology of arachidic acid in 6.3.2 shows that the relation 'increase in pH is increase in temperature or decrease in chain length', noticed for the phase behaviour, cannot be invoked to explain domain morphologies.

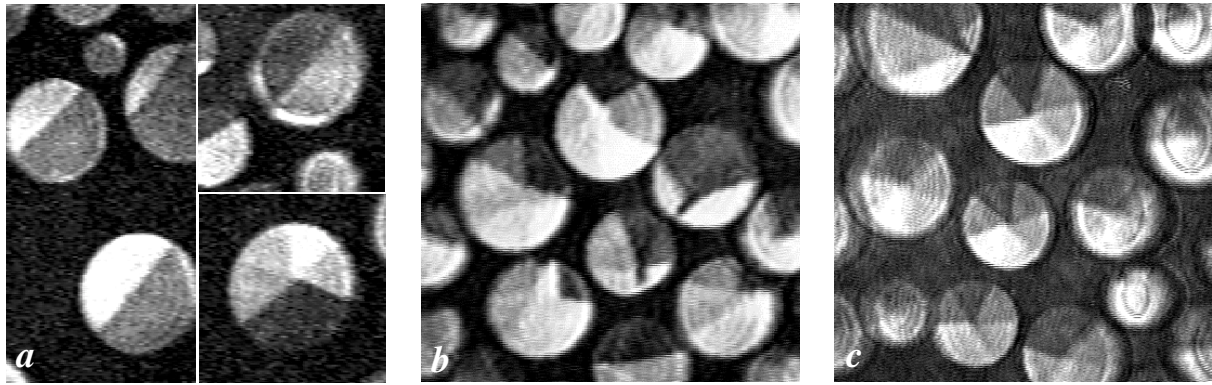


Fig.6.01: Condensed phase domains of palmitic acid at pH 8 (10^{-6} M EDTA), 25°C, are divided into two, three, four and six segments of uniform molecular orientation (a). There is no striking predominance of one domain type; $330 \times 330 \mu\text{m}^2$ (a). Domains of stearic acid on a subsolution of 0.2 ionic strength at pH 9.2 (b) and at pH 11.0 (c) (buffered, with plateau pressure near zero), 25°C. In (b) a texture with one large funnel-like segment extending over the whole domain diameter and three or four smaller wedge shaped segments at the domain edge is predominating. The thinner end of the funnel-like segment has a nearly constant and equal width in all domains of this type. This morphology is observed up to 0.5 M ionic strength. In (c) a texture predominates with six wedge shaped segments of equal size meeting in the domain centre; $290 \times 290 \mu\text{m}^2$ (b, c), $330 \times 330 \mu\text{m}^2$, $290 \times 290 \mu\text{m}^2$ (b,c)

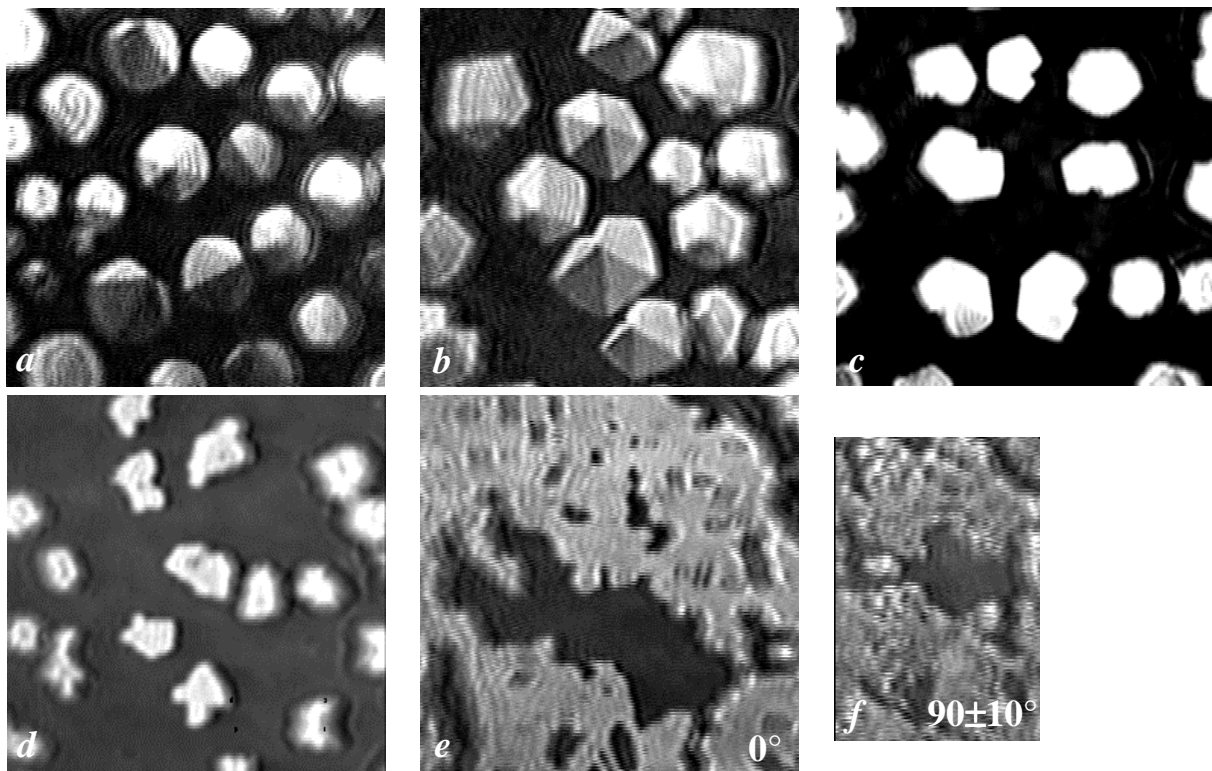
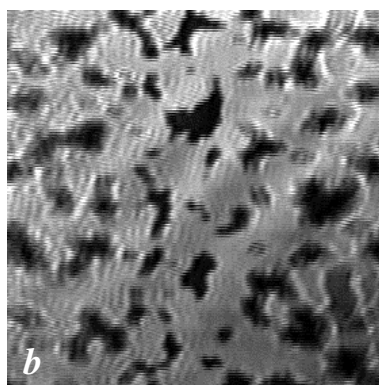
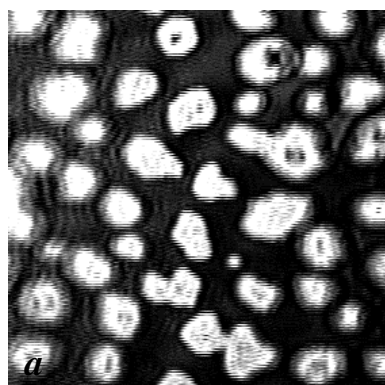


Fig.6.02: Condensed phase domains of arachidic acid grown at pH 12.0 (a), 12.3 (b, c), 12.5 (d, e, f) at 25°C. Between pH 11.7-12.0 the domains are circular and appear with six wedge shaped segments that meet in the domain centre or with three or four segments that have a common point at the domain edge (a) (cf. 6.01 a, c). At pH 12.3 the domains are either hexagons with six segments with the common point of intersection in the domain middle or distorted pentagons with a notch instead of the sixth segment (b, c). Density and tilt angle are uniform within a domain as shown by the example (c). At pH 12.5 the domains readily fuse at higher density of the domains (e). The long range tilt orientational order at pH 12.5 is resolved (f) $90 \pm 10^\circ$



between crossed polarisers (f) (angles between crossed polarisers are given in (e, f)); $250 \times 250 \mu\text{m}^2$ (a,b), $290 \times 290 \mu\text{m}^2$ (c), $200 \times 200 \mu\text{m}^2$ (d,e), $110 \times 160 \mu\text{m}^2$ (f)

Fig.6.03: Irregularly shaped domains of behenic acid at pH 13.0, 25°C (a). Long range tilt order is not resolved any more. The tendency of fusion is very high (b); $230 \times 230 \mu\text{m}^2$

Compression rate in figures 6.01-6.03: $0.02\text{-}0.03 \text{ nm}^2 \text{ molecule}^{-1} \text{ min}^{-1}$

Instead of increasing the pH the series of domain morphologies of arachidic acid can also be run through by increasing the ionic strength and keeping the pH constant. Adding NaCl to a subsolution of pH 12.0 faceted domains like those at pH 12.3 (fig. 6.02 b, c) develop between pNa=1.7-1.3 and at pH 12.3 the domains look like those at pH 12.5 (6.02 d, e) with pNa=1.3.

The effect of polyvalent binding ions on the domain morphology of dissociated fatty acids is demonstrated by the addition of barium ions to the subphase. Giving concentrated BaCl_2 solution dropwise into a solution of pH 12.3, on which a monolayer of arachidic acid has been compressed into the two phase region, and awaiting the diffusion of the metal ions to the monolayer after each added drop, one can observe the gradual and continuous reduction of the tilt angle in the domains and finally the disappearance of the segment structure. Simultaneously the domains become circular and the tendency for domain fusion increases.

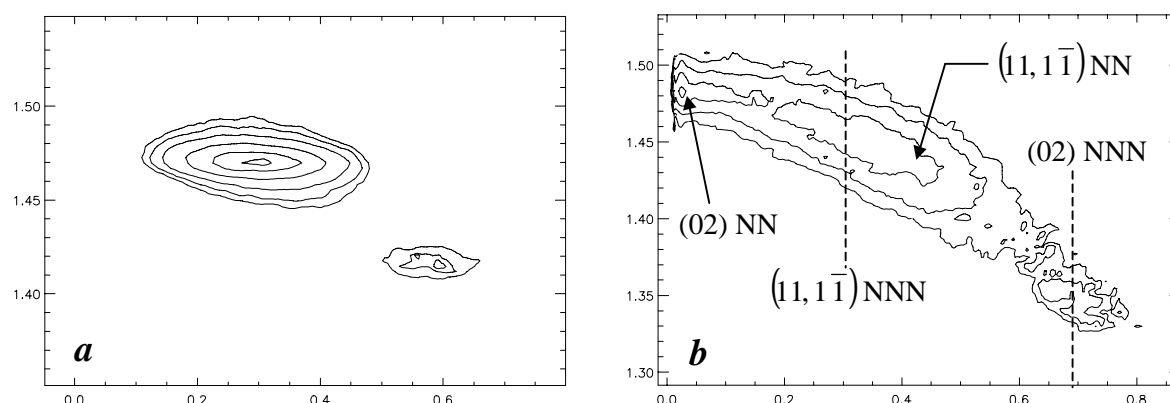


Fig.6.04: Contour plots of the diffracted intensity for arachidic acid monolayers at pH 12.5 (a) and 13.0 (b) at 20 mN/m and 25°C . At pH 12.5 the condensed phase is NNN tilted (a), the pattern at pH 13.0 (b) results from the superposition of the reflections of an NN and an NNN phase [Wei98c]. The (02) NN and (02) NNN reflection positions are easily recognisable. The positions of the (11) NNN reflections can be derived from the relation $Q_{1z} + Q_{2z} = Q_{3z}$ (sketched vertical lines) and that of the (11) NN reflection by assuming the same tilt angle for both phases. The widths of the superimposed peaks in (b) are comparable to those in (a). The

position correlation length for (b) is therefore roughly 100 (tab.VI.1, app.) and this value can be interpreted that translational order is preserved over about 100 lattice spacings (see 3.2.2.2). This value gives also the lower limit for the tilt orientational order. The molecules are uniformly aligned in NN or NNN direction at least over this distance.

6.1.2 Effect of Temperature

Very similar changes in morphology as produced by a change in pH can also be observed by a change in temperature, as demonstrated for arachidic acid. The temperature dependence of the domain morphology of arachidic acid monolayers is illustrated in the figures 6.05a-c. The size of the domains at pH 12.0 was found to be the smaller the lower the temperature. At 16°C the domains look like those at pH 12.3 and 25°C, but are much smaller (a) (cf. fig. 6.02 a).

Drastic changes in morphology occur at pH 12.3. At 25°C the domains are faceted (fig. 6.02 b). At 20°C their shape is irregular and the domains look similar to those at pH 12.5 and 25°C (6.05 b, left half; cf. 6.02 d). With an analyser the inner structure is revealed. The range of tilt orientational order has decreased considerably compared to pH 12.3 and 25°C but it is larger than at pH 12.5 and 25°C. It appears that the domains are built up of many small aggregated faceted domains (6.05 b, right half). At 16°C the condensed phase grows in the form of lamellae, the thickness of which is very small in an early state of growth and it increases up to a limiting value as the monolayer is compressed (c).

It has to be noted that all domain shapes were obtained under conditions of continuous growth. The lamellae at pH 12.3 and 16°C can be transformed into regular faceted forms by heating into the coexistence region to 25°C. In the reverse direction, however, the shape transformation fails. Also at pH 12.0 the larger domains do not split into smaller domains on cooling or fuse to larger domains on heating, but the shape change from faceted to circular and vice versa is reversible with temperature.

Decreasing temperature therefore leads to the reduction of domain size, the increase of the

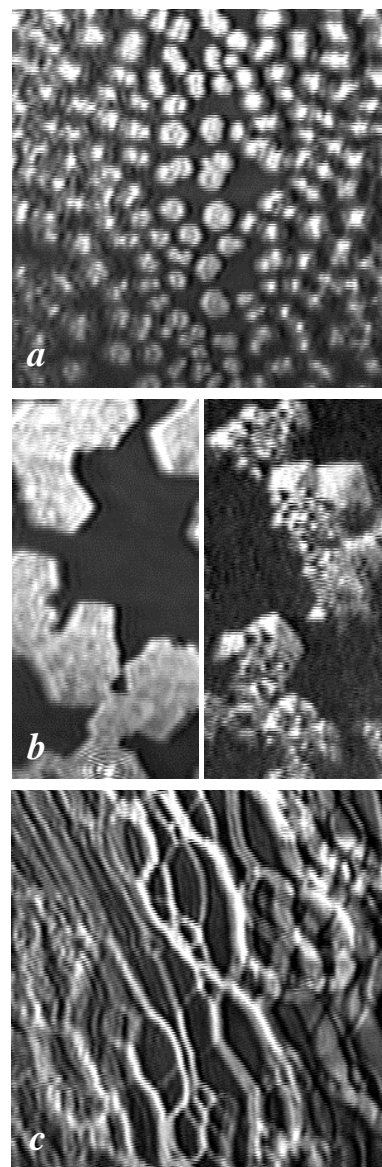


Fig.6.05: LC domains of arachidic acid: pH 12.0, 16 °C (a); pH 12.3, 20°C (right with analyser) (b) and 16°C (c)

boundary length per area and the decrease in the range of tilt orientational order. These are the same effects that result from the *increase* of the pH value.

6.1.3 Influence of Cholesterol

Domains of arachidic acid with a circular boundary line at pH 12.0 and 25°C become cornered and polygonal, when ≥ 1 mol% of cholesterol is added to the spreading solution of arachidic acid. With 1 mol% the morphology in the co-existence region is very similar to that at pH 12.3. However, in the presence of cholesterol the notch at the domain edge is more pronounced and often seems to have its origin

in a missing or incompletely developed sixth segment (fig. 6.08 a). The formation of domains of arachidic acid in a mixture between 5 and 20 mol% cholesterol is illustrated in the figures 6.08b-i. The images *b-i* do not differ for the cholesterol concentrations 5, 10 and 20 mol% investigated, except for the area fraction occupied by the domains which becomes smaller as the amount of cholesterol increases. Hence the cholesterol concentrations are not distinguished in the following discussion.

The monolayer of the arachidic acid/cholesterol mixture, spread in the fluid region, appears inhomogeneous with small grains, that indicate the formation of aggregates (b, grains are bright, area: $0.7 \text{ nm}^2/\text{mol}$. (cf. fig. 6.07)). When the area is decreased and the pressure of the expanded phase increases, the

Fig.6.06: Sketch of a cholesterol molecule and of arachidic acid in all-trans conformation. The cholesterol molecule consists of three parts: a planar and rather rigid steroid skeleton, which reaches up to 9 or 10 carbon atoms of an extended alkyl chain, a flexible iso-octyl chain and a hydroxyl group in 3 β position. Only 4% of the surface area of cholesterol are hydrophilic, though it is an amphiphile with the OH as the polar head group. In mixtures with phospholipids the cholesterol molecules were found to be located such that the steroid ring with the chain is confined to the hydrophobic part of the bilayer and the OH groups lie in the same plane as the lipid ester carbonyl groups [Mor95]

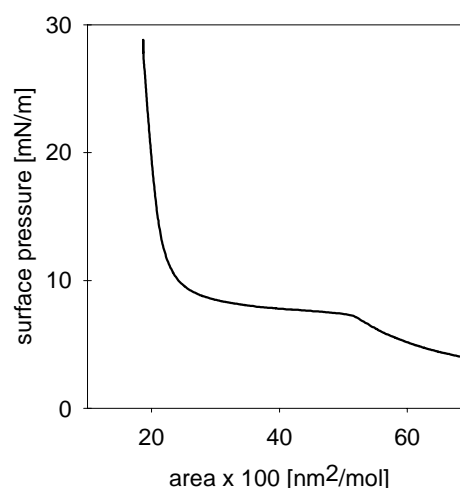
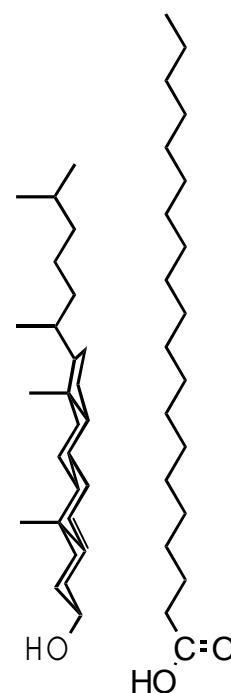
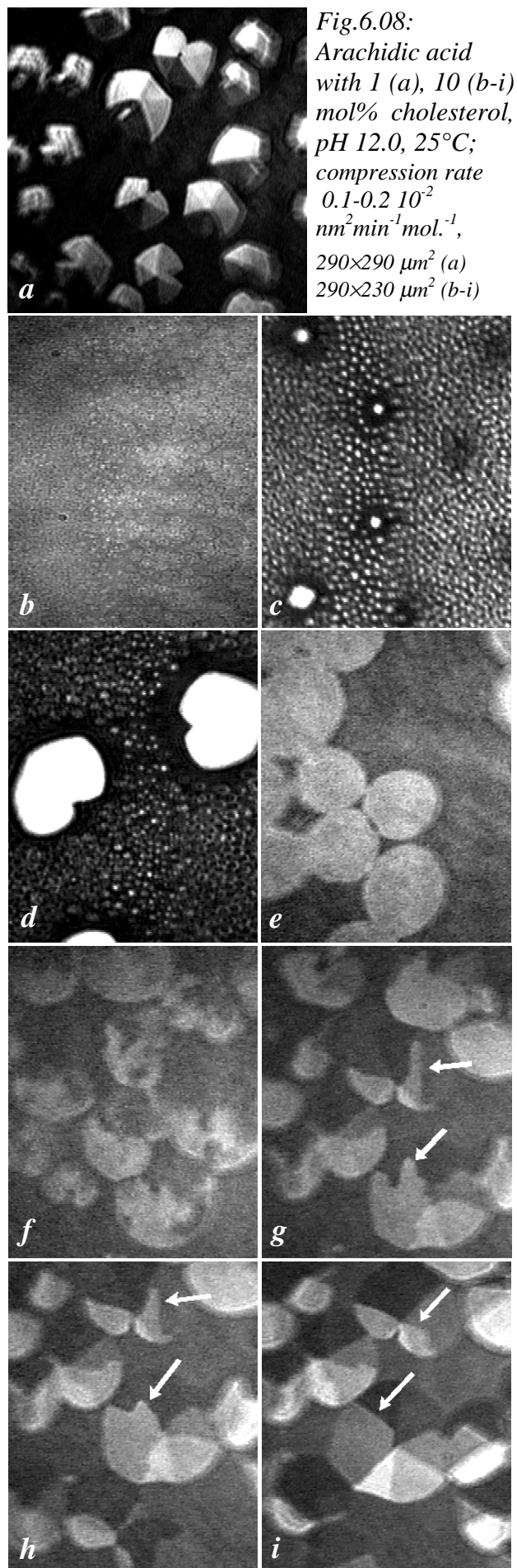


Fig.6.07: Isotherm of arachidic acid with 5.0 mol% cholesterol, 25°C, pH 12.0, compression rate $0.01 \text{ nm}^2/(\text{min mol.})$. The features of the isotherm are representative for the concentrations up to 20 mol%.

grains segregate and become larger. In the two-phase coexistence region initially regions appear that are free of aggregates and that look like dark holes in the monolayer. On further compression eventually bright seeds form in the centre of these holes and grow at the expense of the surrounding aggregates (c). The dark areas obviously represent depleted regions, where a diffusion gradient provides material for the growth of the domain. The content of cholesterol in the domains is probably very small and independent of the cholesterol concentration in the mixture as the domains look the same for all cholesterol concentrations. The aggregates, the size of which does not change any more and which are possibly small domains of arachidic acid with cholesterol that are hindered to grow, are dissolved at the edge of the dark areas. During the growth process the concentration of cholesterol in the depletion region will be enriched. Figure 6.08d shows some domains in an advanced state of growth. The presence of the „halos“ indicates that the domains are still growing. With an analyser an inner structure is observed like that in *a*. The formation of depletion regions around each growing domain prevents the nuclei from emerging in too close vicinity and provides their regular distribution. During growth, however, the domains aggregate as is shown in the figures 6.08e-i. The tendency for aggregation is much more pronounced



than without cholesterol. In time the domains become rounded as atmospheric carbon dioxide penetrates into the subphase and reduces the pH. In figure 6.08e the monolayer is compressed to the limiting area and the molecules in the domains are untilted so that no inner structure is observed with an analyser. In this state the aggregated domains, enclosed in a homogeneous matrix of arachidic acid and cholesterol, partially fuse.

When now the monolayer is expanded slightly below the pressure where the molecules become untilted, irregularly distributed patches with different shades of grey appear on the domains, each shade representing a region where the molecules are uniformly tilted in a certain direction in the monolayer plane (f). On further decreasing the surface pressure, i. e. on increasing the tilt angle, some of these patches grow in area and arrange such that a pattern is formed that already indicates the typical segmented inner structure of the domains (g). The process of the arrangement of the molecular orientations is very quick which points to a high mobility of the hydrocarbon chains in this stage. In figure 6.08g one can see that the orientation of the molecules and the segments with respect to the domain boundary corresponds to that of an unimpaird domain, while the boundaries between the segments are strongly curved and not well defined. The straightening of the boundaries between the segments, that proceeds as the monolayer is expanded, occurs more slowly than the formation of the segments (the straightening of a segment boundary in two different domains is illustrated in *g-i*. The defect lines are marked by arrows). This experiment demonstrates that the inner domain structure is not determined by the growth conditions, but corresponds to the state of lowest energy. It seems unlikely that the segment structure before compression to the untilted state is somehow preserved during this state and reappears on expansion.

6.1.4 Influence of Polyethyleneimine (PEI) in the Subphase

In the previous chapters we have seen the effect of the degree of head group dissociation on the morphology of fatty acid monolayers. The effect of the sodium ions, which have to be added for adjusting the pH, is assumed to be negligible. If a solute is in the subphase, that reacts with the fatty acids in the monolayer and interacts with the carboxylate, as is found for polyvalent metal ions or basic polymers, such as PEI, the monolayer properties are affected on the one hand by the binding of the solutes and on the other hand by the dissociation of the fatty acid molecules. Hence, knowing about the effects of dissociation one should be able to conclude on the specific effects of the solute. In 6.1.1 an experiment with barium ions in the subphase was described that indicates strong binding interactions between the ions and carboxylate. Neighbouring head groups are compressed by the ions and the monolayer

molecules forced into the upright position. In this chapter and in 6.3.3 the influence of a dilute PEI solution on fatty acid monolayers is examined.

The polyethyleneimine used is a highly branched water-soluble polymer containing primary, secondary and tertiary amine groups and an average molecular weight of 1800 g/mole [Pol00]. The pH of an aqueous solution of PEI of mM concentration is about 10.

Fatty acid monolayers, that are in the condensed state on water, are fluid and do not exert a surface pressure at large molecular areas, if spread on a dilute solution of PEI at ambient temperature. On compression the surface pressure suddenly increases below a definite area and finally a plateau region is entered, in which condensed phase domains are formed (fig. 6.09) [Chi91a,b].

In contrast to the compression isotherm the plateau pressure of the expansion isotherm strongly decreases with increasing expansion rate (fig. 6.09 a). The tilted/untilted transition pressure of arachidic acid is increased by about 8 mN/m on PEI compared to the monolayer on water. Also the increase of the collapse pressure and enhanced stability against dissolution has been reported for stearic acid on PEI solution [Hwa99]. The increase of monolayer stability has been realised to be the essential effect of PEI.

The domains grown on PEI solution are rather small and it is hardly possible to determine their texture by means of BAM. Deeper insight is obtained by another experimental approach.

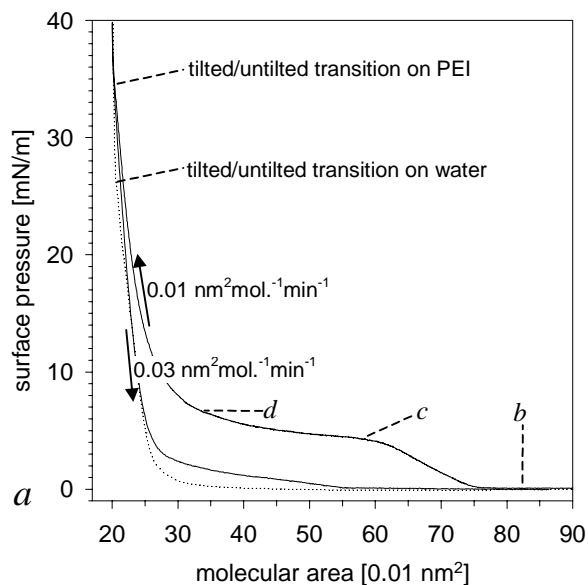
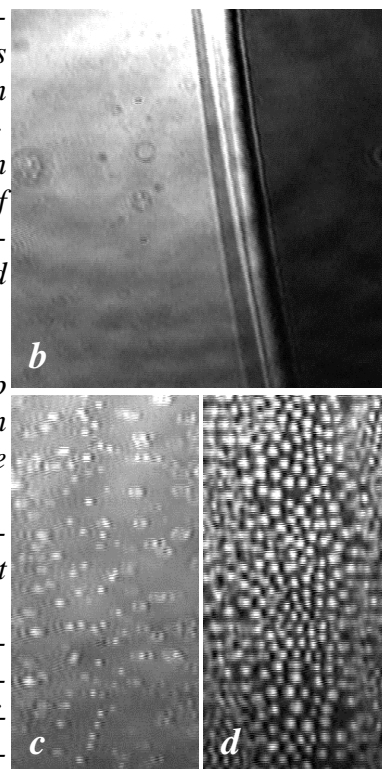


Fig.6.09: (a) Hysteresis of arachidic acid on 1 mM PEI solution at 25°C (for comparison also the isotherm of arachidic acid on water is shown (dotted)). The width of the hysteresis increases with increasing expansion velocity, the compression isotherm is almost unaffected by the velocity.

The bright region in (b) is caused by an inhomogeneous adsorption of a layer of PEI to the fluid fatty acid monolayer.

Small domains develop and grow in the two phase region (c,d). Due to automatic contrast adjustment the background in (c,d) appears with different brightness.



410×410 (b), 140×290 μm² (c,d)

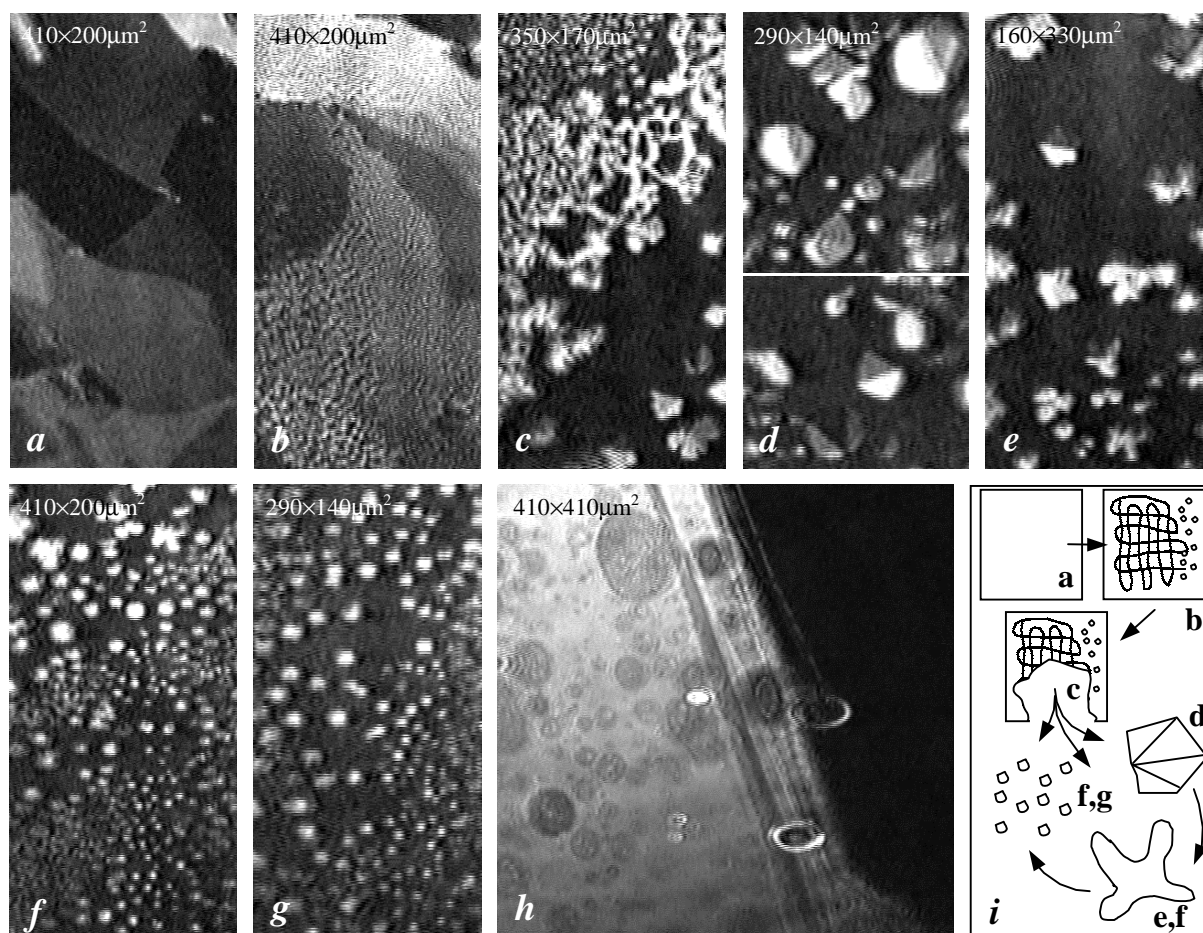


Fig.6.10: Change of a stearic acid monolayer after injection of PEI into the water subphase

A monolayer of stearic acid on water at 25°C is compressed between two Langmuir floats slightly above zero pressure. The entire monolayer is in the condensed state and no fluid phase exists (fig. 6.10 a). Then a concentrated solution of PEI is injected into the subphase behind the barriers. After a while a change in the appearance of the monolayer is observed and an increase of the surface pressure. The contrast between regions of different tilt directions decreases and a fine structuring of the condensed phase is revealed (b). Simultaneously holes emerge in the condensed film, that grow in size. These changes indicate the formation of a two phase region and the conversion of a part of the condensed phase into a fluid phase, while the remaining, initially dense layer of the condensed phase disintegrates into lamellae, that are linked in a network, and into compact domains of different size (c). The large domains are either faceted or of dendritic shape and have textures identical to those observed for arachidic acid at pH 12 (d, e; cf. fig. 6.02 a, b). For the dendritic domains a domain type with four protrusions is predominant. In the course of time the larger domains vanish and finally only very small domains are left in coexistence with the fluid phase (f, g). It seems that the large domains are transformed to the small ones by splitting of the dendritic domains (e, bottom). By this way the domain size becomes more uniform and the same state is reached as

when the monolayer is compressed into the two-phase region on PEI solution (cf. 6.10 g with 6.09 d). This indicates that this state is the equilibrium state. 6.10h shows a piece of the adsorbed polymer layer after expansion to zero pressure. Compared with the state before monolayer compression (fig. 6.09 b) the polymer film contains now many holes. In 6.10h the described morphological changes are depicted schematically.

6.2 Forces Governing Domain Texture and Shape

The peculiar property of an air-water interface to uniformly orient amphiphilic molecules leads to a unique phase behaviour of matter accumulated there. Dipolar interactions, originating from this interfacial asymmetry, contribute to the variety of shapes of domains that emerge in the main phase transition of several monolayer systems. The domain shape often sensitively depends on temperature, chemical composition, the subphase and the relative portions of the two coexisting phases.

There are two independent approaches for interpreting domain features. The first one was derived from the observation by fluorescence microscopy that there are two phases in the coexistence region both of which appeared to be homogeneous and isotropic. It considers the interplay between line tension and electrostatic repulsion [Kel87] and is most similar to the treatment of thin films of a ferromagnetic fluid within a non-ferromagnetic fluid [Lan92]. The second approach [Qiu91, Fis94a] tries to explain the inner structure of domains as detected by polarised fluorescence microscopy and Brewster-angle microscopy and is based on the continuum elasticity theory developed for smectic liquid crystals [Nel80]. A comprehensive theory, however, that is able to account for the various domain types and textures that exist and which combines the elements of both approaches is still to be expected.

6.2.1 Electrostatic Forces

A monolayer consists of an array of dipoles with a component normal to the monolayer plane. In the coexistence region of the main phase transition charge or dipole density of condensed phase domains and fluid phase are different. The dipole interactions in the condensed phase are described by using the resulting dipole density μ , which is the difference between the dipole densities of condensed and fluid phase (see 2.3.3). The free energy of a domain has the form [McC91, Van90]:

$$F = F_{\mu} + F_{\lambda} + F_0 = I\mu^2 + P\lambda + F_0 \quad (6.01)$$

F_{λ} : energy of line tension, F_{μ} : dipole energy, F_0 : remaining energy contributions, μ : differen-

ce in dipole density between fluid and condensed phase, $\mu^2 I$: integral of the electrostatic energy between all dipoles in the domain, I depends on the domain shape and size, P : domain perimeter; λ : (mean) line tension.

The effect of the repulsive dipolar interactions is opposite to that of the line tension. The repulsive interaction between the molecules within a domain favours a large boundary to area ratio, since the electrostatic energy is lowered by separating the molecules from each other. The line energy in contrast tends to keep the boundary line as short as possible and favours the circular shape (fig. 6.11 a). As the electrostatic energy increases faster with domain size than the line energy, the tendency of the domains to deviate from the circular shape increases with increasing domain area. When the electrostatic forces dominate, ellipses [Seu90], stripes [Hec86] or irregular shapes [Lan86] form (fig. 6.11 b). The inverse effect of line tension and dipole forces can be derived from the following consideration:

Let us consider a domain, the shape of which is governed by line tension and dipole repulsion. If line tension and electrostatic forces balance each other and the domain energy is in a minimum, it holds:

$$dF = 0, \quad dF_\lambda = -dF_\mu : \mu^2 dI = -\lambda dP \quad (6.02)$$

The domain shape is defined by the ratio $\lambda/\mu^2 = -dI/dP = c$ (c is a constant).

If now μ or λ changes, the domain will relax and change its shape until line tension and electrostatic forces have again equilibrated and $dF=0$. The first state may be described by $\lambda/\mu^2 = cI$, the second one with a new μ' and same λ as $\lambda/\mu'^2 = cI$ with $\mu' = a\mu$ (a is a constant factor). The same state may also be obtained by changing λ and keeping μ fixed. Thus a change of μ by a is physically equivalent to a change of λ by I/a^2 .

Besides acting within a domain the dipole forces also lead to long range repulsion between domains. This manifests in an increased order of the spatial distribution of the domains (formation of a hexagonal superlattice [Lös88] (fig. 6.12)) and in a lowered tendency for domain aggregation or fusion.

What is the molecular origin of λ ? The thermodynamic definition of λ is

$$\lambda = \left(\frac{dG}{dP} \right)_{\pi, T} = \left(\frac{dH}{dP} \right)_{\pi, T} - T \left(\frac{dS}{dP} \right)_{\pi, T} \quad (6.03)$$

Where λ is the energy G for increasing the domain boundary by a unit length, i. e. for transferring a certain number of molecules from the domain bulk to the perimeter P . The main contribution to λ should afford the enthalpy term, since the translational and conformational freedom of the molecules is not expected to be very different in the bulk and at the interface.

The enthalpy term reflects the energy for breaking bonds and transferring molecules to the interface. An approximate relation between λ and the fluid-condensed phase transition enthalpy ΔH_{LE-LC} is obtained by assuming proportionality between the surface of a molecule and the bonding enthalpy: $\Delta H_{LE-LC}/N_L \approx \pi d \lambda$ (N_L : Loschmidt number, $\Delta H_{LE-LC}/N_L$ corresponds to the bonding enthalpy of a molecule, πd : perimeter of a cylinder) [Mul91]. Proportionality between the surface of a molecule and the bonding enthalpy is reasonable to assume for isotropic bonding forces, such as van-der-Waals forces. A linear relationship between surface tension and heat of evaporation is observed for various substances. That is evident especially from *n*-alkanes, where the number of carbon atoms is proportional to the heat of evaporation as well as to the surface tension [Bir97].

Finally a note how the electrostatic repulsion of charged molecules is taken into account. At high ionic strength, as is the case in the experiments at high pH, the charges of the monolayer molecules are strongly shielded by the counter ions. Charges and counter ions form dipoles (cf. fig. 4.07) and the Coulomb interactions between the charges are replaced by the weaker interactions between dipoles. At low counter ion concentration Coulomb repulsion prevails and charged domains cannot be described by equation 6.01 [And87].

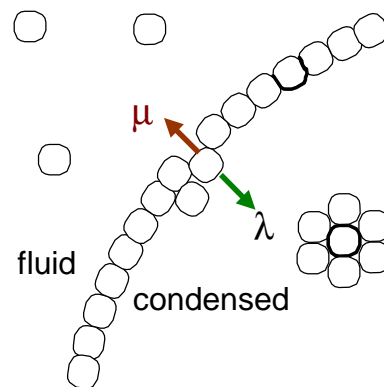
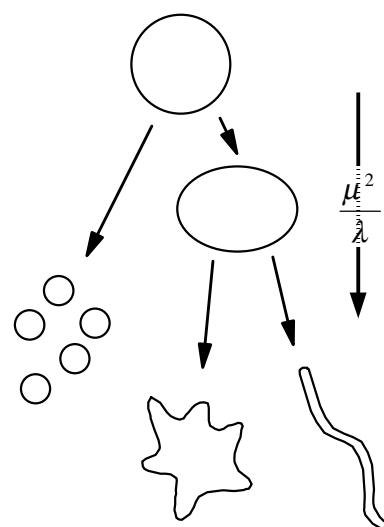


Fig.6.11: (a) Opposite effect of line tension and dipole forces.



(b) The electrostatic forces favour a large boundary to area ratio of the condensed phase. A certain domain shape as the result of the action of μ and λ is defined by the ratio μ^2/λ . image fr. [Seu95]

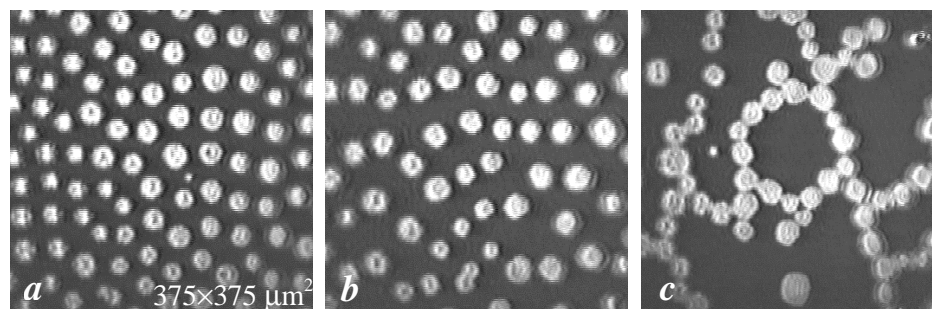


Fig.6.12: 'superlattice' formation (a, b) and domain aggregation (c) in an arachidic acid monolayer at high pH. There are more defects in the

superlattice at pH 12.3 (b) than at pH 12.0 (a) (cf. 3.2.2.2 and fig. 3.06). At pH 12.3 also the tendency for aggregation is higher than at pH 12.0. Due to the electrostatic repulsion the domains aggregate in rows and form loose networks in the lapse of time at pH 12.0 and at pH 12.3(c) (cf. stripe formation of single domains, fig. 6.11 b)

6.2.2 Forces Determining Domain Texture

Regarding the texture one may write for the energy of a domain

$$F = \int \left\{ \frac{K_s}{2} (\nabla \cdot \mathbf{c})^2 + \frac{K_b}{2} (\nabla \times \mathbf{c})^2 \right\} dx dy \mathbf{(1)} + F_{def} \mathbf{(2)} + L\varepsilon \mathbf{(3)} + \oint \lambda dl \mathbf{(4)} \quad (6.04)$$

The numbers in brackets behind each energy term denote the part of the domains in figure 6.13, the energy of which is described by the corresponding term.

The curled brackets of the first expression contain the two second order terms of the Landau-expansion for describing the bulk elasticity. It accounts for the energy cost of distortions in long range tilt order (cf. fig. 3.12). This expression was originally applied to textures in smectic liquid crystals [Lan86] and it is also consistent with the symmetry of monolayer phases [Riv95]. $\nabla \cdot \mathbf{c}$ is a splay distortion (for definition of \mathbf{c} see fig. 3.08). A splay motif would be if all the molecules are tilted along the radial directions emerging from the centre of a circle with all chain ends pointing into the same direction. The motif of $\nabla \times \mathbf{c}$, the bending distortion, is a set of concentric circles where all molecules are uniformly aligned on the circumference. In domains both motifs are often superimposed. The first order term for splay is allowed for Langmuir monolayers, not for smectic liquid crystals due to broken inversion symmetry in monolayers. For systems large compared to molecular size higher order terms can be neglected. The linear term for splay can be included in the line energy via Gauss law and that for bending is zero for achiral molecules (since the rotation changes sign when aligning the molecules once clockwise and once counterclockwise on the circle of the bending motif mentioned, where there should be no energy difference for achiral molecules). The factors K_s and K_b are a measure of the elasticity of the phase. The most favourable state is reached when all molecules are aligned parallel, where the expression becomes zero (fig. 3.12 a).

F_{def} is the energy of the defect core, which is mostly found in the middle or at the edge of a domain. It is energetically

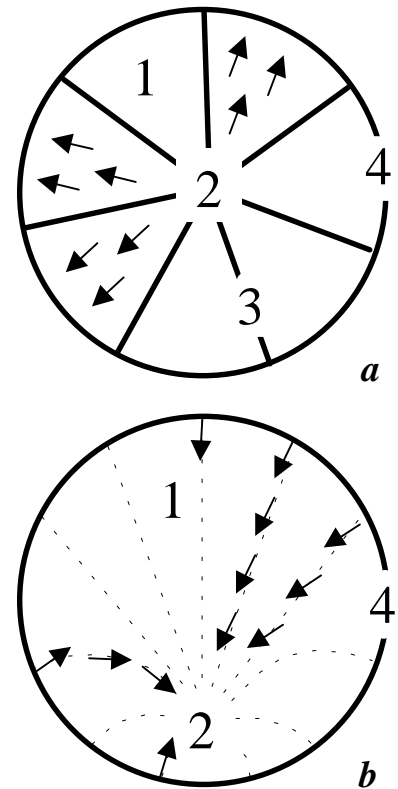


Fig. 6.13: Two textures representing basic features encountered in monolayer domains. A domain with segments of uniformly aligned molecules (a) and a boojum pattern as observed for pentadecanoic acid with splay and bending and without defect lines (b); the numbers refer to the energy terms in eq. 6.04

unfavourable compared to regions with uniform tilt [Lan86] and F_{def} certainly depends on the number of defect lines crossing in this point [Fis94a].

The energy of the defect lines is proportional to the overall length of the defect lines L (term 3). In continuum elasticity theory [Fis94a] it is assumed that the pseudohexagonal lattice continues across the boundary between two segments of different tilt. The defect arm is considered as a narrow region where the tilt azimuthal angle has to pass several energy minima, when it jumps to exactly 60° corresponding to the angle between neighbouring hexatic bond directions. However, as there have been observed numerous domains, the inner structure of which does not comply with this theory (jumps in angle at the segment boundary different from 60°) and owing to the observation that a fluorescence dye, added in small amount to the spreading solution, accumulates between the segments of a methyl ester at low temperature [Qiu91], it might be more reasonable to assume that the segment boundaries correspond to grain boundaries with high defect concentration, so that the lattice correlation is weak. While the bond order might be short ranged near to the boundary, the tilt orientational order continues to exist. At the segment edge the molecules abruptly change their orientation and create a sharp boundary line. Its energy may depend on the angle between \mathbf{c} and the tangent to the boundary or on the change in \mathbf{c} between two neighbouring segments.

Term 4 is the energy of the closed boundary line of the domain. The line tension λ is developed into a Fourier series ($\lambda(0) = \lambda(2\pi)$)

$$\lambda = \lambda_0 + \lambda_1 \cos \varphi + (\lambda_2 \cos 2\varphi + \dots) \quad (6.05)$$

λ_0 is the isotropic, λ_1, λ_2 are anisotropic line tensions (λ in eq. 6.01 is averaged over the entire boundary). It appears that line tension anisotropy is sufficiently described by the first angle dependent term (see chapter 6.3.4, [Hen93]). The angle φ gives the orientation of the molecules at the boundary with respect to the boundary line. The sinus terms are omitted, since there is no difference in line tension if the molecule is tilted to one side (φ_1) or the opposite side ($-\varphi_1$) of the surface normal when chiral interactions are absent.

In segmented domains investigated so far the molecules tend to be oriented either perpendicular (fig. 6.13 a, b; [e.g. Hen93, Ove94, Fis94a, deM98, Wei98a,b]) or parallel [e.g. Lan86, Fis94b, Fis96, Wei98a,b] to the domain boundary. Neglecting the higher anisotropy terms and expressing φ by the product between the unit vectors \mathbf{c} , \mathbf{n} and \mathbf{l} (unit vector of boundary tangent) equation 6.05 adapted to the different cases is:

- preferred molecular orientation perpendicular to the boundary and towards the domain centre (cf. fig. 6.13 b): $\lambda = \lambda_0 + \lambda_1(\mathbf{cn})$,

towards the domain boundary (cf. fig. 6.13 a): $\lambda = \lambda_0 - \lambda_1(\mathbf{cn})$

- preferred molecular orientation parallel to the boundary:

$\lambda = \lambda_0 - \lambda_1(\mathbf{cl})$, where \mathbf{c} and \mathbf{l} are equally oriented.

Anisotropic line energy therefore arises from the deviation of the orientation of the molecules at the domain boundary from a preferred orientation with respect to the boundary line. The reason for the preference of a certain orientation is not yet clear.

The dominance of the boundary energy increases with domain size as the gradient terms in term 1 scale independently of the radius. According to simulations of the pentadecanoic acid boojum texture by Loh and Rudnick [Loh98] the experimentally observed shape can be explained by line tension anisotropy alone. The relative values of K_s and K_b seem to be of minor importance. Rivière and Meunier [Riv95] found for the boojum a higher value of K_s than K_b , despite almost only splay and little bending is observed (fig. 6.13 b). From this they concluded on the prominent role of the boundary conditions.

The equilibrium texture, of course, corresponds to the minimum of F . So some qualitative conclusions on the development of domain textures can be drawn:

with regard to bending energy a domain has the lowest energy, when the tilt direction of the molecules is the same all over the domain. The line tension anisotropy, however, tends to orient the molecules at the boundary, say normal to it. If the boundary energy is large enough, bending in the molecular orientations in the bulk is produced causing an increase in the elastic energy. A boojum pattern is formed (fig. 6.13 b). If the phase however is too rigid, i.e. K_s and K_b are too high, then a solution appears to be the division of the domain bulk into segments, in each of which the tilt direction is uniform. The cost in energy for the creation of defect lines and a defect core is compensated for by the reduction of elastic strain in the bulk and by more favourable boundary conditions. If the defect core is at the domain edge, its energy as well as the overall length of the defect lines are smaller than in domains, where the defect core is in the domain middle. Furthermore, if the defect lines arise from a point at the domain edge, the angles between neighbouring defect lines, which are usually equal [Hen93], are not restricted in their value as in domains, where the defect core is in the centre. On the other hand the anisotropic boundary energy is smaller in domains with centred defect cores because of a smaller deviation of the molecular orientation at the domain boundary from the preferred parallel or perpendicular orientation.

It appears that the commonly encountered textures of segmented domains develop from a domain with initially uniform tilt direction and no segments somewhere during the growth process by a successive increase of the number of segments. This process is driven by the

anisotropy of boundary energy, which decreases with increasing number of segments. That in a monolayer often several textures coexist may have its origin in the small energetic difference of the textures, which are not only determined by boundary anisotropy, and in kinetic effects. In figure 6.14 a way for the evolution of common texture types is proposed.

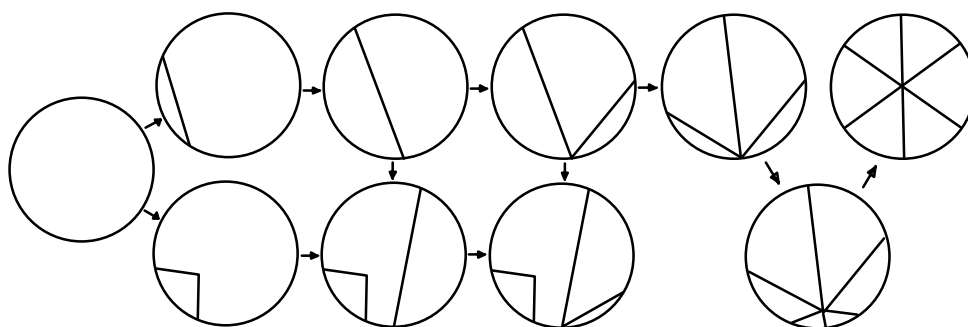
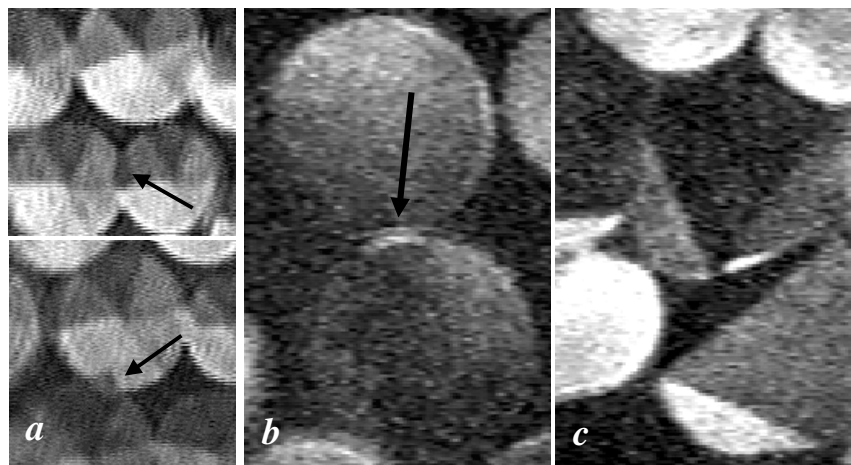


Fig.6.14: Suggested evolution of domain textures leading to textures with 2, 3, 4 and 6 segments of uniform tilt direction. It should be energetically most favourable when the different segments start to develop from a common point at the domain edge.

Figures 3.18, 6.08, 6.15 demonstrate the ease with which the molecules in a domain can change the tilt direction.

Fig. 6.15: When domains get into contact, sometimes a change of the tilt direction of the molecules in the contact region is observed (a, b). With the segmented domains of stearic acid at pH 11.0 (cf. fig. 6.01 c) a small segment is formed in the contact region between two domains (a). The tilt direction in this segment equals that in a segment neighbouring the initially contacting segment.



This indicates that the adopted tilt directions in a domain are the energetically most favourable ones with the lowest defect line energies. In the upper image of (a) (and possibly also in the lower one) the new segment extends over both contacting domains, which have fused by this way [Joh99a].

When a monolayer of palmitic acid (on 0.1M brine, 29°C) is compressed until the domains are in tight contact, the domains, having a boojum pattern when separated (b), adopt segmented structures (c). This implies that the anisotropic boundary energy decreases, the bulk elastic constants increase, or the energy of the defect lines decreases. I think, that especially the boundary energy is affected, when instead with a fluid phase the domain boundary is in contact with condensed phase or a thin region of fluid phase enriched with possible impurities. On the other hand one has to take into account the increase of pressure at the plateau end, which will affect the bulk properties.

115×115μm² (a), 165×245μm² (b,c)

6.3 Explanation and Interpretation

6.3.1 On the Effect of pH

In 6.1.1 we have seen, that increasing degree of dissociation of the condensed phase domains (the fluid phase is already completely dissociated (5.2.1, 5.2.2)) leads to the increase of the ratio of domain perimeter to domain area, to the decrease in the regularity of the domain distribution and to the decrease in the range of tilt orientational order. Increasing ratio of domain perimeter to domain area manifests on the one hand in the decrease of compactness and regularity of the domain shape and on the other hand in the decrease of the average domain size.

The increase of the boundary length per area of the condensed phase can be explained as resulting from either the increase of the electrostatic repulsion μ or the decrease of the line tension λ with increasing pH (6.2.1). The difference in dipole density between condensed and fluid phase $\mu = \mu_{fl} - \mu_{LC}$ is related to the difference of the surface potentials of fluid and condensed phase by $\Delta V_{fl} - \Delta V_{LC} = \mu / (\epsilon \epsilon_0) + \Psi_{0,fl} - \Psi_{0,LC}$ (eq. 4.07). The difference $\Delta V_{fl} - \Delta V_{LC}$ can be determined from surface potential measurement. ΔV_{fl} is the surface potential at A_{fl} and ΔV_{LC} is obtained by linearly extrapolating the tangent on the surface potential curve at A_{fl} to A_{LC} ($\Delta V = \Delta V_{fl} + x_{LC}(\Delta V_{LC} - \Delta V_{fl})$, eq. 4.08) [Mil87]. The potentials $\Psi_{0,fl}$ and $\Psi_{0,LC}$ cannot be determined directly. They might be approximated as $\Psi_0 = \sigma l / (\epsilon \epsilon_0)$ (Debye-Hückel-approximation), which corresponds to the assumption of a layer of dipoles from carboxylate and counter ions separated by the distance l beneath the monolayer (fig. 4.07 b) and which allows to express Ψ_0 in the form of a dipole density $\mu' = -\sigma l$.

Figure 6.16 shows the surface potential isotherms for pH 12.0 and 12.7. At $A > A_{fl}$ ΔV_{fl} decreases with decreasing mean molecular area. This is rarely observed, since the molecular density increases (4.2.3). The decrease in ΔV_{fl} can be explained by the reduction of $\Psi_{0,fl}$ (increase of $-\Psi_{0,fl}$, fig. 5.07 b) with diminishing area. Besides Ψ_0 also a decrease in μ_{fl} , caused by reorientation of the molecules, of the head groups or of the interfacial water molecules, may contribute to the decrease in ΔV_{fl} . The tangents to the potential curves at A_{fl} have zero slopes in both cases, which implies that $\mu + \mu' = 0$ within the resolution limit for ΔV of 10mV. From calculation according to the Gouy-Chapman-Stern theory (5.2.2) one obtains, that $\Psi_{0,fl} - \Psi_{0,LC} = +30\text{mV}$ for $c(\text{MX}) = 0.01-0.03$ (pH 12.0-12.7), $A_{fl} = 0.70 \text{ nm}^2/\text{mol.}$, $A_{LC} = 0.20 \text{ nm}^2/\text{mol.}$, $D_{H,fl/LC} > 0.9$. As $\Delta V_{fl} - \Delta V_{LC} \approx 0$ this suggests that $\mu_{LC} > \mu_{fl}$.

The order of the domain ‘superlattice’ is a measure for the electrostatic repulsion between the domains and the fact that it decreases with increasing pH indicates the decrease of an obviously present but not resolved excess dipole density of condensed or fluid phase.

The drastic change of domain shape and the decrease in domain size with increasing pH can therefore only be caused by the decrease in λ . The plateau width in the isotherms decreases with increasing pH (fig. 5.06). Regarding the equivalence of T and pH, according to eq. 4.05, ΔH_{fl-LC} and hence λ (see 6.2.1) decrease with increasing pH. The decrease in the chain bonding energy and λ can be inferred from the increase in the molecular tilt angle (cf. eq. 3.05) with increasing pH as is revealed by GID (app. VI).

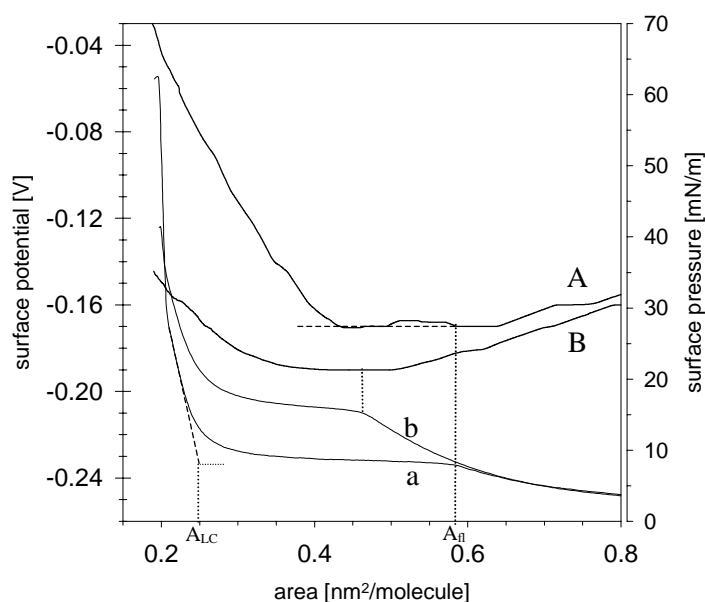


Fig.6.16: Surface potentials (upper curves) and π -A isotherms of arachidic acid at pH 12.0 (A, a) and 12.7 (B, b) at 20°C. $\Delta V_{fl}-\Delta V_{LC}$ is determined by linearly extrapolating the tangent on the surface potential curve at A_{fl} to A_{LC} (sketched for A) [Mil87]. A_{fl} is the molecular area of the fluid phase at the onset of the plateau, and A_{LC} , the molecular area of the condensed phase, is obtained by extrapolating the steep part of the isotherm at low molecular area to the onset plateau pressure; compression rate: $0.015 \text{ nm}^2 \text{ mol}^{-1} \text{ min}^{-1}$

6.3.2 On the Effect of Temperature

A decrease in temperature has been observed to result in an increase in the ratio of domain perimeter to domain area and in a decrease of the range of tilt orientational order just like an increase of the pH value (6.1.2).

λ is expected to increase with decreasing temperature. With *n*-alkanes, alkenes and alkanols it is found that the surface tension $\tau \propto -T$ over a range of several hundred °C [Bir97]. λ should be proportional to the fluid-condensed phase transition enthalpy, which decreases linearly with increasing temperature (fig. 6.17, see discussion in 6.2.1).

The difference in the mean molecular areas of the coexisting phases $A_{fl}-A_{LC}$, i. e. the difference in the molecular densities of the phases increases inversely with decreasing tempe-

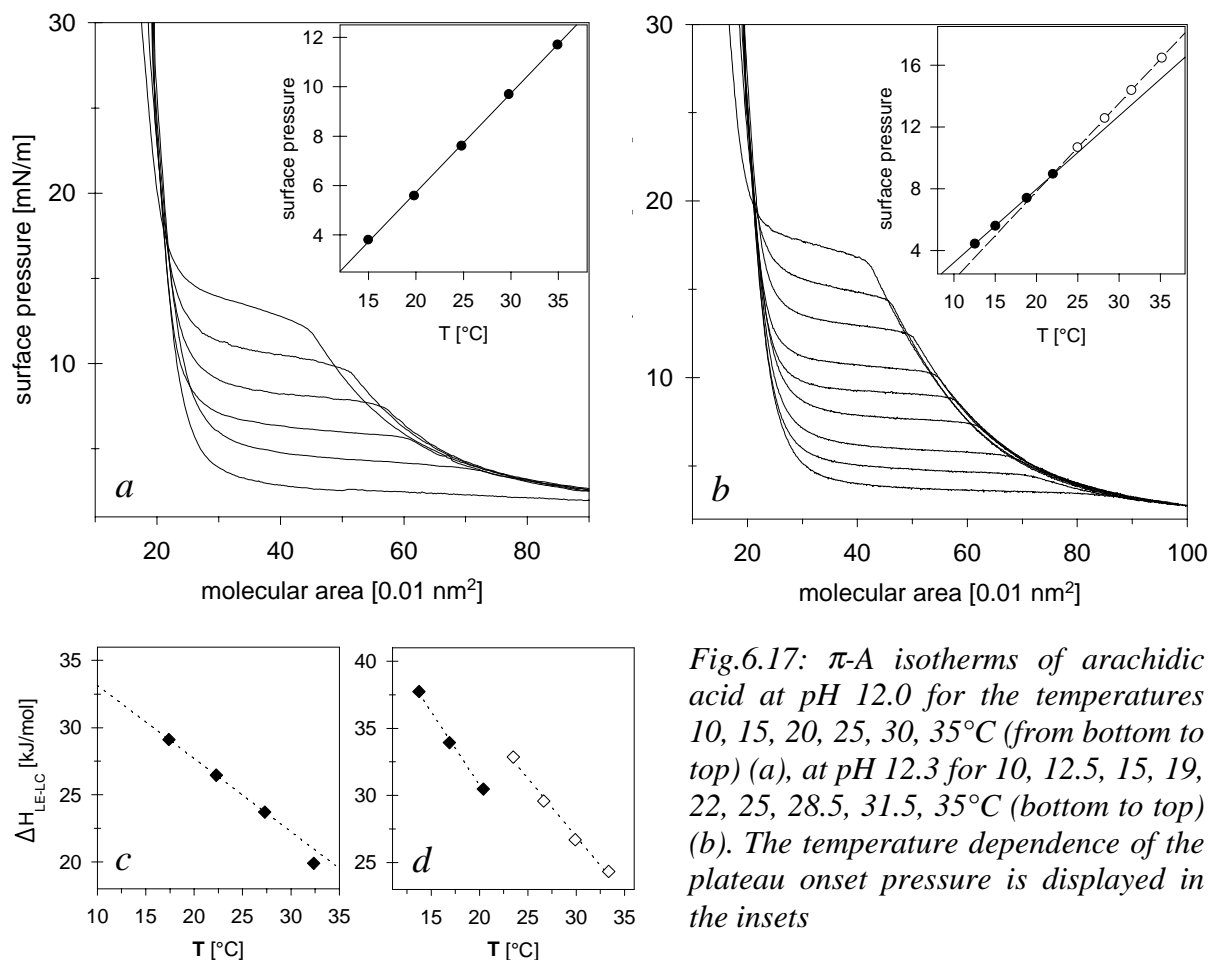


Fig.6.17: π -A isotherms of arachidic acid at pH 12.0 for the temperatures 10, 15, 20, 25, 30, 35°C (from bottom to top) (a), at pH 12.3 for 10, 12.5, 15, 19, 22, 25, 28.5, 31.5, 35°C (bottom to top) (b). The temperature dependence of the plateau onset pressure is displayed in the insets

Enthalpy difference between fluid (LE) and condensed phase (LC) ΔH_{LE-LC} . derived from the isotherms by means of eq. 4.05 for pH 12.0 (c) and pH 12.3 (d). If the enthalpy of the LE phase is assumed to vary continuously with the temperature, (d) indicates different enthalpies and therefore different phases of the condensed phases below and above 20°C (figs. 6.05 c and 6.02 b). The areas of the condensed phase determined from the isotherms are not the exact values as determined by structure analysis, so that the evaluated ΔH values should not be taken quantitative

perature ($A_{fl}-A_{LC}\sim 1/T$). Consequently μ increases with decreasing temperature, provided that the changes of the molecular dipole moments with temperature are negligible or the same in both phases. The morphological changes observed on lowering the temperature can therefore be explained as being due to the increase of the repulsive dipolar forces, which scale with μ^2 and outweigh the linearly increasing line tension.

The prerequisite for arguing with these forces is the presence of equilibrium domain shapes. It is well known that number, size and the shapes of domains can strongly depend on the growth conditions [Hel88, Wei97b]. Proof, that the condensed phase morphology, produced by growth, is the equilibrium morphology, is provided by the reversibility of shape transformations under non-growth conditions and the independence of the morphology of the

compression rate (6.1.2, 6.3.4). The decrease in size and consequent increase in number of the domains with decreasing temperature at pH 12.0 is also conceivable to be due to the increase of the nucleation rate. However, the proportionality between critical nucleus size, which governs the nucleation rate, and the line tension also suggests a higher μ , which corresponds to a smaller effective λ , for the lower temperature [Hel88].

The plot of the plateau onset pressures versus temperature yields a discontinuity between 20 and 25°C for pH 12.3 (fig. 6.17 b, inset). This is also reflected by the derived phase transition enthalpies ΔH_{fl-LC} . This discontinuity indicates a phase change, that could be induced by too strong electrostatic repulsive forces and be the reason for the drastic change in the appearance of the condensed phase. However, by the comparison of data from X-ray analysis for pH 12.0 at 15°C and 25°C on the one hand and of 15°C and 25°C at pH 12.3 on the other no severe difference is revealed (tab.VI.1, app.).

The range of tilt orientational order in the domains in figure 6.05b, which look like aggregates of many very small domains, is reduced to the size of the segments of the small domains. The range of tilt orientational order decreases with increasing μ , which leads to the reduction of the intermolecular attractive interactions and as a consequence to the reduction of the size of the condensed phase domains. Very similar domains are formed on increasing the pH, where also a decrease of the intermolecular attractive interactions is assumed (6.3.1).

Examining the morphological features of a dissociable monolayer we have seen, that in contrast to the phase behaviour (fig. 5.06) the increase of the pH corresponds to the decrease of temperature. This is, because domain texture and shape result from the balance of forces, exhibiting a temperature and pH dependence different from that of phase transition energies.

6.3.3 On the Influence of PEI

PEI dissolved in mM concentration in water gives a weakly basic solution of pH \approx 10. Fatty acids spread on a solution of this pH without PEI dissolve or show the same behaviour as on water. Since the behaviour on PEI solution is different, there must be specific interactions

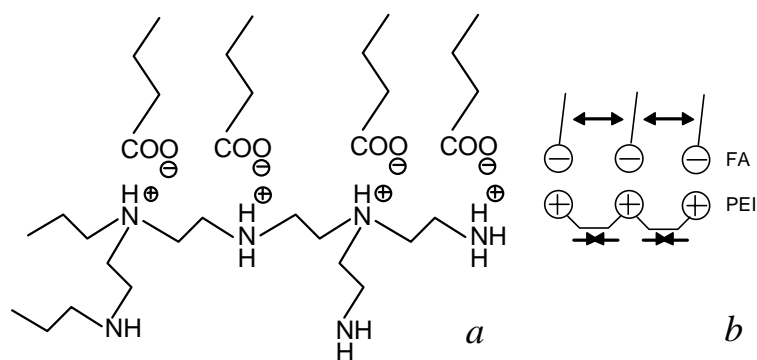


Fig.6.18: The stretched polymer is bound to the fatty acid monolayer of opposite charge by electrostatic forces

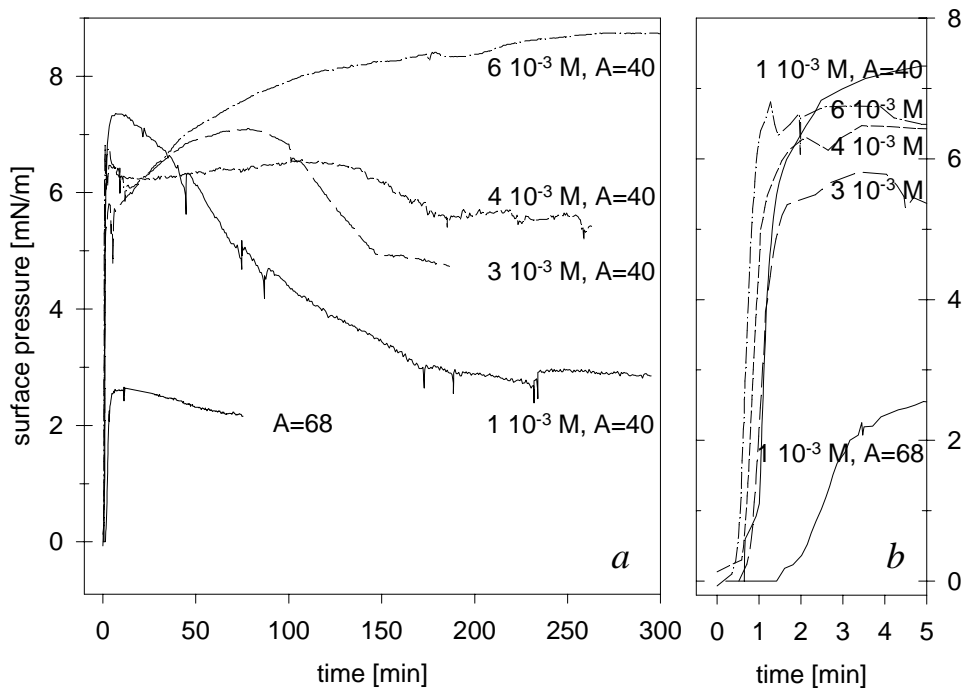


Fig.6.19:
Variation of
surface pressure
during adsorp-
tion of PEI onto
a monolayer of
arachidic acid
for various PEI
concentrations,

A: mean molecu-
lar area between
fixed barriers

between PEI and the fatty acids in the monolayer. Figure 6.09b provides evidence that PEI adsorbs onto the monolayer as a thin layer. The amino groups of the PEI will react with the fatty acids under salt formation according to figure 6.18a. The PEI molecules become highly charged, so that at low ion concentration in the solution they adopt a stretched and rigid conformation and the adsorbed polymer layer is only thin [Vor98]. The interaction between the fatty acids and PEI depends on the subphase pH. It is strongest, when the number of ammonium and carboxylate is equal, which is the case at about pH 10 [Ha99]. In figure 6.09b one can see that at zero pressure the polymer adsorbs only to a part of the monolayer with homogeneous thickness, while other parts seem to be completely free of polymer (dark region). The reason for this may be, that the polymer adsorption is initially confined to the patches of condensed phase, that appear after spreading, as their molecular density is much higher than that of the gaseous phase.

The question arises about the strength of interaction between polymer and monolayer. Is the interaction so strong, that structure, morphology and phase behaviour of the monolayer are determined by the polymer or does the polymer only provide a high degree of dissociation of the monolayer, which then behaves just like at high pH? This question might be elucidated by comparing the influence of PEI with that of a base in the solution.

At high pH the surface pressure of the fluid phase approaches zero asymptotically and is above 2 mN/m below $1 \text{ nm}^2/\text{mol}$. (fig. 5.06). On PEI solution, on the contrary, the pressure of the fluid phase is zero at large areas and increases abruptly at a certain point (fig. 6.09 a). The

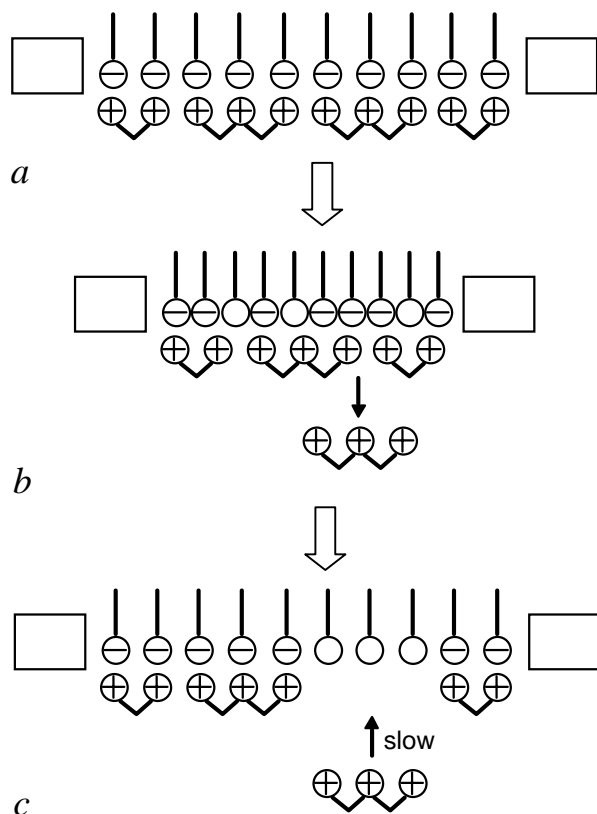


Fig.6.20: At large separation of the monolayer molecules in the fluid phase for each molecule in the monolayer there is a counter charge in the polymer film (a, fig. 6.18). Reducing the area the polymer is too rigid to adjust to the change in area and PEI molecules are ripped off the monolayer and diffuse into the subphase. The charge density of the remaining adsorption layer is lower than the molecular density in the monolayer, so that a portion of the monolayer is undissociated (b). The degree of dissociation decreases with decreasing area, which leads to the increase of the structural order in the monolayer (fig. 6.21). When the monolayer is now quickly expanded, the surface pressure decreases and a hysteresis results in the isotherm, because of the reduced charge density in the monolayer. The filling of the gaps in the polymer layer by PEI molecules from the subphase proceeds so slowly, that holes remain in the expanded film (6.10 h)

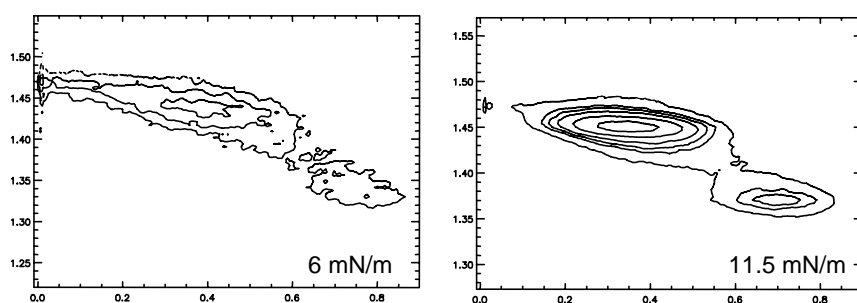


Fig.6.21: Diffracted intensity plots of an arachidic acid monolayer on 1 mM PEI solution, 25°C

repulsion between the molecules in the fluid phase, which is responsible for the finite pressure, is possibly neutralised on PEI solution, because the monolayer molecules are linked by the adsorbed polymer network (fig. 6.18 b).

On compression the surface pressure increases and passes over to a plateau region, at the onset of which domains nucleate (fig. 6.09 c). If, in a multicompart ment trough (fig. 4.01), an arachidic acid monolayer is spread on water subphase and then transferred on PEI solution, the pressure rises very rapidly at the beginning and then varies with time in a non-reproducible way (fig. 6.19). The value of the initial pressure increase depends on the fixed mean molecular area and coincides with the corresponding pressure in the isotherm. The quick initial pressure increase is reproducible and hardly dependent on the PEI concentration for a definite fixed area (fig. 6.19 b). It reflects the adsorption process and the reaction of the

polymer with the monolayer. It is reasonable to assume that the pressure increase is caused by the electrostatic repulsion due to the dissociation of the fatty acid amphiphiles. A penetration of the very hydrophilic PEI into the monolayer is unlikely. The further slow changes in the pressure with time probably reflect changes in the degree of monolayer dissociation due to reorientations of the adsorbed polymer and the penetration of atmospheric carbon dioxide into the subphase.

That the essential effect of PEI is to ionise the fatty acid monolayer is confirmed by the morphological changes occurring on polymer adsorption. The boundary between fluid and condensed phase is elongated considerably by the formation of lamellae and small domains from an initially dense condensed monolayer (fig. 6.10). In an intermediate stage relatively large faceted domains develop, which are the same as those observed at pH 12.3 (cf. figs. 6.10 d, 6.02 b). This indicates that the coupling between PEI and fatty acid monolayer is loose and that the adsorbed polymer layer produces a degree of dissociation, that is comparable to that on an alkaline subsolution of pH near 12.3. Atomic force microscopy experiments of Chi et al. [Chi98] indicate that the small domains in the figures 6.09d, 6.10g are faceted and have the same textures as the larger domains resolved by BAM. However, the assumption of the authors that this texture originates in specific PEI-fatty acid interactions cannot be supported, since the same textures appear on alkaline subphase without PEI. The morphological changes of the fatty acid monolayer, that are observed during PEI adsorption are based on the increase of the ratio μ^2/λ (cf. figs. 6.10 i, 6.11 b).

That the interaction between positively charged polymer segments and dissociated fatty acid molecules is only weak and that the structure of the monolayer is hardly determined by the polymer, but mainly by the degree of dissociation, is evident from the coincidence of the structural parameters for arachidic acid on PEI and at high pH (app VI, cf. figs. 6.04, 6.21).

A hysteresis of the expansion isotherm, that is observed with PEI, is not observed at high pH. This fact suggests at the first sight an influence of PEI exceeding that of changing the degree of dissociation. There are, however, indications, which allow to interpret the appearance of the hysteresis just as to be due to a decrease in the degree of dissociation. A model for the process leading to the hysteresis is presented in figure 6.20.

6.3.4 Faceting of Monolayer Domains

There are several examples of monolayers, which form domains with sharp edges and corners, that look like two dimensional crystals with facets (arachidic acid on PEI [Chi98], sodium dodecyl sulfate [Fle91, Ber91], 1-0-hexadecylglycerol (racemate and enantiomer) [Rie93, Bre94, Geh96, Vol96], 1,2-hexadecanediol [Wei97a], fatty acid methyl esters [Fis94b, Fis96], 1-hexadecyl-2-(2-tetradecyl-palmitoyl)-glycero-3-phosphocholine [Die91, Die94], *S*-1-palmitoyl-glycerol in heptane atmosphere [Har98]). Facets usually reflect a regular lattice and long range positional order, which, however, is not possible in one or two dimensions (see 3.2.2.1). Their appearance in disordered systems like monolayers is therefore not yet completely understood [Ho92]. In this section the faceting of three selected monolayer systems is investigated, that form polygonal domains under different experimental conditions and an explanation for facet formation is offered, that relies on the fundamental forces in domains discussed in 6.2.

6.3.4.1. Variation of an Arachidic Acid Monolayer with pH

When the pH of the subphase of an arachidic acid monolayer is increased from 11.7-12.0 to 12.3 polygonal domains grow with sharp corners and edges, that are straight or have a relatively low curvature (fig. 6.22, 6.02 a-c).

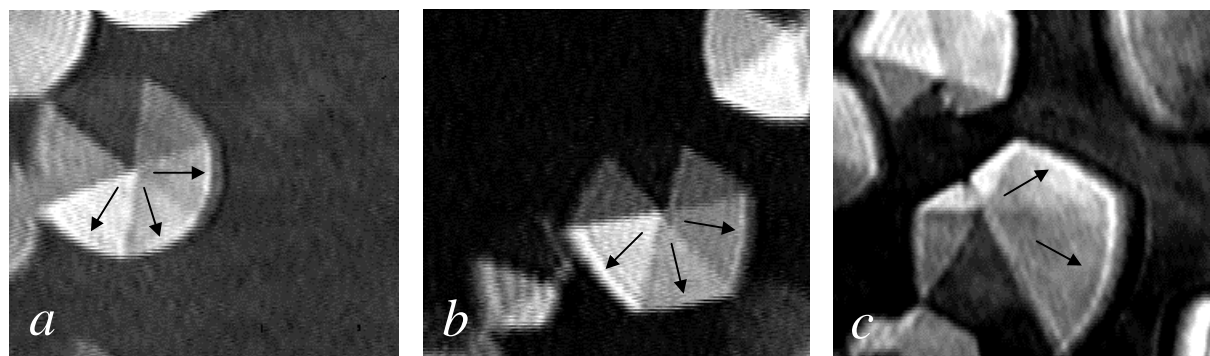
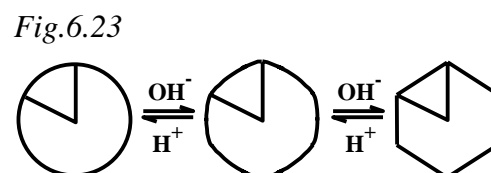


Fig.6.22: Domains of arachidic acid grown on alkaline subphase at pH 12.0 (a), pH 12.3 with hexagons and pentagons coexisting (b,c). The molecular tilt direction is along the bisector in each segment (arrows); 25°C; 165×180 μm^2

If a regular hexagon is formed from a circle, the perimeter extends by 5%. It has been discussed previously that a decrease in λ with increasing pH seems to be the reason for this increase in boundary length accompanying the shape transformation (see 6.3.1).

In order to explain the domain faceting as the result



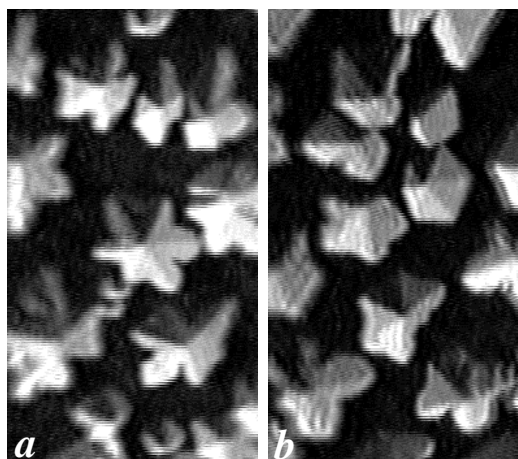


Fig.6.24: Relaxation of the dendritic non-equilibrium shapes of arachidic acid at pH 12.3 into the faceted equilibrium shape (a to b); 25°C; 290×160 μm²

of the action of different forces, one has to ensure, that the faceted shape is an equilibrium shape and not produced by anisotropic growth. This condition can be proven by two ways. In the first case domains are grown at pH 12.0 or 12.3 and the monolayer is kept in the two-phase region at fixed area. When now the pH of the subphase is slowly increased or reduced by the addition of base or acid, a gradual and reversible transformation between rounded and faceted shape can be observed with variation of pH (fig. 6.23). In the second case the kinetic behaviour of the monolayer is investigated. At highest compression

rates ($\geq 0.7 \text{ nm}^2 \text{ mol}^{-1} \text{ min}^{-1}$) dendritic domains are obtained (fig. 6.24 a). The relaxation into the compact faceted shape, which is driven by a decrease in the line tension and in the energy of the defect lines, needs about 20 sec (b). The fact, that the relaxation stops with the faceted form, indicates that this represents an equilibrium state. When the film is left to stand for some hours, the degree of faceting continuously decreases and finally the circular form is recovered due to the neutralisation of the subphase by atmospheric CO_2 .

It is noticed that during the extreme compression and relaxation conditions, where the domains change their size and shape within shortest periods of time, the texture is always perfectly developed like upon entering the plateau at low rate. This indicates that the process of setting up the inner domain structure, i.e. the set up of the long range tilt order and arrangement of the defect lines, is governed by strong forces producing the equilibrium texture (see also fig. 6.08 f-i).

6.3.4.2 Variation of a Monolayer of Heptadecanoic Acid Methyl Ester with Temperature

Circular domains of the ester, to which 0.8 mol% of cholesterol was added, were grown at 32°C and then cooled down to 27°C. Within only two degrees from 29 to 27°C faceting became more and more pronounced and eventually dendrites emerged along the segment boundaries, while the domain stretches. The dendrites and the domain body distort to fine stripes from which further arms sprout (fig. 6.25 a-e).

The transformation is completely reversible and upon heating the droplets and their texture are reformed. The temperature range of shape transformation depends very sensitively on the

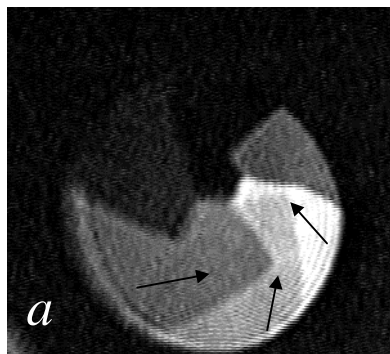
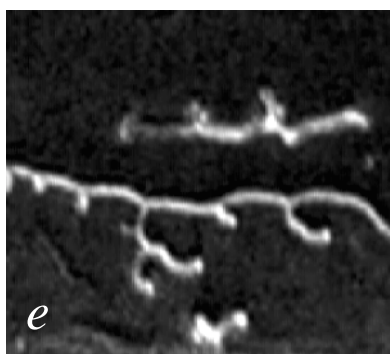
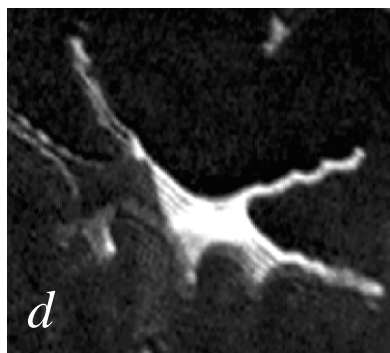
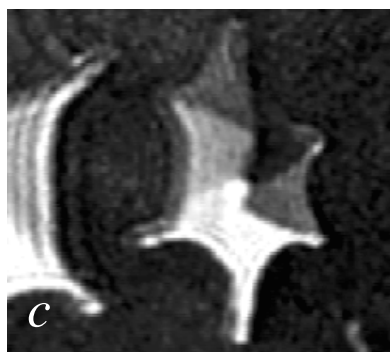
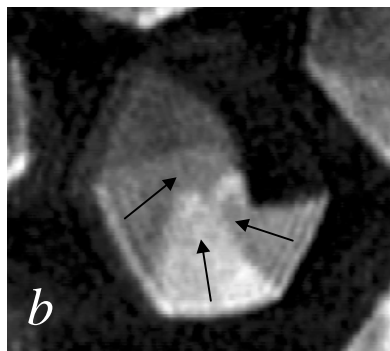


Fig.6.25: Domains of heptadecanoic acid methyl ester at 32°C (a). Between 29 and 27°C shape transformation begins with continuous faceting. The completely faceted state (b) is passed by forming dendrites at the edges of the segments with slightly negative curvature (c). Looking like waves the dendrites elongate and the domain body stretches (d). Eventually stripes develop with equidistant branching (e); a completely stretched domain is visualised in the upper half of the image. The spreading solution contained 0.8 mol% of cholesterol. The arrows in (a, b) indicate the tilt direction;



220×250 μm² (a), 180×205 μm² (b,c), 250×330 μm² (d), 205×250 μm² (e)

amount of cholesterol added. Below 0.5% complete faceting was not achieved on cooling, and above 1% the domains deteriorate so quickly that intermediate states could not be observed.

The corresponding isotherms between 27 and 32°C are presented in figure 6.26. At 27°C the monolayer is condensed at zero surface pressure. Between 27 and 29°C there is no measurable increase in pressure, but the higher compressibility at 29°C indicates the existence of a very low plateau. Possibly a triple point is passed on decreasing the

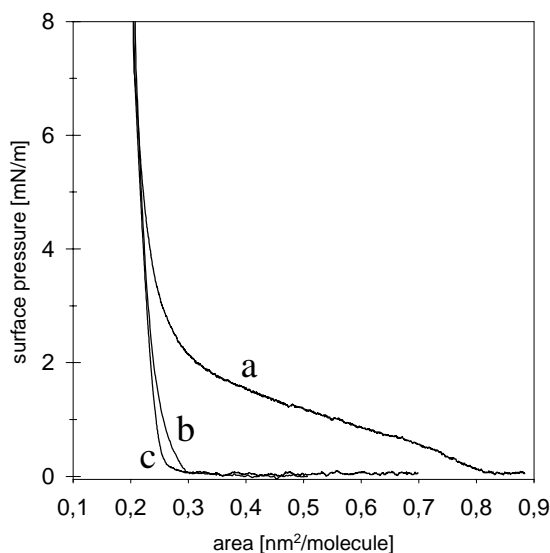


Fig.6.26: π-A isotherms of heptadecanoic acid methyl ester with 0.8 mol% cholesterol at 32°C (a), 29°C (b), and 27°C (c). The enhanced compressibility at 29°C indicates the development of a plateau. At 32°C the plateau appears at about 0.5 mN/m at 0.74 nm²mol.⁻¹; 0.02 nm²mol.⁻¹min⁻¹

temperature from 29 to 27°C. This is supported by the observation of foam patterns, that could indicate G-LE coexistence.

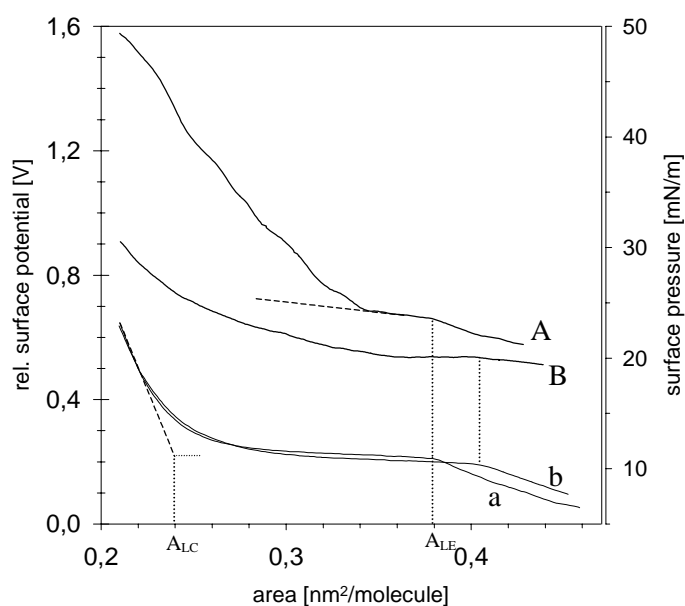
As with arachidic acid at high pH the boundary of the condensed phase of the ester enlarges so strongly with decreasing temperature, that fine lamellae are developed from compact domains. The polygonal shape with a larger perimeter than the circular one appears as an intermediate state. As discussed under 6.3.2 this shape transformation is ascribed to the increase of μ with decreasing temperature. It is conceivable that the drastic change in shape within a few degrees is caused by passing the triple point. Following the hatched vertical line at fixed monolayer area in figure 5.02 one can see that the change in the molecular density and hence in μ is very large at the triple point. The cholesterol is assumed to have only the function of facilitating domain faceting by lowering the line tension (see 6.3.5).

6.3.4.3. Variation of Composition in a Mixture of 1-O-hexadecyl-*rac*-glycerol (ETD) and 1-Palmitoyl-*rac*-glycerol (ESD)

ESD and ETD represent very similar molecules that differ only in that instead of the ester group in ESD there is an ether group in ETD. Pure ETD forms facets above 30° and on cooling the shape distorts while the texture develops splay and bending. The elongations become thinner with falling temperature [Vol96]. This behaviour is opposite to that of pure ESD, which forms circular domains at all temperatures and even the addition of cholesterol has no effect. This indicates higher electrostatic interactions or a lower line tension for ETD than for ESD.

Surface potential measurements of pure ETD and ESD reveal, that μ is much larger for ETD

*Fig. 6.27: Surface potentials (upper curves) and π -A isotherms of ETD (A, a) and ESD (B, b) at 29°C. The potential values do not refer to the clean water surface as zero point and the potential curves for ETD and ESD are shifted relative to each other vertically in the diagram. The evaluation of the plots is described in fig. 6.16.
 $\Delta V_{LC}-\Delta V_{LE}$ (ETD, A): 100-170 mV
 $\Delta V_{LC}-\Delta V_{LE}$ (ESD, B): 3-14 mV
 Compr. rate: $0.02 \text{ nm}^2 \text{ mol}^{-1} \text{ min}^{-1}$*



than for ESD (fig. 6.27). After the kinks in the surface potential curves, that coincide with the beginning of the plateau in the surface pressure-area isotherms, there is a short linear region for both ETD and ESD. This part is linearly extrapolated to determine $\Delta V_{LE}-\Delta V_{LC}$, which is directly proportional to μ (see 6.3.1, $\Psi_0=0$). In at least four measurements with both ESD and ETD $\Delta V_{LC}-\Delta V_{LE}$ was found to be between 100 and 170 mV for ETD and between 3 and 14 mV in the case of ESD. With ETD:ESD (60:40 mol%) mixtures the potential differences from several measurements were lying in a broad range from 60 to 150 mV.

Now mixed monolayers were prepared from ETD:ESD (60:40) to pure ETD in order to continuously vary the magnitude of the forces and observe the change in domain shape. ETD and ESD are miscible above ETD:ESD (50:50) [DeW98a]. Figure 6.28a-c demonstrate the gradual increase of faceting of domains grown to about the same mean molecular area, when the portion of ETD is raised. At about 60% ETD the domains appear still rounded as in pure ESD (a). As the amount of ETD is increased the curvature of the boundary at each of the seven segments reduces (b) until faceting is complete with pure ETD (c).

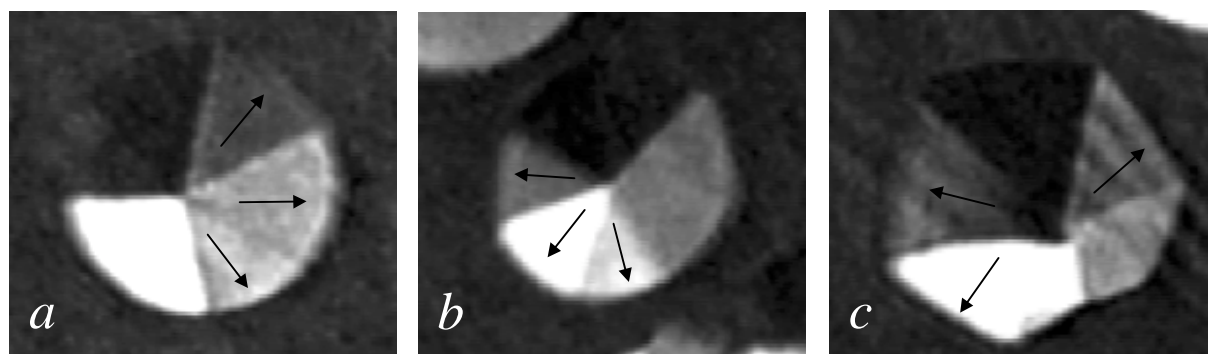


Fig. 6.28: In mixtures of ETD with ESD the degree of faceting of the condensed phase domains gradually increases on increasing the portion of ETD in the mixture; ETD:ESD (mol%)= 65:35 (a), 85:15 (b), 100:0 (c); The arrows indicate the tilt direction; 31.5°C, 150×165 μm^2

In each case the irregularly shaped domains formed at high compression rates relax immediately into the stable growth forms shown. Consequently these shapes developed at a slow rate represent the equilibrium shapes.

6.3.4.4 Discussion

It has been demonstrated, that faceting occurs with rather different substances and at various conditions. This indicates, that faceting is caused by the action of general and fundamental forces and is not related to peculiar chemical properties or a phase transition. There has been

the attempt to explain this phenomenon on the basis of the hexagonal lattice symmetry commonly encountered in monolayer systems analogous to the facet formation on 3D crystals [Cos92]. If, however, domain facets would develop along 2D lattice directions, one would expect only the occurrence of patterns with straight edges and hexagonal symmetry like those shown in the figures 6.22b and 6.25b. There are, however, many instances for domains exhibiting facets, but with a symmetry deviating from hexagonal like that in figure 6.22c showing pentagons or in 6.28b with sevenfold symmetry. Moreover facets are found with varying curvature. In another approach the faceted shape of monolayer domains is assumed to be produced by anisotropic growth along the domain perimeter and too slow relaxation into the circular shape [Ber91]. However, in the above experiments it has been proved, that faceting is an equilibrium process. This implies that the shape transformation is caused by the action of fundamental forces as are described in chapter 6.2. From the experiment it is evident, that the parameters μ and λ substantially contribute. The increase in the ratio μ^2/λ is the prerequisite, that a domain can adopt a shape deviating from circular. But why do the domains adopt a regularly faceted and not an arbitrary irregular shape (cf. fig. 6.11 b)? An answer can be given by regarding the forces the domain texture is based on. In each segment of the investigated domains the molecules are all aligned uniformly and oriented either to the boundary or to the centre of the domain and no splay or bending is observed. As the textures of the rounded and faceted forms coincide, the defect point energies are equal. So only the last two energy terms of equation 6.04 have to be considered. Expressing λ_0' by (μ/μ') ² (see 6.2.1) equation 6.05 becomes

$$\lambda' \cong \lambda_0 \left(\frac{\mu}{\mu'} \right)^2 \pm \lambda_1 (\mathbf{cn}) \quad (\text{for } \lambda_1 \ll \lambda_0) \quad (6.06)$$

for preferential tilt direction perpendicular to the boundary line as observed in 6.3.4.1-3 (see 6.2.2).

Equation 6.06 provides the basis for the explanation of facet formation. When μ increases or the isotropic line tension λ_0 of the domain boundary decreases, the anisotropic terms gain in weight. This means that the boundary energy depends to a larger extent on the orientation of the molecules at the boundary as expressed by the cosine terms. The boundary energy can be minimised by orienting the molecules at the boundary parallel to the boundary normal \mathbf{n} . This is achieved either by orienting the molecules, which would result in a splay texture (fig. 6.13 b) or, if the elastic energy for producing splay is too large, by reducing the curvature and stretching the boundary line of *each single segment* within the domain, while the area of one segment and the domain on the whole remains constant. In the final faceted state the molecules are aligned perpendicular to the boundary and \mathbf{cn} is 1 or -1. Furthermore equation

6.06 says, that faceting can occur only, when the molecules are tilted, since with upright molecules \mathbf{c} and hence the anisotropic terms are zero. A relation between line tension anisotropy and molecular tilt angle is indeed suggested by experimental findings [Qiu92, Die94].

On forming a regular hexagon from a circle with six segments the defect line energy rises by 10%, but as faceting is complete, its contribution to the domain shape seems to be of minor importance.

6.3.5 On the Influence of Cholesterol

In 6.1.3 it has been demonstrated, that a trace of cholesterol on the order of 1 mol% suffices to produce faceting of usually circular domains of arachidic acid at pH 12.0.

Weiss and McConnell [Wei85] found, that the LE-LC interface of DPPC domains increases by a factor of 10-100 or more, when some cholesterol is added. Cholesterol is assumed to preferentially adsorb to the two-dimensional LE-LC interface and to reduce the line tension behaving like a "line active" agent. According to the notion presented in 6.3.4.4 faceting in the presence of cholesterol can be explained by assuming, that cholesterol reduces λ_0 to a larger extent than λ_1 .

The question arises whether the line tension is reduced by the adsorption of cholesterol molecules to the domain boundary or by structural changes induced by the incorporation of cholesterol into the domain body. A decrease in the attractive interactions between the fatty acid molecules under the influence of cholesterol is expected to decrease λ_0 (6.2.1).

In order to elucidate this point the essential properties of cholesterol in mixtures with saturated long chain amphiphiles will be briefly discussed. A more detailed treatment is given in [Joh00]. From studies with bilayer membranes it is known that cholesterol influences on the one hand the translational order of the lattice and on the other hand the conformational order of the neighbouring chains. In membranes in the liquid crystalline phase, which is comparable to the fluid phase in monolayers, cholesterol increases the degree of trans ordering of neighbouring chains over the length of the rigid steroid ring system (≈ 10 carbon atoms, see fig. 6.06) [Mor95]. This ordering effect, which increases with the amount of incorporated cholesterol, is analogous to that of decreasing temperature [Mor95, Vis90]. In the gel state, however, which corresponds to the condensed phase in monolayers, cholesterol breaks the structure and disturbs the translational order of the membranes (acting as "crystal breaker") and the orientational order of the hydrocarbon chains, which is accompanied by an

increase of the mean molecular area A_{xy} . This effect can be attributed to the bad fit of the geometry of the cholesterol molecule to a lattice site in the ordered membrane lattice.

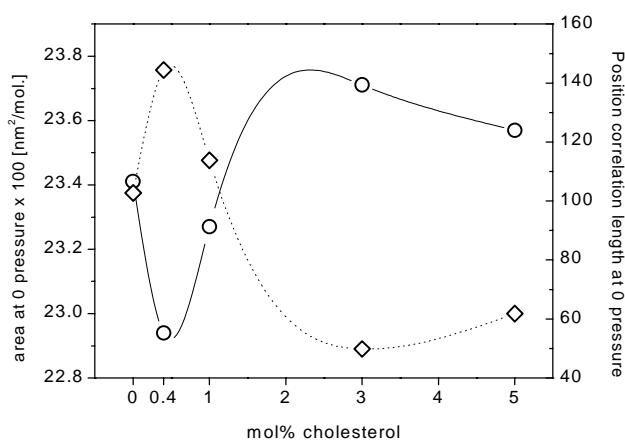


Fig.6.29: Variation of the in-plane area A_{xy} (solid line, circles) and the position correlation length of the (11)-reflections (dotted line, diamonds) in dependence of the cholesterol concentration. The data were obtained by linear extrapolation to zero surface pressure to obtain a qualitative comparison of these parameters.

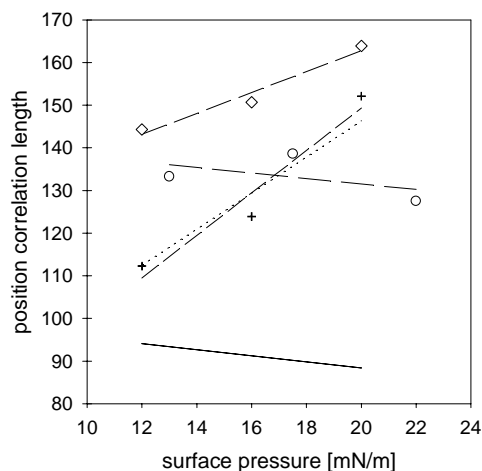


Fig.6.30: Pressure dependence of the position correlation length of the (11)-reflections for 0 mol% (solid line), 0.4 mol% (hatched-long, circles), 1.0 mol% (hatched-middle, diamonds), 3.0 mol% (hatched-short, crosses), 5.0 mol% (dotted) cholesterol. The lines represent linear fits, for clarity only the data for 0.4, 1.0, 3.0 mol% are shown

Subtle details on the interaction between cholesterol and fatty acids in monolayers at pH 12.0 are obtained by X-ray analysis at very low cholesterol concentrations. There is little known yet about the properties of mixtures with traces of cholesterol. Figure 6.29 shows the dependence of the inter-lipid interactions, as expressed by the position correlation length PCL (see 3.2.2.2), and A_{xy} on the cholesterol concentration. The inverse relation between the magnitudes of the PCL and A_{xy} complies with the considerations in 3.2.2.2 (eq. 3.05). The change in A_{xy} is caused by a corresponding change of the tilt angle (eq. 3.06; tab.VI.2, app.). The surprising effect is the reduction in A_{xy} and t below ≈ 1 mol% cholesterol. The increase in A_{xy} and the decrease in the lattice order (PCL) above ≈ 1 mol% cholesterol reflects the "crystal breaker" effect of cholesterol in the condensed phase. At about 3 mol% the saturation concentration of cholesterol in the condensed phase seems to be reached (a limit in miscibility is indicated by the phase separation revealed in 6.1.3).

The evaluation of the X-ray data for this system (fig. 6.29-30, app. VI, [Joh00]), taking into account the cholesterol effects in membranes described above, provides information about the influence of cholesterol on the molecular and structural order in monolayers (and bilayers) of long chain amphiphiles, which may be generalised as follows:

1. Cholesterol increases the conformational order of the aliphatic chains.

The conformational order increases with increasing cholesterol concentration (increasing conformational order is reflected by a decreasing molecular cross section A_0 (tab. VI.2, app.))

2. Cholesterol increases the lattice order by decreasing the tilt angle t and the molecular area A_{xy} (the lattice order is expressed by the position correlation length).

The lattice order increases with increasing cholesterol concentration

3. a) Cholesterol decreases the lattice order by increasing A_{xy} and hence t because of the bad fit of the cholesterol molecule into the ordered lattice of the aliphatic chains ("crystal breaker" effect)

The lattice order decreases with increasing cholesterol concentration

b) The mismatch of the geometry of the cholesterol molecule with a lattice site decreases with increasing surface pressure

4. The points 2 and 3 counterbalance each other and with increasing pressure the balance is shifted to point 2 (fig. 6.30)

5. There is no correlation between the change in chain order and that in the lattice order

For the extrapolation into the two-phase region to about 8 mN/m (cf. fig. 6.07) the lattice order and hence the attractive intermolecular interactions are found slightly higher with 1 % cholesterol than with 0 %. Consequently cholesterol of 1 mol% leads to the increase of λ rather than to its decrease supporting the assumption, that the domain faceting is caused by the "line activity" of adsorbed cholesterol molecules.

During the formation of the domain texture upon entering the tilted phase by decreasing the pressure in the figures 6.08f-i, first the segments develop and finally the defect lines between the segments straighten slowly. The segments develop by orienting the common tilt direction of the molecules within a fraction of the domain area with respect to the domain boundary. Hence this process is obviously governed by the line tension anisotropy. The straightening of the defect lines corresponds to the minimisation of the defect line energy (eq. 6.04, term 3). The low driving force for this process compared to that for orienting the molecules indicates, as already noted in 6.3.4.4, that the energy of the defect lines is lower than that of the boundary line.

6.3.6 Non-Equilibrium Shapes

In this section it is shown that the line tension anisotropy also determines domain shapes developing under non-equilibrium conditions.

In order to observe a pattern that deviates from circular for arachidic acid at pH 12.0, very high compression rates around $0.70 \text{ nm}^2 \text{ mol}^{-1} \text{ min}^{-1}$ are required. The boundary of the domains grown under this condition is irregular but relatively smooth (fig. 6.31 a). It contains notches and cusps, but distinct growth directions do not appear. The inner domain structure, however, is faultless. The relaxation process is very fast (less than 1 sec) and ends up with the circular form. When the pH of the subphase is changed to 12.3 and the same compression conditions are applied, domains develop, the shape of which is distinctly different from that at pH 12.0. When the defect lines cross in the domain centre and growth is uniform, six arms emerge radially from the domain centre pointing in the six symmetry directions, which gives the domains a star-like appearance (fig. 6.31 b). The dendrites grow along the segment edges prolonging the defect lines. The fact, that the relaxation is slower at pH 12.3 (≈ 20 sec) than at pH 12.0 (≈ 1 sec) is an indication of the lower effective line energy at pH 12.3 compared to pH 12.0 This has already been assumed previously (6.3.1, 6.3.4.1/4).

The domain shapes in equilibrium are determined by the balance between electrostatic forces and line tension (including anisotropy) (fig. 6.31 d). When the domains do not grow in equilibrium, their shape additionally depends on the velocity of diffusion and attachment of the molecules from the fluid phase to the domain body. The formation of protrusions or dendrites at a domain growing under supersaturation is favoured by the electrostatic repulsion

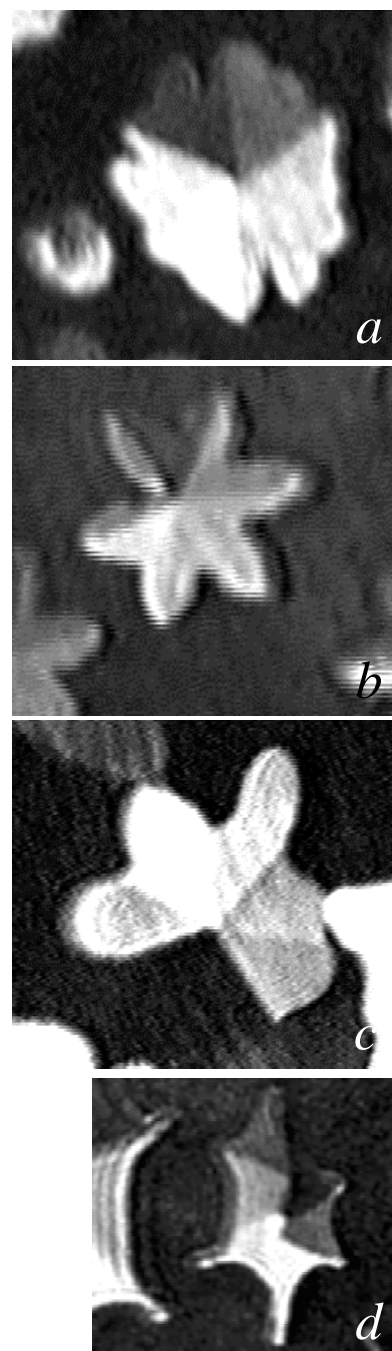


Fig.6.31:
(a-c) Non-equilibrium growth shapes of arachidic acid at pH 12.0 (a) and pH 12.3 (b), 28°C , $0.7 \text{ nm}^2 \text{ mol}^{-1} \text{ min}^{-1}$ and of ESD (c), 31.5°C , $0.04 \text{ nm}^2 \text{ mol}^{-1} \text{ min}^{-1}$; $185 \times 205 \mu\text{m}^2$ (d) equilibrium shape of heptadecanoic acid methyl ester (=fig. 6.25 c)

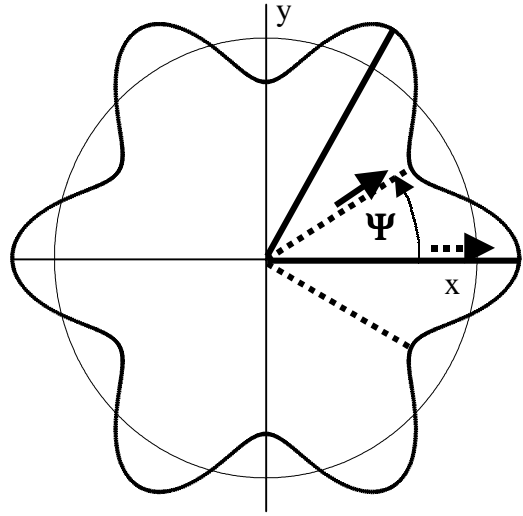
between the molecules in the domain and by concentration gradients due to limited diffusion velocity [Nit86]. The formation of protrusions is counterbalanced by the line tension, that tends to minimise the length of the boundary line. The velocity of attachment of molecules and protrusion formation competes with the velocity the molecules are equally distributed in the domain by means of the line tension. The smaller λ the larger the degree of branching of the domain boundary and vice versa. If the attachment of molecules is energetically more favourable at certain positions of the domain boundary than at others, protrusions emerged at the energetically more favourable positions will be smoothed less quickly and therefore continue growth to form dendrites in definite, often symmetrical directions. Examples of such anisotropic growth represent the figures 6.31b,c. The formation of regular dendrites is often assumed to originate in directional bonding forces between the domain molecules. A relation between growth and bonding or lattice directions is obvious for stiff, crystalline material, such as amphiphilic amides [Mel97a, Mel97b, Geh98]. Growth along bonding directions is possibly also the reason for the formation of dendrites along the bisector of the segments in ESD (fig. 6.31 c). X-ray measurements indicate, that there are particularly strong bonding interactions between the ESD molecules along their tilt direction, which is along the segment bisector (cf. fig. 6.28) [DeW98a, Geh96]. The preferential growth along the defect lines for arachidic acid at pH 12.3, however, seems to have a different origin. Firstly, no directions of enhanced bonding interactions are expected to exist in almost completely dissociated fatty acid monolayers, which is supported by the low PCLs (tab.VI.2, app.). Secondly, there is no reason to assume lower bonding forces at pH 12.0, where protrusions develop arbitrarily indicating isotropic growth (fig. 6.31 a). Figure 6.31d suggests that dendrite formation between two segments corresponds to the most favorable state with respect to the domain forces. As explained above, this would also account for dendrite formation between two segments at non-equilibrium conditions. By integrating over the domain boundary according to equation 6.05 it can be shown that the line energy is smaller when dendrites develop at segment edges than when they develop in the middle of the segments (fig. 6.32). This can be easily understood as in the first case the tendency of the molecules being aligned normal to the boundary (expressed by the line tension anisotropy) is satisfied better than in the latter case. When the dendrites emerge from the segment edges, one has to consider, that the defect line energy is increased, while the line tension decreases. However, the finding that the defect lines can be easily prolonged considerably by the dendrites (fig. 6.25 d), suggests, that the defect line energy is negligible compared to the line tension, which is in agreement with previous remarks (6.3.5).

Fig.6.32: Calculation of the line energy for dendrite formation between two segments (case I, segment marked by solid lines, cf. fig. 6.31 b) and in the middle of a segment (case II, defect lines indicated by dotted lines, cf. 6.31 c), using as boundary a cosine function laid over a circle with $x=\cos\varphi(1+0.2\cos6\varphi)$, $y=\sin\varphi(1+0.2\cos6\varphi)$ and $0\leq\varphi<2\pi$.

The line energy is $F_\lambda = \int (\lambda_0 - \lambda_1 \mathbf{c} \cdot \mathbf{n}) dl$.

In case I the tilt azimuthal angle ψ is 30° with respect to the x -axis (solid arrow), in case II it is 0° (dotted arrow). Integration result: $F_\lambda = 8.16\lambda_0 - 7.2\lambda_1$ (I) and $F_\lambda = 8.16\lambda_0 - 4.8\lambda_1$ (II). So there can be remarkable energy difference between I and II when anisotropic line energy is present favouring growth at the segment edges.

(for the details of the calculation see app. IV)



6.4 Quantification of the Line Tension Anisotropy

In the two foregoing chapters the forces, that govern the equilibrium texture and shape of domains, have been described and discussed. It has been demonstrated how the shape of the domain boundary can be explained as the results of the interplay between dipolar repulsive forces and line tension. Particularly important is the role of the anisotropy of the line tension, which originates in the domain texture and the orientation of the tilted molecules with respect to the domain boundary. It accounts for peculiar domain features, that can be observed, like the formation of facets and the development of dendrites at the border of two domain segments. The investigations suggest, that the shape of condensed phase domains is solely a function of the relative dipole density μ , the isotropic line tension λ_0 , and the first term of the anisotropic line tension λ_1 . The defect line energy, which may also vary with the shape, appears to be negligible against these terms.

So far the parameter λ_1 has been used only qualitatively and domain shapes interpreted by means of the ratio λ_0/λ_1 . In this chapter a way is shown, that allows to determine λ_1 by evaluating the continuous shape transformation from circular to faceted in mixtures of ESD and ETD (cf. 6.3.4.3). Whereas there have been described some experiments in the literature [Mul91, Wur00], according to which the average line tension λ of condensed phase domains is on the order of 10^0 - 10^1 pN, no value could be given yet for λ_1 . Also the physical origin of this parameter is still unclear (for the origin of λ_0 see 6.2.1). The knowledge of the absolute

values of these parameters is important, as it enables to calculate domain shapes, to quantify the influence of factors, such as cholesterol, on the domain shape, and to gain insight in the physical origin of these forces.

6.4.1 Theoretical Basis

According to equation 6.02 λ and μ are related by

$$\lambda(x) = -\frac{dI}{dP}(x) \cdot \mu(x)^2 \quad (6.07)$$

x is the concentration of ETD in the ETD/ESD mixture.

The domain perimeter P is defined as

$$P(x) = \int_0^{2\pi} \left| \frac{dX}{d\varphi} \right| d\varphi = \int_0^{2\pi} [r^2(\varphi) + r'^2(\varphi)]^{1/2} d\varphi \quad ; \quad \bar{X} = r(\varphi) \bar{e}_r \quad (6.08)$$

r is the angle (Θ) dependent distance from the domain centre to the domain boundary ($r = \text{const.}$ for a circle), see also figure 6.33. The integral I is calculated from [Van90]

$$\begin{aligned} I(x) &= \frac{1}{2} \iint_{|\varphi - \varphi'| > \delta} \frac{1}{|\bar{X} - \bar{X}'|} \left| \frac{d\bar{X}}{d\varphi} \right| \left| \frac{d\bar{X}'}{d\varphi'} \right| d\varphi d\varphi' \quad (6.09) \\ &= \iint_{|\varphi - \varphi'| > \delta} \left\{ \cos(\varphi - \varphi') [r(\varphi)r(\varphi') + r'(\varphi)r'(\varphi')] - \sin(\varphi - \varphi') [r'(\varphi)r(\varphi') - r(\varphi)r'(\varphi')] \right\} \\ &\quad \left\{ r^2(\varphi) + r^2(\varphi') - 2r(\varphi)r(\varphi') \cos(\varphi - \varphi') \right\}^{-1/2} d\varphi d\varphi' \end{aligned}$$

δ is the intermolecular distance.

$\mu(x)$ is obtained from surface potential measurement, $I(x)$ and $P(x)$ from an analysis of the domain shapes at different mixing ratios.

The average line tension $\lambda(x)$ for a certain mixing ratio is then obtained by applying equation 6.07.

According to equation 6.06 the line energy is

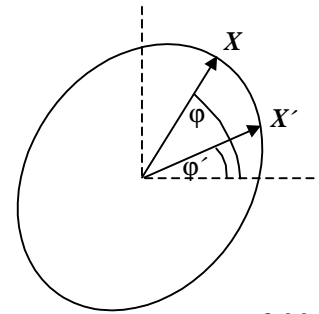


Fig.6.33

$$\lambda(x) P(x) = \lambda_0(x = x_0) P(x) \left(\frac{\mu(x = x_0)}{\mu(x)} \right)^2 + \lambda_1 \int_0^{2\pi} \left| \frac{d\bar{X}}{d\varphi} \right| \frac{\rho\rho}{c\hbar} d\varphi \quad (6.10a)$$

$$\lambda(x) \left(\frac{\mu(x)}{\mu(x = x_0)} \right)^2 = \lambda_0(x = x_0) + \lambda_1 \left(\frac{\mu(x)}{\mu(x = x_0)} \right)^2 \frac{1}{P(x)} \int_0^{2\pi} \left| \frac{d\bar{X}}{d\varphi} \right| \frac{\rho\rho}{c\hbar} d\varphi \quad (6.10b)$$

λ_0 and λ_1 are obtained by linear regression of eq. 6.10b. x_0 is the starting concentration, above which shape transformation occurs; λ_1 is assumed to be independent of x and λ_0 to be changed only by electrostatic forces (6.3.4.4).

6.4.2 Shape Analysis

The degree of faceting has been analysed as a function of the ETD/ESD mixing ratio. A measure for faceting of a domain segment is the magnitude of ΔA per cutting length l (see fig. 6.34 a). The BAM images of a number of domains have been analysed and the parameters ΔA , l , the trunk area A_{tr} (=domain segment area- ΔA) and γ of about 50 selected domain segments have been determined for each of the four mixing ratios 65, 80, 90, 95 mol% ETD. The procedure for determining these values is described in figure 6.35.

The distribution of the measured γ and segment areas ($\Delta A + A_{tr}$) for 65 mol% ETD are presented in figure 6.36a,b.

Assuming a constant curvature of the segment boundary, the degree of faceting is expressed by the ratio of the segment radius r to the radius of boundary curvature R (see fig. 6.34 c). With no faceting $r/R=1$ and with complete faceting $r/R=0$. The r/R values for all the measured segments and concentrations are plotted in figure 6.37a-d. Statistical mean and standard deviation are included as hatched and dotted line, respectively. No relation is recognisable neither between the segment or domain size (r) and the degree of faceting (r/R) nor between the width of a segment (γ , α) and the degree of faceting (not shown). Statistical mean and standard deviation of r/R are plotted versus the mixing ratio in figure 6.38.

The points can be connected by an analytical function of the form $r/R = ax_{ESD}^b$ (x : mol% ESD) (hatched curve).

6.4.3 Calculation

In order to calculate λ from eq. 6.07, one has to determine P , I and μ as functions of the ETD/ESD mixing ratio, i. e. as functions of the domain shape. Since the shape transformation on a single domain is considered, the domain area must be kept constant. P is easily calculated as the seven-fold of the boundary length of a single segment, which is described by a constant radius of curvature. More difficult is the determination of I according to eq. 6.09. For the faceted shapes, $\delta=0.5$ nm and the integration function used several millions of integration steps were needed for a single value of I (the accuracy depends on δ and it increases with increasing number of integration steps), and with SIGMA PLOT software, which was used so

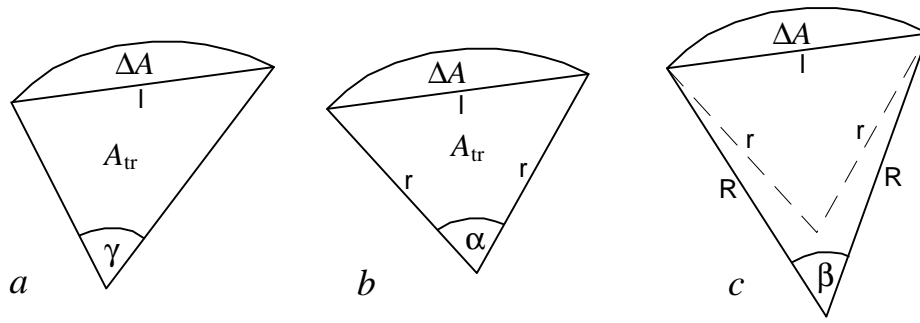


Fig.6.34: From the contour of a domain segment the values ΔA , l , A_{tr} and γ are derived (see fig. 6.35) (a). An ideal segment with equal side lengths r is constructed by leaving ΔA , l , A_{tr} unchanged: $r=(l^4+16A_{tr}^2)^{1/2}/2l$, $\alpha=\arcsin(2A_{tr}/r^2)$ (b). It is assumed that the curvature of the segment boundary is constant; R is the radius of curvature and the ratio r/R decreases with increasing degree of faceting. R is calculated from the segment parameters by the expression:

$$\Delta A = R^2/2(\beta - \sin \beta) = R^2/2 \left[\arccos \left(1 - \frac{l^2}{2R^2} \right) - \sqrt{1 - \left(1 - \frac{l^2}{2R^2} \right)^2} \right] \quad (c)$$

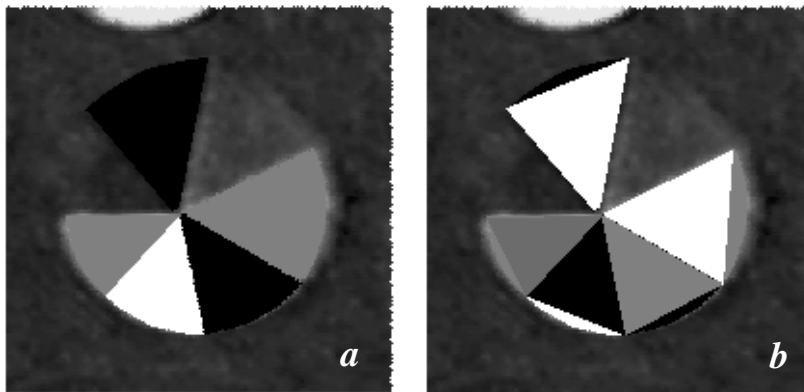


Fig.6.35: In a first step the contours of selected segments of imaged domains were gone over and filled with colour by means of a graphic software (a). Thus the segment areas could be easily determined by means of an image processing software, which also allowed to

measure lengths and angles. In a second step a triangle was drawn on the segment in order to determine ΔA and A_{tr} (b)

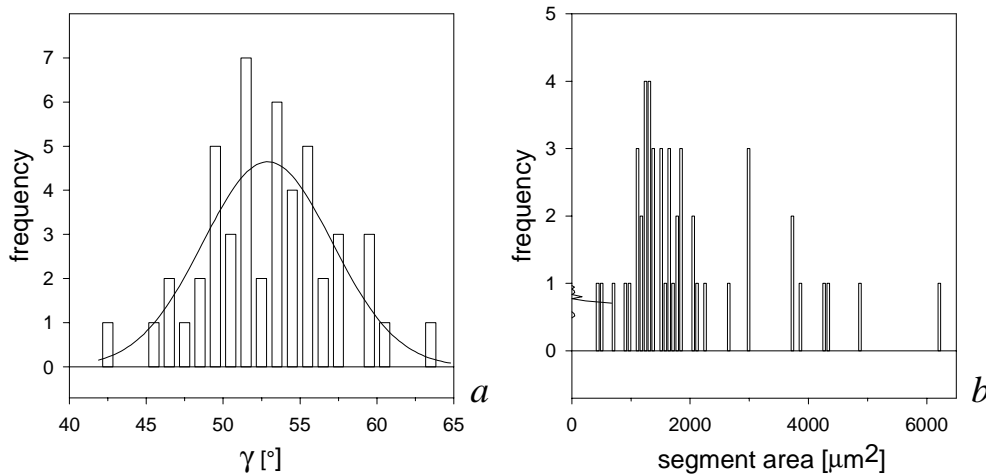


Fig.6.36: The mean angle of the evaluated segments is $52.9 \pm 4.2^\circ$ (a). Distribution of segment areas (b)

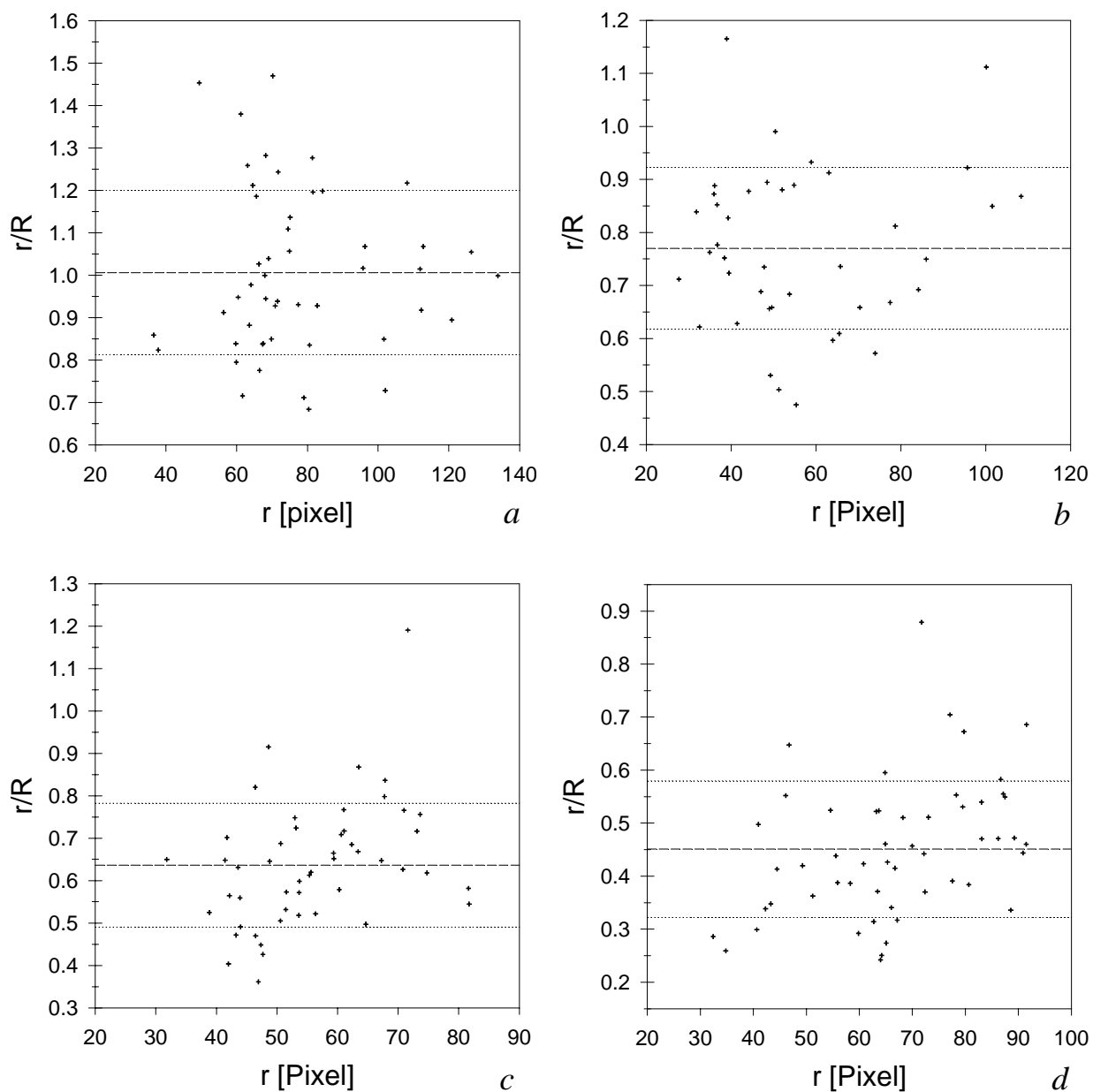


Fig.6.37: Segment evaluation. ETD:ESD (mol%)= 65:35 (a), 80:20 (b), 90:10 (c), 95:5 (d). Mean values for r (stand. dev. in brack.) [μm]: 63(17) (a), 46(17) (b), 46(9.5) (c), 55(13) (d); 122 pixel=100 μm

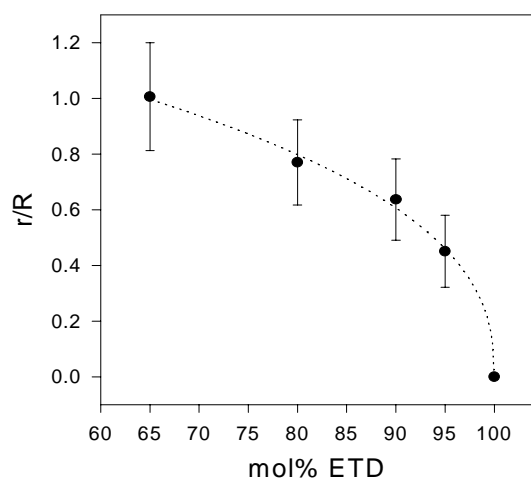


Fig.6.38:
The degree of faceting, expressed by the ratio r/R increases with increasing concentration of ETD following a power law of the form $r/R = ax_{ESD}^b$ (x : mol% ESD, $a=0.243$, $b=0.397$)

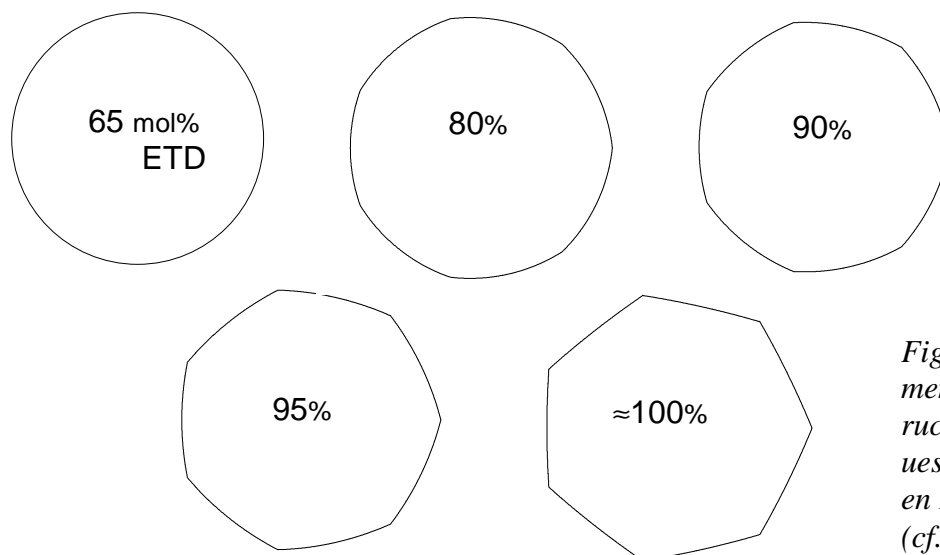


Fig.6.39: 'Ideal' 7-segmented domains constructed from the r/R values measured at the given ETD concentrations (cf. fig. 6.38)

far due to its convenience, calculation took an extremely long time (1-2 weeks for a single I value). A λ value derived from the first incomplete calculations is estimated to be on the order of 1 pN, which is in the right order of magnitude. This encourages to continue this approach. The conditions will be improved by applying a simpler integration function and a quicker calculating software.

$\mu(x)$ is assumed to vary linearly with the mixing ratio according to $\mu(x_{\text{ETD}}) = x_{\text{ETD}}(\mu_{\text{ETD}} - \mu_{\text{ESD}}) + \mu_{\text{ESD}}$. This relation holds under the assumption that the ETD/ESD mixing ratio in the condensed phase is the same as in the expanded phase and that the molecular densities with respect to expanded or condensed phase are equal for pure ETD and pure ESD as well as for the pure compounds and the mixture. μ_{ESD} and μ_{ETD} are determined from the relation $\mu = \epsilon_0 \cdot (\Delta V_{\text{LC}} - \Delta V_{\text{LE}})$ (ϵ is set 1, see 4.2.2). For the potential difference 10 mV is chosen in the case of ESD and 150 mV in the case of ETD (cf. 6.3.4.3). According to the above assumption the value for a ETD:ESD (60:40 mol%) mixture calculated from the potentials of the pure compounds is 94 mV. This is in the measured range (cf. 6.3.4.3).

When $\lambda(x)$ and $\mu(x)$ are known λ_0 and λ_1 are obtained from equation 6.10b.

7. Structure of Dissociated Fatty Acid Monolayers

In the following sections the structural details of fatty acid monolayers on alkaline subphase are investigated on the molecular level. Macroscopic electrostatic parameters, such as electrical potential and surface ion concentration, are determined satisfactorily within certain limits by theory, but information on arrangement, order and specific bonding interactions of the monolayer molecules can only be provided by experiment or simulation. So far no direct information is available on these aspects for monolayers of partially dissociated fatty acids at the air/water interface. Such information is important, since on the one hand the tuning of the intermolecular interactions in the monolayer by varying the degree of dissociation and the consequence on the phase behaviour may provide fundamental insight into the structuring principles of matter. On the other hand, as already mentioned, the interactions of solutes with the monolayer may be understood by the comparison of the phase behaviour in the absence of the solutes with that in their presence (cf. 6.1.4).

7.1 X-ray Analysis

7.1.1 Influence of pH on Chain Order

The lateral electrostatic repulsion between the fatty acid molecules in the monolayer increases with increasing pH and degree of dissociation. As a consequence the chain distance perpendicular to the chain axes increases (fig. 7.01, for arachidic acid) and the trans-ordering of the chains decreases indicating the reduction of the chain interactions. The degree of trans-ordering correlates with the degree of herringbone order and orthogonal unit cell distortion (see 3.2.2.3, fig. 3.07 and 4.5.3, fig. 4.24). The negative signs of the distortion parameter d_0 in figure 7.02

indicate, that the unit cell perpendicular to the chain axes is stretched perpendicular to the tilt direction due to the herringbone ordering (see 4.5.3). From figure 7.02 one can see that the herringbone order decreases, i. e. the conformational disorder of the chains increases and the unit cell perpendicular to the chain axes becomes more hexagonal with increasing pH. The relation between d_0 and pH is nearly linear above pH 9 (for deriving the corresponding unit cell dimensions expressed by the two elliptical axes a , b perpendicular to the chain axes, see

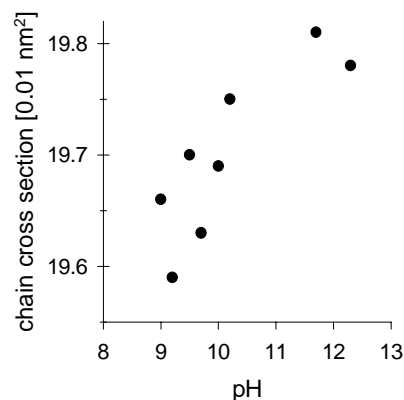


Fig.7.01: The conformational order of arachidic acid chains decreases with increasing pH

4.5.3). Below pH 9, however, the chain order appears to remain unchanged up to pH 9. At pH 12 and 15°C the unit cell perpendicular to the chain axes is almost undistorted hexagonal like stearic acid at pH 9.2 and 25°C. This is in agreement with the findings by M. K. Durbin et al. [Dur94], according to which nonadecanoic acid is undistorted hexagonal at 30°C. This analysis

pH	a ($\pi=0$) [0.1 nm]	b ($\pi=0$) [0.1 nm]	A _{xy} ($\pi=0$) [0.01 nm ²]	π_{PT} [mN/m]	tilt at π_{PT} [°]
2.0	5.46	8.64	23.55		
5.6	5.38	8.63	23.19		
9.0	5.19/5.03	8.66/8.97	22.49	14.9	21.0
9.2	5.19/5.01	8.64/8.91	22.42	13.7	21.3
9.5	5.18/5.02	8.63/8.93	22.34	10.0	23.2
9.7	5.18/4.99	8.62/8.89	22.32	7.5	24.0
10.0	4.98	8.90	22.15	4.7	25.2
10.2	4.99	8.95	22.29		
11.7	4.98	9.01	22.41		
12.0	5.02	9.53	23.84		
12.3	4.98	9.53	23.70		

Tab.7.1: Lattice parameters a , b , A_{xy} of arachidic acid extrapolated to surface pressure zero. The two values for a and b between pH 9.0 and 9.7 refer to the extrapolations from the NN tilted phase (1st value) and the NNN tilted phase (2nd value). π_{PT} is the NN/NNN transition pressure; the values from pH 9.0 to 12.3 refer to 15°C

confirms the relation stated for the monolayer phase behaviour, that the increase of pH corresponds to the increase of temperature or the decrease in chain length.

7.1.2 Influence of pH on Head Group Order

Figure 7.01 reveals that close chain packing is maintained over all the investigated pH range. Thus the molecules can only respond to a change in the interactions by changing the tilt angle and the head group distance in tilt direction (cf. fig. 3.11). This is demonstrated by means of table 7.1, which shows, that the lattice parameters strongly vary with the pH in tilt direction, while they hardly change perpendicular to the tilt direction.

Figure 7.03 shows the variation of the tilt angle and molecular area as a function of the pH value. Very surprising is the decrease in tilt angle and area above about pH 8 with a minimum between pH 10 and 11, since the increasing degree of dissociation and surface charge density would suggest a gradual expansion of the monolayer. A small decrease in area between pH 9 and 10 and subsequent expansion of a stearic acid monolayer was also detected by J. A. Spink [Spi63] from isotherm

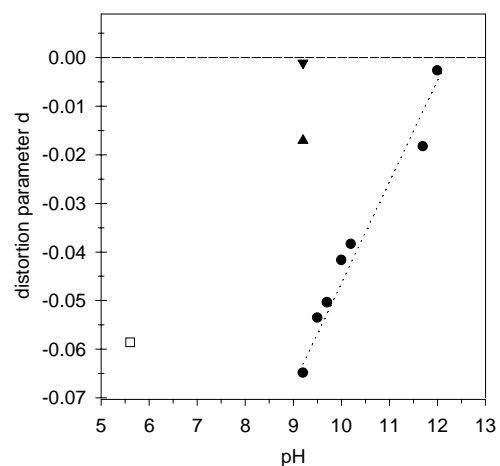


Fig.7.02: Degree of herringbone chain ordering in dependence of pH. ● arachidic acid, 15°C; □ arachidic acid, 20°C; ▲ stearic acid, 15°C; ▼ stearic acid, 25°C

measurements. The interpretation of isotherm measurements, however, is doubtful at this pH, since stearic acid monolayers become unstable at around pH 10 [Avi99].

How can the decrease in area be explained? An answer to this can only be tentative, since information on structures and processes at the interface is hardly available. For the possible interactions, that arise between the head groups of partially dissociated fatty acid monolayers and that are affected by the degree of dissociation, one has to take into account steric and electrostatic interactions, which are both repulsive for the present system, and bonding interactions. As the

monolayer is charged, a role could also play charged solutes, the concentration of which is strongly enriched at the charged interface. In the present case this concerns the borate and sodium ions. The possible influences on the molecular area are discussed in the following.

1. Steric interactions

Steric interactions are due to the volume requirement of the head groups. This not only refers to the pure head groups of the amphiphiles, but also involves solvent molecules interacting with them [Jaq91, Arb98, Pop95, Wal99]. Infrared measurements of fatty acid monolayers on water provide evidence that water molecules are hydrogen bonded to fatty acid head groups [Ger93a, b; Joh01]. The steric head group interactions should therefore be influenced by the orientation and arrangement of these water dipoles, which depends on the type of head group and the surface charge density [Wal99, Mir98, Du94]. The stronger electrostatic attraction of the solvent molecules to charged than to neutral molecules (ion-dipole compared to dipole-dipole interaction) may increase the tendency of water molecules to penetrate between the head groups in a partially dissociated monolayer and to increase the lattice spacings. With increasing dissociation and decreasing distance between the head group charges, however, the energy of the dipoles in the head group layer increases, so that water dipoles are forced to leave this region. On the other hand the electrostatic energy is lowered, if the space between charged head groups is occupied by water molecules that serve as a dielectric. The prevalence of a certain effect in dependence of the pH perhaps contributes to the pH dependence of the area as observed. Besides head group dehydration, a reason for the decrease in molecular area

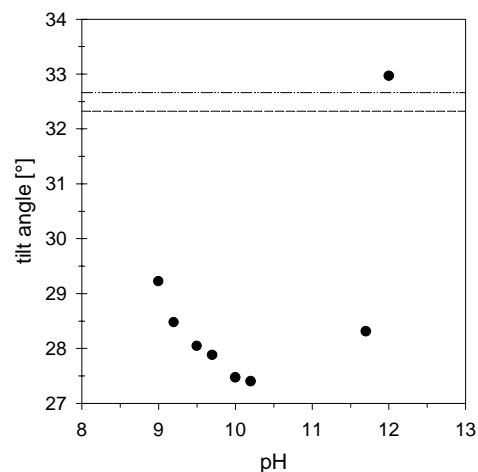


Fig.7.03: Dependence of the tilt angle extrapolated to zero pressure on the pH. ● arachidic acid, 15°C; hatched line: pH 2.0 (25°C); hatched-dotted line: pH 5.6 (20°C)

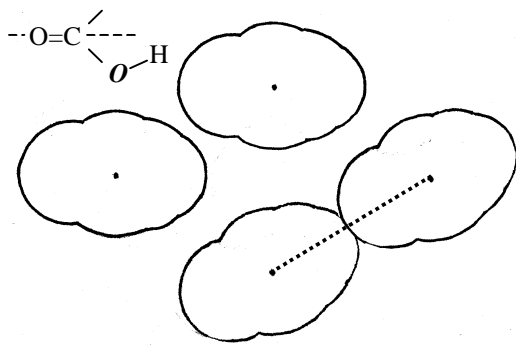


Fig.7.04: Shown are four carboxyl groups drawn with van-der-Waals radii (distances of closest approach, [Sae84, Kit73]) projected on the monolayer plane and placed on the four sites of a lattice unit. The side view is given on the top left. A carboxyl group lies in a plane perpendicular to the monolayer plane.

The prerequisite for hydrogen bonding may be a certain freedom of head group mobility. The latter is provided by tautomerism at the carboxyl group

and large conformational disorder of the chain section next to the head group, that is indicated by simulations of fatty acid monolayers on water [Oka99].

Hydrogen bonding is facilitated by the fact that O-H-O angles need not be linear (moderately strong hydrogen bonds are formed with O-H-O angles between 130 and 180° (table 7.2)). With both oxygens equally immersed into the subphase, the O...O distance of neighbouring head groups aligned along a line (lower right pair) is 0.28/0.30 nm for 0.50/0.52 nm head group distance (out of/in NN tilt direction) as found for pH 9.0 and 15°C at zero pressure (table 7.1). This distance is sufficient for the formation of moderately strong hydrogen bonds

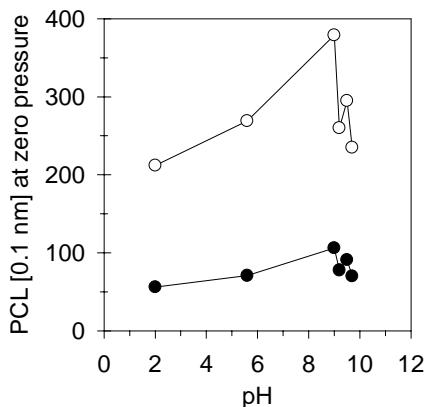


Fig.7.05 (left): Position correlation length of arachidic acid monolayers as a function of pH for the NN phases. Open circles: (02), closed circles (11) reflections.

Fig.7.06 (right): The pressure dependence of the position correlation length decreases with increasing pH.

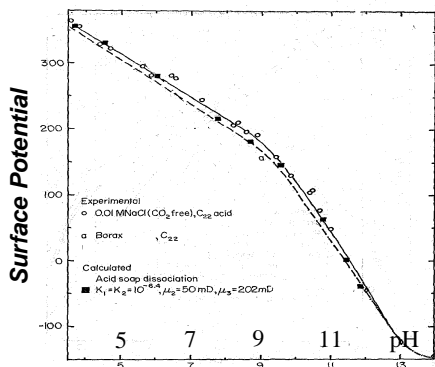
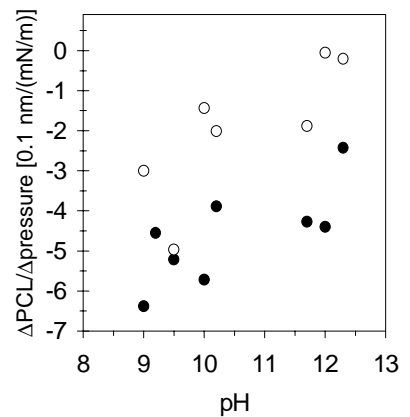


Fig.7.07: Change in the slope of the surface potential-pH plot for behenic acid at pH 9, from [God66]

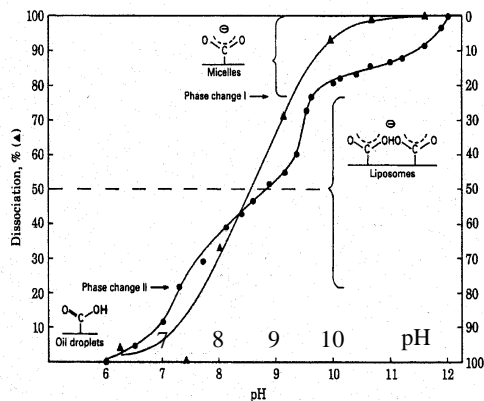


Fig.7.08: The titration curve for a fatty acid dispersion reflects the stability of the state of half dissociation and reveals rapid dissociation above pH 9. From this three „head group

up phases“ were proposed, each of which is confined to a certain range of pH. One phase is carboxyl, the next acid soap and the third one carboxylate for the highest pH values, from [Hai83]

above pH 8 could also be a lower steric requirement of the carboxylate head group compared to the head group of a neutral fatty acid.

2. *Effect of solutes*

The sodium ions are expected to attach relatively loosely to oppositely charged carboxylate groups mainly by electrostatic forces [Car88] and they probably remain hydrated when adsorbing to the monolayer being separated from the head groups by one or more layers of solvent [Boc70, Rit99]. An adsorbed ion together with a carboxylate therefore constitutes a dipole (cf. fig. 4.07) and for a certain degree of monolayer dissociation the electrostatic repulsion of the head groups decreases with increasing ion adsorption as the electrostatic repulsion of charges in the monolayer is partially replaced by the weaker repulsion between parallel dipoles. A decrease of the electrostatic repulsion by adsorption of the ions alone, however, cannot be the reason for monolayer condensation as with lower pH, where charges are compensated by bound protons, the area is more expanded.

An influence of the borate buffer is unlikely. First the adsorption of boric acid or borate would be driven by dispersion forces only, which, because of the rather low molecular mass, are small, and borate, the portion of which prevails above pH 9.2, is repelled from the equally charged surface. Second a varying effect on the monolayer with changing surface charge density should only be exerted by the charged borate ($[\text{H}_3\text{BO}_3]_0$ is constant), the concentration of which at the interface, however, is negligible.

3. *Bonding interactions*

In mixed monolayer systems, and a fatty acid monolayer on alkaline subphase is a mixture between neutral fatty acid and carboxylate, the deviation of properties, such as the molecular area, from the mean of the pure compounds, has been early ascribed to peculiar ion-ion, ion-dipole or dipole-dipole interactions between the unlike head groups [Mar18]. With increasing dissociation the dipole-dipole interactions between neutral molecules are replaced by stronger ion-dipole interactions between carboxyl and carboxylate. In order for the area to decrease, the ion-dipole interactions have to outweigh the repulsive ion-ion interactions between half of the molecules. The ion-ion interactions are weakened by the presence of the counter ions. Highest condensation is expected, when the monolayer is half dissociated. As the pH increases over this point the ion-ion interactions gain in weight and the monolayer expands again.

Another possibility to explain the decrease in area is by assuming hydrogen bonding between the carboxylic head groups [Ale41]. The lattice spacings found are suitable for the formation

of moderate hydrogen bonds, if a certain freedom of head group arrangement is provided (tables 7.1, 7.2, fig. 7.04). There is evidence, that hydrogen bonds are particularly stable, when the carboxyl groups are attached to long alkyl chains [Smi73]. At neutral pH a hydrogen may bridge the carbonyl oxygen and the hydroxyl oxygen of two neighbouring carboxyls. Water molecules could stabilise this bonding. At higher pH the hydrogen bonds couple pairs of carboxylic acid and the corresponding anion. Hydrogen bonds between the acid and the anion are known to be much stronger than those between the uncharged molecules [Pan98], so that the area minimum is again expected at half dissociation.

Experimental findings and calculations according to the Gouy-Chapman theory indicate, that the state of half dissociation is reached at around pH 9 [table 7.3, Bag66, Ave90, Bin91, Hai83]. And indeed, maximal inter-lipid bonding interactions at pH 9 are evident from the analysis of the position correlation length (fig. 7.05). The position correlation length increases continuously up to pH 9, but suddenly drops steeply on passing this value. A sharp discontinuity at pH 9 is exhibited by both the (11) and (02) reflections. The fact, that not all the points of a curve refer to the same temperature has no substantial effect on the course of the position correlation length. Furthermore the correlation length perpendicular to the tilt direction, in the case of figure 7.05 for the (02) reflection, is found to be independent of the chain length and hence the temperature [Kag99]. That bonding is maximal at pH 9 is in agreement with findings according to which fatty acid monolayers are most stable to collapse and dissolution at this pH [Ave90]. The change in the position correlation length must reflect the change in the head group interactions, since the chain interactions are not directly affected by the pH. The maximum bonding at 50% dissociation suggests the presence of ion-dipole or hydrogen bonds.

In the past there has been controversy about which type of binding – ion-dipole or hydrogen bonding – is responsible for changes of monolayer properties [Dav61]. In the present case,

*Tab.7.2:
Classification of
hydrogen bonds
[Jef97]*

H-bond A-H-B	Strong	Moderate	Weak
bonding	mostly covalent	mostly electrostatic	electrostatic
Bond length A-B	2.2-2.5 Å	2.5-3.2 Å	3.2-4.0 Å
Bond angle A-H-B	175-180°	130-180°	90-150°
Bond energy	60-170 kJ/mole	17-60 kJ/mole	< 17 kJ/mole
Examples	Acid salts, HF complexes	Acids, Alcohols, Hydrates, all biological molecules	C-H—O/N bonds

however, this question might be superfluous, since the main contribution to hydrogen bonding is electrostatic for bond distances larger than 2.5 Å (table 7.2). Especially weak hydrogen bonds with a larger donor-acceptor distance are satisfactorily described by dipole-dipole or ion-dipole interactions while covalent bonding due to electron delocalisation between the bound partners gains in weight as the donor-acceptor distance decreases [Jef97, All75].

The difference between the position correlation lengths at pH 9 and pH 10 is obvious and it implies that the area minimum at pH 10 cannot be based on strong attractive interactions at this pH only. There possibly steric interaction are deciding.

Figure 7.06 shows that below pH 12 the cohesion of the molecules decreases with increasing pressure and that with increasing pH the pressure dependence of the correlation length becomes smaller.

*Tab. 7.3:
Electrostatic parameters for the experimental conditions from Gouy-Chapman-Stern theory (5.2.2)*

pH _b	[Na ⁺] $\cdot 10^3$ [mole/l]	ψ_0 [mV]	1/ κ [nm]	D _H	A _{Na}	pH ₀
8.7	1.17	-223	8.87	0.42	0.23	4.9
9.0	1.87	-222	7.01	0.66	0.43	5.2
9.2	2.42	-219	6.17	0.79	0.54	5.5
9.5	3.39	-214	5.20	0.91	0.64	5.9
9.7	4.56	-207	4.49	0.96	0.68	6.2

7.1.3 Model of Fatty Acid Head Group Structure

A discontinuous change in the properties of fatty acid monolayers at 50% dissociation (\approx pH 9) is revealed for the chain order, the positional order of the lattice, the L₂/O_v phase transition pressure (see chapter 7.3) and the surface potential [God63, God66], (fig. 7.07). A conspicuous inflection point at around pH 9 is also found in the titration curve of a dispersion of fatty acids [Hai83], (fig. 7.08). It marks the transition from carboxylate to acid soap. From this it is inferred, that there is hydrogen bonding between neutral acid and anion in the partially dissociated fatty acid monolayer and that the change in the monolayer properties with pH is due to the dependence of the degree of hydrogen bonding and the strength of head group bonding interactions on the degree of monolayer dissociation. Correspondingly the shape of

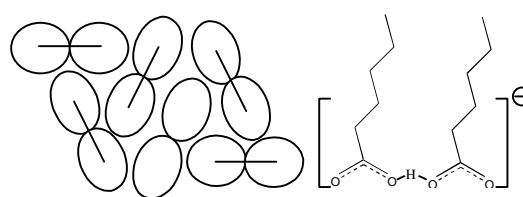


Fig.7.09: Fatty acid head groups associated in pairs of carboxyl and carboxylate by hydrogen bonding. A fraction of head groups may be hydrogen bonded to water

the PCL-pH plot (fig. 7.05) is interpreted in the following way: below pH 9 inter-lipid binding increases due to the formation of H-bridged acid-anion pairs of carboxyl and carboxylate. Bonding strength is maximal at the carboxyl/carboxylate ratio of 1 (pH≈9). Above pH 9 the acid-anion dimers are gradually replaced by pairs of anions as the pH is increased. Consequently the attractive force between the molecules decreases. As the ratio between PCL (02) and PCL (01) in figure 7.05 is approximately the same from pH 2 to pH 9, the bonding interactions are not preferred along certain lattice directions. The value of the ratio itself of about 4 is normal [Kag99]. The relation between position correlation length and pressure in figure 7.06 might reflect, that the degree of hydrogen bonding reduces with increasing pressure. A model of the head group structure of a fatty acid layer at an interface at 50% dissociation is presented in figure 7.09.

That the discontinuity found at pH 9 for various properties originates in a change of hydrogen bonding interactions is supported by simple calculations. Considering hydrogen bonding between acid-anion pairs and electrostatic repulsion as the only intermolecular interactions that vary with pH, the shape of the plot in figure 7.05 reflecting the head group interactions can be understood (fig. 7.10). The calculation shows that the hydrogen bonding energy is in the order of the ion-ion repulsion between half of the molecules and may outweigh the latter.

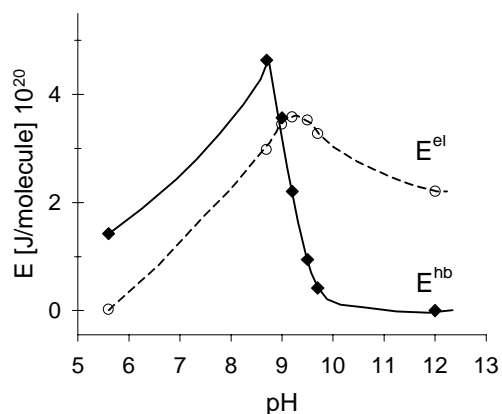


Fig.7.10: Hydrogen bonds are assumed between pairs of neutral carboxyls (energy per bond $E_{COOH/COOH}$) and between pairs of carboxyl and carboxylate (E_{COOH/COO^-}). The bonding energy per molecule E^{hb} varies with the pH and the relative number of both kinds of bonding pairs: $E^{hb}=[0.5E_{COOH/COOH} + D_H(E_{COOH/COO^-} - E_{COOH/COOH})]$ for $D_H < 0.5$ and $E^{hb}=[E_{COOH/COO^-}(1-D_H)]$ for $D_H > 0.5$ (D_H taken from tab. 7.3). The energy E^{hb} of moderate hydrogen bonds with O...O distances of 0.25-0.32 nm are in the range of 17-63 kJ/mole (tab. 7.2). In the calculation the lower limit of 17 kJ/mole is substituted for $E_{COOH/COOH}$ and the upper limit of 63 kJ/mole for E_{COOH/COO^-} .

The electrostatic repulsion is described by the Debye-Hückel approximation, where the diffuse double layer at the interface is regarded as a charged capacitor. The electrostatic energy per molecule E^{el} is the energy for charging this capacitor, the plates of which are separated by the Debye length κ^{-1} : $E^{el}=[e^2(D_H-A_{Na})^2]/[2\epsilon\epsilon_0\kappa A]$ (values according to table 7.3). The total energy is the difference of the two absolute energy contributions.

7.1.4 Conclusion

Speculations about the existence of acid soaps in fatty acid monolayers are already very old [Ale41, Spi63]. Although the existence of hydrogen bonded carbonyl in fatty acid monolayers at the air/water interface has been demonstrated by IR measurement [Ger93b, Joh01], (see 7.2), so far the question could not be solved, if besides interfacial water also neighbouring fatty acids are involved in the hydrogen bonding. X-ray measurements of the molecular area and lattice order strongly indicate the formation of hydrogen bonds between neighbouring fatty acids at the lipid-solution interface, which would account for the peculiar pH dependence of various properties observed. A model for the head group structure is presented, that is based on the formation of discrete hydrogen bridged acid-anion dimers at the interface. However, it is conceivable that there is a quick proton exchange between neighbouring head groups involving the entire head group layer and constituting a continuous proton conducting sheet [Hai83]. Such two-dimensional networks of hydrogen bonds between hydrophilic groups (including water molecules) are assumed at phospholipid/water interfaces [Toc90, Bog87] and at surfaces of proteins [Car98]. One might object that such acid-anion pairs are not stable in aqueous environment [All98]. However, the conditions at the interface are much different from that in bulk (ref. water structure, polarity, cf. fig. 5.08).

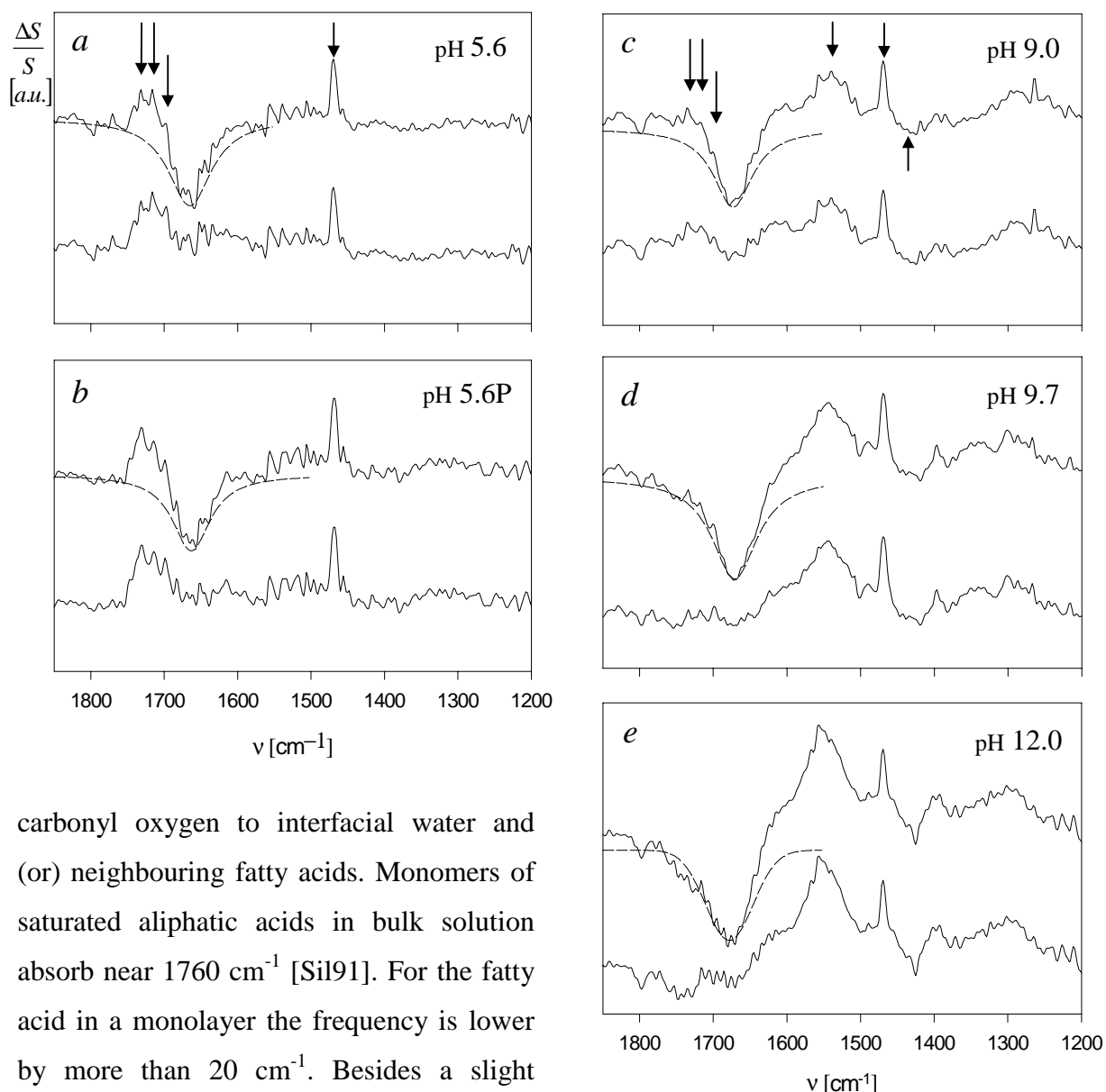
The results of the X-ray measurements are supported and supplemented in the following section by infrared measurements, which provide details on the environment and bonding situation of the single molecule in the monolayer

7.2 Study of the Head Group Bonding by PM-IRRAS

7.2.1 Peak Analysis

1. Peak assignment

For arachidic acid monolayers on water and alkaline solution six IR bands are resolved in the wave number region from 1800 to 1200 cm^{-1} , that correspond to vibrations in the aliphatic chain and in the head group of the ionised and unionised fatty acid amphiphile (fig. 7.11). The carbonyl stretching vibration of the unionised fatty acid is split into three bands at around 1734, 1715 and 1700 cm^{-1} . The splitted band reveals the presence of non-hydrogen (H-) bonded (1734 cm^{-1}), singly H-bonded (1715 cm^{-1}) and doubly H-bonded carbonyl groups (1700 cm^{-1}) in the monolayer [Ger93b, Men95] and is caused by the variation of the strength and thus the stretching frequency of the carbonyl bond due to the hydrogen bonding of the



carbonyl oxygen to interfacial water and (or) neighbouring fatty acids. Monomers of saturated aliphatic acids in bulk solution absorb near 1760 cm^{-1} [Sil91]. For the fatty acid in a monolayer the frequency is lower by more than 20 cm^{-1} . Besides a slight possible shift due to the different optical situation in reflection-absorption compared to transmission spectroscopy [Ger94], the lowering of the stretching frequency of the carbonyl group in the monolayer may reflect a changed solvent structure at the interface compared to that in the bulk or a field effect due to the close vicinity of the molecules in the monolayer. The change of the environment of a fatty acid molecule by the change of solvent properties, such as the polarity, is known to reduce the absorption

Fig.7.11: PM-IRRAS spectra of arachidic acid on subphases of varying pH.

The upper spectra represent the original baseline corrected spectra, the lower ones result when the hatched Lorentz peaks, adjusted to the water dips, are subtracted from those.

The arrows indicate the three $\nu(\text{C}=\text{O})$ modes at 1734 , 1715 and 1700 cm^{-1} , the $\delta(\text{CH}_2)$ mode at 1469 cm^{-1} and the $\nu_{as}(\text{COO}^-)$ at 1550 cm^{-1} and $\nu_s(\text{COO}^-)$ at 1430 cm^{-1} , which is negative with respect to the baseline ($\Delta S/S=0$). The spectra a, c-e were recorded at 12.5 mN/m and the pH values given, b at 25 mN/m .

frequency of the carbonyl group up to 25 cm^{-1} [Sil91].

A striking feature at all pH values is the sharp peak due to the methylene bending vibration of the aliphatic chains. The position of the maximum of the Lorentz fit peak varied between 1468 cm^{-1} and 1470 cm^{-1} for all measurements.

At and above pH 9.0 (fig. 7.11 c-e) the bands of the asymmetric and symmetric carboxylate stretching vibrations appear between 1542 cm^{-1} and 1554 cm^{-1} and between 1419 cm^{-1} and 1444 cm^{-1} , respectively. The band of the asymmetric mode is oriented upward relative to the uncovered substrate line, that of the symmetric one downward. The sign of a band in PM-IRRAS depends on the orientation of the transition dipole momentum of the absorbing molecular group with respect to the electric field of the s or p polarised radiation. For upward oriented bands the transition dipole moments are preferentially aligned parallel to the water surface and downward directed bands arise from an orientation of the dipole normal to the interface [Bla94]. The band orientation may also be reversed by slight changes in the optical settings due to a change of the efficiencies for p and s polarisations [Buf91].

2. Peak fitting

The quantitative evaluation of the carbonyl bands is impeded by the presence of a broad dip at around 1670 cm^{-1} . The dip is probably related to the bending vibration of water, observed at 1640 cm^{-1} in the transmission spectrum [Han91, Ber89]. Part of its intensity can be attributed to the different optical responses of covered and uncovered water surfaces, the main contribution, however, may arise from an anisotropic structuring of water at the interface to air in the absence of a film [Bla94]. In order to eliminate the dip for evaluation, a Lorentz peak was adjusted, not fitted, to the contour of the dip half at the higher wave numbers at pH 12.0 (hatched curve in fig. 7.11 e). At pH 12.0 the contribution of the carbonyl bands to the contour is regarded as negligible. This Lorentz peak was changed proportionally in size and adjusted to the height of the water dips in the spectra from the measurements at the other pH values (hatched curves in fig. 7.11). The position of the peak varied between 1663 cm^{-1} and 1678 cm^{-1} , where the frequency was found to shift to higher values with increasing pH, suggesting a pH dependent change of the interfacial water structure. At pH 5.6 the Lorentz peak matches well with the dip half to lower wave numbers, while at the pH above 9.0 coincidence with the dip half to higher wave numbers is observed. This demonstrates that the changes of the width of the dip with pH and its asymmetry are caused by the appearance of bands that superimpose to the water peak and justifies the modelling of the dip by a symmetric function. Finally the Lorentz peaks were subtracted from the original spectra in order to eliminate the water dip.

Lorentz peaks were fitted to the carbonyl bands of the difference spectrum (lower curve in figures 7.11 a-e) and the areas of the Lorentz peaks taken as peak intensities. By this way the presence of doubly, singly and non-H-bonded carbonyl bands is revealed up to pH 9.7 (table 7.4). For all measurements from pH 5.6 to 9.7 the position of the fitted peaks was 1732-1735 cm^{-1} for the non-H-bonded, 1720-1714 cm^{-1} for the singly and 1704-1697 cm^{-1} for the doubly H-bonded species.

As the carboxylate peaks are rather broad, Gaussian fits seemed best suitable for both peaks. It has been reported that both carboxylate peaks are split into two peaks, that are positioned at around 1404 cm^{-1} and 1423 cm^{-1} for the symmetric mode and around 1544 cm^{-1} and 1560 cm^{-1} for the asymmetric one [Ger94]. In the present work the two peaks of the symmetric mode were fitted separately, if they could be discerned well, otherwise they were fitted as a single Gaussian. A split of the peak of the asymmetric mode was hardly pronounced in most cases (see fig. 7.11 c-e), so that it was fitted as a single Gaussian.

pH	N	Peak positions [cm^{-1}]					
		1430	1469	1550	1700	1715	1734
5.6	5	-	32(8) 2.2	-	36(15) 1.2	25(17) 1.1	45(21) 1.6
5.6P	4	-	30(4) 2.2	-	26(13) 1.0	17(2) 0.9	54(8) 1.6
9.0	3	7.3(1) -0.4	25(6) 1.7	61(23) 1.1	10(6) 0.5	11(4) 0.7	36(18) 0.6
9.7	3	12(2) -0.5	23(3) 1.7	73(21) 1.4	11(4) 0.6	8.0(6) 0.7	4.4(1) 0.5
12.0	2	26(7) -1.2	22(1) 1.7	129(3) 2.2	-	-	-

Tab.7.4:
Fitted peak areas. N: number of measurements. 5.6P refers to 25 mN/m, the other values to 12.5 mN/m. The first value of each row is the mean fitted area with the standard deviation given in brackets, the second value the mean peak height (ν [cm^{-1}]: $\nu(\text{C}=\text{O})$ [1734(CO_2H), 1715($\text{CO}_2\text{H}\cdot\text{1H}$ -), 1700($\text{CO}_2\text{H}\cdot\text{2H}$ -)]; $\nu_{\text{as}}(\text{COO}^-)$ [1550]; $\nu_{\text{s}}(\text{COO}^-)$ [1430]; $\delta_{\text{s}}(\text{CH}_2)$ [1469]

7.2.2 Discussion

1. Variation of peak intensities with pH

The measurements at different pH values were performed at 12.5 mN/m and in one case at 25 mN/m. 12.5 mN/m was chosen, because on the one hand the pressure should be at low values, in order to be able to draw conclusions based on previous work for comparable conditions, but on the other hand the pressure must be high enough to have a condensed phase at pH 12 and to allow the comparison of all the measurements up to pH 12.0. For pH 5.6 the intensities of the different carbonyl bands are found roughly equal at 12.5 mN/m (tab. 7.4). At the doubled pressure, the intensity for the non-H-bonded carbonyl is increased with respect to that for the singly and doubly H-bonded forms and with respect to the non-H-bonded carbonyl at

the pressure of 12.5 mN/m. This suggests that the amount of singly as well as doubly H-bonded fatty acid decreases with increasing surface pressure.

On increasing the pH to 9.0 the intensities of the bands assigned to all three carbonyl forms decrease. The intensities for the singly and doubly H-bonded carbonyl are much lower than for the non-H-bonded one. Additionally the two bands of carboxylate appear. Between pH 9.0 and 9.7 the intensity for the non-H-bonded carbonyl drops drastically, while that for the H-bonded forms remains roughly unchanged.

The hydrogen bonding to the carbonyl oxygen of a fatty acid is conceivable either between the fatty acid and interfacial water molecules or (and) between adjacent fatty acids. Gericke et al. found that for fatty acid esters the band at 1704 cm^{-1} is missing and that the carbonyl of esters is only singly H-bonded. They also noticed that in the state of high monolayer compression the band of the singly H-bonded carbonyl of the ester disappears. This they ascribed to the shielding of the carbonyl oxygen by the alcohol in Z-conformation against H-bonding with water. The latter is supported by the findings of Gericke et al., that the degree of H-bonding of esters decreases with increasing chain length of the alcohol in the series *methyl ester* > *ethyl ester* > *n-propyl ester* [Ger94, Ger95]. On the other hand they noticed that fatty acids remain highly H-bonded at high pressures and that the presence of the 1704 cm^{-1} band with fatty acids is involved with an enhanced order of the aliphatic chains [Ger93b, Ger94]. All this suggests, that hydrogen bridges exist between neighbouring fatty acid molecules.

Enhanced conformational order of the chains was revealed by Gericke et al. [Ger93b] with IRRAS at pH 9 for stearic acid. However, the order did not change significantly between pH 2 and 8, but was found drastically increased at pH 9. Moreover their IR analysis revealed a sharp tilting transition of the molecules to the vertical at pH 9. Similarly no tilted phase was found by Datta et al. [Dat00] for heneicosanoic acid at high pH with X-ray diffraction. This is opposite to the results in 7.1, where the lipid interactions change smoothly between pH 2 and 9 and tilted phases are present up to pH 13. Both authors did not add EDTA to the subphase (at least they did not mention), the use of which however is crucial, since tiny amounts of polyvalent metallic impurities are strongly enriched beneath a charged fatty acid monolayer. The strong increase in chain order and the loss of tilt at pH 9, which was noticed by these authors, were probably caused by salt formation.

2. Taking peak intensities for surface concentrations

In table 7.5 the intensities of the H-bonded carbonyl forms, of the non-H-bonded carbonyl

and of the carboxylate are put into relation to each other giving in the sum 100% for each pH value. The error in brackets includes the largest absolute deviation observed in the number N (see tab. 7.4) of measurements performed at each pH. For pH 5.6 the intensity of carboxylate is set as zero, for pH 12.0 as 100%. The carboxylate intensities in percent at pH 9.0 and 9.7 are derived from the relative intensities of the band at 1550 cm^{-1} , taking the intensity for pH 12.0 as 100%. And the relative intensities of the carbonyl bands at pH 9.0 and 9.7 are the mean of the relative intensities, that would result if for the carboxylate intensity the largest measured value is substituted, and those intensities that would result from the smallest measured value for carboxylate.

Tab.7.5: Relative peak intensities giving 100% for each pH. The intensities are taken as surface concentrations. The brackets contain the maximal absolute deviation (in \pm) from N measurements.

	pH 5.6	9.0	9.7	12.0	5.6P
HOC=O	39(15)	35(23)	8(2)	0	52(9)
HOC=O·1H-	31(17)	12(5)	17(14)	0	17(2)
HOC=O·2H-	30(15)	11(7)	22(9)	0	31(14)
COO ⁻	0	42(15)	53(14)	100	0

Under the assumption, that on the one hand the orientation of the transition dipole moments, i. e. the orientation of the head groups, and their magnitudes do not change significantly over all the pH range for carbonyl and carboxylate, and that on the other hand the magnitudes of the transition dipole moments are not much different for the non-, singly and doubly H-bonded carbonyl group, the intensity distribution in table 7.5 corresponds to the surface concentrations of the different fatty acid species. The data of table 7.5 might be over interpreted by regarding them as concentrations, since no data are available to prove the validity of these assumptions, however the experimental findings of other authors, from the own X-ray investigation (7.1) and the conclusions presented below seem to justify these assumptions:

the maximum change in chain tilt of the arachidic acid molecules in the monolayer between pH 5.6 and 12.0 at 15°C is only a few degree and almost equivalent for pH 5.6 and 12.0 (fig. 7.03). Correspondingly the change in the orientation of the head group and the transition dipole moments over this pH range should be small. More unsure is the assumption of constant magnitudes of the transition dipole moments at the different subphase conditions and of equal transition dipole moments for the non-, singly and doubly H-bonded carbonyl group. With increasing degree of protonation, besides a peak shift to lower frequency, the magnitude of the transition dipole moment of the carbonyl stretching vibration is expected to increase [Gün96]. However, investigating the hydrogen bonding of carbonyl groups by different

solvents in the bulk, K. B. Patel et al. [Pat85] assumed equal absorbances for the different carbonyl forms. They pointed out that this arbitrary assumption complies with experimental results and that the error is only small. Gomez-Fernandez and Villalain [Gom98] determined the IR peak intensities of carbonyl and carboxylate for a fatty acid in a membrane and different ratios of fatty acid and carboxylate between pH 7 and 11. By directly relating the peak intensities they obtained a proper titration curve and the expected pK near 9. This indicates that also the change in the magnitude of the transition dipole moments of (non-)H-bonded carbonyl and of carboxyl with pH is small.

The intensity of the methylene band seems to decrease systematically with increasing pH. The difference of the intensities at pH 5.6 and 12.0 is almost 50%. However, the change in the molecular orientation is small (fig. 7.03) and also the decrease in the density of the molecules is negligible with increasing pH. In the condensed phase the molecules are tightly packed and the area per molecule increases only if the tilt angle increases or, very slightly, by increasing conformational chain disorder. Therefore the variation in the intensity of the methylene band is assumed to be due to scattering and the methylene band is not used for scaling. The intensities for the different pH values are related by the factor 1.

3. Concluded variation of surface concentrations with pH

Taking peak intensities for surface concentrations, according to table 7.5 the arachidic acid monolayer is half dissociated at about pH 9 ($D_H \approx 0.5$). This is in agreement with Gouy-Chapman-Stern theory for the buffer concentrations used (table 7.6, for comparison also the data of the subphase pH values hypothetically lowered by 0.3 units from pH 9.0 and 9.7 are given corresponding to extreme experimental tolerance). The deviation between theory and experiment, however, is large for pH 9.7. Theory yields a dissociation degree of more than 90% above pH 9.4. However, the

difference in the intensities of the carboxylate bands at pH 9.7 and 12.0 is conspicuous (fig. 7.11 d, e). Furthermore the presence of the carbonyl triplet is unambiguous at pH 9.7 (fig. 7.11 e), which would certainly not be resolved at a dissociation degree above 90%.

pH _b	[Na ⁺]·10 ³ [mole/l]	D _H	A _{Na}	pH ₀	ψ ₀ [mV]
5.6	0	0.003	0	2.8	-163
8.7	1.87	0.52	0.31	5.0	-216
9.0	1.87	0.66	0.43	5.2	-222
9.4	4.56	0.92	0.64	5.9	-206
9.7	4.56	0.96	0.68	6.2	-207
12.0	10.0	1.00	0.72	8.8	-188

Tab.7.6: Values calculated acc. to GCS-theory

Possibly the Gouy-Chapman-Stern theory fails to predict the true conditions at the monolayer, because it does not consider hydrogen bonding.

Regarding the intensities as concentrations, table 7.5 shows that the portions of singly and doubly H-bonded fatty acid, which are always approximately equal, strongly decrease between pH 5.6 and 9.0, while the change for the non-H-bonded fatty acid is insignificant. Between pH 9.0 and 9.7 the situation reverses and a drastic decrease of the amount of non-H-bonded fatty acid is found, while that of H-bonded fatty acid remains roughly unchanged. The decrease in the degree of hydrogen bonding from pH 5.6 to 9.0 can be explained as due to a decreasing concentration of hydronium ions at the monolayer, by which the carbonyl oxygen is protonated stronger than by water (according to Gouy-Chapman-Stern the surface pH_0 increases from 2.8 to 5.2, table 7.6) and to the increasing amount of carboxylate, which has the effect, that the number of adjacent neutral molecules, which could hydrogen bond to each other, reduces. Unclear at first sight is the jump in intensity for the non-H-bonded fatty acid above pH 9.0. However, a discontinuity at this pH value has also been observed previously (see 7.1) and been interpreted as the result of the breaking of hydrogen bonded acid-anion pairs accompanied by rapid dissociation (i. e. strong increase of carboxylate at the expense of carboxyl) above pH 9. The latter is not reflected by the carboxylate intensity at pH 9.7, which is not much higher than that at pH 9.0. The value seems to be somewhat too low. Possibly the peak area has been underestimated. Because of the small number of neutral fatty acids at this pH, it is conceivable that the presence of H-bonded carbonyl bands at pH 9.7 is only due to hydrogen bonding to water. The frequencies for the singly and doubly H-bonded carbonyl do not change until pH 9.7. This indicates that the character of the hydrogen bonds is preserved.

7.2.3 Conclusion

Combining interpretation and results from X-ray and IR investigation, the following tentative picture on the structure and head group bonding of fatty acid monolayers on alkaline subsolution is provided:

- In a monolayer on water at 12.5 mN/m fatty acid head groups are unbound, singly, and doubly H-bonded to approximately equal portions.
- The head groups of neutral fatty acids on aqueous subphase ($\text{pH} \approx 5.6$) are hydrated and the water molecules are bound to the head groups via hydrogen bonding to the carbonyl oxygen.
- In addition at pH 5.6 neighbouring fatty acids may be hydrogen bridged. The possibility that there is only hydrogen bonding between fatty acids and not between fatty acids and water is unlikely, since hydrogen bonding also occurs with esters [Ger94, Ger95] and in that case it must be with water.

- At pH 9.0 nearly half of the lipids are dissociated, acid-anion dimers of carboxyl and carboxylate have formed and a fraction of about 20% of carboxyl is bonded to water.
- Between pH 9 and 10 monolayer dissociation strongly increases, but a fraction below 20% is still hydrogen bonded to water molecules.
- At pH 12.0 almost all the molecules are dissociated. One part of the carboxylate may be associated with water, the other with the counterions. Different forms of association for the carboxylate group have been considered as the reason for the broad or splitted bands.

7.3 Effect of pH on the Stability of Monolayer Phases

Although fatty acids are relatively simple molecules, their monolayers exhibit a rich polymorphism with at least 7 solid phases (fig. 3.19) [Kja87, Dut87, Stä45, Bib91, Ove93b, Sch93, Riv94, Riv96, Tee97, Dur97, Shi94]. Up to now it is not understood what is responsible for such a variety of phases. The portion of phases with tilted molecules is predominant. The main directions of tilt are NN at the lower pressures in the phase diagram and NNN at intermediate pressures. The phase diagram of long chain alcohols differs from that of fatty acids in, that instead of the three tilted phases L_2 , L_2' , O_v it contains only one NNN-tilted phase. The untilted phases are the same [Shi94]. As in both amphiphiles only the head groups are different, it has been concluded that the untilted high pressure phases are a consequence of chain interactions, while the stability of the tilted phases is essentially determined by the head group interactions. Hence it is interesting to investigate what happens, when the fatty acid head groups are ionised on increasing the subphase pH, since by this the head group interactions are changed.

7.3.1 Phase Shifting due to Head Group Ionisation

In isotherms phase transitions may be indicated as horizontal plateaus or as kink, that mark a change in slope. Plateaus usually indicate discontinuous, kinks continuous phase transitions. Figure 7.12a illustrates the discontinuity of the low-pressure phase transition between tilted phases of arachidic acid below 20°C for pH 9. The discontinuity gradually decreases with increasing temperature and above 20°C the transition is not detectable any more in the isotherms.

The transition from tilted to untilted phases at high pressure appears as a plateau or as a kink over the entire accessible temperature range. Figure 7.12b shows that the pressure of the transition between the tilted phases decreases with increasing pH. Also the degree of discontinuity, expressed by the plateau width, reduces to a large extent between pH 5.6 and

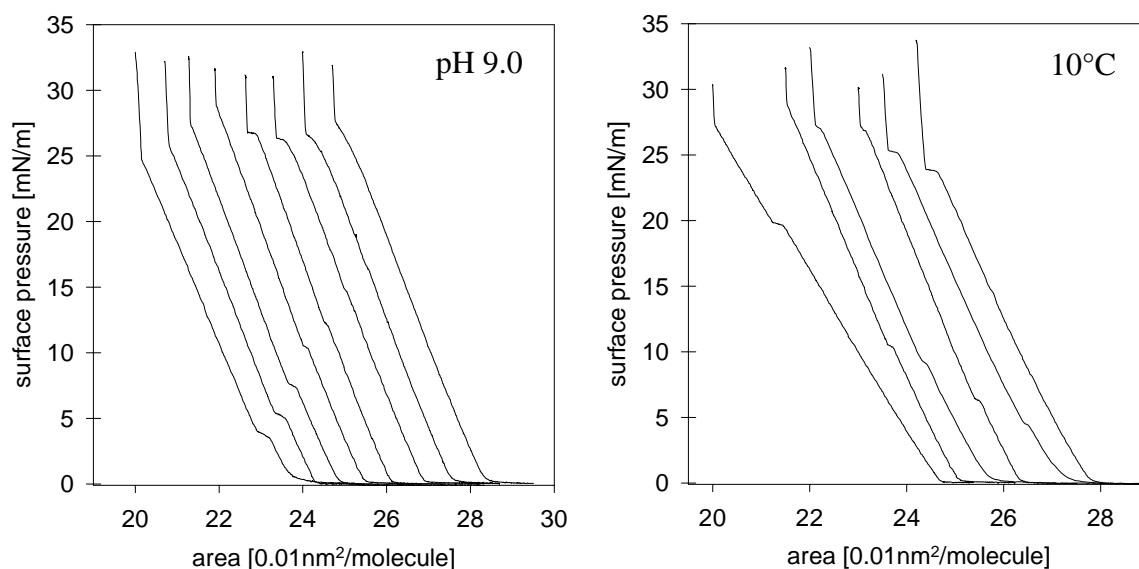


Fig.7.12

(a) Surface pressure-area isotherms of arachidic acid at pH 9.0 for 2, 4, 7, 10, 12, 15, 17, 20°C (from left to right)

(b) Isotherms at pH 5.6, 9.0, 9.2, 9.5, 9.7, ≈ 10.5 (from left to right) at 10°C

The isotherms are shifted along the area axis for clarity

pH 9.0 and slightly between pH 9.0 and pH 9.7. The opposite behaviour is observed for the high-pressure transition. There the discontinuity of the transition becomes more and more pronounced as the pH increases. The isotherms also reveal that the compressibility of the monolayer is larger at pH 5.6 than above pH 9.

Figure 7.13 demonstrates the influence of the subphase pH on the monolayer phases of arachidic acid. The open symbols (triangles and circles) mark the phase transitions between the tilted phases L_2 , L_2' , O_v and the untilted phases S and LS. The values were determined from the kink points (triangles) or the small plateaus (circles) in the high pressure region of the isotherms (cf. fig. 7.12 a, for pH 9.0) and agree with the values determined by BAM (see below).

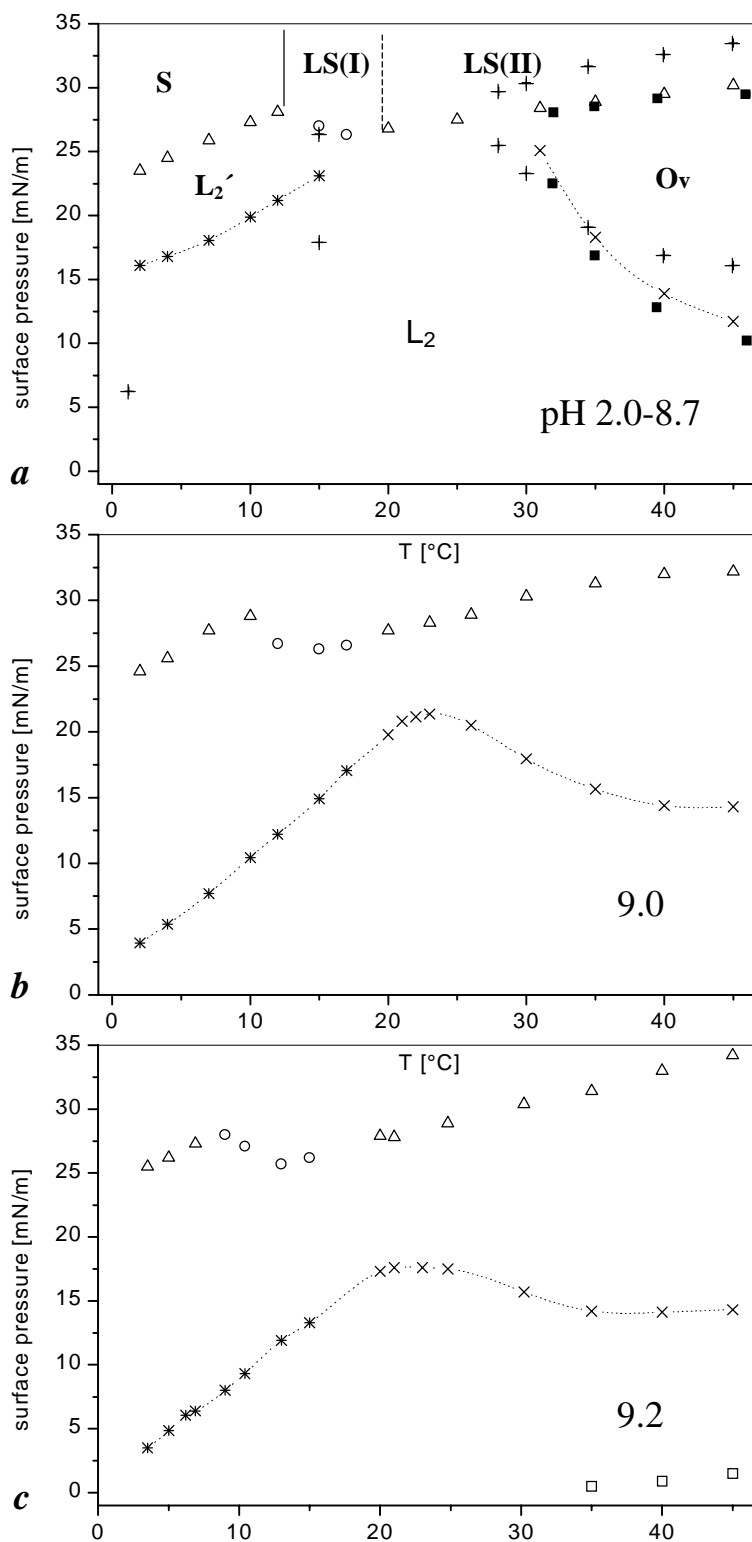
The circles mark the transition between the L_2' phase and the distorted hexagonal LS(I) phase. The LS(I) phase is separated from the hexagonal rotator phase LS(II) by a continuous transition towards higher temperatures (dotted line in 7.13 a) and from the S phase by a discontinuous transition towards lower temperatures (solid line) [Lau97]. This is reflected by the sudden change from a kink to a plateau in the isotherms at the S/LS(I) boundary and the continuous transformation from a plateau to a kink with increasing temperature at the LS(I)/LS(II) transition (fig. 7.12 a). The LS(I) phase is enclosed between about 12 and 20°C at pH 5.6 and with increasing pH it shifts to lower temperatures into the range from about 8 to 15°C at pH 9.7. This phase shift is illustrated by the transformation of a kink to a plateau and

the continuous growth of the plateau width with increasing pH in the high pressure region of the corresponding isotherms at 10°C (fig. 7.12 b).

The shape of the boundary between untilted and tilted phases changes only insignificantly with pH. In the branch at high temperatures the transition pressures increase from pH 2.0 to 8.7 (fig. 7.13 a) and remain unchanged from pH 8.7 to 10.5.

At pH 5.6 there are two transitions between tilted phases (fig. 7.13 a). One transition is between the NN tilted L_2 phase and the NNN tilted L_2' phase at low temperatures. It is discontinuous (symbolised by *) and reflected by a plateau in the low pressure region of the corresponding isotherms (fig. 7.12 a). The transition pressures determined with BAM coincide for compression as well as expansion exactly with those points in the isotherms, where the pressure starts to rise at the end of a plateau. The second transition between tilted phases is between the L_2 and the O_v

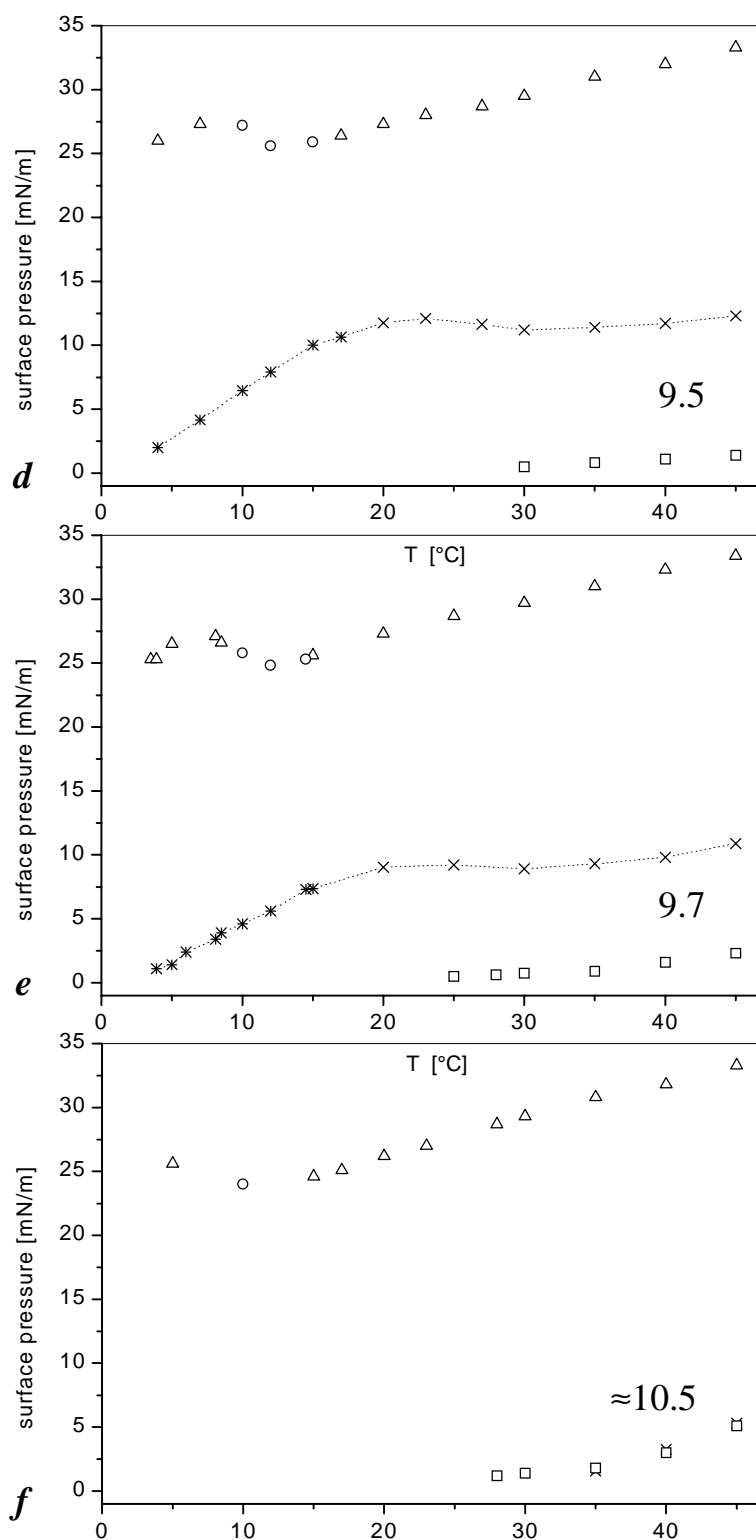
Fig.7.13: pH-dependence of the phase boundaries of arachidic acid monolayers between 2 and 45°C for (a) pH 2.0 (■), 5.6 (Δ,○,*,×), 8.7 (+); (b) 9.0; (c) 9.2; (d) 9.5; (e) 9.7; (f) ≈10.5. For meaning of symbols see text



(NNN) phase at high temperatures. There is no feature in the isotherms indicating this transition, but with BAM changes in the reflectivity are detected in the mono-layer pattern on passing the phase boundary (see below).

As the pH value is enhanced the boundaries of the tilting transitions approach each other and merge smoothly at about pH 9.0 combining the L_2 and the O_v phase to one NNN tilted phase [Joh98]. The NN/NNN boundary now continuously shifts to lower pressures until it vanishes at pH 10.5, leaving one single NNN and the untilted phases. The NN/NNN transition points at pH 10.5 (7.13 f, behind open squares) were determined by extrapolation, because the buffering capacity of the borate buffer for pH 10.5 proved to be too low and the measured values for the transition pressures were hence

overestimated. The values of the points of the boundary to the untilted phases, however, refer to this buffer solution, but as they are scarcely affected by the pH, they serve as a reasonable guide in the diagram. Over all the temperature range linearity between the pH and the L_2 - L_2' or L_2 - O_v (NN/NNN) transition pressure was found above pH 9.0 (fig. 7.14). The only deviation from this occurs above 35°C, where the transition pressures at pH 9.0 and 9.2



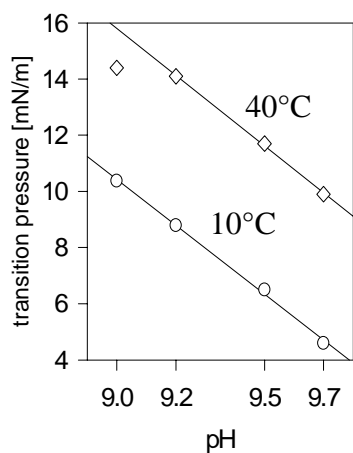
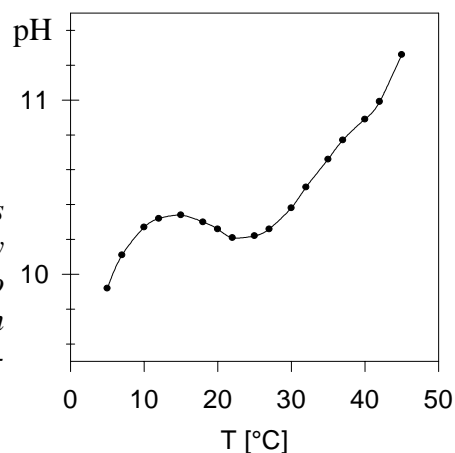


Fig.7.14: Linear pH-dependence of the NN/NNN transition pressure at 10 and 40°C above pH 9

Fig.7.15: pH values extrapolated linearly (cf. fig. 7.14) to zero NN/NNN transition pressure as a function of temperature



approach with increasing temperature. From this linear relationship the pH values can be determined, at which the NN/NNN transition pressure is zero (fig. 7.15).

Figure 7.15 shows, that in arachidic acid monolayers, besides the untilted phases, only one tilted phase exists in the measured temperature range for pH values higher than 10.

7.3.2 Optical changes at the phase transitions

Whether a phase transition is discontinuous or continuous can be seen directly by observing the movement of the monolayer molecules by means of BAM. A discontinuous transition between two tilted phases as well as between a tilted and an untilted phase is characterised by the discontinuous change of the molecular orientation at a propagating domain boundary. In contrast, during a continuous phase transition the image contrast changes gradually within a certain region due to a continuous reorientation of the molecules. In addition with BAM the transition between tilted and untilted phase can be distinguished from that between two tilted phases. The morphological changes during the four types of phase transitions (continuous and discontinuous transition between tilted and untilted phase, continuous and discontinuous one between tilted phases), which were the same for all pH values investigated, are described in the following. The continuity of the transitions as derived from the isotherms is confirmed.

Three subsequent stages of compression at the plateau of the discontinuous transition between the L_2' and the LS(I) phase are presented in figure 7.16. Patches with different shades of grey represent domains in which the molecules are tilted in certain azimuthal directions (7.16 a), while the tilt angle in the monolayer is uniform. On reducing the molecular area (across the plateau) the untilted phase, appearing homogeneously grey, starts to spread over the surface and grows in area at the expense of the tilted phase (7.16 b, c). Patches of the tilted phase are in coexistence with the untilted phase and when compression is

stopped, the movement of the domain boundaries interrupts. At the end of the plateau the image is uniformly grey. This process is reversed on expansion.

Figure 7.17 is an example for a continuous transition between tilted and untilted phases (triangles in fig. 7.13). The contrast between the domains decreases continuously on compression until the image is homogeneous at the kink point. The loss of contrast is due to the reduction of the tilt angle with growing surface pressure.

At the discontinuous transition between the two tilted phases L_2 and L_2' or the merged tilted phase at low temperatures (indicated by * in fig. 7.13) one observes at some places in the BAM image the development of domains with a new shade of grey that grows in area when the monolayer is compressed. The

growth of such a domain is presented in figure 7.18. In figure 7.18b a thin strip with a new tilt direction is about to be formed at the borders of the black domains in the centre of the image. There are fluctuations in the orientation of the molecules at the borderline which appears notched. At this stage the image seemed to be less sharp suggesting that the molecules are in slight movement. This may be caused by the loosening of the tilt-bond coupling at the NN/NNN-transition, when the molecular chains swing into a new direction. The movement of the chains is obviously least restricted at the domain boundaries where the growth of new domains is initiated. In 7.18c the fronts of the two domains, emerged at the edges of the black areas, have propagated and the borderlines are now smooth. The domains of equal azimuthal orientation of the molecules (indicated by identical brightness) approach each other and

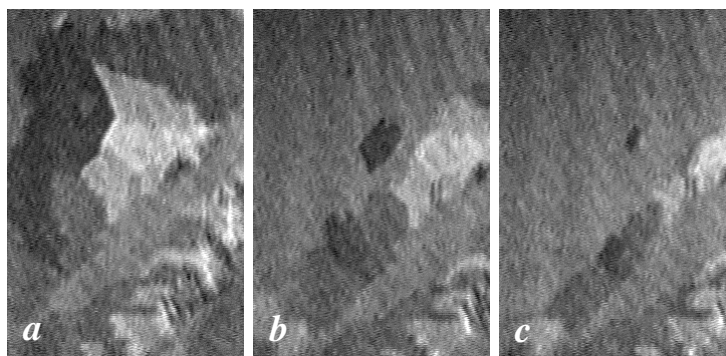


Fig.7.16a-c: As the discontinuous tilted/untilted phase transition is traversed during increasing pressure, the homogeneously appearing untilted phase spreads and replaces the mosaic-like tilted phase. When the phase transition has finished, the image is homogeneous (not shown); pH 9.2, 10°C (27 mN/m). Image size: 195×290 μm²

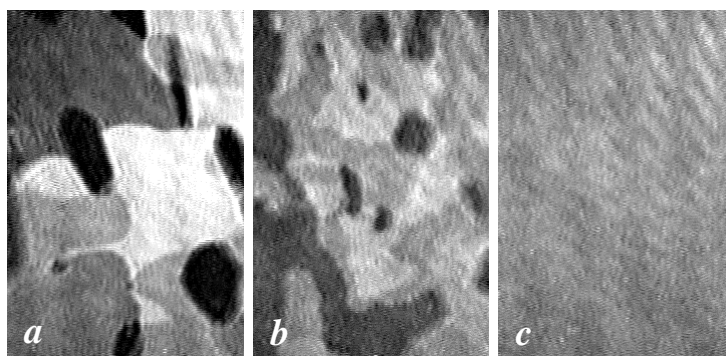


Fig.7.17a-c: For the continuous tilted/untilted phase transition the image contrast gradually decreases with increasing pressure until the monolayer is homogeneous at the kink point in the isotherm; pH 5.6, 25°C (27.5 mN/m). Image size: 195×290 μm²

eventually merge to form a single domain (7.18 e, f). The identical tilt direction in both domains might indicate that the molecules, starting from the domain edge, adopt the most favourable orientation with respect to the brighter phase, at the expense of which the domains grow.

The process of a continuous transition between the L_2 and the O_v phase or the merged tilted phase at high temperatures (symbolised by \times in fig. 7.13), is shown in figure 7.19. Figures 7.19a-h represent a compression

cycle where (a-d) are subsequent stages of compression traversing the phase boundary from one tilted phase (a) to the other (d). No domain boundary is shifting. The domains continuously adopt a different reflectivity and their boundaries are extinguished by mutual influencing of the chain orientations in neighbouring regions, which fuse and lead to new domain shapes. On expanding (e-h) back into the other tilted phase (h) a similar pattern as the original

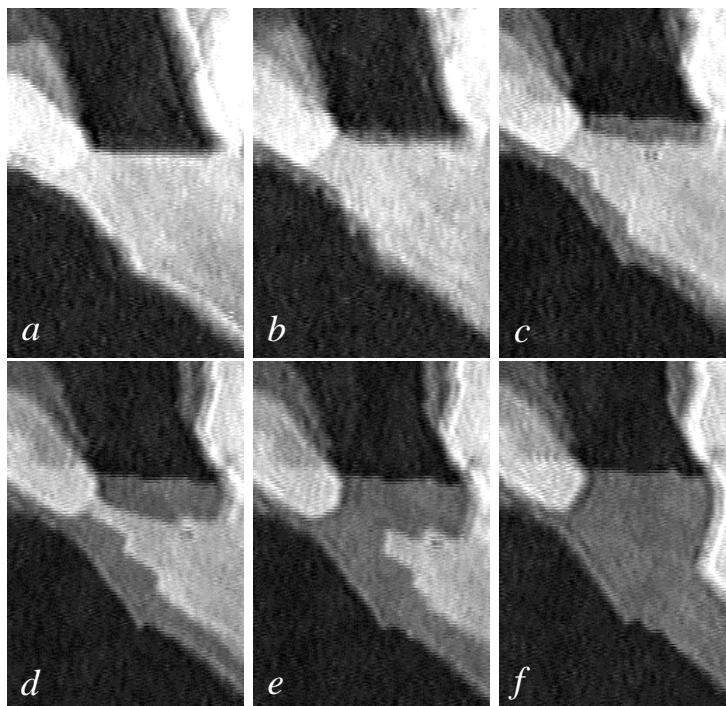
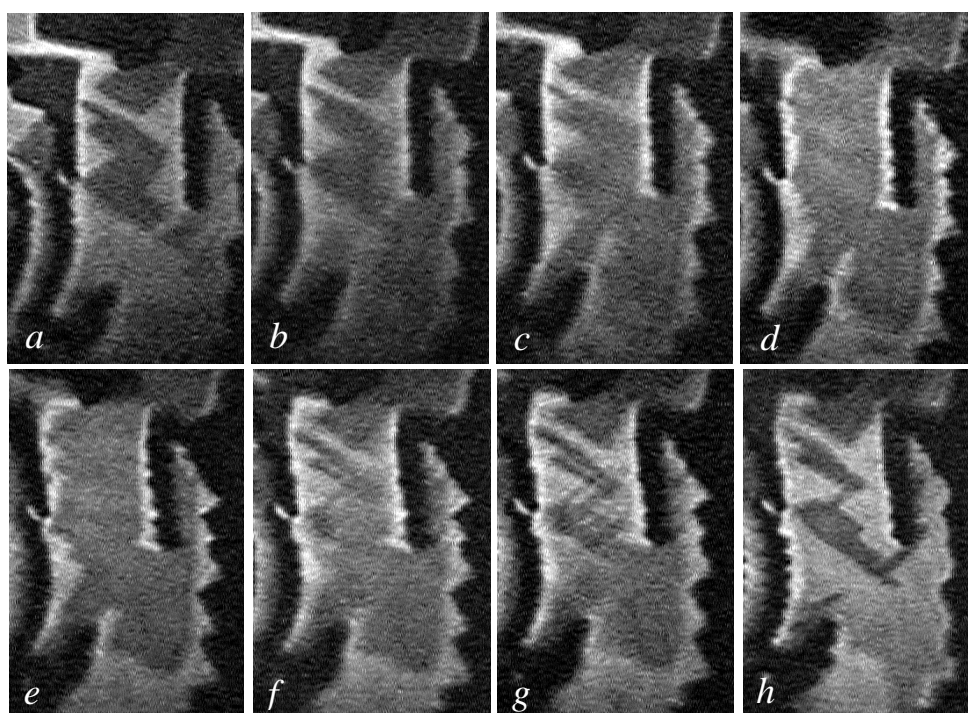


Fig.7.18a-f: Subsequent stages of the discontinuous NN/NNN phase transition; pH 8.7, 15°C (17.9 mN/m). Image size: 140×205 μm^2

Fig.7.19a-h: Subsequent stages of a phase transition cycle at the continuous NN/NNN transition; (a-d) compression, (e-h) expansion; pH 5.6, 35°C (18.3 mN/m). Image size: 350×520 μm^2



one (a) is obtained. The explanation that with repeated cycles always very similar domains are recovered may be as follows. The contour of the domain in the centre of figure 7.19a may be imprinted in the lattice by lattice defects accumulated at the domain perimeter. The uniform tilt orientation enhances the order of the lattice in the domain area. When the orientation of the molecules and the optical structure of the monolayer change at the transition, the defects are bridged because of the long ranging alignment of the molecules and are therefore invisible (7.19 d, e). They may partially heal but the contour of the old domain essentially persists. When the previous phase is entered again the molecules swing back into the original orientations and within the original boundaries as then the most favourable state concerning the energies of the domain boundaries may be reached for this phase.

7.3.3 Indications of a Superior Division of the Phase Diagram

The result of the isotherm and BAM measurements is, that the $L_2'/LS(I)$ and the L_2/L_2' transition are discontinuous, while all the others (L_2'/S , $L_2/LS(II)$, $O_v/LS(II)$ and L_2/O_v) are continuous. In some literature [Riv94, Kag99] the L_2/O_v transition was regarded as discontinuous first order, which is in contradiction to the results of the present work.

From the phase diagrams (fig. 7.13) one can see, that the temperature, where the L_2 and L_2' (merged phase) transition becomes continuous, is nearly independent of the pH. The change in type of transition seems to mark an almost vertical boundary, that, including the $LS(I)$ and $LS(II)$ phase boundary, divides the fatty acid phase diagram in two superior parts.

The temperature range, within which the continuity of the NN/NNN transition changes, i. e. the width of this boundary, was tried to establish by means of BAM for two pH values: for pH 9.2 the transition was found to be continuous above 24°C and discontinuous below 18°C. The range in between was hard to resolve, because the movement of the molecules was relatively slow and the contrast of the image was poor compared to lower pressures for higher pH values. It is conceivable that the type of transition changes continuously over this temperature range. At pH 9.7 the mobility of the molecules at the transition was high and the range, within which a change in transition type was realised, could be narrowed to 1°C between 25 and 26°C.

The existence of a vertical phase boundary in this temperature range has been inferred from theoretical considerations [Kag93b, Kag95b] and is indicated by some experimental observations [Lau97, Pet96]. The reason, that nobody yet succeeded to prove its existence with certainty, may be that, besides the experimental difficulties due to its vertical position, the transition is hindered kinetically [Lau97]. According to the theory [Kag93b, Kag95b] this

boundary separates herringbone ordered phases at low temperatures from herringbone disordered phases in the high temperature part of the diagram (dividing the L_2 phase into L_{2d} (disordered) and L_{2h} (ordered)). It is conceivable that an effect of this boundary and the underlying structural feature is the separation of the NNN phases L_2' and O_v by the NN L_2 phase and their fusion near the LS(I)/LS(II)/ L_2' (or L_2)-triple point [Tee97], which occurs at the presumed location of the boundary. This feature may also be responsible for the inflection point between 15 and 25°C in the curve of figure 7.15 showing the pH values necessary to reach zero NN/NNN transition pressure.

7.3.4 Possible Explanations of the Phase Shifting

A horizontal shift of the phase boundaries by about 4°C to lower temperatures on increasing the pH from 5.6 to 9.7 is revealed by the shift of the LS(I) phase. The phase shift can be explained by the reduction of the attractive interactions between the lipids with increasing degree of dissociation and electrostatic head group repulsion. The same effect is caused by a decrease in chain length [Bib90].

Much more drastic is the influence of the pH on the shift of the boundaries between the tilted phases. The movement of the boundaries of arachidic acid in dependence of the pH is very similar to that of fatty acid/ester or acid/alcohol mixtures in dependence of the mixing ratio [Tee97, Shi94, Dur95, Fis95]. This can be easily understood by regarding the fatty acid monolayer on alkaline subphase as a mixture between neutral fatty acid and carboxylate, the ratio of which changes with the pH [Joh98]. While with acid/alcohol mixtures the L_2 phase disappears at about equal proportions of the two compounds [Shi94, Dur95, Fis95], with fatty acid monolayers on alkaline subphase this happens above pH 10 (fig. 7.15), when the monolayer is almost pure carboxylate. The latter follows from the solution of the Gouy-Chapman-Stern equation for pH > 10 (table 7.6).

It is obvious that the shift of the phase boundaries between the tilted phases in the lipid mixtures is caused by the change in the head group interactions with changing mixing ratio, since the chains of the different compounds are the same. Consequently a key to the understanding of the richness of phases in amphiphilic monolayers appears to be the understanding of the head group interactions. As discussed in 7.1.2 for these electrostatic, steric and bonding interactions and the role of the solutes have to be taken into account. The similarity in the phase behaviour of dissociated fatty acids and of fatty acid/ester, alcohol mixtures as noticed above suggests, that the solutes are not specifically responsible for this phase behaviour, since in the latter system no ions and surface charges are present and the

sodium ions beneath the charged fatty acid monolayer are expected to essentially influence only the lateral electrostatic interactions in the monolayer by electrical screening, compensation of head group charges and by changing the degree of dissociation.

A measure for the head group interactions represents the mean molecular area of the monolayer, the value of which includes steric, electrostatic and bonding interactions. This suggests to search for a relation between phase transition pressure and mean molecular area. The latter may be treated as equivalent to the head group size. Indeed in the literature the idea is followed, that the NN/NNN transition pressure is coupled to a definite molecular area, or equivalently, to a definite molecular tilt angle (for fatty acids and derivatives around 20°) [Tee97, Shi92, Sch97, Sch99]. This idea shall be illustrated as follows: the tilt angle (t) corresponds to a certain molecular area A_{xy} , according to $A_{xy}\cos t=A_0$ (I) [Tip91, Kja89], where A_0 is the cross sectional area of a chain. As the compressibility $\Delta A_{xy}/\Delta\pi$ (<0) is usually found to be constant, the area A_{xy}' at the transition pressure π' is derived from: $A_{xy}' = \pi' \cdot \Delta A_{xy}/\Delta\pi + A_{xy}(\pi=0)$ (II) (t' is obtained from (I)). Accordingly, when assuming a certain value for the tilt angle t' (or area A_{xy}') at the transition and equal compressibilities, the transition pressure (π') decreases with decreasing molecular area at zero pressure ($A_{xy}(\pi=0)$). Alternatively expressed, the NN/NNN transition pressure decreases with decreasing head group size.

In the present case, however, the change in the transition pressure cannot be explained in this way. When comparing the two isotherms for pH 9.2 and 9.5 in figure 7.12b, one can see that the compressibilities are equal and that the NN/NNN transition pressures are well separated, while the pressures of the transition to the untilted phase are quite the same. The coinciding widths of the plateaus indicate very similar jumps in area at the transitions. Hence, if according to the above concept A_{xy}' is the same at the NN/NNN transitions for both pH values, the difference between the transition pressures should be similar at the tilted/untilted and at the NN/NNN transition. This, however, is not found. Furthermore X-ray measurements reveal, that t' is not constant, but increases by more than 4° between pH 9 and pH 10 at 15°C (tab.7.1).

Insight in the stability of NN and NNN phase and hence the magnitude of the transition pressure is obtained by a simple model considering the steric interactions between compressible spheres in place of the head groups (see 3.2.2.4). According to this the presence of either NN or NNN phase depends on the interplay between chain and head group interactions. While the NNN phase seems to be favoured by the chain interactions, especially at small tilt angles [Kag93a, Kuz98], the NN phase is the more favourable in this model, i. e. the NN/NNN transition pressure is the higher, the lower the compressibility and the stronger

the steric interactions between the head groups are. Strong steric interactions are exerted by large head groups, so that qualitatively the same relation results between head size and transition pressure as with the idea of a constant transition area A_{xy} discussed above. The model of compressible heads, however, allows to consider also a possible direction dependence (anisotropy) of the compressibility (fig. 3.16). The decrease in the NN/NNN transition pressure with increasing dissociation could be explained by a higher compressibility of carboxylate compared to carboxyl along the [11] lattice direction (d'' in fig. 3.16 c).

X-ray measurements supported by IR measurements (7.1, 7.2) indicate bonding interactions between the fatty acid head groups.

In figure 7.20 the NN/NNN L_2/O_v transition pressure is plotted versus the pH for 40°C. The coincidence with the graphs in figure 7.05 is easily noticed. From figure 7.13a one can see that the variation of the transition pressure with the pH, as is shown in figure 7.20, is similar for temperatures higher than 40°C. Below this temperature the transition pressure increases only slightly or even slightly decreases with increasing pH up to pH 9, but the rapid and linear decrease of the transition pressure beyond this pH value applies to the whole L_2/O_v transition range. The correlation between the head group bonding interactions and the L_2/O_v transition pressure is significant. This finding is surprising and important, since it indicates that the NN L_2 phase, which is characteristic of fatty acid monolayers, is stabilised by head group bonding interactions. In terms of the above model of compressible spheres the correlation between bonding interactions and transition pressure can be explained by the increase in the steric interactions and in the tendency of the head groups to separate due to hydrogen bonding.

The L_2/L_2' transition was not investigated in such detail. From the few points in figure 7.13a, however, it appears that the transition pressure rapidly decreases already above pH 5.6.

The high sensitivity of the NN/NNN (L_2/O_v) transition pressure to changes in the head group interactions is demonstrated by the noticeable difference in pressure between pH 2 and pH 5.6. It is apparently caused by the small difference in the degree of dissociation in the order of one percent, which is hard to resolve by other methods [Ave90, Mir98].

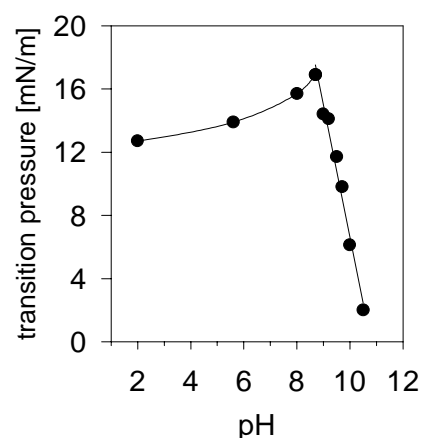


Fig.7.20: Variation of the L_2/O_v phase transition pressure with pH for arachidic acid at 40°C

7.3.5. An Alternative Mechanism for the NN/NNN Transition

It is generally assumed, that the NN/NNN transition occurs by the rotation of the tilted molecular chains by 30° (or 30° plus multiples of 60°) [Lau99].

Inspecting the morphological changes in monolayers during NN/NNN phase transitions, however, it appears that not all the molecules move at the transition. This was also noticed previously [Sch93]. It is therefore conceivable, that the NN/NNN transition is based on a different mechanism without chain rotation and that the change in the tilt direction is just driven by energy differences at the domain boundaries. The latter is indicated by the observations described above (fig. 7.18, 7.19).

This notion is supported by the fact, that rotation of the molecules is even observed between two phases with NN tilt at the L_2/L_2'' transition [Riv96]. A mechanism for an NN/NNN transition working without chain rotation is proposed in figure 7.21. Similar shifts of atoms or molecules at phase transitions are found in 3D systems (e. g. martensitic transformation).

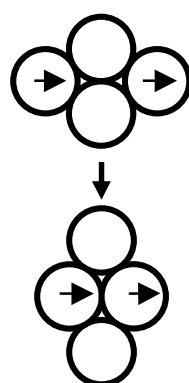


Fig.7.21: Proposed mechanism for an NN/NNN transition without chain rotation. The circles indicate the head groups, the arrows the tilt direction. The position of the grey circles illustrate the transition from NNN tilt (above) towards NN tilt (below)

7.4 Disclosure of Lipid-Solute Interactions by Simple Isotherm Measurement

In this chapter an idea is presented how information on the influence of solutes on the head group interactions of a lipid monolayer may be obtained from the surface pressure-area isotherm. Series of mixtures between water and a number of compounds were prepared and the change in the isotherm of an arachidic acid monolayer was investigated in dependence of the subphase composition.

1. Change of head group hydration

Figure 7.22 shows the isotherms of arachidic acid on solutions of different ethanol concentration. The NN/NNN and tilted/untitled phase transitions are well visible. Both transition pressures decrease almost equally with increasing ethanol content of the subphase, the difference between the two values, however, slightly increases (tab. 7.7). The parallel shift of the isotherms to lower pressures corresponds to the decrease of molecular area and tilt angle at zero pressure. The reduction of the head group area in the presence of the alcohol is

ascribed to the removal of solvent molecules between the amphiphilic head groups. The positive surface pressure of a monolayer can be regarded as an osmotic pressure, which arises from the tendency of the amphiphilic head groups to separate at the solvent surface (eq. 4.02). If the solvent is removed, the attractive chain interactions dominate and the head group distance is reduced by reducing the chain tilt angle (eq. 3.05). Figure 7.22 provides evidence that the lipid head groups are hydrated (meaning close contact between head groups and water molecules, that tend to penetrate between the head groups, not a fixed shell of immobile solvent molecules around the head groups, see app. V) and that

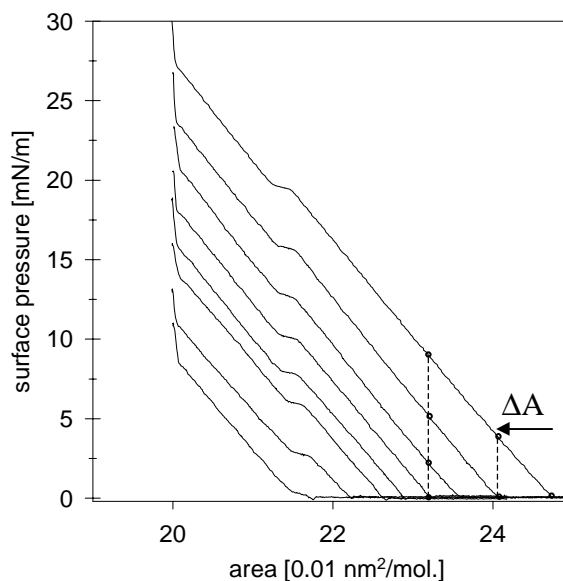


Fig.7.22: Isotherms of arachidic acid monolayers on water/ethanol mixtures at 10°C. Visible are the NN/NNN and tilted/untitled phase transitions (cf. fig. 7.12). From top to bottom: 0, 1, 2, 3, 4, 5, 7, 9 vol% ethanol

the head groups are dehydrated by adding alcohol or by increasing the surface pressure. The correspondence between the increase in the ethanol concentration and the increase in the surface pressure is illustrated by the hatched vertical lines in the figure.

How can the dehydrating effect of this and other solutes (see below) be explained? This question, to which no sure answer exists yet, might have large implication for the understanding of the action of such solutes in biological systems, as for instance of the capability of alcohols of changing the conformation of proteins [Hir98, Kle90, Aru97]. It is well known that ethanol forms hydrogen bonded aggregates $(EtOH)_n$ in the pure liquid and in non-polar solvents [Sto77, Lea88]. Recent experiments indicate that ethanol self-aggregates even in dilute aqueous solution. The size of these aggregates is assumed to increase with increasing alcohol concentration [Miz95, Nis95]. Now it is conceivable that such aggregates, due to the surface activity of the alcohol [Son77], settle in one or more layers beneath the lipid monolayer and replace the water molecules in the head group region (model in fig. 7.23). The alcohol molecules should preferentially accumulate

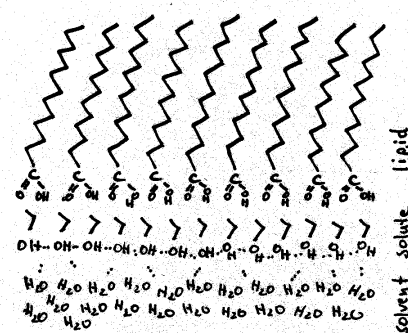


Fig.7.23: Model for the dehydration mechanism of solutes. The orientation of the ethanol molecules with the OH pointing to the water phase seems most likely

beneath a monolayer, since, as already mentioned, this region is much less polar than the bulk solution (fig. 5.08). According to this idea the dehydrating efficiency of the solute should be the higher, the larger the adsorbed aggregates, the smaller the gaps between separate adsorbed aggregates, the stronger the cohesion of the molecules within the aggregates and the higher the hydrophobic character of the molecules.

A measure for the dehydration efficiency of a solute is the ratio of the decrease in molecular area (at a certain pressure) per increase in solute concentration $\Delta A/\Delta c$. ΔA versus c is plotted for a number of solutes in figure 7.24. ΔA has been calculated by multiplying the difference in the

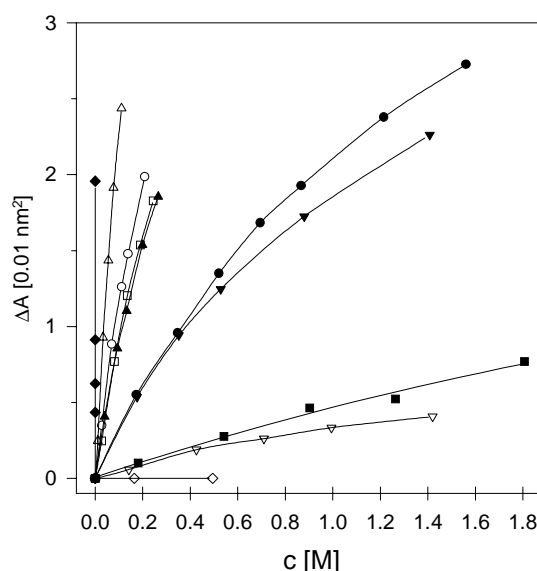


Fig.7.24: Condensation of an arachidic acid monolayer at 10°C by solutes in the water subphase; ●: ethanol, ○: 2,2,2-trifluoroethanol ■: ethylene glycol, □: 1-propanol, ▲: 2-propanol, △: 1-butanol, ▼: acetic acid, ▽: DMSO, ◆: Cu^{2+} , ◇: glucose (density data: [Rid86,Dau98])

tilted/untilted transition pressures π_{PT} (2) (tab. 7.7) of pure water and solute with the isotherm compressibility $\Delta A/\Delta\pi$. For the compressibility the same value of $-0.145 \cdot 10^{-2} \text{ nm}^2 \text{ mol}^{-1} \text{ m(mN)}^{-1}$ has been substituted for all solutes. This value is the mean of the compressibilities determined from X-ray analysis for some solutes and different solute concentrations (tab. 7.8) (the coincidence of the isotherm compressibilities for arachidic acid on water and on $10^{-4} \text{ M Cu}^{2+}$ solution for 20°C is shown by X-ray analysis in [Joh99b]). According to figure 7.24 the condensing, i. e. the dehydration efficiency, decreases in the order:

$\text{Cu}^{2+} > 1\text{-butanol} > 2,2,2\text{-trifluoroethanol} > 1\text{-propanol} \geq 2\text{-propanol} > \text{ethanol} > \text{acetic acid} > \text{ethylene glycol} > \text{DMSO} > \text{Glucose}$

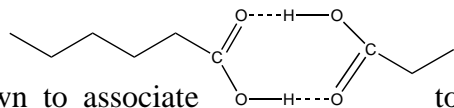
With the exception of Cu^{2+} one finds, that the dehydration efficiency increases with increasing apolar and decreasing polar portion, i. e. with increasing hydrophobicity of the solute molecule. This supports the dehydration mechanism proposed above.

2. Indication of carboxylic acid dimer formation

If isotherms of arachidic acid are measured on mixtures of acetic acid in water, significant monolayer condensation is observed, which is due to collapse and/or dissolution (fig. 7.25). The solubility increases with increasing acetic acid concentration. X-ray measurements with 2

and 5 vol% acetic acid indicate that the decrease in area is due to collapse formation. They reveal that the monolayer transforms into 3 D matter the quicker the higher the solute concentration.

Carboxylic



acids are known to associate to dimers in apolar solvents and in the gas phase [Jun94]. Dimer formation between acetic and arachidic acid could explain the enhanced tendency for collapse formation. On dimer formation the end of the monolayer lipid pointing to the subphase becomes more hydro-phobic, since the end is a methyl group and the carboxylic head group is shielded from the water phase by dimer

formation. Consequently the untying of the lipid from the water surface and its incorporation into a 3 D collapse phase is facilitated. Slight monolayer condensation was also noticed for some water alcohol mixtures during two subsequent compression-expansion cycles, but by far not to such an extent.

3. Change of head group interactions

According to the model of compressible spheres presented in 3.2.2.4 (fig. 3.16), a change in the head group interactions manifests in the shift of the tilt angle at the NN/NNN transition (fig. 3.17). For equal isotherm compressibilities pressure and tilt angle are equivalent, so that a change in the difference of tilted/untilted and NN/NNN transition pressure ($\Delta_{1,2}$ in tab. 7.7) indicates a change in the head group compressibilities. With ethanol $\Delta_{1,2}$ is slightly above the value for pure water and it increases with increasing ethanol concentration. A very similar behaviour is found for ethyleneglycol. Much more pronounced is this effect with DMSO. Essentially no influence on the head group interactions is revealed for trifluoroethanol, n-, i-propanol, butanol, acetic acid and glucose. It seems contradictory that hydrogen bonding is assumed above between arachidic and acetic acid without significant effect on the arachidic acid head group interactions. In comparison the increase in $\Delta_{1,2}$ with increasing pH is very large and comprehensible, since the head group interactions are affected considerably on dissociation. A large effect is also revealed for the copper ions, which are known to bind to and strongly interact with carboxylate [Spi55, Joh99b]. Surprising is the fact, that $\Delta_{1,2}$

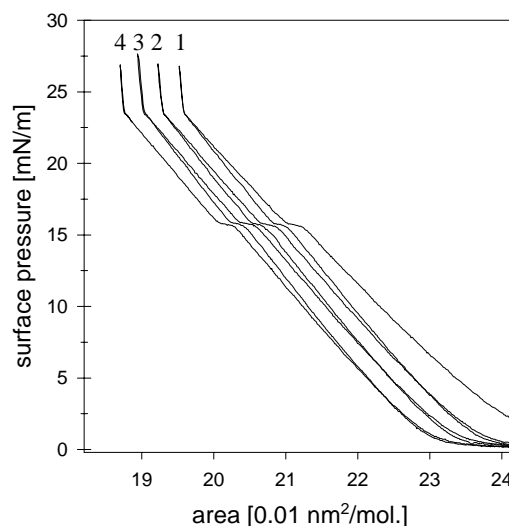


Fig.7.25: Shift of the isotherm of arachidic acid (1-4) on a solution of 1 vol% acetic acid in water on subsequent compression and expansion; 10°C; $0.28 \text{ nm}^2 \text{ mol}^{-1} \text{ min}^{-1}$

decreases with increasing ion concentration. This indicates that the interactions between the head group copper/carboxylate complexes is completely different from that between (sodium)/carboxylate groups.

Solute	v%	$\pi_{PT}(1)$	$\pi_{PT}(2)$	$\Delta_{1,2}$	ΔA	Solute	v%/M	$\pi_{PT}(1)$	$\pi_{PT}(2)$	$\Delta_{1,2}$	ΔA
no	0	19.9	27.3	7.4	0		2	6.9	14.5	7.6	1.86
ethanol	1	16.0	23.5	7.5	0.55	1-butanol	0.1	17.8	25.6	7.3	0.25
	2	13.1	20.7	7.6	0.96		0.3	13.4	20.9	7.5	0.93
	3	10.3	18.0	7.7	1.35		0.5	9.7	17.4	7.7	1.44
	4	8.1	15.7	7.6	1.68		0.7	6.5	14.1	7.6	1.91
	5	6.4	14.0	7.6	1.93		1	2.8	10.5	7.7	2.44
	7	2.9	10.9	8.0	2.38	acetic acid	1	16.0	23.6	7.6	0.54
	9	0.5	8.5	8.0	2.73		2	13.2	20.8	7.6	0.94
	2,2,2-trifluoroethanol	0.2	17.3	24.9	7.6		0.35	3	11.1	18.7	7.6
0.5		13.9	21.2	7.3	0.88		5	7.7	15.4	7.7	1.73
0.8		11.0	18.6	7.6	1.26	8	4.0	11.7	7.7	2.26	
1		9.7	17.1	7.4	1.48	DMSO	1	19.2	26.9	7.7	0.06
1.5	6.0	13.6	7.6	1.99	3		18.4	26.0	7.6	0.19	
ethylene-glycol	1	19.3	26.6	7.3	0.10		5	17.7	25.5	7.8	0.26
	3	18.0	25.4	7.4	0.28		7	16.8	25.0	8.2	0.33
	5	16.6	24.1	7.5	0.46		10	16.1	24.5	8.4	0.40
	7	15.8	23.7	7.9	0.52	D-(+) glucose	0.165 M	19.8	27.3	7.5	0.00
	10	13.9	22.0	8.1	0.77		0.494 M	19.8	27.2	7.4	0.00
1-propanol	0.2	18.1	25.6	7.5	0.25	CuSO ₄	1 μ M	17.7	24.3	6.6	0.44
	0.6	14.6	22.0	7.4	0.77		3 μ M	17.2	23.0	5.8	0.62
	1	11.7	19.0	7.3	1.20		4 μ M	16.1	21.0	4.9	0.91
	1.4	9.4	16.7	7.3	1.54		5 μ M	10.7	13.8	3.1	1.96
	1.8	7.4	14.7	7.3	1.83	base	pH 5.6	19.9	27.3	7.4	
2-propanol	0.3	17.1	24.5	7.4	0.40		pH 9.0	10.5	28.8	18.3	
	0.7	13.9	21.4	7.5	0.86		pH 9.2	9.3	27.1	17.8	
	1	12.0	19.7	7.7	1.10		pH 9.5	6.5	27.2	20.7	
	1.5	9.0	16.7	7.7	1.54		pH 9.7	4.6	25.8	21.2	

Tab.7.7: Shift of phase transition pressures $\pi_{PT}(1)$ (NN/NNN), $\pi_{PT}(2)$ (tilted/untitled) [mN/m] and reduction in head group area ΔA (determination see text) [0.01 nm²/mol.] of an arachidic acid monolayer in dependence of the solute concentration at 10°C. A change in $\Delta_{1,2}$ ($=\pi_{PT}(2)-\pi_{PT}(1)$) with respect to pure water subphase is assumed to indicate a change in the arachidic acid head group interactions

	v%	$-\Delta A/\Delta\pi$	$A(\pi=0)$
no solute	0	0.144/0.141	23.1/22.8
1-butanol	0.3	0.143/0.149	22.1/22.0
	0.6	0.137/0.153	21.4/21.3
acetic acid	2	0.134/0.160	22.2/22.3
	5	0.150/0.149	21.5/21.4
1-heptadecanol	0.03	0.137 (NNN)	20.6 (NNN)

Tab.7.8: Compressibilities $\Delta A/\Delta\pi$ [0.01nm²/mol./(mNm⁻¹)] and molecular areas for zero pressure $A(\pi=0)$ [0.01nm²/mol.] determined by X-ray analysis for arachidic acid monolayers and some solutes at 10°C. The couples of values A/B refer to NN/NNN phase

8. Summary and Outlook

The point of main effort in this work was the investigation of the correlation between the degree of dissociation in fatty acid monolayers at the air/solution interface and their thermodynamic, morphological and structural features. The monolayers were characterised by means of film balance and surface potential measurements, Brewster-angle microscopy, X-ray diffraction and IR reflection absorption spectroscopy.

The gradual change of the subphase pH and hence of the portion of charged molecules in the monolayer allows to fine-tune the intermolecular interactions and the balance between repulsive electrostatic and attractive forces. It is revealed that slight changes in pH produce significant effects on phase behaviour, structure and morphology of fatty acid monolayers. Using arachidic acid as representative for the fatty acids a change in the monolayer phase diagram is observed already between pH 2 and 5.6 (fig. 7.13 a), where the fraction of dissociated molecules is almost negligible (according to the Gouy-Chapman-Stern theory on the order of a percent, tab. 7.6). This indicates the sensitivity of the stability of monolayer phases on changes in the intermolecular interactions. Between pH 8 and 10 an abrupt change in the structural properties is detected, and macroscopic phase behaviour and morphology of arachidic acid change drastically above about pH 12.

At high pH fatty acids, that are condensed on water subphase develop a fluid phase and exhibit a plateau region in the isotherms, which can be attributed to a state of coexistence of fluid and condensed monolayer phase. The pH values at which different fatty acids develop a plateau depends on the chain length and the temperature. The solubility decreases with increasing chain length and from arachidic acid fatty acid monolayers are stable and suitable for investigation within the accessible temperature range up to pH 13. Lower homologues can be stabilised against dissolution by salting-out. The surface pressure of the two phase region increases linearly with pH (fig. 5.06), which demonstrates for the thermodynamic behaviour of the monolayer the equivalence of an increase in pH with an increase in temperature or a decrease in chain length (also the latter are linear functions of the plateau onset pressure). The increase in plateau pressure with increasing pH is ascribed to the increase in the degree of dissociation and the consequent decrease in the fluid-condensed phase transition enthalpy due to enhanced electrostatic repulsion in the condensed phase. This means that fatty acid monolayers still contain neutral fatty acids and are able to dissociate up to about pH 13 where dissociation is assumed to be complete (fig. 5.06). Above pH 12.0 the difference in electrostatic energy caused by a change in pH by 0.3 units corresponds to the dispersion

energy of a CH₂-chain segment for arachidic acid. It would be interesting to find a quantitative relation between pH, plateau onset pressure and degree of dissociation, which reproduces the linearity between pH and plateau pressure and proves the assumption, that the change in the plateau pressure arises from incomplete monolayer dissociation.

The following model is proposed for the composition of a heterogeneous fatty acid monolayer in the state of fluid-condensed coexistence (fig. 5.08): the fluid phase with a larger molecular area is completely dissociated. The condensed phase of higher molecular density is only partially dissociated, although surface charge density and potential are higher than for the fluid phase. Hence an increase in the subphase pH affects predominantly the condensed phase. The weakly electrostatically binding counter ions, like the used sodium ions, are enriched at the interface and partially adsorb to the charged monolayer.

It is shown that the morphological features size and shape of condensed phase domains in the two phase region and the range of tilt orientational order are determined by the balance of repulsive electrostatic and attractive interactions between the monolayer lipids. Relations are revealed between the microscopic monolayer morphology and the intermolecular interactions on the molecular level.

An increase in the pH in arachidic acid monolayers between pH 12 and 13 leads to the decrease in the average domain area, to the increase in the domain perimeter per area and to the decrease in the range of tilt orientational order. The same effects as for an increase in the degree of dissociation are found for a decrease in temperature at constant pH. In both cases these changes can be explained by the increase in the ratio of μ to λ . The difference in the dipole densities of condensed and fluid phase μ is a measure for the repulsive interactions, and the mean line tension λ is determined by the attractive interactions. Surface potential measurements and the increase in the tendency for domain aggregation and fusion between pH 12.0 and 12.7 indicate, that μ is near zero and slightly decreases with increasing pH. However, the increase in the intermolecular distance and chain tilt (fig. 7.03, cf. eq. 3.05), the increase in the chain cross section (fig. 7.01) and the decrease in the degree of herringbone order and chain conformational order (fig. 7.02) with increasing pH point to the decrease in the intermolecular interactions in the condensed phase and therefore to the decrease in λ with increasing monolayer dissociation. The decrease in the intermolecular interactions also accounts for the decrease in the extent of tilt order with increasing pH. Its range decreases from several tens of μm at pH 12.0 to approximately 100 molecular distances at pH 13 (fig. 6.04). In this context it is interesting to note, that stable, compact domains still form at pH 13, where the monolayer is assumed to be completely dissociated.

Both λ and μ are expected to increase with decreasing temperature. λ is expected to increase linearly with decreasing temperature (6.3.2), μ should vary like $A_{fl}-A_{LC}$ inversely with temperature, provided that the change in the dipole moments of the molecules in the fluid and in the condensed phase with temperature is negligible or comparable. Moreover a change in μ needs a change in λ^2 , in order to observe the same effects on domain morphology. Hence with decreasing temperature the repulsive are expected to outweigh the attractive interactions.

This demonstrates, that with respect to the morphological behaviour, in contrast to the thermodynamic and structural behaviour, an increase in pH corresponds to a decrease in temperature.

It is shown that the microscopic structure within condensed phase domains and peculiar shape transformations, such as faceting, are the result of the action of forces that are based on intermolecular interactions, and not the result of growth conditions. These forces arise from the tilt of the rod-like molecules. Elastic energy, defect line energy and defect core energy are produced when the preferred parallel tilt order of the molecules is disturbed and the molecules change their tilt direction sharply or continuously. For a reason not yet known tilted molecules prefer to adopt a definite orientation with respect to the domain boundary. Deviation from this direction is connected with a cost in energy. This energy creates an anisotropic contribution to the line energy, λ_1 . It is found to be much larger in magnitude than the defect line energy. The line tension can be imagined to be composed of an isotropic term λ_0 and an anisotropic term λ_1 . The consideration of these forces allows to understand also domain shapes formed under non-equilibrium conditions.

A way is offered how the values λ_0 and λ_1 could be determined from the analysis of equilibrium domain shapes. The work is still in progress. If these values are known, an important step is done in predicting domain shapes and more information on the origin of λ_1 could be obtained. Since a relation between λ_1 and the chain tilt angle is probable, a future perspective could be to determine the dependence between them.

The smooth shapes of arachidic acid domains at pH 12.0 become faceted, when a trace of cholesterol is added to the monolayer. In order to examine, whether the change in the morphology is caused by the incorporation of cholesterol in the condensed fatty acid phase or by interaction of cholesterol with fatty acid molecules at the domain boundary, X-ray measurements on arachidic acid-cholesterol mixtures with very low amount of cholesterol were performed. The results suggest, that the effect of cholesterol is based on its 'line activity'. Surprising and new results are obtained with respect to cholesterol-lipid interactions.

The results demonstrate that only traces of cholesterol can cause conspicuous changes in the structure of lipid monolayers and that the study of lipid/cholesterol mixtures with very low cholesterol concentrations may contribute to the understanding of the cholesterol interactions at the molecular level, the knowledge of which is still incomplete. Due to the relevance of cholesterol for function and built up of biological membranes these measurements should also be applied to monolayers of membrane lipids.

For several properties of fatty acid monolayers a discontinuity was found in the dependence on the subphase pH at around pH 9, corresponding to 50% monolayer dissociation. Examples are the degree of herringbone ordering, the magnitude of the position correlation length or the value of the NN/NNN phase transition pressure (figs. 7.02, 7.15, 7.20). An unexpected result is also the condensation of the monolayer above pH 8, in spite of the increasing degree of dissociation. This behaviour is ascribed to pH-dependent head-head or head-solvent interactions. From the pH dependence of the position correlation length it is inferred, that on dissociation of the monolayer neutral and dissociated fatty acids associate to hydrogen bridged acid-anion dimers and that the number of dimers is maximal and bonding between the head groups strongest at 50% dissociation (\approx pH 9).

This idea is supported by IR reflection absorption measurements on arachidic acid monolayers. The observed variation of the intensities of the splitted carbonyl bands with pH suggests, that there is hydrogen bonding not only between the fatty acid and water, but also between adjacent fatty acid molecules in the monolayer.

A highly interesting point is the imagination of a two-dimensional hydrogen bonding network, where there is a quick proton exchange between neighbouring head groups. Transport processes through biological membranes are assumed to occur via proton diffusion along the membrane surface, which is quicker than the diffusion in the aqueous bulk. Under appropriate experimental conditions fatty acid monolayers could possibly serve as model system for investigating this phenomenon.

In the chapters 6.3.5 and 7.1 it has been demonstrated, that from X-ray peak widths and the derived position correlation lengths details on the bonding interactions between lipids are obtained with good accuracy and meaningfulness. In the literature this important facility has been scarcely made use of so far. This tool could be developed further and become more useful by establishing a relation between the value of the position correlation length and the inter-lipid bonding energy.

Monolayers of fatty acids and other amphiphiles exhibit a variety of different phases, the origin of which is not understood. On increasing the subphase pH and the portion of carboxylate

in the fatty acid monolayer very similar changes in the phase diagram are observed as for fatty acid/fatty alcohol or ester monolayer mixtures with decreasing portion of neutral acid. The transition pressure between NN and NNN phases shifts drastically to lower values, while the phase boundaries between the untilted phases and between untilted and tilted phases are hardly affected. This demonstrates the influence of the lipid head group interactions on the stability of tilted monolayer phases. A simple model was developed, which relates the shift in the NN/NNN transition pressure to steric interactions between the head groups. In order to verify it and to gain more insight in the monolayer phase behaviour a task in the future will be to modify lipid head groups in a defined way and to investigate the influence on transition pressures between tilted phases. The detailed analysis of the change of the L_2/O_v transition pressure with pH reveals strong resemblance to the dependence of the position correlation length on the pH value. This finding suggests, that the NN phase in fatty acids, which is not present in monolayers of alcohols, is stabilised by hydrogen bonding between the fatty acid head groups. The investigation of the bonding interaction – by measuring the position correlation length – in other mixed monolayer systems, where a relation between transition pressures and mixing ratio exists, would certainly contribute to the elucidation of this point.

It is shown how information on the interaction of a monolayer with solvent and solute molecules of the subphase can be obtained from simple isotherm measurement. The performed experiments with arachidic acid monolayers on subphases of solute/water mixtures suggest, that the fatty acid head groups are strongly hydrated and that on pressure increase the distance between the head groups is reduced by the squeezing out of solvent molecules. It is assumed that solutes less polar than water interact with the monolayer on the one hand by reducing the degree of head group hydration and thus the area of the head group and on the other hand by changing the steric interactions between the lipid head groups. It is noticed that the interaction of solutes with monolayers can be different from that with bilayers, from which follows that monolayers at the air/water interface cannot serve as model systems for biological membranes in any respect (especially not with respect to solute-lipid interactions), and that they should better be replaced by monolayers at an oil/water interface for this purpose.

By comparing the behaviour of dissociated monolayers in the absence of solutes, that interact with the charged monolayer, such as polyvalent metal ions or polymers, with the behaviour in the presence of these solutes, information is obtained about specific monolayer-solute interactions. This is demonstrated in an example with an arachidic acid monolayer and polyethyleneimine in the subphase.

9. References

- [Ale41] Alexander, A. E. *Proc. Roy. Soc. London A* **1941/42**, 179, 470
- [All75] Allen, L. C. *J. Am. Chem. Soc.* **1975**, 97, 6921
- [Als89] Als-Nielsen, J.; Kjaer, K. *X-ray Reflectivity and Diffraction Studies of Liquid Surfaces and Surfactant Monolayers* In: *Phase Transitions in Soft Condensed Matter B*; Riste, T.; Sherrington, D., eds.; Plenum: New York, Vol. 211; p. 113
- [And87] Andelmann, D.; Brochard, J.; Joanny, J. F. *J. Chem. Phys.* **1987**, 86, 3673
- [Arb98] Arbel-Haddad, M.; Lahav, M.; Leiserowitz, L. *J. Phys. Chem. B* **1998**, 102, 1543
- [Aru97] Arunkumar, A. I.; Kumar, T. K. S.; Yu, C. *Internat. J. Biol. Macromolecules* **1997**, 21, 223
- [Asg00] Asgharian, B.; Cadenhead, D. A. *Langmuir* **2000**, 16, 677
- [Ave75] Aveyard, R.; Heselden, R. *J. Chem. Soc. Faraday Trans 1* **1975**, 71, 312
- [Ave82] Aveyard, R. *Can. J. Chem.* **1982**, 60, 1317
- [Ave90] Aveyard, R.; Binks, B. P.; Carr, N.; Cross, A. W. *Thin Solid Films* **1990**, 188, 361
- [Ave98] Aveyard, R.; Binks, B. P.; Chen, J.; Esquena, J.; Fletcher, P. D. I.; Buscall, R.; Davies, S. *Langmuir* **1998**, 14, 4699
- [Avi99] Avila, L. V. N.; Saraiva, S. M.; Oliveira, J. F. *Colloids Surf.* **1999**, 154, 209
- [Bag66] Bagg, J.; Haber, M. D.; Gregor, H. P. *J. Colloid Interface Sci.* **1966**, 22, 138
- [Ber89] Bertie, J. E.; Ahmed, M. K.; Eysel, H. H. *J. Phys. Chem.* **1989**, 93, 2210
- [Ber91] Berge, B.; Faucheux, L.; Schwab, K.; Libchaber, A. *Nature* **1991**, 350, 322
- [Ber91] Berge, B.; Faucheux, L.; Schwab, K.; Libchaber, A. *Nature* **1991**, 350, 322
- [Bib90] Bibo, A. M.; Peterson, I. R. *Adv. Mater.* **1990**, 2, 309
- [Bib91] Bibo, A. M.; Knobler, C. M.; Peterson, I. R. *J. Phys. Chem.* **1991**, 95, 5591
- [Bin91] Binks, B. P. *Adv. Colloid Interface Sci.* **1991**, 34, 343
- [Bir97] Birdi, K. S. *Surface Tension and Interfacial Tension of Liquids* In: *Handbook of Surface and Colloid Chemistry*; Birdi, K. S., ed.; CRC: New York, 1997; p. 71
- [Bla94] Blaudez, D.; Buffetau, T.; Cornut, J. C.; Desbat, B.; Escafre, N.; Pezolet, M.; Turllet, J. M. *Thin Solid Films* **1994**, 242, 146
- [Blo90] Bloch, M. J.; Yun, W. *Phys. Rev. A* **1990**, 41, 844
- [Boc70] Bockris, J. O'M.; Reddy, A. K. N. *Modern Electrochemistry*; Plenum Press: New York, 1970, Vol 2; pp. 741ff
- [Bog87] Boggs, J. M. *Biochim. Biophys. Acta* **1987**, 906, 353
- [Böh93] Böhm C. *Thesis*; Mainz; 1993
- [Bre94] Brezesinski, G.; Rietz, R.; Kjaer, K.; Bouwman, W. G.; Möhwald, H. *Il Nuovo Cimento* **1994**, 16, 1487
- [Bre00] Brezesinski, G. *private communication*

- [Bro92] Brock, J. D. *Bond-Orientational Order In: Bond-Orientational Order in Condensed Matter Systems*; Strandburg, K. J., ed.; Springer-Verlag: New York, 1992; pp. 1-31
- [Buf91] Buffetau, T.; Desbat, B.; Turllet, J. M. *Appl. Spectrosc.* **1991**, *45*, 380
- [Car88] Carrell, C. J.; Carrell, H. L.; Erlebacher, J.; Glusker, J. P. *J. Am. Chem. Soc.* **1988**, *110*, 8651
- [Car98] Careri, G. *Progr. Biophys. Molecular Biol.* **1998**, *70*, 223
- [Cev87] Cevc, G.; Marsh, D. *Phospholipid Bilayers*; Wiley: New York, 1987; pp. 29-36
- [Chi91a] Chi, L. F.; Johnston, R. R.; Ringsdorf, H. *Langmuir* **1991**, *7*, 2323
- [Chi91b] Chi, L. F.; Johnston, R. R.; Ringsdorf, H. *Makromol. Chem.* **1991**, *46*, 409
- [Chi98] Chi, L. F.; Gleiche, M.; Fuchs, H. *Langmuir* **1998**, *14*, 875
- [Cos92] Costas, M. E.; Knobler, C. M. *Rev. Mex. Fis.* **1992**, *38*, 791
- [Dah98] Dahmen-Levison, U.; Brezesinski, G.; Möhwald, H. *Progr. Colloid Polym. Sci.* **1998**, *110*, 269
- [Dat00] Datta, A.; Kmetko, J.; Richter, A. G.; Yu, C.-J.; Dutta, P.; Chung, K.-S.; Bai, J.-M. *Langmuir* **2000**, *16*, 1239
- [Dau98] Daubert, T. E.; Danner, R. P. *Physical and Thermodynamic Properties of Pure Chemicals: Data Compilation*; Taylor&Francis: Washington, 1998
- [Dav61] Davies, J. T.; Rideal, E. K. *Interfacial Phenomena*; Academic Press: London, 1961; p. 236
- [Dav63] Davies, J. T.; Rideal, E. K. *Interfacial Phenomena*; Academic Press: New York, 1963
- [deM98] de Mul, M. N. G.; Mann, J. A. *Langmuir* **1998**, *14*, 2455
- [DeW98a] DeWolf, C.; Bringezu, F.; Brezesinski, G.; Möhwald, H.; Howes, P.; Kjaer, K. *Physica B* **1998**, *248*, 199
- [DeW98b] DeWolf, C.; Brezesinski, G.; Weidemann, G.; Möhwald, H.; Kjaer, K.; Howes P. *J. Phys. Chem.* **1998**, *102*, 3238
- [Die91] Dietrich, A.; Möhwald, H.; Rettig, W.; Brezesinski, G. *Langmuir* **1991**, *7*, 539
- [Die94] Dietrich, A.; Brezesinski, G.; Möhwald, H.; Dobner, B.; Nuhn, P. *Il Nuovo Cimento* **1994**, *16*, 1537
- [Du94] Du, Q.; Freysz, E.; Shen, Y. R. *Phys. Rev. Lett.* **1994**, *72*, 238
- [Dur94] Durbin, M. K.; Malik, A.; Ghaskadvi, Shih, M. C.; R.; Zschack, P.; Dutta, P. *J. Phys Chem.* **1994**, *98*, 1753
- [Dur95] Durbin, M. K.; Shih, M. C.; Malik, A.; Zschack, P.; Dutta, P. *Colloids Surf. A.* **1995**, *102*, 173
- [Dur97] Durbin, M. K.; Malik, A.; Richter, A. G.; Ghaskadvi, R.; Gog, T.; Dutta, P. *J. Phys Chem.* **1997**, *106*, 8216
- [Dut87] Dutta, P.; Peng, J. B.; Lin, B.; Ketterson, J. B.; Prakash, M.; Georgopoulos, P.; Ehrlich, S. *Phys. Rev. Lett.* **1987**, *58*, 2228
- [Fai96] Fainerman, V. B.; Vollhardt, D.; Melzer, V. *J. Phys. Chem* **1996**, *100*, 15478

- [Fle91] Flesselles, J.-M.; Magnasco, M. O.; Libchaber, A. *Phys. Rev. Lett.* **1991**, *67*, 2489
- [Fis94a] Fischer, T. M.; Bruinsma, R. F.; Knobler, C. M. *Phys. Rev. E* **1994**, *50*, 413
- [Fis94b] Fischer, B.; Tsao, M.-W.; Ruiz-Garcia, J.; Fischer, T. M.; Schwartz, D. K.; Knobler, C. M. *J. Phys. Chem* **1994**, *98*, 7430
- [Fis95] Fischer, B.; Teer, E.; C. M. Knobler *J. Chem. Phys.* **1995**, *103*, 2365
- [Fis96] Fischer, B.; Tsao, M.-W.; Ruiz-Garcia, J.; Fischer, T. M.; Schwartz, D. K.; Knobler, C. M. *Thin Solid Films* **1996**, *284-5*, 110
- [Fra79] Frahm, J.; Diekmann, S. *J. Colloid Interface Sci.* **1979**, *70*, 440
- [Gai66] Gaines, G. L., Jr. *Insoluble Monolayers at Liquid-Gas Interfaces*; Wiley: New York, 1966
- [Geh96] Gehlert, U. *Thesis*; Berlin; 1996
- [Geh98] Gehlert, U.; Weidemann, G.; Vollhardt, D.; Brezesinski, G.; Wagner, R.; Möhwald, H. *Langmuir* **1998**, *14*, 2112
- [Ger93a] Gericke, A.; Hühnerfuss, H. *Proc. SPIE-Int. Soc. Opt. Eng.* **1993**, *2089*, 570
- [Ger93b] Gericke, A.; Hühnerfuss, H. *J. Phys. Chem.* **1993**, *97*, 12899
- [Ger94] Gericke, A. *Thesis*; Hamburg; 1994
- [Ger95] Gericke, A.; Hühnerfuss, H. *Ber. Bunsenges. Phys. Chem.* **1995**, *99*, 641
- [God63] Goddard, E. D.; Ackilli, J. A. *J. Colloid Sci.* **1963**, *18*, 585
- [God66] Goddard, E. D.; Smith, S. R.; Kao, O. *J. Colloid Interface Sci.* **21** (1966) 320
- [God67] Goddard, E. D.; Kao, O.; Kung, H. C. *J. Colloid Interface Sci.* **1967**, *24*, 297
- [Gom98] Gomez-Fernandez, J. C.; Villalain, J. *Chem. Phys. Lip.* **1998**, *96*, 41
- [Gra47] Grahame, D. C. *Chem. Rev.* **1947**, *41*, 441
- [Gün96] Günzler, H.; Heise, H. M. *IR-Spektroskopie*, 3. Ed.; VCH: Weinheim, 1996; p. 237
- [Gut95] Gutberlet, T.; Vollhardt, D. *J. Colloid Interface Sci.* **1995**, *173*, 429
- [Ha99] Ha, K.; Kim, J.-M.; Rabolt, J. F. *Thin Solid Films* **1999**, *347*, 272
- [Hai83] Haines, T. H. *Proc. Natl. Acad. Sci. USA* **1983**, *80*, 160
- [Han91] Handke, M.; Milosevic, M.; Harrick, N. J. *Vib. Spectrosc.* **1991**, *1*, 251
- [Har67] Harrick, N. J. *Internal Reflection Spectroscopy*; Wiley: New York, 1967
- [Har98] Harke, M.; Motschmann, H. *Langmuir* **1998**, *14*, 313
- [Hay87] Hayden, B. E. *Reflection Absorption Infrared Spectroscopy In: Vibrational Spectroscopy of Molecules on Surfaces*; Yates, J. T., Jr; Madey, T. E., eds; Plenum Press: New York and London, 1987; pp. 267-344
- [Hec86] Heckl, W. M.; Möhwald, H. *Ber. Bunsenges. Phys. Chem.* **1986**, *90*, 1159
- [Hel87] Helm, C. A.; Möhwald, H.; Kjaer, K.; Als-Nielsen, J. *Biophys. J.* **1987**, *52*, 381
- [Hel88] Helm, C. A.; Möhwald, H. *J. Phys. Chem.* **1988**, *92*, 1262
- [Hen91] Henon, S.; Meunier, J. *Rev. Sci. Instrum.* **1991**, *62*, 936
- [Hen93] Henon, S.; Meunier, J. *J. Chem. Phys.* **1993**, *98*, 9148

- [Hir98] Hirota, N.; Mizuno, K.; Goto, Y. *J. Mol. Biol.* **1998**, *275*, 365
- [Ho92] Ho, T. L. *Faceting in Bond-Oriented Glasses and Quasicrystals* In: *Bond-Orientational Order in Condensed Matter Systems*; Strandburg, K., ed.; Springer: New York, 1992; pp 216-254
- [Ho97] Ho, C.; Stubbs, C. D. *Biochemistry* **1997**, *36*, 10630
- [Hos93] Hosoi, K.; Ishikawa, T.; Tomioka, A.; Miyano, K. *Jpn. J. Appl. Phys.* **1993**, *32*, 135
- [Hön91] Hönig, D.; Möbius, D. *J. Phys. Chem* **1991**, *95*, 4590
- [Hön92] Hönig, D.; Overbeck, G. A.; Möbius, D. *Adv. Mater.* **1992**, *4*, 419
- [Hön94] Hönig, D. *Thesis*; Göttingen; 1994
- [Hua92] Huang, C. C. *Nature of Phase Transitions Related to Stacked Hexatic Phases in Liquid Crystals* In: *Bond-Orientational Order in Condensed Matter Systems*; Strandburg, K., ed.; Springer: New York, 1992; pp. 78-136
- [Huo99] Hou, Q.; Dziri, L.; Desbat, B.; Russell, K. C.; Leblanc, R. M. *J. Phys. Chem.* **1999**, *103*, 2929
- [Hwa99] Hwang M.-J.; Kim, K. *Langmuir* **1999**, *15*, 3563
- [Isr82] Israelachvili, J.; Pashley, R. *Nature* **1982**, *300*, 341
- [Isr96] Israelachvili, J.; Wennerström, H. *Nature* **1996**, *379*, 219
- [Jac90] Jacquemain, D.; Grayer Wolf, S.; Leveiller, F.; Lahav, M.; Leiserowitz, L.; Deutsch, M.; Kjaer, K.; Als-Nielsen, J. *J. Am. Chem. Soc.* **1990**, *112*, 7724
- [Jac91] Jacquemain, D.; Leveiller, F.; Weinbach, S. P.; Lahav, M.; Leiserowitz, L.; Kjaer, K.; Als-Nielsen, J. *J. Am. Chem. Soc.* **1991**, *113*, 7684
- [Jef97] Jeffrey, G. A. *An Introduction to Hydrogen Bonding*; Oxford University Press: New York, 1997
- [Joh98] Johann, R.; Weidemann, G.; Vollhardt, D. *Annual Report*; HASYLAB DESY: Hamburg, 1998; p. 417
- [Joh99a] Johann, R.; Vollhardt, D. *Mater. Sci. Eng. C* **1999**, *8-9*, 35
- [Joh99b] Johann, R.; Siegel, S.; Vollhardt, D. *Annual Report*; HASYLAB DESY: Hamburg, 1999; p. 694
- [Joh00] R. Johann; C. Symietz; D. Vollhardt; G. Brezesinski; H. Möhwald *J. Phys. Chem.* **2000**, *104*, 8512
- [Joh01] R. Johann, D. Vollhardt, H. Möhwald *Colloids Surf A*, in press
- [Jun94] Breitmaier, E.; Jung, G. *Organische Chemie I: Grundlagen, Stoffklassen, Reaktionstypen*; Thieme: Stuttgart, 1994, 3. ed.; p. 258
- [Kit73] Kitaigorodsky, A. I. *Molecular Crystals and Molecules*; Academic Press: New York, 1973; p. 20
- [Kag93a] Kaganer, V. M.; Osipov, M. A.; Peterson, I. R. *J. Chem. Phys.* **1993**, *98*, 3512
- [Kag93b] Kaganer, V. M.; Loginov, E. B. *Phys. Rev. Lett.* **1993**, *71*, 2599
- [Kag95a] Kaganer, V. M., Peterson, I. R.; Kenn, R. M.; Shih, M. C.; Durbin, M.; Dutta, P. *J. Chem. Phys.* **1995**, *102*, 9412

- [Kag95b] Kaganer, V. M.; Loginov, E. B. *Phys. Rev. E* **1995**, *51*, 2237
- [Kag99] Kaganer, V. M.; Möhwald, H.; Dutta, P. *Rev. Modern Phys.* **1999**, *71*, 779
- [Kat92] Strandburg, K. J. *Computer Simulation Studies of Bond-Orientational Order In: Bond-Orientational Order in Condensed Matter Systems*; Strandburg, K. J., ed.; Springer-verlag: New York, 1992; pp. 32-77
- [Kel78] Kellner, B. M. J.; Müller-Landau, F.; Cadenhead, D. A. *J. Colloid Interface Sci.* **1978**, *66*, 597
- [Kel87] Keller, D. J.; Korb, J. P.; Mc Connell, H. M. *J. Phys. Chem.* **1987**, *91*, 6417
- [Kja87] Kjaer, K.; Als-Nielsen, J.; Helm, C. A.; Laxhuber, L. A.; Möhwald, H. *Phys. Rev. Lett.* **1987**, *58*, 2224
- [Kja89] Kjaer, K.; Als-Nielsen, J.; Helm, C. A.; Tippman-Krayer, P.; Möhwald, H. *J. Phys. Chem.* **1989**, *93*, 3200
- [Kle86] Klein, M. V.; Furtak, T. E. *Optics*, 2nd ed.; Wiley: New York; 1986
- [Kle90] Klemm, W. R. *Alcohol*; Pergamon Press, 1990, Vol. 7; pp. 49-59
- [Kno90a] Knobler, C. M. *Science* **1990**, *249*, 870
- [Kno90b] Knobler, C. M. *Adv. Chem. Phys.* **1990**, *77*, 397
- [Kra00] Krasteva, N.; Vollhardt, D.; Brezesinski, G. *J. Phys. Chem.* **2000**, *104*, 8704
- [Kuz98] Kuzmenko, I.; Kaganer, V. M.; Leiserowitz, L. *Langmuir* **1998**, *14*, 3882
- [Lak83] Lakhdar-Ghazal, F.; Tichadou, J.-L.; Tocanne J.-F. *Eur. J. Biochem.* **1983**, *134*, 531
- [Lan86] Langer, S. A.; Sethna, J. P. *Phys. Rev. A* **1986**, *34*, 5035
- [Lan92] Langer, S. A.; Goldstein, R. E.; Jackson, D. P. *Phys. Rev. A* **1992**, *46*, 4894
- [Lau97] Lautz, C.; Fischer, T. M.; Kildea, J. *J. Chem. Phys.* **1997**, *106*, 7448
- [Lau99] Lautz, C.; Fischer, Th. M. *Eur. Phys. J.* **1999**, *7*, 263
- [Lea88] Leaist, D. *Can. J. Chem.* **1988**, *66*, 1129
- [Lid94] Lide, D. R. *Handbook of Chemistry & Physics*, 75th ed.; CRC Press: Florida, 1990
- [Loc97] Lochhead, M. J.; Letellier, S. R.; Vogel, V. *J. Phys. Chem* **1997**, *101*, 10821
- [Loh98] Loh K. K.; Rudnick, J. *Phys. Rev. Lett.* **1998**, *81*, 4935
- [Lon52] Long, F. A.; McDevit, W. F. *Chem. Rev.* **1952**, *51*, 119
- [Lös88] Lösche, M.; Duwe, H.-P.; Möhwald, H. *J. Colloid Interface Sci.* **1988**, *126*, 432
- [Mac90] MacRitchie, F. *Chemistry at Interfaces*; Academic Press: San Diego, 1990
- [Mar18] Marsden, J.; Schulman, J. H. *Trans. Faraday Soc.* **1938**, *34*, 748
- [McC91] McConnell, H. M. *Annu. Rev. Phys. Chem.* **1991**, *42*, 171
- [McF93] McFate, C.; Ward, D.; Olmstedt III, J. *Langmuir* **1993**, *9*, 1036
- [McL77] McLaughlin, S. *Curr. Topics Membr. Transp.* **1977**, *9*, 71
- [Mel97a] Melzer, V. *Thesis*; Berlin; 1997

- [Mel97b] Melzer, V.; Weidemann, G.; Vollhardt, D.; Brezesinski, G.; Wagner, R.; Struth, B.; Möhwald, H. *Supramol. Sci.* **1997**, *4*, 391
- [Men95] Mendelsohn, R.; Brauner, J. W.; Gericke, A. *Annu. Rev. Phys. Chem.* **1995**, *46*, 305
- [Mil86a] Miller, A. *Thesis*; TU München; 1986
- [Mil86b] Miller, A.; Knoll, W.; Möhwald, H. *Phys. Rev. Lett.* **1986**, *56*, 2633
- [Mil87] Miller, A.; Helm, C. A.; Möhwald, H. *J. Physique* **1987**, *48*, 693
- [Mir98] Miranda, P. B.; Du, Q.; Shen, Y. R. *Chem. Phys. Lett.* **1998**, *286*, 1
- [Mit93] Mitchell, J. K. *Fundamentals of Soil Behaviour*, 2nd ed; John Wiley & Sons: New York, 1993; pp. 100-130
- [Miz95] Mizuno, K.; Miyashita, Y.; Shindo, Y.; Ogawa, H. *J. Phys. Chem* **1995**, *99*, 3225
- [Möh89] Möhwald, H. *The phases and phase transitions in lipid monolayers* In: *Phase transitions in soft condensed matter*; Riste, T., Sherrington, D., ed., Vol 211; pp. 145-159
- [Moo90] Moore, B. G.; Knobler, C. M.; Akamatsu, S.; Rondolez, F. *J. Phys. Chem.* **1990**, *94*, 4588
- [Mor95] Morrow, M. R.; Singh, D.; Lu, D.; Grant, C. W. M. *Biophys. J.* **1995**, *68*, 179
- [Mul91] Muller, P.; Gallet, F. *Phys. Rev. Lett.* **1991**, *67*, 1106
- [Mur92] Murray, C. A. *Experimental Studies of Melting and Hexatic Order in Two-Dimensional Colloidal Suspensions* In: *Bond-Orientational Order in Condensed Matter Systems*; Strandburg, K. J., ed.; Springer-verlag: New York, 1992; pp. 137-215
- [Mye91] Myers, D. *Surfaces, Interfaces and Colloids*; VCH Verlagsges.: Weinheim, 1991
- [Nel80] Nelson, D. R.; Halperin, B. I. *Phys. Rev. B* **1980**, *21*, 5312
- [Nis95] Nishi, N.; Takahashi, S.; Matsumoto, M.; Tanaka, A.; Muraya, K.; Takamuku, T.; Yamaguchi, T. *J. Phys. Chem.* **1995**, *99*, 462
- [Nit86] Nittmann, J.; Stanley, H. E. *Nature* **1986**, *321*, 663
- [Ois97] Oishi, Y.; Takashima, Y.; Suehiro, K.; Kajiyama, T. *Langmuir* **1997**, *13*, 2525
- [Oka99] Okamura, E.; Fukushima, N.; Hayashi, S. *Langmuir* **1999**, *15*, 3589
- [Ove93a] Overbeck, G. A. *Thesis*, Göttingen, 1993
- [Ove93b] Overbeck, A. G.; Möbius, D. *J. Phys. Chem.* **1993**, *97*, 7999
- [Ove94] Overbeck, G. A.; Hönig, D.; Möbius, D. *Thin Solid Films* **1994**, *242*, 213
- [Pan98] Pan, Y.; McAllister, M. A. *J. Am. Chem. Soc.* **1998**, *120*, 166
- [Pat72] Patil, G. S.; Matthews, R. H.; Cornwell, D. G. *J. Lipid Research* **1972**, *13*, 574
- [Pat75] Patil, G. S.; Matthews, R. H.; Cornwell, D.G. *Adv. Chem. Ser.* **1975**, *144*, 44-66
- [Pat85] Patel, K. B.; Eaton, G.; Symons, M. C. R. *J. Chem. Soc., Faraday Trans. I* **1985**, *81*, 2775
- [Pet96] Peterson, I. R.; Kenn, R. M.; Goudot, A.; Fontaine, P.; Rondelez, F.; Bouwman, W. G.; Kjaer, K. *Phys. Rev. E.* **1996**, *53*, 667

- [Pol00] Polysciences, Inc.; polymer/monomer catalogue, 1998-2000
- [Pop95] Popovitz-Biro, R.; Majewski, J.; Wang, J. L.; Leiserowitz, L.; Lahav, M.; Kjaer, K.; Als-Nielsen, J. In *Organic Thin Films and Surfaces: Directions for the Nineties*; Ulman, A., Ed.; Academic Press: New York, 1995, Vol. 20; pp. 145-181
- [Qiu91] Qiu, X.; Ruiz-Garcia, J.; Stine, K. J.; Knobler, C. M. *Phys. Rev. Lett.* **1991**, *67*, 703
- [Qiu92] Qiu, X.; Ruiz-Garcia, J.; Knobler, C. M. *Progr. Colloid Polym. Sci.* **1992**, *89*, 197
- [Rid86] Riddick, J. A.; Bunger, W. B.; Sakano, T. K. *Organic Solvents: Physical Properties and Methods of Purification*, 4th ed.; Wiley: New York, 1986
- [Rie93] Rietz, R.; Brezesinski, G.; Möhwald, H. *Ber. Bunsenges. Phys. Chem.* **1993**, *97*, 1394
- [Rit99] Ritchie, I. M.; Bailey, S.; Woods, R. *Adv. Colloid Interface Sci.* **1999**, *80*, 183
- [Riv94] Rivière, S.; Hénon, S.; Meunier, J.; Schwartz, D. K.; Tsao, M.-W.; Knobler, C.M. *J. Chem. Phys.* **1994**, *101*, 10045
- [Riv95] Rivière, S.; Meunier, J. *Phys. Rev. Lett.* **1995**, *74*, 2495
- [Riv96] Rivière-Cantin, S.; Hénon, S.; Meunier, J. *Phys. Rev. E* **1996**, *54*, 1683
- [Sae84] Saenger, W. *Principles of Nucleic Acid Structure*; Springer Verlag: New York, 1984; pp. 39, 54
- [Sal62] Salem, L. *J. Chem. Phys.* **1962**, *37*, 2100
- [Sak98] Schmidt, M. *Anorganische Chemie*, Bd 1; Wissenschaftsverlag: Mannheim, 1991
- [Sch93] Schwartz, D. K.; Knobler, C. M. *J. Phys. Chem.* **1993**, *97*, 8849
- [Sch97] Schmid, F.; Lange, H. *J. Chem. Phys.* **1997**, *106*, 3757
- [Sch99] Schmid, F.; Stadler, C.; Lange, H. *Colloids Surf. A.* **1999**, *149*, 301
- [Seg65] Segerman, E. *Acta Cryst.* **1965**, *19*, 789
- [Seu90] Seul, M.; Sammon, M. J. *Phys. Rev. Lett.* **1990**, *64*, 1903
- [Seu95] Seul, M.; Andelman, D. *Science* **1995**, *267*, 476
- [Shi92] Shih, M. C.; Bohanon, T. M.; Mikrut, J. M.; Zschack, P.; Dutta, P. *J. Chem. Phys.* **1992**, *96*, 1556
- [Shi94] Shih, M. C.; Durbin, M. K.; Malik, A.; Zschack, P.; Dutta, P. *J. Chem. Phys.* **1994**, *101*, 9132
- [Sie97] Siegel, S. Ph. D. Thesis, Berlin, 1997
- [Sil91] Silverstein, R. M.; Bassler, G. C.; Morrill, T. C. *Spectrometric Identification of Organic Compounds*, 5th ed.; Wiley: New York, 1991; pp. 91-164
- [Skj89] Skjeltorp, A. T.; Helgesen, G. *Qualitative Aspects of Condensation, Ordering and Aggregation In: Phase Transitions in Soft Condensed Matter, Series B*; Riste, T.; Sherrington, D., eds.; Plenum: New York, 1989; Vol. 211, pp. 23-43
- [Sir97] Sirota, E. B. *Langmuir* **1997**, *13*, 3849
- [Smi73] Smith, R.; Tanford, C. *Proc. Nat. Acad. Sci.* **1973**, *70*, 289

- [Smi90] Smit, B.; Hilbers, P. A. J.; Esselink, K.; Rupert, L. A. M.; van Os, N. M.; Schlijper, A. G. *Nature* **1990**, *348*, 624
- [Smi93] Smith, D. E.; Haymet, A. D. J. *J. Chem. Phys.* **1993**, *98*, 6445
- [Son77] Sonntag, H. *Lehrbuch der Kolloidwissenschaft*; VEB Dt. Verlag d. Wissensch.: Berlin, 1977; p. 42ff
- [Spi63] Spink, J. A.; Sanders, J. V. *Trans. Faraday Soc.* **1955**, *51*, 1154
- [Spi63] Spink, J. A. *J. Colloid Interface Sci.* **1963**, *18*, 512
- [Sta71] Stanley, H. E. *Introduction to Phase Transitions and Critical Phenomena*; Oxford University Press: Oxford, 1971; pp. 95, 96
- [Stä45] Ställberg-Stenhagen, S.; Stenhagen, E. *Nature* **1945**, *156*, 239
- [Sto77] Stokes, R. H. *J. Chem. Soc. Faraday Trans. I* **1977**, *73*, 1140
- [Sur88] Suresh, K. A.; Nittmann, J.; Rondelez, F. *Europhys. Lett.* **1988**, *6*, 437
- [Tee97] Teer, E.; Knobler, C. M.; Lautz, C.; Wurlitzer, S.; Kildae, J.; Fischer, T. M. *J. Chem. Phys.* **1997**, *106*, 1913
- [Tip91] Tippman-Krayer, P.; Möhwald, H. *Langmuir* **1991**, *7*, 2303
- [Toc90] Tocanne, J. F.; Teissié, J. *Biochim. Biophys. Acta* **1990**, *1031*, 111
- [Tsa95] Tsao, M.-W.; Fischer, T.; Knobler, C. *Langmuir* **1995**, *11*, 3184
- [Van90] Vanderlick, T. K., Möhwald, H. *J. Phys. Chem.* **1990**, *94*, 886
- [Vie94] Vierl, U.; Löbecke, L.; Nagel, N.; Cevs, G. *Biophys. J.* **1994**, *67*, 1067
- [Vist90] Vist, M. R.; Davis, J. H. *Biochemistry* **1990**, *29*, 451
- [Vog88] Vogel, V.; Möbius, D. *J. Colloid Interface Sci.* **1988**, *126*, 408
- [Vol96] Vollhardt, D.; Gehlert, U. *Tenside Surf. Det.* **1996**, *33*, 197
- [Vor98] Vorberg, K. *Thesis*; Potsdam; 1998
- [Wal95] Wallqvist, A.; Berne, B. J. *J. Phys. Chem.* **1995**, *99*, 2885
- [Wal99] Walker, R. A.; Gragson, D. E.; Richmond, G. L. *Colloids Surf. A* **1999**, *154*, 175
- [Wei85] Weiss, R. M.; McConnell, H. M. *J. Phys. Chem.* **1985**, *89*, 4453
- [Wei96] Weidemann, G.; Vollhardt, D.; Lang, S.; Bringezu, F.; DeWolf, C.; Annual Report, DESY HASYLAB (Hamburg), 1996, p. 459
- [Wei97a] Weidemann, G. *Thesis*; Berlin; 1997
- [Wei97b] Weidemann, G.; Vollhardt, D. *Langmuir* **1997**, *13*, 1623
- [Wei98a] Weidemann, G.; Brezesinski, G.; Vollhardt, D.; Bringezu, F.; de Meijere, K.; Möhwald, H. *J. Phys. Chem.* **1998**, *102*, 148
- [Wei98b] Weidemann, G.; Brezesinski, G.; Vollhardt, D.; Möhwald, H. *J. Phys. Chem.* **1998**, *102*, 1224
- [Wei98c] Weidemann, G.; Brezesinski, G.; Vollhardt, D.; Möhwald, H. *Langmuir* **1998**, *14*, 6485
- [Wur00] Wurlitzer, S.; Steffen, P.; Wurlitzer, M.; Khattari, Z.; Fischer, Th. M. *J. Chem. Phys.* **2000**, *113*, 3822

Appendix

I. Substances used

A) Monolayer lipids

1. Fatty acids $\text{CH}_3(\text{CH}_2)_n\text{COOH}$: myristic acid (Sigma, 99-100%), pentadecanoic acid (Merck, 99%), palmitic acid (Merck, 99%), stearic acid (Sigma, $\approx 99\%$), arachidic acid (Merck, $>99\%$), behenic acid (Merck)
2. Palmityl acetate (Sigma, $\approx 99\%$)
3. Heptadecanoic acid methyl ester (Sigma, $\approx 99\%$)
4. 1-Monostearoyl-rac-glycerol (Sigma, $\approx 99\%$)
5. 1-0-hexadecyl-rac-glycerol (Sigma, $\approx 99\%$)
6. Cholesterol (Sigma, 99+%)

B) Spreading solvent

n-Heptane (Merck, 99.3%) (+5 vol% ethanol (Merck, $>99.8\%$))

C) Subphase

Ultra-pure water with specific resistance above 18 M Ω cm from a Millipore desktop (pH \approx 5.6)

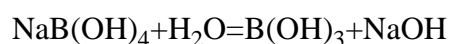
D) Subphase additives

NaCl (Fluka, $>99.5\%$), $\text{NaBO}_2 \cdot 4\text{H}_2\text{O}$ (Avocado, 98%), H_3BO_3 (Isocommerz, GDR, $>99\%$), ethylenediamine tetraacetic acid (Aldrich, 99.9995%), NaOH (1 N (Titrisol), Merck), HCl (1 N Titrisol, Merck), polyethyleneimine/branched/MW1800 (Polysciences, Inc., 99%), ethanol (Merck, $>99.8\%$), 2,2,2-trifluoroethanol (Sigma), ethylene glycol (Fluka, $\geq 99.5\%$), 1-propanol (Fluka, $>99.5\%$), 2-propanol (Merck, $>99.7\%$), 1-butanol (Merck, $\geq 99.5\%$), acetic acid (Merck, $>99.8\%$), DMSO (Sigma, $\geq 99.9\%$), D-(+) glucose (Sigma, 99.5%), $\text{CuSO}_4 \cdot 5\text{H}_2\text{O}$ (p.a.)

All substances were used as received

E) Calculation of buffer concentration

Equilibrium ($<0.01\text{M}$ borate): $\text{B}(\text{OH})_3 + \text{H}_2\text{O} = \text{B}(\text{OH})_4^- + \text{H}^+$, $K_S = 5.80 \cdot 10^{-10}$



Equations:

1. $K_S = [\text{B}(\text{OH})_4^-][\text{H}^+]/[\text{B}(\text{OH})_3] = 5.80 \cdot 10^{-10}$
2. $[\text{B}(\text{OH})_4^-] + [\text{B}(\text{OH})_3] = [\text{B}(\text{OH})_4^-]_0 + [\text{B}(\text{OH})_3]_0$ (index 0: added concentrations)
3. $[\text{OH}^-] + [\text{B}(\text{OH})_4^-] = [\text{H}^+] + [\text{Na}^+] (= [\text{B}(\text{OH})_4^-]_0)$

$$4. [H^+][OH^-]=K_W=10^{-14}$$

$$\Rightarrow [B(OH)_4^-]_0=(K_S[B(OH)_3]_0+K_WK_S/[H^+]+K_W)/[H^+]-[H^+]-K_S$$

pH	[B(OH) ₃]/M	[B(OH) ₄ ⁻]/M
8.0	0.005	0.000291
8.7	0.004	0.001169
9.0	0.0032	0.00187
9.2	0.0026	0.00242
9.5	0.0018	0.00339
9.7	0.0015	0.004556
10.0	0.0007	0.00474
10.5	0	0.006

F) Correction of base concentration when adding EDTA

EDTA is a weak acid. It has been added in the fully protonated form (C₂N₂H₄²⁺)(C₄O₈H₁₀²⁻) abbreviated as YH₄. In the buffer solutions [EDTA]=10⁻⁵, 10⁻⁶ M, so correction is not necessary. In solutions of pH≥11.7 [EDTA]=10⁻³-10⁻⁴ M, so more NaOH has to be added than without EDTA.

Equations:

$$1. K_{S1}=[YH_3^-][H^+]/[YH_4]=10^{-2.0}$$

$$K_{S2}=[YH_2^{2-}][H^+]/[YH_3^-]=10^{-2.67}$$

$$K_{S3}=[YH^{3-}][H^+]/[YH_2^{2-}]=10^{-6.16}$$

$$K_{S3}=[Y^{4-}][H^+]/[YH^{3-}]=10^{-10.26}$$

$$2. [YH_4]_0=[YH_4]+[YH_3^-]+[YH_2^{2-}]+[YH^{3-}]+[Y^{4-}]$$

$$3. [H^+]+[Na^+](=[NaOH]_0)=[YH_3^-]+2[YH_2^{2-}]+3[YH^{3-}]+4[Y^{4-}]+[OH^-]$$

$$4. [H^+][OH^-]=K_W$$

The required [NaOH]₀ is obtained by calculating [YH₃⁻], [YH₂²⁻], [YH³⁻], [Y⁴⁻] with the desired [EDTA] from eqs. 1, 2, 4 and substituting the desired [OH⁻] in eq. 3.

II. Salt effects

The solubility of a non or weakly polar solute in water is affected by the presence of an electrolyte. The decrease of the solubility in water by the addition of salt is known as ‘salting out’. Few cases are known, where the solubility is enhanced by salt, which is referred to as ‘salting in’. Salting out corresponds to an increase and salting in to a decrease of the energy of transfer of the solute $\Delta\xi$. There are many examples that $\Delta\xi$ varies linearly with the electrolyte concentration for salting out up to molar concentrations [Lon52]. These salt effects are not yet understood in detail and they are assumed to arise from a large number of different types of intermolecular interactions, the magnitude of which will strongly depend on the properties of both the solute and the salt components.

The change of $\Delta\xi$ of the solute from pure water to salt solution arises from a change of the solute-solute, ion-solvent, ion-solute or (and) solute-solvent interactions.

A feature of the molecules considered is their poor solubility in water, so that solute-solute interactions do not play a role.

There are different approaches for describing the salt effects, that consider the change of the structure and properties of water induced by ions. One, for instance, is based on the observed correlation between the degree of salting out and the contraction of solvent volume as salt is added [Lon52]. Other approaches consider the change of the electrostatic conditions in the solvent when ions are present [Lon52 and ref. therein]. Repulsive electrostatic interactions occur between ions and apolar solutes due to the formation of image charges of equal sign at the water-solute interface. The ions are repelled from the solute molecules, which can be regarded as cavities of low dielectricity within the highly polar solvent, and a layer depleted of ions is created around the solute.

The same effect has been revealed at the air/water interface by measuring an increase of the surface tension with increasing concentration of dissolved salt. A depleted surface region is predicted according to the Gibbs adsorption equation:

$$\Gamma = -\frac{d\tau}{RTd \ln c} \quad (\text{II.1})$$

where τ is the surface tension, c is the concentration of an ion and Γ is the surface excess concentration, which can be negative or positive. A negative Γ indicates, that the solute concentration at the surface is lower than in bulk. The surface tension increases with ion concentration, since on creating new surface area energy is expended for repelling the ions from the surface.

Also the solute-solvent interactions, which can be specific, are altered by ions. The finding that the salting-out of acids is increased in the presence of small cations and decreased with small anions and that the effect is reversed with bases, can be explained by the alignment of the water dipoles around an ion. The outer part of the hydration shell of strongly solvated small ions either consists of hydrogen or oxygen atoms of the water dipoles, depending on the charge of the ion in the centre. These groups are suggested to interact with the hydrogen of the acid or the lone pair of the base producing the effects mentioned.

A rather simple experimental approach for determining a value for the salting out efficiency of a salt solution was introduced by Aveyard et al. [Ave75, Ave82, Ave98], which proved to be quite accurate. There the free energy of a solute in salt solution $\Delta\xi$ was equated to the energy for producing the interface between solute and solution and regarded as equivalent to the energy for the formation of a macroscopic interface, which can be directly determined by measuring the surface or interfacial tension. Accordingly the free energy of salting out $\Delta(\Delta\xi)$ (difference in transfer energy between salt solution and pure water) is:

$$\Delta(\Delta\xi) = \Delta\tau A N_A \quad (\text{II.2})$$

where A is the surface area of the solute, N_A the Avogadro number and $\Delta\tau$ the difference of the surface or interfacial tensions of salt solution and pure water.

The relation shows that the free energy of salting out increases with increasing surface tension and hence increasing surface depletion (cf. eq. II.1). This implies that the essential contribution to salting out is the repulsive ion-solute interaction.

Correspondingly the prerequisite for salting in are attractive interactions between ion and solute. This explains why salting in is especially observed with large ions, where dispersion forces are large, or when there are specific interactions between ions and functional groups of the solute, as in the example of acids and bases mentioned above [Lon52, Ave98].

In the case of charged solutes, such as dissociated fatty acids, the ions effect the solubility also by charge shielding. According to:

$$\Delta G = \pi A + q \Psi_0 \quad (\text{II.3})$$

where π is the monolayer pressure and A the area per molecule in the monolayer; ΔG is the expense in energy for a desorbed molecule with charge q to enter the monolayer again and it decreases with decreasing surface potential Ψ_0 . Ψ_0 , however, becomes smaller with increasing salt concentration (fig. 5.07 c).

III. Dispersion energy of a tilted cylinder densely packed between six neighbours

Eq 3.13 can be written as (see fig. A1) [Kag93]:

$$F_{0i} = -g \frac{L - 2d_i |\mathbf{n}\mathbf{u}|}{d_i^5 (1 - (\mathbf{n}\mathbf{u})^2)^5}$$

\mathbf{n} and \mathbf{u} are unit vectors.

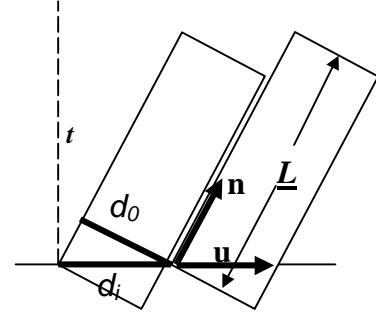


Fig.A1

Figure A2 shows the cylinder positions 0, 1, 2 and 3 in the untilted state ($\mathbf{n}\perp\mathbf{u}$). The distance between next points is d_0 . On changing the tilt direction about ψ with respect to the NN direction (line g) the distances a, b and c of points 1-3 towards a line perpendicular to the tilt direction through 0 stretch to a' , b' , c' :

$$a = d_0 \cos \psi$$

$$b = d_0 \cos(60^\circ - \Psi)$$

$$c = d_0 \cos(60^\circ + \Psi)$$

$$a' = a \frac{1}{\cos t} \quad \text{the same relation holds between b and b', c and c'}$$

ψ varies between 0° (NN) and 30° (NNN).

The new distances in the monolayer plane different from d_0 become (fig. A3):

$$d_1^2 = d_0^2 \sin^2 \Psi + a'^2 \quad \Rightarrow \quad d_1 = d_0 \sqrt{\sin^2 \Psi + \frac{\cos^2 \Psi}{\cos^2 t}}$$

$$d_2^2 = d_0^2 \sin^2 (60^\circ - \Psi) + b'^2 \quad \Rightarrow \quad d_2 = d_0 \sqrt{\sin^2 (60^\circ - \Psi) + \frac{\cos^2 (60^\circ - \Psi)}{\cos^2 t}}$$

$$d_3^2 = d_0^2 \sin^2 (60^\circ + \Psi) + c'^2 \quad \Rightarrow \quad d_3 = d_0 \sqrt{\sin^2 (60^\circ + \Psi) + \frac{\cos^2 (60^\circ + \Psi)}{\cos^2 t}}$$

The angles α_1 , α_2 , α_3 and φ are determined from:

$$\cos \alpha_1 = (d_2^2 + d_3^2 - d_1^2) / 2d_2d_3$$

$$\cos \alpha_2 = (d_1^2 + d_3^2 - d_2^2) / 2d_1d_3$$

$$\cos \alpha_3 = (d_1^2 + d_2^2 - d_3^2) / 2d_1d_2$$

$$\cos \varphi = (d_0^2 + d_1^2 - (a'-a)^2) / 2d_0d_1$$

Hence the interaction energies between the central rod and a nearest neighbour at positions 1, 2 and 3 of fig. A3 are:

$$F_{01} = -g \frac{L - 2d_1(\sin t \cos(\Psi - \varphi))}{d_1^5 (1 - \sin^2 t \cos^2(\Psi - \varphi))^{\frac{5}{2}}}$$

$$F_{02} = -g \frac{L - 2d_2(\sin t \cos(\alpha_3 - \Psi + \varphi))}{d_2^5 (1 - \sin^2 t \cos^2(\alpha_3 - \Psi + \varphi))^{\frac{5}{2}}}$$

$$F_{03} = -g \frac{L - 2d_3(\sin t \cos(\alpha_2 + \Psi - \varphi))}{d_3^5 (1 - \sin^2 t \cos^2(\alpha_2 + \Psi - \varphi))^{\frac{5}{2}}}$$

Considering only *nearest neighbour interactions* the total energy per rod is:

$$F_l = -g (F_{01} + F_{02} + F_{03}) = f(\Psi, t)$$

For aliphatic chains g in fig. 3.22 and 3.23 was taken as 4098 kJ/mole [Sal62]

Fig.A2

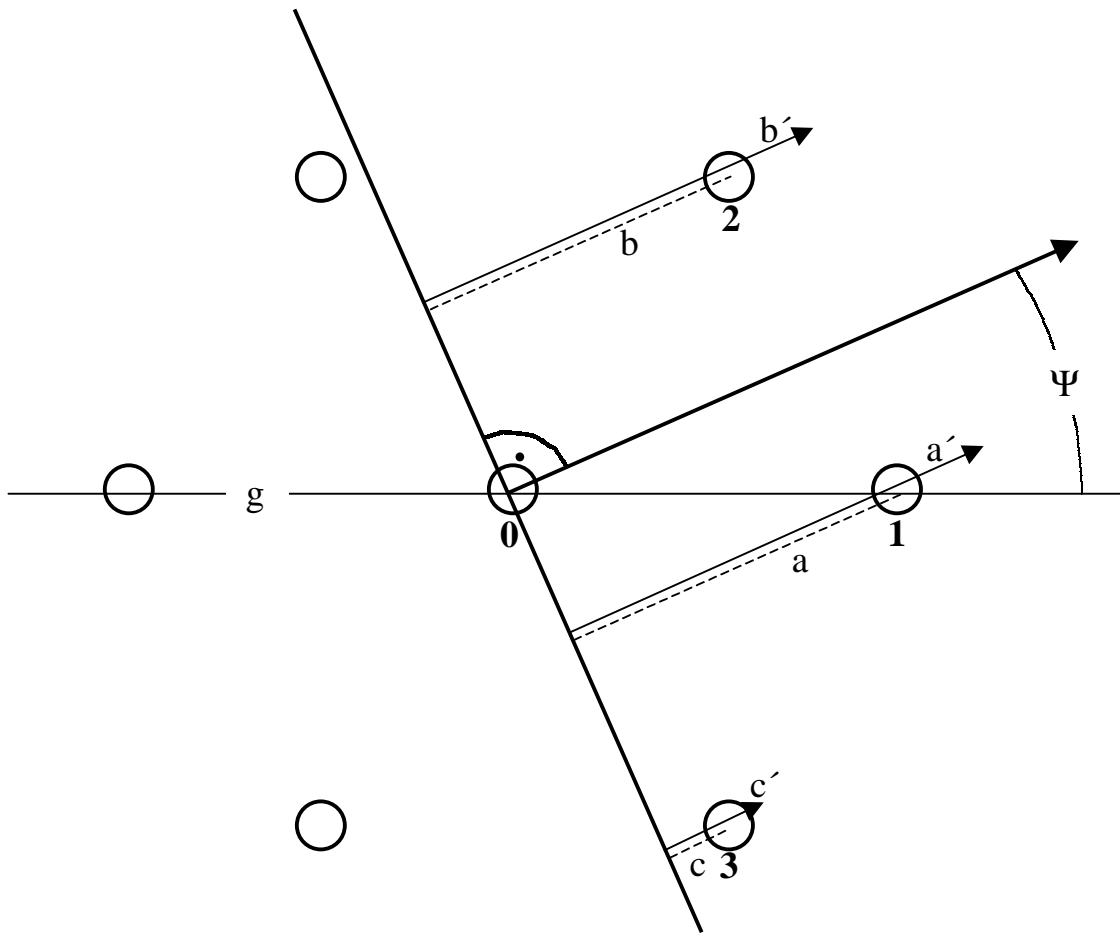
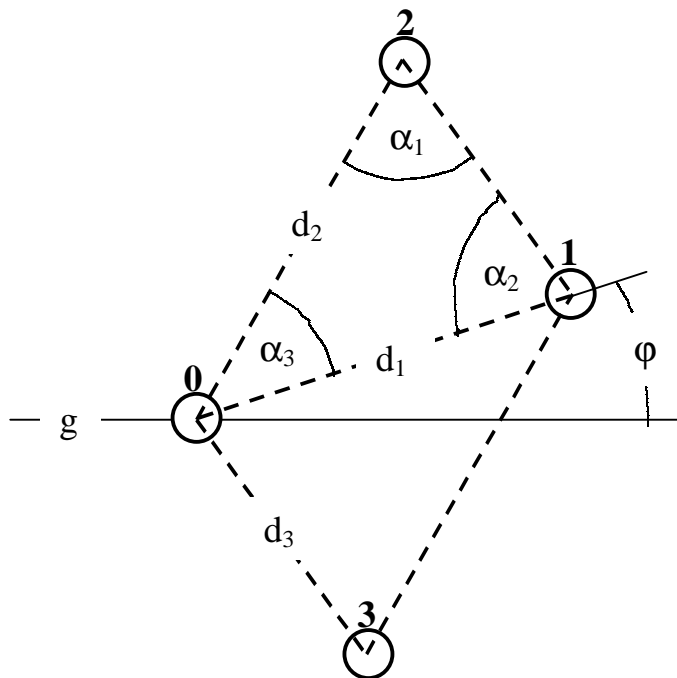
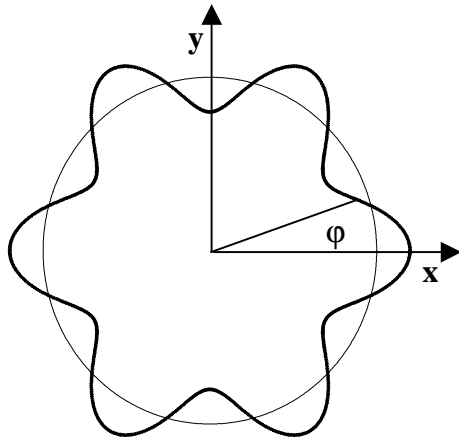


Fig.A3



IV. Calculation of line energy (fig. 6.32)



$$x = \cos\varphi (1 + 0.2 \cos 6\varphi),$$

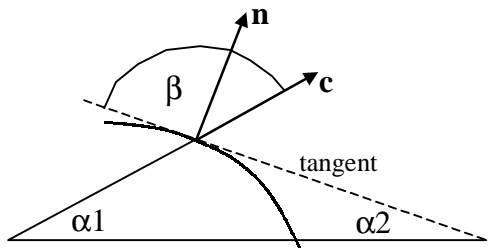
$$y = \sin\varphi (1 + 0.2 \cos 6\varphi)$$

Fig.A4

The line energy $F_\lambda = \int (\lambda_0 - \lambda_1 \mathbf{c} \cdot \mathbf{n}) dl$ is calculated by summing over the perimeter increments

Δl numerically according to: $F_\lambda = \lambda_0 \sum \Delta l - \lambda_1 \sum (\mathbf{c} \cdot \mathbf{n} \Delta l)$;

$$\Delta l = (\Delta x^2 + \Delta y^2)^{1/2};$$



\mathbf{c} indicates the tilt direction of the molecules in a segment,

\mathbf{n} is the normal vector to the domain boundary

Fig.A5

According to fig. A5 it holds

$$\mathbf{c} \cdot \mathbf{n} = c \cdot n \cdot \cos(\beta - 90^\circ) = c \cdot n \cdot \sin\beta$$

$$\beta = 180^\circ - (\alpha_1 + \alpha_2);$$

$$\tan \alpha_2 = \left| \frac{dy}{dx} \right| = \frac{(\cos \varphi + 0.2 \cos \varphi \cos 6\varphi - 1.2 \sin \varphi \sin 6\varphi)}{(-\sin \varphi - 0.2 \sin \varphi \cos 6\varphi - 1.2 \cos \varphi \sin 6\varphi)}$$

The integral was calculated from $\varphi=0$ to 30° (the value of the whole perimeter is 12 times as large) with $\alpha_1=0^\circ$ for case II in fig. 6.32 and $\alpha_1=30^\circ$ for case I.

V. On monolayer-subphase interactions

1. Head group-solvent interactions

The arrangement and bonding of head groups cannot be considered separately from the structure and order of the water molecules next to the head groups, since both influence each other. The structure of water beneath a monolayer will be different from that at the interface to air, which is determined by the tendency of the water molecules to minimise the number of unsaturated bonds. Beneath a monolayer the orientation and binding of water molecules will be affected by polarising electric fields, arising from the monolayer, and the presence of free electron pairs or hydrogens on the head groups to which water can bind. From surface force measurements Israelachvili and Pashley [Isr82] suggested, that the clathrate-like hydrogen bonding structure around hydrophobic molecules is destroyed when polar molecules are placed next to the hydrophobic ones. This would illustrate the influence of polar groups on the nearby water structure.

It is known that the nucleation of ice crystals is facilitated under monolayers of long chain alcohols on water. The arrangement of the hydroxyl head groups makes the monolayer to serve as a template of an ice surface, which causes the reorientation and epitaxial growth of the water molecules beneath the monolayer [Jac91, Pop95, Arb98]. The ability of alkanols to induce the growth of ice crystals is much more pronounced than with fatty acids. Beneath monolayers of neutral fatty acids, in contrast, the structural order and hydrogen bonding network of the interfacial water were found to be heavily disrupted [Mir98]. On the other hand an ionised monolayer creates a surface electric field, which exerts an orienting force upon the water dipoles. At high surface charge density at high pH this field can orient several layers of water molecules and strengthen the lateral hydrogen bonds between the molecules [Wal99] producing an ice-like surface structure of water [Du94, Mir98].

Water molecules at the interface may be bonded to polar head groups more strongly than to other water molecules and form a hydration sheath around a head group, where the water molecules are in a state, that is different from interfacial or bulk water. This does not necessarily mean that the water molecules are tightly fixed, the exchange of water molecules with the surrounding is rather more slowly than between water aggregates in the bulk [Mye91]. The hydrated head group should behave different from an unsolvated one in that it occupies a larger volume. In some instances the concept of head group hydration provides a satisfactory explanation for changes of the in-plane head group area in mono- or bilayers (see chapters 7.1.2, 7.4).

The observation, that uncharged hydrophilic solutes or surfaces in water are hindered to fuse or aggregate and seem to repel each other at short distances, is often ascribed to the, so called, hydration or solvation force, also referred to as ‘negative hydrophobic force‘ (cf. 2.3.2.1). It is assumed to be due to the steric repulsion of water layers, that tightly adhere to hydrophilic surfaces. However, surface force measurements performed by Israelachvili and Wennerström provide a different picture. They demonstrate that the interaction between molecularly smooth and rigid surfaces is attractive at short range below 2 nm [Isr96]. Within this distance the oscillation of force with distance suggests the arrangement of water and other solvents in layers, where energy has to be expended for each sheet of solvent to be removed. For surfaces that are not molecularly smooth, like biological surfaces, however, this energy barrier, and hence the extent of water structuring are strongly reduced. With such surfaces often repulsion is observed at short range. Israelachvili and Wennerström [Isr96] assumed that the reason for this is entropic repulsion, that arises from the restriction of the thermal motion of protruding surface groups or tilting head groups, rather than the repulsion of water layers.

Computer simulations on the distribution of oil-surfactant micelles in water between two surfactant-oil monolayers reveal, to the surprise of the authors [Smi90], that the region near the interfaces is depleted of micelles. Both micelle and monolayer surfaces correspond to biological surfaces (unsmooth), so that this result can be interpreted as the consequence of entropic repulsion between micelles and interfaces.

2. The applicability of monolayers at air as model systems for lipid bilayers is limited

For monolayers at the air/water interface the situation should be different. The amphiphiles there are expected to have a lower vertical mobility, i. e. a lower tendency to protrude into the subphase, than amphiphiles at an oil/water interface or in a bilayer. The protruding of a lipid from a monolayer at the air/water interface is accompanied with an increase in energy due to the loss of chain contact area (eq. 3.04, L reduces). In a monolayer at the oil/water interface or in a bilayer, however, the gap left by the protruding lipid is filled by another alkane, so that protrusion should be much more facilitated from these interfaces. Consequently a monolayer at the air should appear more rigid than a monolayer at an oil/water interface or a bilayer and also the extent of entropic repulsion at the interface should be smaller.

The difference in the behaviour of a monolayer at the air/water interface and a bilayer is demonstrated by the following example. As discussed in 7.4 the presence of short chain alcohols in the aqueous subphase leads to the reduction of the molecular monolayer area, because of head group dehydration. For lipid bilayers, in contrast, it is found that the head group area and chain tilt angle are increased by alcohol [Vie94, Ho97]. The different effect of

short chain alcohols on bilayers and monolayers at air can be explained again by considering the chain interactions. Like a relative vertical shift of the molecules in a monolayer at air also an increase in the chain tilt is accompanied by a decrease in the chain contact area (eq. 3.05) and therefore energetically unfavourable. In lipid bilayers the loss of contact due to tilt between the chains within a layer can be compensated by an increase in the interaction with the chains in the opposite layer. Hence the molecules in bilayers should be tilted much easier than in monolayers at the air/water interface.

The reason for the increase in the tilt angle in the presence of alcohol in bilayers is probably, that alcohol molecules, which are much shorter than the lipids are incorporated in the bilayer in the head group region and increase the area per bilayer lipid. The chains of the bilayer adjust to the change in area by tilting. In monolayers at air the incorporation of the alcohols is energetically too costly. This example demonstrates that the applicability of monolayers at the air/water interface as model systems for bilayers is limited. A much higher similarity exists between bilayers in water and monolayers at an oil/water interface.

VI. X-ray diffraction data

1 Arachidic acid on pH solution

pH 2 (HCl), 25°C

Units: [$K_{x/z}$, FWHM]=10 nm⁻¹, [d, a, b]=
0.1 nm, [A_{xy} , A_0]=0.01 nm², [t]=degree,
[π]=mN/m, [PCL]=0.1 nm

π	$K_x(11)$	FWHM	$K_x(02)$	FWHM	$K_z(11)$	FWHM	$K_z(02)$	FWHM
4	1.3827	0.0357	1.4658	0.0135	0.6829	0.232	0	
12	1.4320	0.0348	1.4770	0.0172	0.5605	0.24	0	
20	1.4812	0.0300	1.4932	0.02	0.4005	0.275	0	
25	1.5136	0.0317	1.5136	0.0317	0.11		0	
30	1.5150	0.0538	1.5150	0.0538	0		0	

π	d02	d11	a	b	t	A_{xy}	A_0
4	4,2865	4,5441	5,359	8,573	30,2	22,97	19,85
12	4,2540	4,3877	5,121	8,508	24,6	21,79	19,82
20	4,2079	4,2420	4,912	8,416	17,4	20,67	19,72
25	4,1512	4,1512	4,793	8,302	4,8	19,90	19,83
30	4,1473	4,1473	4,789	8,295	0	19,86	19,86

on water, 10°C

π	$K_x(11)$	FWHM	$K_x(02)$	FWHM	$K_z(11)$	FWHM	$K_z(02)$	FWHM
4	1.4096	0.0416	1.4466	0.0151	0.723	0.254	0	
8	1.4367	0.0538	1.4488	0.0174	0.668	0.277	0	
12	1.4650	0.0512	1.4512	0.0198	0.608	0.292	0	
16	1.4908	0.0801	1.4563	0.0198	0.533	0.284	0	
20	1.4832	0.0231	1.5660	0.0391	0.229	0.263	0.445	0.259
21.5	1.4872	0.0223	1.5860	0.0388	0.199	0.265	0.385	0.269
23.5	1.4931	0.0191	1.6085	0.0283	0.154	0.255	0.292	0.268
25	1.4972	0.0190	1.6270	0.0242	0.039	0.315	0.177	0.259

π	d02	d11	a	b	t	A_{xy}	A_0
4	4.3434	4.4574	5.1932	8.6868	30.8617	22.5564	19.3626
8	4.3368	4.3733	5.0642	8.6736	28.2982	21.9625	19.3378
12	4.3296	4.2889	4.9369	8.6593	25.5352	21.3752	19.2873
16	4.3145	4.2146	4.8300	8.6290	22.2801	20.8388	19.2830
20	4.0123	4.2362	4.9879	8.0245	16.0830	20.0128	19.2295
21.5	3.9617	4.2248	4.9940	7.9233	13.8661	19.7846	19.2081
23.5	3.9062	4.2081	4.9946	7.8125	10.5648	19.5102	19.1795
25	3.8618	4.1966	4.9989	7.7236	4.4808	19.3049	19.2459

on water, 20°C

π	$K_x(11)$	FWHM	$K_x(02)$	FWHM	$K_z(11)$	FWHM	$K_z(02)$
5	1.4045	0.032	1.4624	0.0131	0.6856	0.248	0
10	1.4367	0.0342	1.4683	0.0132	0.6154	0.249	0
16	1.4731	0.0388	1.4762	0.0203	0.5023	0.230	0
32	1.5296	0.0729	1.5296		0		0

π	d02	d11	a	b	t	A_{xy}	A_0
5	4.30	4.47	5.24	8.59	29.8	22.51	19.5
10	4.28	4.37	5.09	8.56	26.5	21.77	19.5
16	4.26	4.27	4.93	8.51	21.5	20.98	19.5
32	4.11	4.11	4.74	8.22	0.0	19.48	19.5

pH 9.0, 15°C

π	Kx(11)	FWHM	Kx(02)	FWHM	Kz(11)	FWHM	Kz(02)	FWHM
2	1.4184	0.0227	1.4529	0.0106	0.657	0.251	0	
7	1.4413	0.0231	1.4589	0.0119	0.601	0.249	0	
12	1.4621	0.0316	1.4634	0.0145	0.535	0.237	0	
17	1.4739	0.0208	1.4901	0.0323	0.25	0.215	0.496	0.25
23	1.4899	0.0307	1.5244	0.044	0.197	0.252	0.353	0.283
30	1.4902	0.0334						
HB	1.4900	0.0363	1.5347	0.0153				

π	d02	d11	a	b	t	Axy	Ao
2	4.3246	4.4298	5.1576	8.6492	28.3000	22.3043	19.6384
7	4.3068	4.3594	5.0545	8.6136	25.8000	21.7688	19.5989
12	4.2936	4.2974	4.9636	8.5871	22.9000	21.3117	19.6320
17	4.2166	4.2630	4.9407	8.4332	18.5000	20.8330	19.7564
23	4.1217	4.2172	4.9081	8.2435	13.8000	20.2298	19.6458
30	4.2163	4.2163	4.8686	8.4327	0.0000	20.5277	20.5277
HB	4.0941	4.2169	4.9194	8.1882	0.0000	20.1406	20.1406

pH 9.2, 15°C

π	Kx(11)	FWHM	Kx(02)	FWHM	Kz(11)	FWHM	Kz(02)	FWHM
2	1.4222	0.0296	1.4566	0.0123	0.6364	0.2430	0.0000	
7	1.4455	0.0315	1.4621	0.0133	0.5878	0.2530	0.0000	
12	1.4721	0.0437	1.4680	0.0169	0.5189	0.2380	0.0000	
15	1.4752	0.0271	1.4934	0.0227	0.2599	0.2260	0.5253	0.2220
20	1.4879	0.0372	1.5232	0.0475	0.2165	0.2500	0.4152	0.2500
27	1.5242	0.0950			0		0	

π	d02	d11	a	b	t	Axy	Ao
2	4.3136	4.4179	5.1435	8.6272	27.5181	22.1871	19.6773
7	4.2974	4.3467	5.0386	8.5947	25.2377	21.6527	19.5860
12	4.2801	4.2682	4.9239	8.5602	22.1288	21.0748	19.5227
15	4.2073	4.2592	4.9386	8.4146	19.2853	20.7781	19.6121
20	4.1250	4.2229	4.9156	8.2500	15.5586	20.2769	19.5338
27	4.1223	4.1223	4.7600	8.2446	0	19.6221	19.6221

pH 9.5, 15°C

π	Kx(11)	FWHM	Kx(02)	FWHM	Kz(11)	FWHM	Kz(02)	FWHM
2	1.4229	0.0256	1.4573	0.0115	0.627	0.25	0	
7	1.4431	0.0287	1.4617	0.0123	0.574	0.244	0	
12	1.4633	0.0382	1.4660	0.0141	0.512	0.248	0	
17	1.4756	0.0236	1.4901	0.0269	0.25	0.216	0.506	0.26
23	1.4909	0.0344	1.5219	0.0418	0.200	0.252	0.38	0.38
30	1.5212	0.085			1.5652	0.045	1.5187	0.071

π	d02	d11	a	b	t	Axy	Ao
2	4.3115	4.4158	5.1410	8.6230	27.1587	22.1655	19.7216
7	4.2985	4.3540	5.0494	8.5971	24.7632	21.7050	19.7092
12	4.2859	4.2938	4.9612	8.5719	22.0121	21.2632	19.7132
17	4.2166	4.2581	4.9330	8.4332	18.6527	20.8008	19.7082
23	4.1285	4.2144	4.9008	8.2570	14.3732	20.2329	19.5996
30	4.1304	4.1304	4.7694	8.2608	0.0000	19.6996	19.6996
HB	4.0143	4.1372	4.8275	8.0286	0.0000	19.3792	19.3792

pH 9.7, 15°C

π	Kx(11)	FWHM	Kx(02)	FWHM	Kz(11)	FWHM	Kz(02)	FWHM
1	1.4204	0.0314	1.4584	0.0127	0.6328	0.2770	0.0000	
6	1.4443	0.0293	1.4639	0.0136	0.5728	0.2420	0.0000	
8	1.4536	0.0364	1.4666	0.0161	0.5475	0.2440	0.0000	
10	1.4695	0.0209	1.4649	0.0493	0.2967	0.1870	0.5921	0.3010
16	1.4812	0.0140	1.5005	0.0250	0.2382	0.1870	0.4881	0.2250
22	1.4997	0.0181	1.5323	0.0380	0.1759	0.2630	0.3289	0.2340
26.7	1.5242	0.0860	1.5242	0.0860	0		0	

π	d02	d11	a	b	t	Axy	Ao
1	4.3083	4.4235	5.1546	8.6165	27.4342	22.2076	19.7102
6	4.2921	4.3504	5.0465	8.5842	24.7045	21.6600	19.6776
8	4.2842	4.3226	5.0063	8.5684	23.5687	21.4481	19.6589
10	4.2892	4.2757	4.9321	8.5783	22.0307	21.1543	19.6097
16	4.1874	4.2421	4.9200	8.3748	17.8170	20.6018	19.6137
22	4.1005	4.1896	4.8736	8.2010	12.5229	19.9841	19.5087
26.7	4.1223	4.1223	4.7600	8.2446	0	19.6221	19.6221

pH 10.0, 15°C

π	Kx(11)	FWHM	Kx(02)	FWHM	Kz(11)	FWHM	Kz(02)	FWHM
2	1.4230	0.0247	1.4582	0.0117	0.623	0.252	0	0
7	1.4610	0.0167	1.4421	0.0310	0.32	0.233	0.64	0.243
12	1.4700	0.0206	1.4709	0.0310	0.287	0.248	0.58	0.223
17	1.4814	0.0236	1.4972	0.0316	0.235	0.207	0.47	0.23
23	1.4964	0.0441	1.5218	0.0471	0.16	0.260	0.32	
30	1.5221	0.0811			1.6210	0.0670	1.5687	0.0386

π	d02	d11	a	b	t	Axy	Ao
2	4.3089	4.4154	5.1416	8.6177	27.01	22.1546	19.74
7	4.3570	4.3006	4.9448	8.7139	23.93	21.5442	19.69
12	4.2717	4.2743	4.9365	8.5433	21.4189	21.0871	19.6307
17	4.1966	4.2414	4.9151	8.3932	17.4281	20.6269	19.6800
23	4.1288	4.1989	4.8763	8.2576	11.8750	20.1334	19.7025
30	4.1280	4.1280	4.7666	8.2559	0	19.6762	19.676
HB	4.0053	3.8761	4.4291	8.0107	0	17.7402	17.74

pH 10.2, 15°C

π	Kx(11)	FWHM	Kx(02)	FWHM	Kz(11)	FWHM	Kz(02)	FWHM
2	1.4181	0.0253	1.4604	0.0124	0.625	0.249	0	
7	1.4598	0.0209	1.4357	0.0277	0.322	0.225	0.65	0.237
12	1.4704	0.0240	1.4686	0.0490	0.269	0.214	0.534	0.269
17	1.4818	0.0303	1.4971	0.0326	0.225	0.214	0.45	0.227
23	1.4994	0.0462	1.5221	0.0599	0.15	0.269	0.3	0.25
30	1.5217	0.0632			1.5205	0.061	1.5628	0.031

π	d02	d11	a	b	t	Axy	Ao
2	4.3024	4.4307	5.1686	8.6047	27.2089	22.2371	19.7764
7	4.3764	4.3041	4.9431	8.7528	24.2588	21.6329	19.7227
12	4.2784	4.2731	4.9322	8.5567	20.0507	21.1015	19.8225
17	4.1969	4.2402	4.9132	8.3938	16.7298	20.6204	19.7476
23	4.1280	4.1905	4.8635	8.2559	11.1499	20.0765	19.6975
30	4.1291	4.1291	4.7678	8.2581	0.0000	19.6866	19.6866
HB	4.0205	4.1323	4.8171	8.0409	0.0000	19.3670	19.3670

pH 11.7, 15°C

π	Kx(11)	FWHM	Kx(02)	FWHM	Kz(11)	FWHM	Kz(02)	FWHM
3	1.4515	0.0187	1.4055	0.0323	0.349	0.232	0.711	0.234
7	1.4605	0.0170	1.4316	0.0263	0.324	0.243	0.649	0.250
12	1.4715	0.0183	1.4631	0.0390	0.272	0.217	0.54	0.262
17	1.4825	0.0235	1.4924	0.0373	0.214	0.193	0.431	0.265
23	1.5078	0.0487	1.5129	0.0639	0.09	-	0.18	-
30	1.5220	0.0682	1.5220	0.0682	0		0	

π	d02	d11	a	b	t	Axy	Ao
3	4.4704	4.3288	4.9472	8.9409	26.6221	22.1163	19.7716
7	4.3889	4.3021	4.9355	8.7779	24.3700	21.6615	19.7314
12	4.2944	4.2699	4.9211	8.5889	20.3270	21.1335	19.8175
17	4.2101	4.2382	4.9049	8.4202	16.0554	20.6501	19.8446
23	4.1531	4.1671	4.8172	8.3061	6.7850	20.0063	19.8662
30	4.1282	4.1282	4.7669	8.2565	0.0000	19.6789	19.6789

pH 12.0, 15°C

π	Kx(11)	FWHM	Kx(02)	FWHM	Kz(11)	FWHM	Kz(02)	FWHM
13	1.4724	0.0233	1.4473	0.0381	0.30	0.282	0.60	0.248
17	1.4870	0.0228	1.4833	0.0395	0.25		0.5	
23	1.5218		1.5609		0.03(?)		0.06(?)	
30	1.5261		1.5892		0		0	

π	d02	d11	a	b	t	Axy	Ao
13	4.3413	4.2673	4.8999	8.6826	22.5172	21.2722	19.6505
17	4.2360	4.2254	4.8750	8.4719	18.6283	20.6505	19.5686
23	4.0254	4.1288	4.8094	8.0507	2.2575(?)	19.3596	19.3596
30	3.9537(?)	4.1172	4.8224	7.9074	0.0000	19.0662	19.0662

AA, pH 12.0, 25°C

π	Kx(11)	FWHM	Kx(02)	FWHM	Kz(11)	FWHM	Kz(02)	FWHM
12	1.4607	0.0244	1.3959	0.0377	0.330	0.256	0.6548	0.222
16	1.4684	0.0202	1.4206	0.0376	0.2868	0.261	0.5829	0.253
20	1.4822	0.0271	1.4426	0.0314	0.2697	0.237	0.4984	0.242
24	1.4915	0.0249	1.4697	0.0323	0.2135	0.310	0.4073	0.241
28	1.5036	0.0251	1.4913	0.0355	0.16	0.29	0.31	0.23
32	1.5185	0.0239	1.5159	0.0239	0	0	0	0

π	d02	d11	a	b	t	Axy	Ao
12	4,5012	4,3015	4,897	9,002	25,2	22,041	19,94
16	4,4229	4,2789	4,889	8,846	22,1	21,624	20,02
20	4,3555	4,2391	4,852	8,711	19,8	21,1346	19,89
24	4,2751	4,2127	4,841	8,550	15,8	20,696	19,91
28	4,2132	4,1788	4,812	8,427	11,9	20,2748	19,84
32	4,1449	4,1449	4,786	8,290	0	19,838	19,84

pH 12.3, 15°C

π	Kx(11)	FWHM	Kx(02)	FWHM	Kz(11)	FWHM	Kz(02)	FWHM
12	1.4568	0.0241	1.4014	0.0465	0.34	0.238	0.68	0.256
17	1.4712	0.0255	1.4440	0.0426	0.295	0.250	0.593	0.244
22	1.4870	0.0320	1.4802	0.0487	0.230	0.233	0.457	0.226
30	1.5210	0.0627	1.5210	0.0627	0		0	

π	d02	d11	a	b	t	Axy	Ao
12	4.4835	4.3130	4.9194	8.9670	25.8840	22.0563	19.8436
17	4.3512	4.2708	4.9016	8.7025	22.2753	21.3282	19.7366
22	4.2448	4.2254	4.8717	8.4896	17.2107	20.6794	19.7535
30	4.1310	4.1310	4.7700	8.2619	0.0000	19.7047	19.7047

pH 12.3, 25°C

π	Kx(11)	FWHM	Kx(02)	FWHM	Kz(11)	FWHM	Kz(02)	FWHM
14	1.4528	0.0233	1.3680	0.0376	0.349	0.242	0.70	0.249
17.5	1.4610	0.0209	1.3950	0.0371	0.310	0.234	0.62	0.209
22	1.4765	0.0194	1.4336	0.0282	0.266	0.227	0.53	0.234
26	1.4908	0.0183	1.4681	0.0259	0.210	0.236		
35	1.5163	0.0199	1.5163	0.0199	0		0	

π	d02	d11	a	b	t	Axy	Ao
14	4.5930	4.3249	4.902	9.186	27.1	22.516	20.05
17.5	4.5041	4.3006	4.894	9.008	24.0	22.0447	20.14
22	4.3828	4.2555	4.868	8.766	20.3	21.333	20.01
26	4.2798	4.2146	4.842	8.600	16.0	20.724	19.92
35	4.1438	4.1438	4.7848	8.288	0	19.827	19.83

pH 12.5, 25°C

π	Kx(11)	FWHM	Kx(02)	FWHM	Kz(11)	FWHM	Kz(02)	FWHM
20	1.4715	0.0264	1.4152	0.0401	0.299	0.237	0.594	0.254
28	1.4954	0.025	1.4717	0.03	0.215	0.261	0.413	0.208
36	1.5181	0.0225			0		0	

π	d02	d11	a	b	t	Axy	Ao
20	4.4398	4.2699	4.8699	8.8796	22.8538	21.6215	19.9242
28	4.2693	4.2017	4.8264	8.5387	15.9961	20.6057	19.8079
36	4.1390	4.1390	4.7793	8.2780	0	19.7815	19.7815

pH 13.0, 25°C

π	Kx(11)	FWHM	Kx(02)	FWHM	Kz(11)	FWHM	Kz(02)	FWHM
20 ¹			1.3402	0.0896			0.7332	0.2480
20 ²			1.4816	0.0328			0	

π	d02	d11	a	b	t	Axy	Ao
20 ¹	4.6882		4.9	9.3765	28.6836	23.1	
20 ²	4.2408			8.4816			

¹ NNN peak

² NN peak

1 Stearic acid on pH solution

pH 9.2, 15°C

π	Kx(11)	FWHM	Kx(02)	FWHM	Kz(11)	FWHM	Kz(02)	FWHM
2.3	1.4192	0.0258	1.4739	0.0125	0.5835	0.2710	0.0000	
10	1.4584	0.0285	1.4861	0.0160	0.4817	0.2620	0.0000	
16	1.4864	0.0279	1.4993	0.0200	0.3596	0.2600	0.0000	
18	1.5041	0.0270	1.4940	0.0400	0.1200		0.2400	
25	1.5220	0.0285			0		0	

π	d02	d11	a	b	t	Axy	Ao
2.3	4.2630	4.4274	5.1807	8.5259	25.6922	22.0852	19.9018
10	4.2280	4.3083	5.0069	8.4559	21.0010	21.1689	19.7627
16	4.1909	4.2273	4.8955	8.3818	15.6509	20.5163	19.7556
18	4.2056	4.1774	4.8129	8.4112	9.1262	20.2411	19.9849
25	4.1282	4.1282	4.7669	8.2565	0	19.6789	19.6789

pH 9.2, 25°C

π	Kx(11)	FWHM	Kx(02)	FWHM	Kz(11)	FWHM	Kz(02)	FWHM
2	1.4020	0.0278	1.4761	0.0107	0.5876	0.2730	0.0000	
8	1.4311	0.0255	1.4835	0.0111	0.5051	0.2420	0.0000	
13.5	1.4559	0.0274	1.4912	0.0121	0.4469	0.2570	0.0000	
16	1.4887	0.0197	1.4605	0.0227	0.2225	0.3120	0.4121	0.2500
21	1.5020	0.0162	1.4880	0.0200	0.1297	0.3480	0.2652	0.2560
27	1.5143	0.0137			0		0	

π	d02	d11	a	b	t	Axy	Ao
2	4.2566	4.4816	5.2711	8.5132	26.2413	22.4370	20.1246
8	4.2354	4.3905	5.1339	8.4708	22.4275	21.7439	20.0993
13.5	4.2135	4.3158	5.0248	8.4270	19.6683	21.1721	19.9368
16	4.3021	4.2206	4.8433	8.6042	16.3542	20.8363	19.9933
21	4.2226	4.1832	4.8155	8.4451	9.9953	20.3337	20.0251
27	4.1492	4.1492	4.7911	8.2985	0	19.8795	19.8795

pH 9.7, 25°C

π	Kx(11)	FWHM	Kx(02)	FWHM	Kz(11)	FWHM	Kz(02)	FWHM
1	1.4029	0.0301	1.4774	0.0109	0.5700	0.2520	0.0000	
8	1.4375	0.0286	1.4861	0.0113	0.4818	0.2480	0.0000	
10	1.4361	0.0250	1.4802	0.0218	0.2480	0.3140	0.4867	0.2570
18	1.4996	0.0150	1.4833	0.0150	0.1472	0.3530	0.2918	0.2290
27			1.5138	0.0126	0		0	

π	d02	d11	a	b	t	Axy	Ao
1	4.2529	4.4787	5.2682	8.5057	25.5437	22.4049	20.2150
8	4.2280	4.3709	5.1059	8.4559	21.3805	21.5878	20.1021
10	4.3752	4.2448	4.8542	8.7503	18.8869	21.2381	20.0947
18	4.1899	4.2360	4.9094	8.3798	11.0590	20.5698	20.1878
27	4.1506	4.1506	4.7927	8.3012	0	19.8926	19.8926

Measured data points and corresponding phases

Fatty acid	T [°C]	pH	Surface pressures [mN/m]
Arachidic acid	25	2.0	NN 4, 12, 20, 25; U: 30
		12.0	NNN: 12, 16, 20, 24; U: 32
		12.3	NNN: 14, 17.5, 22, 26; U: 35
		12.5	NNN: 20, 28; U: 36
		13.0	NNN: 20
	20	5.6	NN: 5, 10, 16; U: 32
	15	9.0	NN: 2, 7, 12; NNN: 17, 23; U: 30
		9.2	NN: 2, 7, 12; NNN: 15, 20; U: 27
		9.5	NN: 2, 7, 12; NNN: 17, 23; U: 30
		9.7	NN: 1, 5, 7; NNN: 9, 15, 21; U: 26.7
		10.0	NN: 2; NNN: 7, 12, 17, 23; U: 30
		10.2	NN: 2; NNN: 7, 12, 17, 23; U: 30
		11.7	NNN: 3, 7, 12, 17, 23; U: 30
		12.0	NNN: 13, 17, 23; U: 30
		12.3	NNN: 12, 17, 22; U: 30
		10	5.6
	Stearic acid	25	9.2
9.7			NN: 1, 8; NNN: 10, 18; U: 27
15		9.2	NN: 2, 10, 16; NNN: 18; U: 25

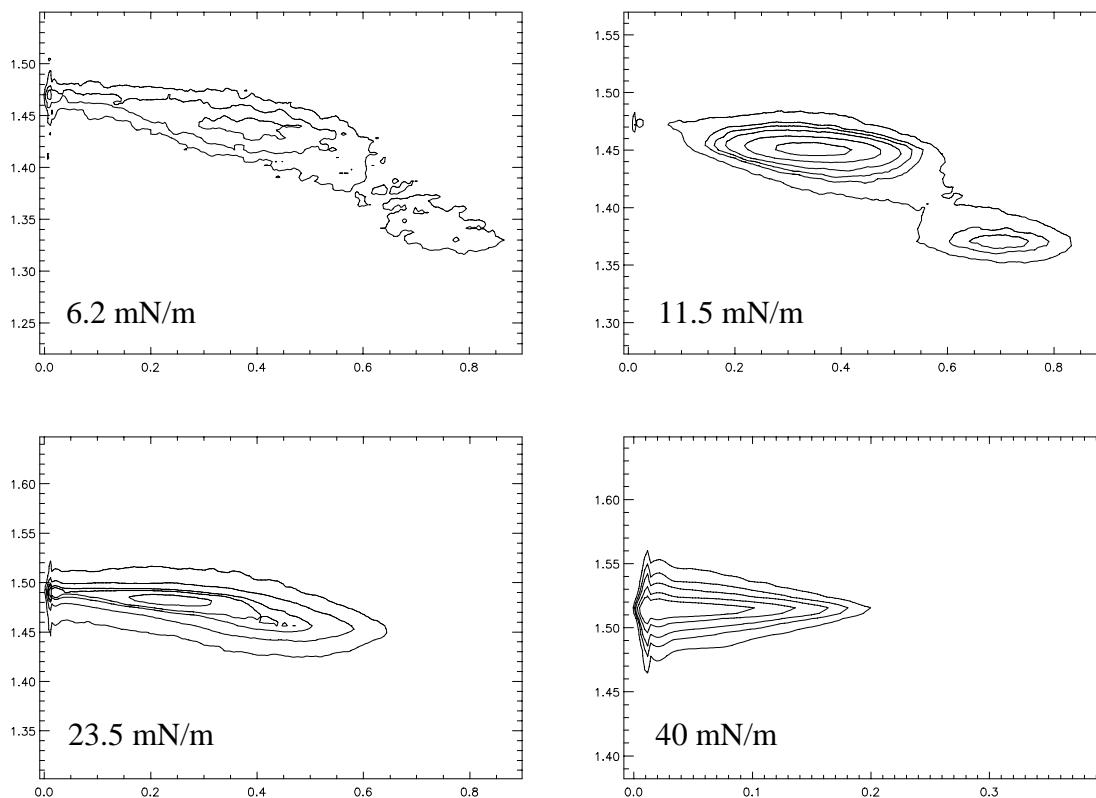
3. Arachidic acid on $1 \cdot 10^{-3}$ M polyethyleneimine solution at 25°C

π	Kx(11)	FWHM	Kx(02)	FWHM	Kz(11)	FWHM	Kz(02)	FWHM
6.2 ¹	1.4374	0.0460	1.3377	0.0713	0.365	0.355	0.741	0.281
6.2 ²	1.41	0.12	1.4648	0.0272	0.537	0.285	0	0
11.5	1.4515	0.0278	1.3710	0.0441	0.351	0.246	0.698	0.238
23.5	1.4849	0.0232	1.4547	0.0366	0.200	0.350	0.446	0.272
40	1.5164	0.0182	1.5164	0.0182	0		0	

π	d(11)	d(02)	a	b	t	A _{xy}	A ₀	$\xi(11)$	$\xi(02)$
6.2 ¹	4.3712	4.6970	4.938	9.394	28.8	23.196	20.33	44.2	28.2
6.2 ²	4.4562	4.2894	5.21	8.58	24.0	22.369	20.43	16.7	77.1
11.5	4.3288	4.5829	4.911	9.166	27.0	22.506	20.04	75.3	46.2
23.5	4.2314	4.3192	4.854	8.639	16.2	20.964	20.13	92.2	56.1
40	4.1435	4.1435	4.785	8.287	0.0	19.825	19.82	123.1	123.1

¹ NNN peak

² NN peak



Contour plots for arachidic acid on $1 \cdot 10^{-3}$ M PEI solution at 25°C

4. Arachidic acid cholesterol mixtures on subsolution of pH 12.0 at 25°C

0.4 mol% Cholesterol

π	Kx(11)	FWHM	Kx(02)	FWHM	Kz(11)	FWHM	Kz(02)	FWHM
13	1.4671	0.0171	1.4204	0.0265	0.298	0.231	0.594	0.264
17.5	1.4787	0.0166	1.4469	0.0246	0.256	0.229	0.52	0.226
22	1.4883	0.0177	1.4698	0.0223	0.224	0.224	0.44	0.215
34	1.5185	0.0178	1.5185	0.0178	0		0	

π	d02	d11	a	b	t	Axy	Ao
13	4,4235	4,2827	4,894	8,847	22,7	21,65	19,97
17.5	4,3425	4,2491	4,872	8,685	19,6	21,16	19,93
22	4,2749	4,2217	4,855	8,550	16,8	20,75	19,87
34	4,1378	4,1378	4,778	8,276	0,0	19,77	19,77

1 mol%

π	Kx(11)	FWHM	Kx(02)	FWHM	Kz(11)	FWHM	Kz(02)	FWHM
12	1.4649	0.0161	1.4216	0.0237	0.3041	0.2309	0.5910	0.2389
16	1.4785	0.0156	1.4492	0.0224	0.2607	0.2206	0.4950	0.2954
20	1.4920	0.0147	1.4764	0.0166	0.2148	0.2575	0.42	0.247
32	1.5176	0.0167						

π	d02	d11	a	b	t	Axy	Ao
12	4,4198	4,2892	4,905	8,840	22,9	21,68	19,98
16	4,3356	4,2497	4,875	8,671	19,3	21,14	19,95
20	4,2557	4,2113	4,846	8,512	16,1	20,62	19,82
32	4,1402	4,1402	4,781	8,280	0	19,79	19,79

3 mol%

π	Kx(11)	FWHM	Kx(02)	FWHM	Kz(11)	FWHM	Kz(02)	FWHM
12	1.4605	0.0196	1.3982	0.031	0.3171	0.238	0.6449	0.218
16	1.4723	0.0181	1.4300	0.0280	0.2710	0.244	0.5465	0.277
20	1.4852	0.0155	1.4618	0.0217	0.2291	0.226	0.42	0.32
32	1.5168	0.0164						

π	d02	d11	a	b	t	Axy	Ao
12	4,4938	4,3021	4,900	8,988	24,6	22,02	20,02
16	4,3938	4,2676	4,882	8,788	20,8	21,45	20,05
20	4,2983	4,2305	4,860	8,597	16,7	20,89	20,01
32	4,1424	4,1424	4,783	8,285	0	19,81	19,81

5 mol%

π	Kx(11)	FWHM	Kx(02)	FWHM	Kz(11)	FWHM	Kz(02)	FWHM
12	1.4615	0.0195	1.4032	0.0290	0.3139	0.418	0.6260	0.222
16	1.4739	0.0176	1.4352	0.0280	0.2700	0.214	0.5350	0.271
20	1.4867	0.0159	1.4633	0.0233	0.2268	0.253	0.4090	0.307
32	1.5167	0.0159	1.5167	0.0159				

π	d02	d11	a	b	t	Axy	Ao
12	4,4778	4,2991	4,901	8,956	24,1	21,94	20,04
16	4,3779	4,2630	4,881	8,756	20,5	21,37	20,01
20	4,2938	4,2263	4,855	8,588	16,4	20,85	20,00
32	4,1427	4,1427	4,784	8,285	0	19,82	19,82

5. Arachidic acid on water/solute mixtures at 10°C

0.3 vol% n-Butanol

π	K_x(11)	FWHM	K_x(02)	FWHM	K_z(11)	FWHM	K_z(02)	FWHM
2	1.4415	0.0590	1.4489	0.0167	0.666	0.289	0	0
5	1.4626	0.0600	1.4512	0.0164	0.621	0.318	0	0
8	1.4884	0.0790	1.4546	0.0167	0.566	0.313	0	0
11	1.5024	0.1102	1.4583	0.0209	0.494	0.259	0	0
13.5	1.4840	0.0237	1.5689	0.0293	0.225	0.254	0.436	0.236
15	1.4885	0.0207	1.5852	0.0329	0.194	0.267	0.378	0.273
16.5	1.4921	0.0205	1.6070	0.0306	0.152	0.278	0.295	0.261
18	1.4970	0.0184	1.6275	0.0215	0.057	0.330	0.186	0.253

π	d02	d11	a	b	t	A_{xy}	A_o
2	4.3365	4.3588	5.0417	8.6730	28.1205	21.8636	19.2828
5	4.3296	4.2959	4.9477	8.6593	26.0589	21.4218	19.2441
8	4.3195	4.2214	4.8384	8.6391	23.5501	20.8997	19.1590
11	4.3086	4.1821	4.7832	8.6171	20.6096	20.6087	19.2897
13.5	4.0048	4.2340	4.9878	8.0097	15.7677	19.9752	19.2235
15	3.9637	4.2212	4.9869	7.9273	13.5829	19.7665	19.2137
16.5	3.9099	4.2110	4.9974	7.8198	10.5572	19.5394	19.2087
18	3.8606	4.1972	5.0005	7.7213	5.2658	19.3051	19.2236

0.6 vol% n-Butanol

π	K_x(11)	FWHM	K_x(02)	FWHM	K_z(11)	FWHM	K_z(02)	FWHM
1	1.4668	0.0554	1.4523	0.0173	0.604	0.292	0	0
3	1.4849	0.0621	1.4547	0.0175	0.565	0.275	0	0
4.5	1.4920	0.0819	1.4564	0.0195	0.532	0.282	0	0
6	1.5012	0.1032	1.4579	0.0221	0.499	0.272	0	0
8	1.4815	0.0262	1.5598	0.0346	0.241	0.276	0.459	0.236
9.5	1.4861	0.0215	1.5797	0.0319	0.206	0.261	0.404	0.254
11.5	1.4919	0.0196	1.6047	0.0288	0.153	0.288	0.307	0.261
13	1.4972	0.0184	1.6247	0.0227	0.066	0.345	0.199	0.258

π	d02	d11	a	b	t	A_{xy}	A_o
1	4.3264	4.2836	4.9301	8.6527	25.3578	21.3296	19.2745
3	4.3192	4.2314	4.8535	8.6385	23.5784	20.9635	19.2133
4.5	4.3142	4.2113	4.8250	8.6284	22.2216	20.8158	19.2698
6	4.3098	4.1854	4.7878	8.6195	20.8187	20.6341	19.2869
8	4.0282	4.2411	4.9882	8.0564	16.7855	20.0936	19.2374
9.5	3.9775	4.2280	4.9913	7.9549	14.4817	19.8528	19.2220
11.5	3.9155	4.2115	4.9955	7.8310	10.8133	19.5597	19.2124
13	3.8673	4.1966	4.9960	7.7346	5.8164	19.3208	19.2213

0.03 vol% n-Heptadecanol

π	K_x(11)	FWHM	K_x(02)	FWHM	K_z(11)	FWHM	K_z(02)	FWHM
1	1.5008	0.0877	1.4576	0.0191	0.5153	0.274	0	0
3.5	1.4806	0.0243	1.5595	0.0451	0.241	0.246	0.4688	0.238
5	1.4849	0.0222	1.5770	0.0353	0.223	0.223	0.4249	0.258
7.5	1.4916	0.0181	1.6059	0.0289	0.166	0.243	0.319	0.247
9	1.4958	0.0171	1.6231	0.0223	0.083	0.203	0.2171	0.251

π	d02	d11	a	b	t	Axy	Ao
1	4.3106	4.1866	4.7891	8.6213	21.4434	20.6443	19.2152
3.5	4.0290	4.2437	4.9921	8.0579	16.9534	20.1129	19.2388
5	3.9843	4.2314	4.9936	7.9685	15.4362	19.8958	19.1781
7.5	3.9126	4.2124	4.9984	7.8251	11.4581	19.5566	19.1668
9	3.8711	4.2006	5.0005	7.7422	6.7306	19.3575	19.2241

2 vol% acetic acid

π	Kx(11)	FWHM	Kx(02)	FWHM	Kz(11)	FWHM	Kz(02)	FWHM
3	1.4461	0.0605	1.4496	0.0171	0.658	0.288	0	0
5	1.4581	0.0559	1.4516	0.0170	0.628	0.302	0	0
7	1.4700	0.0649	1.4532	0.0180	0.595	0.288	0	0
11	1.4979	0.0942	1.4578	0.0223	0.509	0.261	0	0
14	1.4816	0.0278	1.5615	0.0423	0.231	0.253	0.446	0.234
16	1.4876	0.0240	1.5842	0.0347	0.197	0.266	0.374	0.269
18	1.4938	0.0218	1.6121	0.0308	0.131	0.318	0.270	0.264
19	1.4984	0.0157	1.6280	0.0202	0.012	0.370	0.156	0.280

π	d02	d11	a	b	t	Axy	Ao
3	4.3344	4.3449	5.0211	8.6689	27.7369	21.7637	19.2630
5	4.3285	4.3092	4.9684	8.6569	26.4086	21.5056	19.2614
7	4.3237	4.2743	4.9169	8.6474	24.9676	21.2592	19.2725
11	4.3100	4.1947	4.8015	8.6201	21.2544	20.6946	19.2870
14	4.0238	4.2408	4.9898	8.0476	16.2116	20.0782	19.2799
16	3.9662	4.2237	4.9899	7.9323	13.6253	19.7908	19.2338
18	3.8975	4.2062	4.9959	7.7950	9.3695	19.4716	19.2119
19	3.8595	4.1933	4.9945	7.7189	3.1642	19.2761	19.2467

5 vol% acetic acid

π	Kx(11)	FWHM	Kx(02)	FWHM	Kz(11)	FWHM	Kz(02)	FWHM
1.5	1.4691	0.0738	1.4526	0.0172	0.599	0.284	0	0
3	1.4808	0.0687	1.4547	0.0203	0.571	0.312	0	0
4.5	1.4904	0.0890	1.4561	0.0202	0.540	0.295	0	0
6	1.5031	0.1003	1.4583	0.0201	0.502	0.262	0	0
8	1.4795	0.0277	1.5539	0.0387	0.246	0.265	0.471	0.239
9.5	1.4843	0.0233	1.5736	0.0361	0.221	0.263	0.424	0.241
11.5	1.4899	0.0194	1.5981	0.0381	0.174	0.279	0.348	0.262
13	1.4950	0.0170	1.6145	0.0238	0.132	0.271	0.259	0.275

π	d02	d11	a	b	t	Axy	Ao
1.5	4.3255	4.2769	4.9202	8.6510	25.1297	21.2824	19.2680
3	4.3192	4.2431	4.8712	8.6385	23.8782	21.0400	19.2391
4.5	4.3151	4.2158	4.8315	8.6302	22.5498	20.8481	19.2542
6	4.3086	4.1802	4.7803	8.6171	20.9030	20.5961	19.2406
8	4.0435	4.2468	4.9903	8.0870	17.2164	20.1783	19.2742
9.5	3.9929	4.2331	4.9922	7.9857	15.3851	19.9331	19.2188
11.5	3.9317	4.2172	4.9965	7.8633	12.2849	19.6447	19.1949
13	3.8917	4.2028	4.9933	7.7834	9.2003	19.4326	19.1826

6. Arachidic acid on $2 \cdot 10^{-4}$ M CuSO_4 -solution at 20°C

Hysteresis: compression from 5-32 mN/m, subsequent expansion from 32-5 mN/m

π	$\mathbf{Kx(11)}$	FWHM	$\mathbf{Kx(02)}$	FWHM	$\mathbf{Kz(11)}$	FWHM	$\mathbf{Kz(02)}$
5	1.4873	0.0426	1.4759	0.0227	0.4415	0.222	0
10	1.5101	0.0506	1.52		0.2781	0.24	0
32	1.5340		1.5114	(1.5279)	0		
10	1.5016	0.0385	1.4853		0.3681	0.229	0
5	1.4689		1.470		0.52	0.266	0

π	$\mathbf{d02}$	$\mathbf{d11}$	\mathbf{a}	\mathbf{b}	\mathbf{t}	$\mathbf{A_{xy}}$	$\mathbf{A_0}$
5	4.26	4.22	4.87	8.51	18.9	20.71	19.6
10	4.13	4.16	4.82	8.27	12.0	19.90	19.5
32	4.16	4.10	4.71	8.31	0.0	19.57	19.6
32	4.11	4.11	4.75	8.22	0.0	19.53	19.5
10	4.23	4.18	4.81	8.46	15.8	20.37	19.6
5	4.27	4.28	4.94	8.55	22.2	21.12	19.5

7. Tables

Tab.VI.1: ref. to arachidic acid (the parameters a, b, A_{xy} , tilt angle and the position correlation length PCL are extrapolated to 20 mN/m. At pH 13 the data refer to the NNN phase); d_0 : distortion parameter

pH	T [$^\circ\text{C}$]	a	b	A_{xy}	$-A_{xy}/\pi$	tilt	PCL_{11}	PCL_{02}	PCL_{11}/π	PCL_{02}/π	$-d_0$
12.0	15	4.84	8.25	19.98	0.193	13.2	70	60	-4.40	-0.05	0.003
12.3	15	4.88	8.58	20.94	0.138	19.4	72	44	-2.42	-0.21	0.034
12.0	25	4.86	8.71	21.15	0.112	19.6	89	59	-0.72	0.41	0.006
12.3	25	4.88	8.88	21.64	0.151	22.2	108	67	2.49	2.49	0.015
12.5	25	4.87	8.89	21.62	0.130	22.9	80	51	0.66	2.37	0.010
13.0	25	4.9	9.4	23.1	-	28.7	-	-	-	-	-

Tab.VI.2: ref. to arachidic acid/cholesterol mixture (concentration of cholesterol in mol%; the A_{xy} and PCL values linearly extrapolated to $\pi = 30$ are not the real values at 30 mN/m as the molecules are untilted above about 28 mN/m)

%chol.	tilt($\pi=0$)	$\mathbf{dA_{xy}/d\pi}$	$\mathbf{A_{xy}(\pi=30)}$	$\mathbf{PCL}_{11}(\pi=30)$	$\mathbf{A_0(\pi=0)}$
0.0	33.2°	-0.1138	20.00	81	19.59
0.4	31.2°	-0.1000	19.94	125	19.62
1.0	33.0°	-0.1325	19.30	187	19.52
3.0	36.5°	-0.1413	19.47	199	19.06
5.0	35.7°	-0.1363	19.48	189	19.14

VII. List of symbols

Π_e :	Equilibrium spreading pressure
τ :	Surface tension
π :	Surface pressure
A :	Monolayer area (per molecule)
A_0 :	Smallest monolayer area per amphiphile, molecular cross section
ξ :	Chemical potential
G :	Free enthalpy
H :	Enthalpy
S :	Entropy
x :	Mole fraction
F_L :	Van-der-Waals energy of an upright rod-shaped aliphatic chain in a monolayer
F_I :	Van-der-Waals energy of a tilted rod-shaped aliphatic chain in a monolayer
LE:	Liquid expanded monolayer phase
LC:	Liquid condensed monolayer phase
\mathbf{c} :	Unit vector of the projection of an amphiphile onto the monolayer plane
\mathbf{n} :	Normal to domain boundary
p_z :	Molecular dipole moment perpendicular to the monolayer plane
μ :	Difference between the dipole densities of coexisting monolayer phases
λ :	(Mean) line tension between coexisting monolayer phases (λ_0 : isotropic line tension, λ_1 : anisotropic line tension)
F_μ :	Dipole energy of a monolayer phase
F_λ :	Energy of line tension
P :	Perimeter of an LC domain
σ :	Surface charge density
q :	Charge
κ^{-1} :	Debye length
Ψ_0 :	Surface potential (Potential at zero distance from a charged surface)
ΔV :	Surface potential (potential drop at an interface)
D_H :	Fraction of dissociated acid (free or sodium salt) in the monolayer
A_{Na} :	Fraction of lipid-sodium salt in the monolayer
$Q_{xy}(\mathbf{K}_x), Q_z(\mathbf{K}_z)$:	Components of the X-ray scattering vector in x-y and z direction

Thesen

1. Durch Veränderung des Subphasen-pH-Wertes und somit des Dissoziationsgrades werden Phasenverhalten, Gitterstruktur, molekulare Ordnung und Morphologie von Fettsäuremonoschichten empfindlich beeinflusst.
2. Fettsäuremonoschichten, die auf Wasser in kondensierter Form vorliegen, werden durch Erhöhung des pH-Werts der Subphase in Abhängigkeit von der Monoschichtfläche entweder in den kondensiert-expandiert Zweiphasenkoexistenzbereich oder in die reine expandierte Phase überführt.
3. Am Beispiel von Arachinsäure wird gezeigt, dass der Plateaudruck des Hauptphasenübergangs von pH 11.5 bis 13 linear mit dem pH-Wert ansteigt. Oberhalb von pH 13 wird die Fettsäuremonoschicht als vollständig dissoziiert angenommen.
4. Folgender Zustand wird für die Arachinsäuremonoschicht im Zweiphasenbereich postuliert: die fluide Phase ist vollständig dissoziiert, die kondensierte nur zum Teil. Ein Teil der dissoziierten Fettsäuremoleküle ist mit den eingesetzten Natriumgegenionen assoziiert. Die Zunahme des Plateaudrucks mit zunehmendem pH ergibt sich durch Erhöhung der Dissoziation der kondensierten Phase.
5. Bezüglich des thermodynamischen Phasenverhaltens von dissoziierbaren Monoschichten entspricht eine Erhöhung des pH-Werts der Subphase einer Erhöhung der Temperatur oder einer Verkürzung der Kettenlänge der Monoschichtmoleküle. Diese Analogie wurde nachgewiesen für die Verschiebung des Plateaudrucks in π -A Isothermen und für die Verschiebung von Phasengrenzen im π -T Phasendiagramm.
6. Grösse, Form und innere Struktur von Domänen der kondensierten Phase im Zweiphasenkoexistenzbereich lassen sich auf intermolekulare Wechselwirkungen zurückführen.
7. Das Verhältnis von Domänenumfang zur Domänenfläche und das Ausmass der Neigungsorientierungsordnung in den Domänen wird bestimmt durch das Wechselspiel von Randlinienspannung und intermolekularer Dipolabstossung. Die Randlinienspannung ist Ausdruck von intermolekularen Kräften und sie ist umso grösser je grösser die attraktiven molekularen Wechselwirkungen sind.
8. Durch Erhöhung des pH-Werts nimmt in Fettsäuredomänen das Verhältnis von Domänenumfang zur Domänenfläche zu und die Reichweite der Neigungsorientierungsordnung in den Domänen ab. Dies ist zurückzuführen auf die Abnahme der molekularen Bindungskräfte mit zunehmendem pH-Wert. Die Vergrösserung der molekularen Fläche und des Kettenneigungswinkels sowie die Abnahme der Konformationsordnung der Ketten und der Kettenpackung mit zunehmendem pH-Wert bestätigen das. Die Veränderung der Dipolkräfte ist demgegenüber vernachlässigbar.
9. Dieselben Veränderungen in der Morphologie von Fettsäuremonoschichten, die durch Erhöhung des pH-Wertes der Subphase erzeugt werden, entstehen durch Erniedrigung der Temperatur. Dies wird auf die Verstärkung der abstossenden Dipolwechselwirkungen mit sinkender Temperatur zurückgeführt. Die Beziehung zwischen pH-Wert und Temperatur wie sie für das Phasenverhalten ermittelt wurde ist somit umgekehrt gültig für das morphologische Verhalten.

10. Die Facettierung von Monoschichtdomänen ist ein Gleichgewichtsvorgang, der die Verringerung der Linienspannung und das Vorliegen geneigter Moleküle voraussetzt. Die Facettenbildung beruht auf der noch unverstandenen Tatsache, dass die geneigten Moleküle in der Domäne eine Orientierung entweder senkrecht oder parallel zur Domänenrandlinie anstreben. Dieses Phänomen lässt sich beschreiben durch Einführung eines einzigen Anisotropieterms für die Randlinienspannung. Diese Randlinienanisotropie erklärt auch die Beziehung zwischen Dendritenbildung und innerer Domänenstruktur unter Nicht-Gleichgewichtsbedingungen.

11. Cholesterin in der Monoschicht bewirkt eine Verminderung der Randlinienspannung durch Anlagerung der Moleküle an den Domänenrand.

12. In der kondensierten Phase einer Fettsäuremonoschicht gelöstes Cholesterin wirkt wie folgt: Cholesterin erhöht die Konformationsordnung der aliphatischen Ketten. Es verstärkt einerseits die molekulare Wechselwirkung und die Gitterordnung durch Verringerung des Neigungswinkels der Ketten. Andererseits erzeugen die Cholesterinmoleküle durch ihre Größe Unordnung im Gitter und schwächen dadurch die molekulare Wechselwirkung. Das Gleichgewicht zwischen beiden Effekten hängt ab von der Cholesterinkonzentration und vom Druck.

13. Eine Diskontinuität in mehreren Eigenschaften von Fettsäuremonoschichten (Kettenpackung, L_2/Ov -Phasenübergangsdruck, Positionskorrelationslänge) bei etwa pH 9, d. h. bei einem Dissoziationsgrad von ca. 50%, und ein Maximum der Positionskorrelationslänge (gleichbedeutend dem Maximum der attraktiven Wechselwirkung zwischen den Kopfgruppen) bei diesem pH lässt auf die Bildung von wasserstoffverbrückten Säure-Anion Dimeren in teilweise dissoziierten Fettsäuremonoschichten schließen.

14. Das Wechselspiel von Ketten- und Kopfgruppenwechselwirkungen zwischen amphiphilen Molekülen ist verantwortlich für die Vielfalt von geneigten Monoschichtphasen.

15. Die Verschiebung des Übergangsdrucks zwischen NN und NNN Phasen durch den pH-Wert der Subphase oder durch in der wässrigen Subphase gelöste Moleküle oder Ionen beruht auf der Veränderung der sterischen Wechselwirkungen zwischen benachbarten Kopfgruppen.

16. Der Einfluss von Polyethylenimin in der Subphase auf Fettsäuremonoschichten beschränkt sich auf die Verminderung der Monoschichtlöslichkeit und auf die Erhöhung des Dissoziationsgrades der Fettsäuremonoschicht auf einen Wert, der dem bei etwa pH 12 entspricht. Spezifische Wechselwirkungen zwischen Ammoniumgruppen des Polymers und dissoziierten Lipiden der Monoschicht gibt es nicht.

Lebenslauf

Johann, Robert

geb. 1970 in Huntsville/USA

Ausbildung

Schulausbildung	1976-1980	Grundschule in Sobernheim
	1980-1982	Realschule in Sobernheim
	1982-1989	Descartes-Gymnasium in Neuburg a. d. Donau
		Abschluss: Abitur
Militärdienst	1989-1991	Soldat auf Zeit
Studium	1991-1997	Universität Regensburg Fachrichtung Chemie Diplom
	1994-1995	1 Semester Auslandsaufenthalt in Canterbury, Kent, GB Abschluss: Diplom
Diplomarbeit		“Bau eines Apparates zum induktiven Schmelzen und die Untersuchung der Ordnungszustände von Au_2InNd , Ag_2InNd und Au_2InLa sowie theoretische Berechnungen an NdO und NdS ”
Promotion	Aug.1997-Okt.2001	Max-Planck-Institut für Kolloid- und Grenzflächenforschung in Golm

Danksagung

An dieser Stelle möchte ich all denjenigen danksagen, die am Gelingen dieser Arbeit einen Anteil haben

Mein besonderer Dank gilt meinem Betreuer Prof. Vollhardt, dass ich in seiner Arbeitsgruppe auf diesem, wie der Umfang der Arbeit zeigt, sehr ergiebigen Gebiet der unlöslichen Monoschichten arbeiten durfte. Ich bin ihm sehr dankbar für den grossen Freiraum, den er mir in der Gestaltung meiner Arbeit gewährte und für die Möglichkeit, eigene Ideen zu entwickeln und sie in Form von Publikationen und Vorträgen zu vertreten. Ich danke ihm für sein stetes Bemühen um einwandfreie Arbeitsbedingungen, die ein reibungsloses Arbeiten ermöglichten.

Nicht weniger danken möchte ich Prof. Möhwald für sein stetes und grosses Interesse an der Arbeit und den Belangen eines jeden Doktoranden an seinem Institut. Ich danke ihm für die wertvolle Unterstützung und die beständige Einladung zu ungezwungener Diskussion, die er sich mit seinen Mitarbeitern in einer solchen Intensität wünscht, dass nach seinen Worten der Betrieb in seinem Büro dem in einem Taubenschlag gleichkommen solle.

Bedanken möchte ich mich auch bei den ehemaligen Angehörigen der Arbeitsgruppe Dr. Gerd Weidemann, Dr. Kerstin Meine und Dr. Volker Melzer für die Zeit, in der sie meine Arbeit begleitet haben. Ihre geradezu selbstlose Hilfsbereitschaft von einer Art, die ich bisher kaum kannte, halfen mir sehr, mich mit der mir neuen Materie und den Gerätschaften vertraut zu machen. Sie begleiteten mich bei den ersten Messungen, und aus zahlreichen Diskussionen mit ihnen habe ich wertvolle Anregungen für meine Arbeit geschöpft.

Dr. Stefan Siegel danke ich für die aufgrund seines ausserordentlichen wissenschaftlichen Interesses stete Diskussionsbereitschaft und für seine Unterstützung in manchen technischen Fragen.

Bei Irina Berndt und Ursula Modrow bedanke ich mich, dass sie mich so herzlich in die Arbeitsgruppe aufgenommen haben, dass sie mir bei den allerersten Versuchen an Filmwaage und Brewsterwinkel-Mikroskop zur Seite gestanden haben und nicht zuletzt für die logistische Unterstützung.

Nadja Krasteva, Dr. Emmrich und zahlreichen ausländischen Gästen, die kamen und gingen, danke ich für das interessante und abwechslungsreiche Arbeitsklima.

Dr. Gerald Brezesinski, einem der geschätztesten Betreuer im Institut, danke ich dafür, dass er sich für meine Anliegen immer Zeit genommen hat, und seinen Mitarbeiter Christian Symietz und Dr. Ursula Dahmen-Levison danke ich für ihre Unterstützung und Rat bei den Röntgen- und Infrarotmessungen.